One- and Multidimensional Liquid Chromatographic and Mass Spectrometric Strategies for the Quality Control of Natural, Synthetic and Therapeutic Peptides

Dissertation

der Mathematisch-Naturwissenschaftlichen Fakultät

der Eberhard Karls Universität Tübingen

zur Erlangung des Grades eines

Doktors der Naturwissenschaften

(Dr. rer. nat.)

vorgelegt von

Ryan Icharia Karongo

aus Nairobi (Kenia)

Tübingen

2022

II

The research described in this thesis was conducted between January 1st 2018 and February 20th 2022 at the Institute of Pharmaceutical Sciences, Division Pharmaceutical (Bio-)Analysis, Eberhard Karls Universität Tübingen under the supervision of Prof. Dr. Michael Lämmerhofer.

Contents

I. Summary

Synthetic and therapeutic peptides are experiencing increasing importance in biopharma over the past decade and the number of peptide drug approvals is steadily increasing. However, generic chromatographic methods for their analysis in quality control often reach their limits, especially for the identification of minor peptide related impurities (< 1%) that tend to co-elute with the active pharmaceutical ingredient (API). Two-dimensional liquid chromatography (2D-LC) instrumentation, since its commercialization, has promoted the development of a broad spectrum of methodologies and applications to address a multitude of pharmaceutical challenges, comprising complex and hard-to-resolve samples (e.g. stereoisomers and structurally similar impurities). The aim of the following work was the development and implementation of 1D- and 2D-LC platform methods for the quality control of peptides, on both an intact and at a building block level (e.g. amino and alkanoic acids). These methods, further facilitate the structural elucidation of novel peptides used for drug discovery research e.g. lipopeptides. Consequently, a variety of challenges regarding peptide purity control and structure elucidation were addressed in this thesis. In particular, a peptide API purity control method by a selective comprehensive reversed phase 2D-LC (sRP×RP), two methods for enantioselective amino acid analysis, a high throuput (2.5 min) 1D-LC and a multiple-heart-cutting 2D-LC (mRP-chiral) method. Furthermore, a direct enantioselective characterization method for 3-hydroxy fatty acids (3-OH-FAs) in lipopeptides, is presented.

First, the sRP×RP was developed as an advanced generic method on an intact peptide level, hyphenated to complementary modes of detection, namely UV-DAD, charged aerosol detection (CAD) and ESI-QTOF-MS/MS in data-dependent (IDA, information dependent acquisition) and data independent acquisition (SWATH, sequential window acquisition of all theoretical fragment ion spectra). Only the main peak, is transferred comprehensively from the generic (low pH, 0.1 % TFA) first dimension (^{1}D) to an orthogonal (high pH, NH_4OH) second dimension (^{2}D). The method provides additional information on critical quality attributes at no extra time and further enables ESI-MS hyphenation by selecting MS compatible conditions for the ^{2}D. This comprehensive sampling strategy permits subsequent quantification utilizing all detectors, especially also on an MS^2 level owing to SWATH technology.

In many instances natural and non-ribosomal synthetized peptides contain D- and uncommon AAs, and therefore, an enantioselective method was required to control their stereochemical integrity on a building block level. In order to improve the weak detection properties of AAs, pre-column derivatization with 6-aminoquinolyl-*N*-hydroxysuccinimidyl carbamate (AQC; AccQ), resulting in favourable chromophoric, fluorophoric and electrospray ionization

properties, was utilized. AQC-AAs are further stronger retained in RP-LC and better chirally recognized on quinine (QN-AX, ZWIX(+)) and quinidine (QD-AX and ZWIX(-)) carbamate selectors. A rapid high-throughput enantioselective amino acid analysis (ReAAA) assay utilizing a short QN-AX core-shell particle column was developed to allow the simultaneous analysis of all proteinogenic AAs within one run (2.5 min). As a proof of principle, an AA supplement sample containing minor D-amino acid impurities was analyzed. However, when uncommon amino acids are present in a sample, especially isobaric analogues, their chromatographic resolution is mandatory prior MS detection. By combining chemoselectivity with enantio/stereoselectivity in a robust and fully automated mRP-chiral-FLD (fluorescence detection)-ESI-QTOF-MS platform, it was possible to resolve all proteinogenic AAs despite the presence of frequently occurring isobars of Leu/Ile (*allo*-Isoleucine, *tert*-Leucine, Norleucine) and Thr (aThr, Hse), especially present in non-ribosomally synthetized lipopeptides (NRLP) from various natural sources.

Lastly, In order to complete the characterization of a NRLP, the stereochemistry of the attached 3-hydroxy alkanoic acids ought to be elucidated, for which an enantioselective UHPLC-ESI-MS/MS assay utilizing an amylose tris(3,5-dimethylphenyl carbamate) based polysaccharide CSP immobilized on 1.6 µm silica particles (CHIRALPAK IA-U) was established. The assignment of the carbon chain length and stereochemistry of 3-OH-FAs ranging from hexanoic (C6) to myristic acid (C14) is presented, observing a consistent gradient elution order of S < R.

II. Zusammenfassung

Synthetische und therapeutische Peptide haben im vergangenen Jahrzehnt, mit einem stetigen Wachstum an Zulassungen von Peptidarzneimitteln, eine zunehmende Bedeutung in der Arzenimitteltherapie erfahren. Generische chromatographische Methoden für ihre Analyse in der Qualitätskontrolle stoßen jedoch häufig an ihre Grenzen, insbesondere bei der Identifizierung von geringfügigen peptidbezogenen Verunreinigungen (< 1 %), die dazu neigen, gemeinsam mit dem pharmazeutischen Wirkstoff (API) zu eluieren. Zweidimensionale hochleistungsflüssigkeitschromatographische (2D-LC) Instrumente haben seit ihrer Kommerzialisierung die Entwicklung eines breiten Spektrums an Methoden und Anwendungen hervorgebracht, um eine Vielzahl von pharmazeutischen Herausforderungen anzugehen, die komplexe und schwer aufzulösende Proben umfassen (z. B. Stereoisomere und strukturell ähnliche Verunreinigungen).

Ziel der folgenden Arbeiten war die Entwicklung und Implementierung von 1D- und 2D-LC-Plattformmethoden zur Qualitätskontrolle von Peptiden, sowohl auf intakter als auch auf Bausteinebene (z. B. Amino- und Alkansäuren). Diese Verfahren erleichtern weiterhin die Strukturaufklärung neuer Peptide, die für die Arzneimittelforschung von Interesse sind, z.B. Lipopeptide. Folglich wurden in dieser Dissertation eine Vielzahl von Herausforderungen in Bezug auf die Kontrolle der Peptidreinheit und die Strukturaufklärung addressiert. Insbesondere eine Peptid-API-Reinheitskontrollmethode durch eine „selective comprehensive" Umkehrphasen 2D-LC (sRP×RP), zwei Methoden zur enantioselektiven Aminosäureanalyse, nämlich eine 1D-LC mit hohem Durchsatz (2,5 min) und eine „multiple-heart-cutting"-2D-LC (mRP-chiral) Methode. Darüber hinaus wird eine Methode zur direkten enantioselektiven Charakterisierung von 3-Hydroxy-Fettsäuren (3-OH-FAs) in Lipopeptiden vorgestellt.

Zunächst wurde die sRP×RP als fortschrittliche generische Methode auf intakter Peptidebene entwickelt, verbunden mit komplementären Detektionsmodi, sprich UV-DAD, Charged-Aerosol-Detektion (CAD) und Elektrosprayionisation-Quadrupol-Flugzeit-Hybrid-Tandem-Massenspektrometrie (ESI-QTOF-MS/MS) in datenabhängiger (IDA, informationsabhängige Erfassung) und datenunabhängige Erfassung (SWATH, sequentielle Fenstererfassung aller theoretischen Fragmentionenspektren). Nur der Hauptpeak wird umfassend von der generischen (niedriger pH, 0,1 % TFA) ersten Dimension (^{1}D) in eine orthogonale (hoher pH, NH_4OH) zweite Dimension (^{2}D) übertragen. Das Verfahren liefert ohne zusätzlichen Zeitaufwand zusätzliche Informationen zu kritischen Qualitätsattributen und ermöglicht ferner die ESI-MS-Trennung, indem MS-kompatible Bedingungen für die ^{2}D gewählt wurden. Diese umfassende Eluatüberführungsstrategie ermöglicht eine nachträgliche Quantifizierung unter

Verwendung aller Detektoren, insbesondere auf MS^2-Ebene aufgrund der SWATH-Technologie.

In vielen Fällen enthalten natürliche und nicht-ribosomal synthetisierte Peptide D- und ungewöhnliche Aminosäuren (AS), weshalb eine enantioselektive Methode erforderlich war, um ihre stereochemische Integrität zu überprüfen. Dafür wurde eine Vorsäulenderivatisierung mit 6-Aminochinolyl-N-hydroxysuccinimidylcarbamat (AQC; AccQ) verwendet, um die schlechten Nachweiseigenschaften von AS auszugleichen, was zu vorteilhaften chromophoren, fluorophoren und Elektrospray-Ionisationseigenschaften führte. Weiterhin werden AQC-AS stärker auf Umkehrphasen retardiert und chiral besser auf Chinin- (QN-AX, ZWIX(+)) und Chinidin- (QD-AX und ZWIX(-)) Carbamat-Selektoren erkannt. Um eine gleichzeitige Analyse aller proteinogenen AAs in einem Lauf zu ermöglichen, wurde eine rapide (2,5 min) Hochdurchsatz-Methode zur enantioselektiven Aminosäureanalyse (ReAAA) unter Verwendung einer kurzen QN-AX Core-Shell-Partikelsäule entwickelt. Als Grundsatzbeweis wurde damit eine Aminosäurehaltige Nahrungsergänzungsprobe analysiert, die geringfügige D-Aminosäureverunreinigungen enthielt. Wenn jedoch ungewöhnliche Aminosäuren in einer Probe vorhanden sind, insbesondere isobare Analoga, ist deren chromatographische Auflösung vor der MS detektion obligatorisch. Durch die Kombination von Chemoselektivität mit Enantio-/Stereoselektivität in einer robusten und vollautomatischen mRP-chiral-FLD(Fluoreszenzdetektion)-ESI-QTOF-MS-Plattform war es möglich, alle proteinogenen AAs aufzulösen, trotz des Vorhandenseins häufig vorkommender Isobaren von Leu/Ile (*allo*-Isoleucin, *tert*-Leucin, Norleucin) und Thr (*allo*-Thrreonin, Homoserin), besonders vorhanden in nicht-ribosomal synthetisierten Lipopeptiden (NRLP) natürlichen Ursprungs.

Schließlich sollte zur Vervollständigung der Charakterisierung eines NRLP die Stereochemie der angehängten 3-Hydroxyalkansäuren aufgeklärt werden, wofür ein enantioselektiver UHPLC-ESI-MS/MS-Assay unter Verwendung einer Amylose-Tris(3,5-dimethylphenylcarbamats) basierten chiralen stationären Phase, immobilisiert auf 1,6-µm-Silicapartikeln (CHIRALPAK IA-U), etabliert wurde. Es wird die Zuordnung der Kohlenstoffkettenlänge und Stereochemie von 3-OH-FAs im Bereich zwischen Hexan- (C6) und Myristinsäure (C14) vorgestellt, wobei eine konstante Elutionsreihenfolge von S < R bei dieser Methode mit Gradientenelution beobachtet wird.

III. List of publications

Publication I

<u>R. Karongo</u>, T. Ikegami, D.R. Stoll, M. Lämmerhofer, A selective comprehensive reversed-phase×reversed-phase 2D-liquid chromatography approach with multiple complementary detectors as advanced generic method for the quality control of synthetic and therapeutic peptides, *Journal of Chromatography A*, 1627 (**2020**) 461430, DOI: 10.1016/j.chroma.2020.461430.

Publication II

<u>R. Karongo</u>, J. Jiao, H. Gross, M. Lämmerhofer, Direct enantioselective gradient reversed-phase ultra-high performance liquid chromatography tandem mass spectrometry method for 3-hydroxy alkanoic acids in lipopeptides on an immobilized 1.6 µm amylose-based chiral stationary phase, *J Sep Sci*, 44 (**2021**) 1875-1883, DOI: 10.1002/jssc.202100104.

Publication III

<u>R. Karongo</u>, M. Ge, C. Geibel, J. Horak, M. Lämmerhofer, Enantioselective multiple heart cutting online two-dimensional liquid chromatography-mass spectrometry of all proteinogenic amino acids with second dimension chiral separations in one-minute time scales on a chiral tandem column, *Anal. Chim. Acta*, 1180 (**2021**) 338858, DOI: 10.1016/j.aca.2021.338858.

Publication IV

<u>R. Karongo</u>, M. Ge, J. Horak, H. Gross, M. Kohout, W. Lindner, M. Lämmerhofer, Rapid enantioselective amino acid analysis by ultra-high performance liquid chromatography-mass spectrometry combining 6-aminoquinolyl-N-hydroxysuccinimidyl carbamate derivatization with core-shell quinine carbamate anion exchanger separation, *Journal of Chromatography Open*, 1 (**2021**) 100004, DOI: 10.1016/j.jcoa.2021.100004.

Publication V - Manuscript

<u>R. Karongo</u>, J. Horak, M. Lämmerhofer, Untargeted full comprehensive online reversed-phase×chiral two-dimensional liquid chromatography-mass spectrometry for enantioselective 6-aminoquinolyl-N-hydroxysuccinimidyl carbamate derivatized amino acid analysis column.

IV. Author Contributions

Publication I

A selective comprehensive reversed-phase×reversed-phase 2D-liquid chromatography approach with multiple complementary detectors as advanced generic method for the quality control of synthetic and therapeutic peptides.

Ryan Karongo:

Conceptualization and investigation
Methodology and formal analysis
Data curation and visualization
Main writing of the manuscript

Assoc. Prof. Dr. Tohru Ikegami:

Supervision and proofreading of the manuscript

Prof. Dr. Dwight R. Stoll:

Proofreading of the manuscript
Funding acquisition

Prof. Dr. Michael Lämmerhofer:

Conceptualization, methodology, supervision and financing of the project
Discussion of results and interpretation
Proofreading and final approval of the manuscript
Corresponding author

Publication II

Direct enantioselective gradient reversed-phase ultra-high performance liquid chromatography tandem mass spectrometry method for 3-hydroxy alkanoic acids in lipopeptides on an immobilized 1.6 µm amylose-based chiral stationary phase.

Ryan Karongo:

Conceptualization and investigation
Methodology and formal analysis
Data curation and visualization
Main writing of the manuscript

Junjing Jiao:

Sample collection
Proofreading of the manuscript

Prof. Dr. Harald Gross:

Proofreading of the manuscript

Prof. Dr. Michael Lämmerhofer:

Conceptualization, methodology, supervision and financing of the project
Discussion of results and interpretation
Proofreading and final approval of the manuscript
Corresponding author

Publication III

Enantioselective multiple heart cutting online two-dimensional liquid chromatography-mass spectrometry of all proteinogenic amino acids with second dimension chiral separations in one-minute time scales on a chiral tandem column.

<u>Ryan Karongo:</u>

Conceptualization and investigation
Methodology and formal analysis
Data curation and visualization
Main writing of the manuscript

Min Ge:

Investigation, methodology and formal analysis

Christian Geibel:

Column packing
Proofreading of the manuscript

Dr.rer.nat Jeannie Horak:

Conceptualization, methodology and supervision
Proofreading of the manuscript
Co-corresponding author

Prof. Dr. Michael Lämmerhofer:

Conceptualization, methodology, supervision and financing of the project
Discussion of results and interpretation
Proofreading and final approval of the manuscript
Corresponding author

Publication IV

Rapid enantioselective amino acid analysis by ultra-high performance liquid chromatography-mass spectrometry combining 6-aminoquinolyl-N-hydroxysuccinimidyl carbamate derivatization with core-shell quinine carbamate anion exchanger separation.

<u>**Ryan Karongo:**</u>

Conceptualization and investigation
Methodology and formal analysis
Data curation and visualization
Main writing of the manuscript

Min Ge:

Investigation, methodology and formal analysis

Dr.rer.nat Jeannie Horak:

Conceptualization, methodology and supervision
Proofreading of the manuscript

Prof. Dr. Harald Gross:

Resources and proofreading of the manuscript

Michal Kohout

Investigation and resources
Proofreading of the manuscript

W. Lindner

Conceptualization and resources
Proofreading of the manuscript

Prof. Dr. Michael Lämmerhofer:

Conceptualization, methodology, supervision and financing of the project
Discussion of results and interpretation
Proofreading and final approval of the manuscript
Corresponding author

Publication V – Revised Manuscript

Comprehensive Online Reversed-phase×Chiral Two-dimensional Liquid Chromatography-Mass Spectrometry with Data-independent SWATH-Acquisition for Untargeted Enantioselective Amino Acid Analysis

<u>Ryan Karongo:</u>

Conceptualization and investigation

Methodology and formal analysis

Data curation and visualization

Main writing of the manuscript

Dr. rer. nat Jeannie Horak:

Conceptualization and proofreading of the manuscript

Prof. Dr. Michael Lämmerhofer:

Conceptualization, methodology, supervision and financing of the project

Discussion of results and interpretation

Proofreading and final approval of the manuscript

Corresponding author

V.   Poster Presentations

DPhG (Germany Pharmaceutical Society) Annual meeting 2018, Hamburg, Germany, October 2nd – 5th.

A Selective Comprehensive 2D-LC Method for the Quality Control of Synthetic (Therapeutic) Peptides

Ryan Karongo, Tohru Ikegami, Dwight Stoll, Michael Lämmerhofer

48th International Symposium on High-Performance Liquid Phase Separations and Related Techniques 2019, Milan, Italy, June 16th – 20th.

A Selective Comprehensive 2D-LC Method for the Quality Control of Synthetic Peptides

Ryan Karongo, Michael Lämmerhofer

30th PhD students meeting of the German Chemical Society Society 2020, Hohenroda, Germany, January 11th – 14th.

Impurity Profiling of Synthetic Peptides by Two-Dimensional Liquid Chromatography

Ryan Karongo, Jeannie Horak, Michael Lämmerhofer

VI.   Oral Presentations

31st PhD students meeting of the German Chemical Society 2018, Hohenroda, Germany, January 11th – 12th.

Enantioselective liquid chromatography of AQC derivatized amino acids in achiral - chiral multiple heart cutting online 2D-LC

<u>Ryan Karongo</u>, Jeannie Horak, Michael Lämmerhofer

31st International Symposium on Pharmaceutical and Biomedical Analysis 2021, Kyoto, Japan, August 29th – September 1st.

One- and Two-Dimensional Methods for the Rapid and Comprehensive Enantioselective Analysis of AQC Derivatized Amino Acids from Natural and Synthetic Peptides

<u>Ryan Karongo</u>, Jeannie Horak, Michael Lämmerhofer

VII. Video Presentations

HPLC Tube - 48th International Symposium on High-Performance Liquid Phase Separations and Related Techniques 2019, Milan, Italy, June 16th – 20th.

A Selective Comprehensive 2D-LC Method for the Quality Control of Synthetic Peptides

<u>Ryan Karongo</u>, Michael Lämmerhofer

VIII. List of abbreviations

^{1}D	First dimension in 2D-LC
1D-LC	One-dimensional liquid chromatography
^{2}D	Second dimension in 2D-LC
2D-LC	Two-dimensional liquid chromatography
3-OH-FAs	3-Hydroxy fatty acids
AQC, AccQ	6-aminoquinolyl-N-hydroxysuccinimidyl carbamate
ReAAA	Rapid enantioselective amino acid analysis
AA	Amino Acid
ACN	Acetonitrile
AcOH	Acetic acid
APCI	Atmospheric pressure chemical ionization
API	Active pharmaceutical ingredient
CAD	Charged aerosol detection
CE	Collision energy
CEM	Channel electron multiplier
CHCl$_3$	Chloroform
CHIRALPAK IA-U	Amylose tris(3,5-dimethylphenyl carbamate) based polysaccharide CSP
cps	Counts per second
CSP	Chiral stationary phase
DAD	Diode array detector
DDA	Data-dependent acquisition
DP	Declustering potential
EIC	Extracted ion chromatogram
BPC	Base peak chromatogram
ELSD	Evaporation light scattering detection
SPAM	Stationary phase assisted modulation
Eq.	Equation
ESI	Electrospray ionization

FLD	Fluorescence detection
FA	Formic acid
FDA	United States Food and Drug Administration
Fig.	Figure
FPP	Fully porous (silica) particles
FWHM	Full width at half maximum
HCl	Hydrochloric acid
HILIC	Hydrophilic interaction liquid chromatography
HPLC	High performance liquid chromatography
HR	High resolution
ICH	International Council for Harmonisation of Technical Requirements for Pharmaceuticals for Human Use
ID	Inner diameter
IDA	Information-dependent acquisition
IS	Internal standard
LC	Liquid chromatography
LC-LC	Heart-cutting 2D-LC
LC×LC	Full comprehensive 2D-LC
LOD	Limit of detection
OPA	o-Phthaldialdehyde
FMOC-Cl	9-Fluorenylmethyl chloroformate
NBD-F	7-Fluoro-4-nitrobenzo-2-oxa-1,3-diazole
VIS	Visible (light spectroscopy)
m/z	Mass-to-charge ratio
MeOH	Methanol
mLC-LC, MHC	Multiple-heart-cutting 2D-LC
MRM	Multiple reaction monitoring
MS	Mass spectrometry
MS/MS	Tandem mass spectrometry
NaOH	Sodium hydroxide

NH₄Ac	Ammonium acetate
NH₄FA	Ammonium formate
NH₄HCO₃	Ammonium carbonate
NH₄OH	Ammonium hydroxide
NMR	Nuclear magnetic resonance
NRLP	Non-ribosomally synthetized lipopeptides
NRP	Non-ribosomal peptide
NRPS	Non-ribosomal peptide synthetase
pH	Potentia hydrogenii
ppm	Parts per million
q2	Collision cell (RF-only quadrupole)
QC	Quality control
QD-AX	Quinidine-derived chiral anion exchanger
QN-AX	Quinine-derived chiral anion exchanger
QqQ	Triple quadrupole
QTOF	Quadrupole time-of-flight
ref.	Reference
RP	Reversed-phase chromatography
S/N	Signal-to-noise
SCX	Strong cation exchanger
sLC×LC	Selective comprehensive 2D-LC
SPE	Solid phase extraction
SPP	Superficially porous (silica) particles (Coreshell particles)
SRM	Selected reaction monitoring
SWATH	Sequential window acquisition of all theoretical fragment ion spectra
TDC	Time-to-digital converter
TFA	Trifluoroacetic acid
THF	Tetrahydrofuran
TIC	Total ion current
TOF	Time-of-flight

RT, t_R	Retention time
UHPLC	Ultra-High-Performance Liquid Chromatography
UV	Ultraviolet (light spectroscopy)
V_0	Dead volume
V_D	Dwell volume
VWD	Variable wavelength detector
WAX	Weak anion exchanger
XIC	Extracted ion chromatogram
ZWIX(-)	Quinidine-derived zwitterionic CSP
ZWIX(+)	Quinine-derived zwitterionic CSP

1. Introduction

1.1 Therapeutic peptides

Peptides along with other molecules, such as proteins, carbohydrates, lipids, and nucleic acids are molecules of life. They are present in every living cell and structure of multicellular organisms. In the past few years, there has been a high demand for peptides as lead molecules for active pharmaceutical ingredients (API) [1, 2]. Mainly, three different approaches are used to synthesize them: (a) isolation from cell culture of biotechnological production of non-ribosomal and ribosomal peptide synthetase machinery, (b) recombinant expression in microorganisms or animals, and (c) chemical synthesis [3]. Each approach carries advantages and disadvantages driven by peptide size, desired modifications or derivatives, time constraints, and economics.

Therapeutic and theranostic peptides occupy an interesting space along the molecular continuum between traditional small molecule drugs and large ones such as proteins [4]. They are predominantly accessible through the synthetic route according to Merrifield [5]. The most important challenge however is their quality, especially with respect to impurities. Considering their biological function, impurities may pose significant consequences that can potentially affect the safety and efficacy of the therapeutic peptide. Following, the need for thorough monitoring and characterization becomes evident [6].

Natural sources of guidance towards the discovery of novel peptides encompass biosynthesis by the well-defined machinery of the ribosome leading to proteinogenic amino acids (AAs) as building blocks [7, 8]. Common examples of synthetically produced peptides of natural origin are Octreotide and Oxytocin. A further source guiding the development of therapeutics are non-ribosomal peptides (NRPs), e.g. Poaeamide [9, 10]. These non-standard peptides contain uncommon features, including non-proteinogenic, D- and *N*-methylated AAs, cyclization motifs (disulphide, amide and ester bonds) and lipophilic sidechains [11-13]. Lipopeptides are a special class of NRPs connected to a lipid moiety, which contain a considerable degree of stereoinformation, S/R configuration, within the peptide backbone and the commonly 3-hydroxylated lipophilic sidechain. Extraction of these compounds from their natural source may deliver multiple diastereoisomers, which have to be recognized and characterized for a full structural elucidation of the active compound [9, 14-16].

Understanding how to control the presence or absence of impurities when transitioning from a recombinant route of manufacture to a synthetic one is critical for the manufacturer [3]. The biggest challenge in peptide synthesis is therefore the purification step. Synthetic peptides may contain structurally related impurities, which are difficult to characterize. These could

originate from raw materials, from the manufacturing process or could be formed during (downstream processing or purification, and/or degradation during storage. Peptide related impurities include (i) deletion and (ii) insertion impurities, (iii) incomplete removal of the protecting group, (iv) oxidation and reduction, (v) dimers, (vi) diastereomers, and (vii) side and end chain impurities [17-19].

Table 1: Limits for reporting impurities according to ICH Q3A.

Maximum daily dose	Reporting threshold	Identification threshold	Qualification threshold
≤2g/ day	0.05%	0.10% or 1.0 mg per day intake (whichever is lower)	0.15% or 1.0 mg per day intake (whichever is lower)
>2g/day	0.03%	0.05%	0.05%

Their classification usually depends on their levels in the final substance, where the critical threshold of identification is set to 0.1 % according to ICH (Q3A) guidelines **Table 1**. In order to effectively detect various potential impurities on a peptide or AA level [3, 6, 20, 21] effectively, it is necessary to adopt a variety of orthogonal LC principles and detection methods such as reversed phase liquid chromatography (RPLC), hydrophilic interaction chromatography (HILIC), ion exchange and chiral chromatography, hyphenated to UV, charged aerosol (CAD) or mass spectrometric (MS) detection.

1.2 Separation Modes - Liquid Chromatography

1.2.1 Reversed phase Chromatography

RPLC is based on a non-polar stationary phase and utilizes organic non-polar solvents for elution, where the separation for a set of analytes will occur according to their individual hydrophobic properties [22-24]. During the 1970s ion exchange chromatography used to be the state of art for the separation of ionic samples, e.g. peptides and AAs, which contain acidic and basic moieties. Since then, however, there has been a great development for the analysis of ionizable compounds with RPLC [24]. The adsorption mechanism of solute molecules has been well investigated and understood, leading to the awareness of the following interactions influencing selectivity [24].

i.   hydrophobic interaction of lipophilic analyte moieties and the alkyl strands of the stationary phase as the dominating retention principle

ii. steric exclusion of larger solute molecules from the stationary phase

iii.   dipole–dipole interaction between a dipolar solute and stationary phase (e.g. a nitrile group for a cyano column)

iv.   hydrogen bonding of an acceptor (basic) or a donor (acidic) solute group, respectively, by a donor (acidic) or an acceptor (basic) group within the stationary phase

v.   cation-exchange or electrostatic interaction between a cationic solute and an ionized silanol

(SiO⁻) within the stationary phase

vi. $\pi-\pi$ interactions between an aromatic solute and a phenyl (phenyl column) or nitrile (cyano column) group

These interactions are regulated by the choice of aqueous-organic modifier and additives. Consequently, pH, solvent type, column, percentage of organic modifier, temperature, and buffer concentration are tuned to control the selectivity in RPLC separation [24]. RPLC is currently the state-of-the-art for the control of peptide impurities, in particular with trifluoroacetic acid (TFA) as an ion-pairing agent, which masks the cationic moieties of peptide analytes and further suppresses the ionization of acidic groups (including silanol groups within the stationary phase), resulting in excellent separations [24]. Nevertheless, there is a certain risk for structurally similar impurities to co-elute with the main compound during analysis and preparative purification steps. Therefore, orthogonal LC separation methods comprising e.g. HILIC, chiral stationary phases (CSPs) and mixed mode stationary phases, are highly recommended.

1.2.2   HILIC – Hydrophilic Interaction Liquid Chromatography

The term "hydrophilic interaction liquid chromatography - HILIC" was first suggested by Alpert in 1990 and refers to the affinity of analytes to water adsorbed to the polar adsorbent surface [25]. Since then there has been an increased popularity and importance of this technique [26-28], where applications range between a large selection of polar molecules [25, 29], including AAs and peptides [25, 30]. In HILIC the stationary phases may consist of non-modified silica or silica modified with polar chemical molecular structure such as amide, diol, zwitterionic sulfobetaine, or aminopropyl. On the basis thereof, the mobile phase contains an amount of water between 3–40% mixed with organic solvent, for instance acetonitrile (60-97% commonly used) or acetone. Just like in RPLC, various buffers are used to control the pH, ionic strength and ionization of the analytes. The retention mechanism is based on the partitioning of polar molecules between the organic bulk mobile phase and the aqueous-rich layer, which is formed on the highly polar/ionic stationary phase. When polar solutes enter the aqueous layer, they interact with the stationary phase. Hydrogen bonding and electrostatic interactions play also

a role for analyte retention, which differs from the retention mechanism in RPLC. Thus, these two modes can be considered as complementary and orthogonal [31-34].

A major advantage in HILIC is the low viscosity and high volatility of the acetonitrile-rich mobile phase, resulting in small back pressures, especially when long columns are used to increase separation efficiency. Additionally, the volatility of the highly organic mobile phase provides great electrospray desolvation efficiency, which leads to an improvement in sensitivity with detectors based on nebulization and evaporation processes, such as electrospray ionization mass spectrometry (ESI-MS), evaporation light scattering detection (ELSD) and charged aerosol detection (CAD) [35-37].

1.2.3 Chiral Chromatography

The impurity analysis of synthetic therapeutic peptides should include principles capable of resolving chiral impurities, either introduced to the API by the starting materials or by degradation [17]. The stereoisomeric purity of a peptide is of prime importance as a critical quality attribute regarding pharma-and toxicology [17-19]. In any product, where two enantiomers exist, one may exhibit the desired activity, while the other is either inactive or toxic. Many examples have shown the undesired effects of one isomer, limiting the overall effectiveness of the API [38]. The presence or absence of stereoisomers can be determined on an intact peptide or amino acid level following peptide hydrolysis and pre-column derivatization [39, 40]. The former strategy is more convenient and straightforward, but often insufficient [38], while the latter reveals the complete chiral D/L-AA profile, but is cumbersome and requires a skilled laboratory. Various areas of research utilize chiral LC [41-46] for the analysis of AAs [20, 47-50] and peptides [38, 51]. Important chiral selectors include chiral crown ethers [52, 53], macrocyclic antibiotics [54-57] polysaccharides [58] and cinchona alkaloid based chiral ion exchangers [38, 59, 60], although no chiral stationary phase has proven to be universally effective for the separation of enantiomers.

Chiral polysaccharide derivatives are based on amylose and cellulose aryl esters and carbamates with methyl, chloro or mixed methyl/chloro substituents, where D-glucose molecules are linked via α- and β-1, 4-glycosidic bonds, respectively. These eventually translate into a helical structure for the former and a rigid linear structure for the latter. A large number of broadly selective chiral columns are available through these structural variations, suitable for the analysis of e.g. oxidized fatty acids present in Lipopeptides [14, 58].

Cinchona alkaloids on the other hand, derived from quinine (+) or quinidine (-) carbamates, appear to be highly stereoselective for the resolution of chiral molecules [48, 61]. In particular they have been successfully applied for amino acid [62-66], oligopeptide [67-70] and lipopeptide [10] analysis using the commercially available zwitterionic chiral CHIRALPAK

4

ZWIX(+) and ZWIX(-) phases, which provide opposite elution orders for enantiomers [38]. They consist of an achiral anion-exchanger (quinine (+) or quinidine (-) carbamate) and a chirally attached carbamate-based cation-exchanger, i.e. amino cyclohexane sulfonic acid, immobilized on fully porous (FPP) or superficially porous (SPP) particles [71]. The corresponding weak anion exchanger phases QD-AX and QN-AX are obtained by substituting the chirally attached amino cyclohexane sulfonic acid moiety with a tert-butyl moiety. SPP supported stationary phases have shown to be favorable in terms of speed, efficiency and pressure drop, but are however not yet commercially available for these selectors [72]. The type and composition of organic solvents (MeOH, ACN, THF) navigate the separation, since these CSPs can be operated in polar organic, HILIC and reversed phase mode [60, 73]. Thus, they can be considered as mixed mode selectors [74, 75].

1.3 Two-dimensional liquid chromatography

Online two-dimensional liquid chromatography has gained tremendous popularity in recent years, largely due to the technological advances in the speed of LC separations (UHPLC with sub-2µm and core shell particle columns), the mechanical modulation valve and software to control it. Its purpose is to collect and modulate the effluent from the first dimension (^{1}D) into the second dimension (^{2}D). The most fundamental principles for any successful 2D-LC separation is based on the orthogonality of the two dimensions: columns with different stationary phase chemistries should be employed to maximize the difference in selectivity for one or more compound pairs which are otherwise difficult to resolve. Poorly or unresolved compounds eluting from the first dimension are further separated in the second dimension [76].
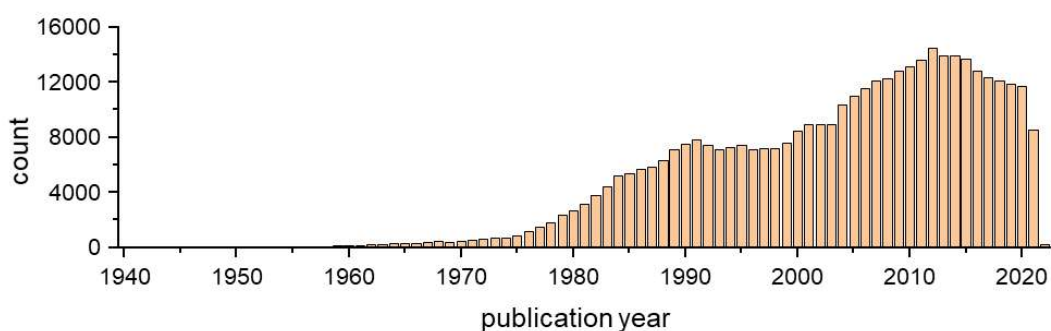

Figure 1: SciFinder Results for "two-dimensional liquid chromatography" in the title.

1.3.1 General principles – Peak Capacity, Undersampling, Orthogonality

The sample dimensionality s, as noted, can be considered as the number of independent variables required to describe the components of the sample mixture, e.g. amino acids differ in the side chain lipophilicity and their chirality as two orthogonal properties [77, 78]. 2D-LC made its early beginnings with Erni and Frei who utilized this technique for the resolution of

complex mixtures [79]. Since then, many advances have been made including the characterization of very complex samples, the universal analysis of less complex samples, but also for the sake of keeping correlation of samples within orthogonal separation conditions. According to Stoll et al. the ^{2}D can be conceptualized as a chemically selective analyzer of the ^{1}D.

1.3.1.1 Peak Capacity

The concept of peak capacity (n_c) is a concept favorably used to evaluate the performance in gradient elution and it describes the largest number of peaks, that can be fit within a separation window, e.g. between the first ($t_{R,1}$) and n^{th} ($t_{R,n}$) eluting peak [80]. For a one-dimensional chromatographic system, it is calculated using the average peak width (W) measured at 4σ (R_s = 1).

$$n_c = \frac{(t_{R,n} - t_{R,1})}{W}$$

(Eq. 1)

The limit of 1D-LC for complex mixtures can be explained using the statistical overlap theory [81]. According to Poisson statistics, the number of peaks in a random chromatogram will never exceed 37% of the potentially available peaks or peak capacity. The required peak capacity in 1D-LC can therefore only be extended increasing the separation time towards infinity, which is impractical. This situation gives rise to the necessity for multidimensional separation especially for complex mixtures.

As long as the following requirements are met, peak capacity can be used according to Gidding's product rule as a metric of the resolving power of a 2D separation [82]. First, the distribution of a mixture of components that is subjected to two or more separation mechanisms is dependent on different factors. Thus, the necessity for orthogonality, that again is predicated on complementary separation mechanisms. Second, the separation in the ^{1}D must be maintained during the transfer process to the ^{2}D: fast sampling of the ^{1}D to avoid "undersampling". Since, at undersampling conditions, peaks already separated in the ^{1}D remix in the sampling loop, losing the separation effect/resolution achieved by the ^{1}D. Thus,

$$n_{c,2D} = {}^1n_c \cdot {}^2n_c$$

(Eq. 2)

Undersampling introduced by the sampling process (especially at high sampling loop volumes) cannot be avoided completely and should be accounted for when calculating the effective peak capacity using the correction factor β [83], whereas t_s is the sampling time (modulation time) and $^1\sigma$ the ^{1}D peak standard deviation.

$$\langle \beta \rangle = \sqrt{1 - 0.214 \cdot \left(\frac{t_s}{\langle {}^1\sigma \rangle} \right)^2}$$

$$\text{for } 0.2 \leq \frac{t_s}{\langle {}^1\sigma \rangle} \leq 16$$

(Eq. 3)

According to Murphy, Schure and Foley (M-S-F), any peak from the ^{1}D should be sampled at least four times across the 8σ peak width to minimize the effect of undersampling [84]. For peak widths of typically 10s, this would result in maximum of 2.5 s sampling time.

As stated above, orthogonality influences the effective peak capacity. The degree of orthogonality is represented by the fraction coverage (f_{coverage}) of the separation space. Considering undersampling and the incomplete use of the separation space, the corrected formula for peak capacity (n*) is therefore:

$$n^*_{c,2D} = {}^1n_c \times {}^2n_c \times \left\langle \frac{1}{\beta} \right\rangle \times f_{\text{coverage}}$$

(Eq. 4)

The fractional utilization of 2D space can be accessed using multiple strategies resulting in orthogonality. For some applications, however, the focus is not the maximization of the peak capacity, but rather the maintenance of the correlation between the first dimension and a complementary second dimension, e.g. desalting applications [85, 86] or peak purity analysis [87].

1.3.1.2 Orthogonality

As above mentioned, 2D-LC methods require a certain degree of orthogonality between the two individual dimensions to attain an advantage over 1D-LC. Hence, orthogonality is an important quality descriptor to determine the performance of a 2D-LC method [26].

Orthogonality is a direct result of dissimilarities in separation mechanisms (selectivity) between the both dimensions in 2D-LC. The selectivity of both dimensions can therefore be adjusted by tuning multiple variables. The stationary and mobile phase are adjusted first, considering that selectivity is very much dependent on the physicochemical properties of the sample like molecular size, charge and hydrophobicity. The stationary and mobile phase should be selected in order to accommodate those properties within their selectivity [88]. In the case of peptides, which are zwitterionic in nature, the pH of the mobile phase plays a major role and must be considered. The stationary phase can be selected in order to sample hydrophobicities and hydrophilicities, in RP-LC and HILIC mode, respectively. [89]

There are a variety of methods, which have been proposed in order to quantify orthogonality, such as the mutual information theory [90], convex-hull [91], asterisk method [92], the nearest neighbor distance approach [93] and the bin counting method [78, 88]. All define high orthogonality as the effective utilization of separation space in both dimensions. Thus, the surface coverage in the two-dimensional space should be maximized, while the degree of correlation between the dimensions should be minimized [94].

A simple and widely used descriptor is the above-mentioned bin counting method, which is further illustrated in **Figure 2**. The first step is to normalize the retention times according to **(Eq.** 5, which transforms the retention time values to range between 0 and 1. Normalization of retention times offers the comparison of multiple 2D-LC data, removes the void space caused by column or system void volumes and allows using the mobile phase gradient as useful boundaries for normalization [88, 89].

$$RT_{i(norm)} = \frac{RT_i - RT_{min}}{RT_{max} - RT_{min}}$$
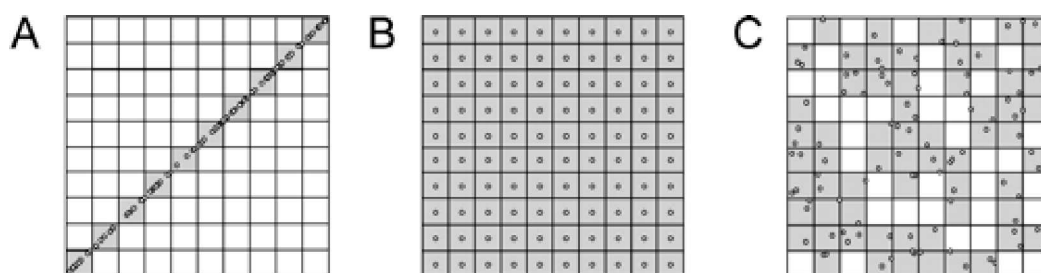
(Eq. 5)

Figure 2: The bin counting principle to determine the orthogonality of a hypothetical (A) a non-orthogonal (10 % surface coverage), (B) a perfectly orthogonal (100% surface coverage, unrealistic) and (C) a randomly orthogonal (65% surface coverage, realistic) separation. Adapted with permission from Gilar et al. [88].

Then the separation space is divided into squared bins, whereas the number of bins corresponds to the number of analyte components. **Figure 2** shows a hypothetical separation, where the separation space is divided into 100 bins, which equals the amount of sample components (dots) within the separations pace. [88] Thus, *f* can be calculated as the ratio of the fraction of bins occupied by dots and the sum of all bins, **(Eq.** 6 illustrates the definition of fraction coverage (*f*).

$$f = \frac{\sum bins}{P_{max}}$$

(Eq. 6)

$\sum$**bins** are the number bins occupied by peaks and P_{max} is the total peak capacity obtained as the sum of all bins. Following, three scenarios are illustrated. In the first scenario (**Figure 2A**),

the selectivity of both dimensions is identical and therefore the correlation maximized, which results in a lining up of all sample components along the diagonal (*f*=0.1). **Figure 2B** illustrates the ideal 2D-LC separation, where there is no correlation between the dimensions (f=1) but is nevertheless unrealistic. **Figure 2C** represents a random data set (f=0.63), which is more realistic. Gilar et. al concluded that in real LCxLC separations, *f* is unlikely to exceed 0.63 [88]. Therefore, according to the above principles, 2D-LC orthogonality (*O*) can be calculated according to **(Eq.** *7*.

$$O = \frac{\sum bins - \sqrt{P_{max}}}{0.63 P_{max}}$$

(Eq. 7)

Following, orthogonality ranges between 0 and 1 and is expressed as a percentage value. This approach was confirmed by Watson et al. [95] with an exception to separations characterized by a low peak capacity, where 63% surface coverage is not sufficient to achieve ideal orthogonal separations. At low peak capacities, the bin count reduces and bin size increases, thus surface coverage is inherently high.

The variety of approaches to determine orthogonality are highly complicated and complicate the comparability and interpretation of the results of 2D separations amongst different research groups. Therefore, their use as a metric measure to compare 2D-LC results between researchers often leads to overrated results [96], and is yet a problem that has to be further dealt with by the community.

1.3.2 2D-LC instrumentation and modes of operation

2D-LC can be implemented either offline or online. In offline 2D-LC the sample collection and analysis steps between the dimensions are independent. The peak capacity is higher, since more time is devoted to prepare and separate the collected fractions in the second dimension. In online 2D-LC the sample collection depends on the speed of the second dimension, and considerable effort has been devoted to enhance the storage capability of fractions during modulation (details will be discussed below). The latter therefore delivers a lower peak capacity in comparison, but the separation is substantially faster (days vs. hours). In the following, 2D-LC will not refer to offline, but to online 2D-LC. Online 2D-LC is normally used in two distinct modes of operation: Heart-cutting (LC-LC) and full comprehensive (LCxLC) mode, whereas instrumental modifications of both allow intermediate modes: multiple heart-cutting (mLC-LC) and selective comprehensive (sLCxLC) mode.

The choice between full comprehensive (LCxLC) and standard heart-cutting (LC-LC) 2D-LC is based on the quantity of effluent/fractions desired to be transferred to the ^{2}D. The former

allows the entirety and the latter only singular fractions to be transferred to the ^{2}D. Both require only two symmetrical loops, where one is filled with effluent, while the other is used as a flow path for analysis, and vice versa (**Figure 3**). For LCxLC in particular the ^{2}D is highly burdened in terms of speed, since the analysis of the content of one loop and the filling of the other must be completed simultaneously (one cycle) [96-99]. Thus, both dimensions are directly dependent (sampling time must be equal to the ^{2}D cycle time). For LC-LC the valve setup is the same, however the above-mentioned constraints are relaxed, since only a few fractions are transferred. Nevertheless, one fraction has to be fully analyzed in the ^{2}D, before the valve can switch to collect a second one.
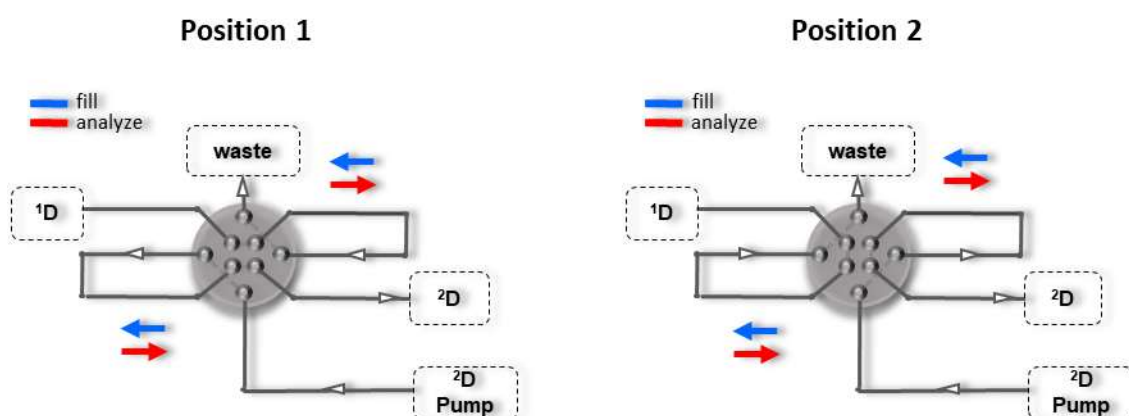

Figure 3: Valve (2-position/4-port) design for LC-LC and LCxLC, equipped with two sampling loops.

Once the sampling time is defined by the maximum allowable speed of the ^{2}D, any change in the ^{1}D flow rate (^{1}F) results in a change in the sample volume transferred to the ^{2}D column. This constraint usually limits the ^{1}F to be lower than optimum in order to avoid sample loss due to overfilling of the loop or flooding the ^{2}D column with a large injection volume. An option to relax this constraint is the utilization of flow splitting after the ^{1}D column [100], which allows the ^{1}F to be optimized independently. Therefore, an improved usage of the ^{1}D separation space can be obtained and unmodified (e.g. validated) 1D methods can be used for the ^{1}D.

The intermediate 2D-LC modes sLCxLC and mLC-LC require the loops to be exchanged with loop decks (**Figure 4**) for the temporary storage of multiple consecutive or distinct fractions, respectively, of ^{1}D effluent. Therefore, specific regions of ^{1}D effluent may be analyzed without restrictions in the second dimension [101, 102].
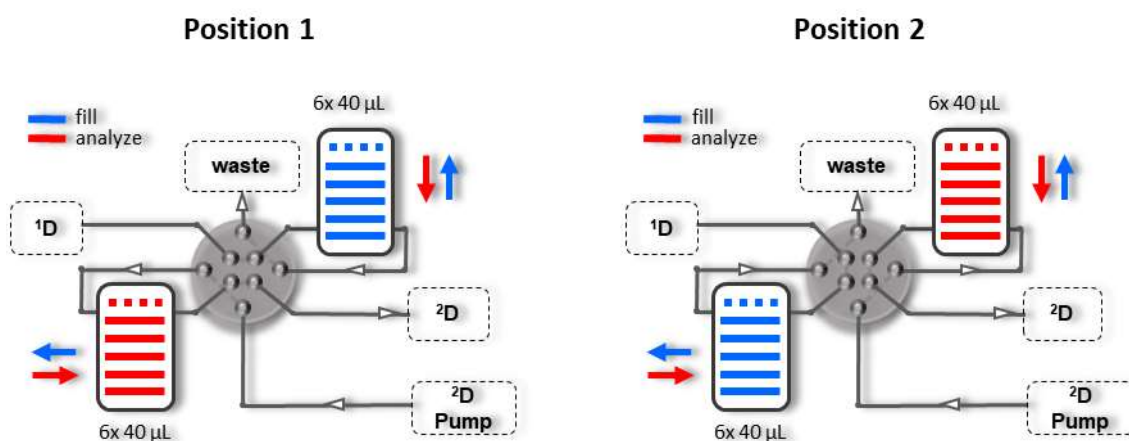
Figure 4: Two sampling loop decks (6-position/14-port valve heads, 6 x 40 μL loops) complementing the main valve (5-position/10-port) for mLC-LC and sLCxLC.

The use of peak parking loop decks and the availability of storing multiple cuts during the modulation process is based on an algorithm for filling and analysing the stored cuts according to certain principles. First, a sampled cut is analyzed as soon as possible as long as the ^{2}D is not occupied. However, if the ^{2}D is occupied, subsequent cuts will be stored in a consecutive manner in the loops of the decks. If all loops are filled, the peak is lost. During analysis, the loop deck is emptied entirely in the reversed order and a flush gradient is run before switching to the next loop deck to avoid contamination.

In normal peak parking mode (only option for sLCxLC), the loop deck is filled entirely before emptying. In the case of mLC-LC, however, smart peak parking mode is possible, which utilizes an algorithm that tries to maximize the number of parked cuts, while minimizing the total runtime (maximum efficiency). In order to satisfy these conditions, the decks are not necessarily filled entirely. In both modes, the peak sampling process is either time based or peak based.

In general, when developing any 2D-LC method, irrespective of the separation mode, much care to detail has to be taken. These include the undersampling problem [103], the usage of 2D separation space, consideration towards sample dimensionalities [77], and detection sensitivity, just to name a few [101, 102]. A special obstacle posed on any online 2D-LC method when fractions are directly transferred from one dimension to the other are mobile phase incompatibilities (modifier, pH and additives), that in worst case scenarios produce peak splitting or breakthrough [104]. One solution, which was utilized in the following work to compensate for possible incompatibilities, at least to a certain extent, is a valve-based approach termed active solvent modulation (ASM) [76] and will be explained to in the following chapter.

1.3.3 Active Solvent Modulation

Sample dilution occurs during both chromatographic dimensions. The dilution process is compounded relative to the starting concentration of the sample during injection, which results in loss of detection sensitivity at the end of the ^{2}D compared to 1D separations. In order to address this negative aspect of 2D separations, the analyte bands eluting from the ^{1}D should be re-focused on the column head of the ^{2}D column. Three options have been described. First, the use of more retentive columns in the ^{2}D. Second, the use of trapping cartridges or columns as part of the interface between the dimensions (SPAM). And third, by transiently weakening the ^{1}D effluent, which becomes the sample solvent during injection into the ^{2}D column (e.g. weak water-rich ^{2}D mobile phase in the case of RP separation). The latter is a valve-based approach termed active solvent modulation (ASM) [76, 105] and is depicted in **Figure 5**. The resulting peak focussing effect compensates the large dilution caused by the increased injection volume (depending on the ASM factor) and eliminates peak shape problems as well as breakthrough of early eluted sample components.
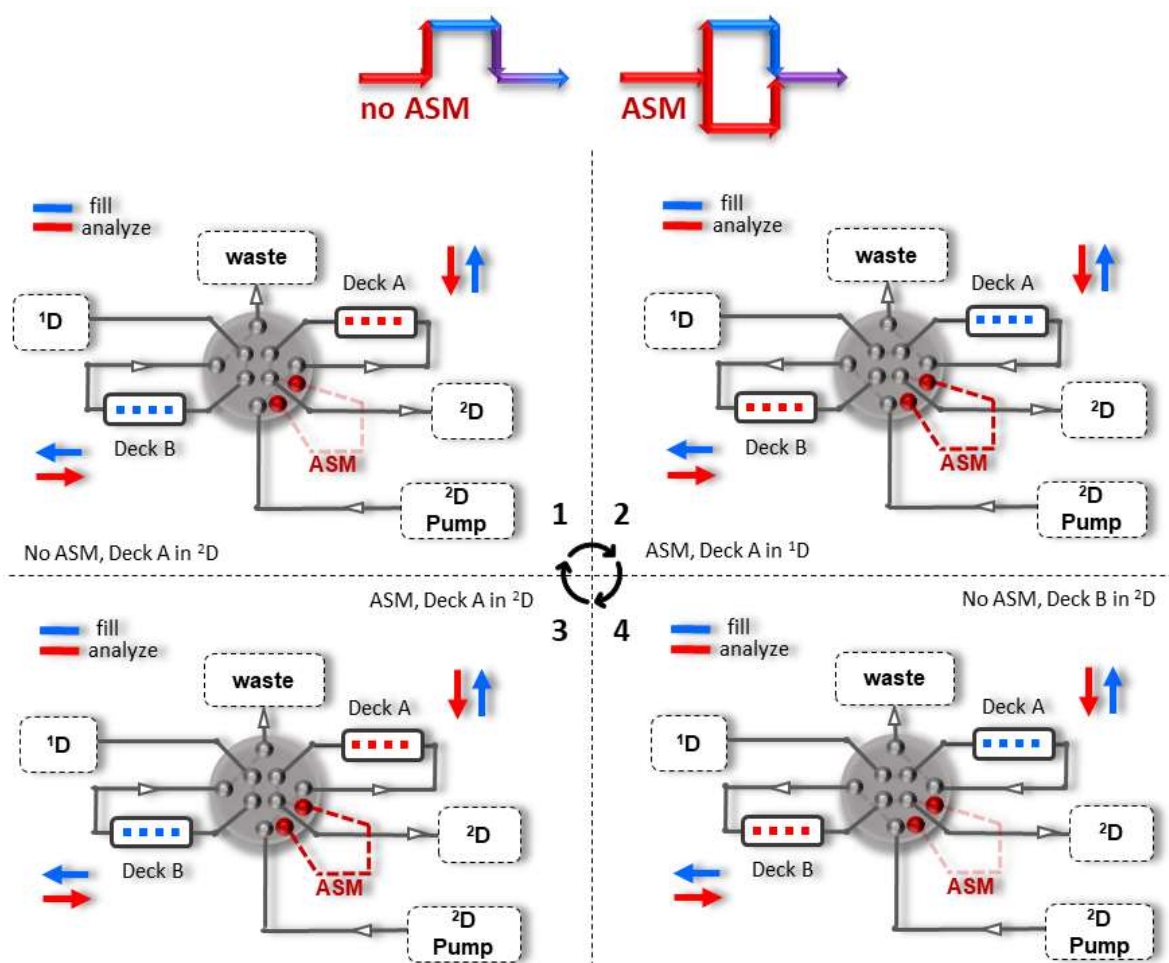

Figure 5: Above: The dilution principle with and without ASM. Below: ASM valve (5-position/10-port) positions during active solvent modulation.

1.3.4 Practical considerations

A number of physical parameters should be considered, before implementing a new 2D-LC method. Instrumental parameters and respective recommendations are summarized in **Table 2**.

Table 2: Practical considerations of physical parameters for the establishment of a 2D-LC method.

^{1}D	Column Length [mm]	A long ^{1}column (100-250 mm) should be selected to provide high efficiencies and allow for separation of a majority of the sample components.
	Inner Diameter [mm]	Thin inner diameters (1.0 - 2.1 mm) should be selected to provide a suitably slow flow for a favorable sampling frequency and selected loop size.
	Particle Size [µm]	Fast separations ($t_0 \leq 1$ min) require N ≤ 25,000 and sub-2µm or sub-3µm core shell particles are most favorable (limited by maximum pressure). Difficult long separations ($t_0 \geq 10$ min) require high efficiencies (N ≥ 100 000), and benefit from relatively large particle diameters (≥5 µm) [101].
	Flow rate [mL/min]	The flow rate influences the ^{2}D cycle time directly.
	Linear velocity [mm/s]	Should be kept constant for method transfer (e.g. for column screening).
	Dwell Volume ^{1}V$_D$ [µL]	Should always be determined and reported to define the gradient delay, which is necessary for method transfers between instruments.
	Peak width at 8σ [min]	Necessary to adjust the ^{2}D sampling rate, since 4 cuts per 8σ peak width are recommended to avoid undersampling.
	t_R [min]	For the calculation of the separation efficiency.
	Efficiency N	Peak capacity in gradient elution.
	^{1}z (split ratio)	Flow splitting should be considered in order to maintain optimum conditions for the ^{1}D, while relaxing the constraints set upon the ^{2}D, else a compromise between ^{1}D peak capacity, instrument specifications regarding ^{1}F and ^{2}D sampling rate. The split should

14			be placed prior detection to avail a real-time reference chromatogram for sampling and maintaining the transfer capillary volume. [100, 106].
	^{2}D	2D-LC Mode	The choice between LC-LC, mLC-LC, LCxLC and sLCxLC determines the separation speed necessary in the ^{2}D.
		Loop setup	Ideally operated in a countercurrent (first-in-last-out) modulator configuration for reduced modulation asymmetry [107].
		Column Length [mm]	The ^{2}D column should be relatively short (50 mm or less), to allow fast separations. In gradient separations, short columns allow high volume ratios (t_G/t_0 = duration of gradient/column dead time), while maintaining short cycle times and reducing the time needed for re-equilibration [101].
		Inner Diameter [mm]	Should be chosen wide to increase $^2V_0$ and therefore minimize the negative effects of transferring large volumes.
		Particle Size [µm]	As small as possible to produce high peak capacities, but is compromised by the maximum possible operating pressure and required separation speed.
		Flow rate [mL/min]	The ^{2}D-flow-rate should be fixed in such a way that the maximum allowable pressure can be reached, since very fast separations are desired [108].
		Linear velocity [mm/s]	Should be kept constant during method transfer or for column screening.
		Injection Volume [µL]	Large injection volumes improve detection sensitivity, but can be detrimental (e.g. solvent mismatch, column overload) to the ^{2}D separation. Analyte focusing conditions (e.g. ASM) can ameliorate the disadvantageous situations [109].
		Dwell Volume ^2V_D [µL]	See Dwell Volume ^1V_D.
		Percentage of $^2V_0$ [%]	Below 15 % of the column dead volume should be injected into the column to limit injection band-broadening effects [24] and below 10 %, to avoid zones of mismatch (e.g. pH) inside the LC column [110].

Diameter ratio ($^2d_c/^1d_c$)	Pareto-optimality results show that highest peak capacity is achieved with $^2d_c/^1d_c$ between 7 and 4. High values of $^2d_c/^1d_c$ benefit the total peak capacity, however have a detrimental effect on dilution [101]. Also, increasing the flow-rate ratio $^2F/^1F$ (by increasing $^2d_c/^1d_c$) reduces band broadening caused by injection [111].
Modulation time [s]	For LCxLC applications, the ^2D modulation time is 0.15 $\sqrt{^1N}$ (e.g. 20 s for ^1N = 1000) and 0.5 $\sqrt{^1N}$ if important peaks elute at t_0, while for mLC-LC, LC-LC and sLCxLC constraints on the overall cycle time are relaxed [101, 112]. Loop size [µL] and filling [%] should be used to adjust the modulation time.
Re-equilibration time [min]	For RP-LC, 2-10 x V_0 is recommended (V_D should be considered). For HILIC and chiral separation the re-equilibration time should be deduced empirically (t_R reproducibility). Full re-equilibration might not be necessary [113]. If possible, ^2F should be increased (same for ^1F) to accelerate re-equilibration.
Gradient time t_G [min]	The gradient time and re-equilibration time should be maximized and minimized, respectively. Both contribute to the modulation time (critical for LCxLC applications).
Sampling rate [cuts/peak]	A sampling rate of 4 cuts per 8σ peak width is recommended to avoid undersampling conditions (Section 1.3.1) [102].
Loop size [µL]	Various loop sizes are available (typically 40, 60 and 100 µL).
Loop filling [%]	The loop volume should be twice the modulation volume, due to the parabolic flow profile (Hagen-Poiseuille flow), resulting from friction with the inner surface of the column [101].
Dilution factor [D_F]	The dilution factor for each dimension is the ratio of analyte concentration at injection and detection [101]. It is largely influenced by dispersion in the ^1D and the ^2D, as well as extra column peak broadening effects, which can be reduced by peak focusing, e.g. by the use of ASM or SPAM [108].

Not all parameters can be held at optimum and, since many of them interact, compromises have to be made. Physico-chemical properties, however, influencing orthogonality (choice of

stationary and mobile phase) and the use of active solvent modulation should be considered in regard to a specific application.

1.4 Detection

The chromatographic separation of analytical samples is accompanied, as a matter of course, with hyphenated detection. The choice of the detector is very much analyte dependent, although a universal detector is highly sought for [114]. An ideal detector is highly sensitive with a correlated (linear or predictable) response to all analytes, independent on the immediate environment (temperature, flow, mobile phase properties), does not produce extra-column peak broadening [24]. However, not a single detector is ideal, which is why complementary detector systems are often necessary [87, 115]. The following detectors have been used in this work to augment each other for the detection of various peptide and related analytes.

1.4.1 UV and fluorescence detectors

The most widely hyphenated detector is the ultra violet (UV) detector introduced by Hovarth and Lipsky in 1966 [116], and nowadays available as variable wavelength (VWD) and diode array (DAD) detectors. With a wide linear range, both minor impurities and APIs are accessible. The compatibility with non-volatile (phosphate) and ion-supressing (TFA) buffer systems and solvent gradients is highly appreciated in reversed-phase peptide analysis. The use of a DAD further allows the acquisition of UV spectra across a chromatogram, which in specific cases allows spectral discrimination of two otherwise co-eluting substances, provided they have different absorbance maxima. Minor differences of peak spectra allow analysis for peak impurities below 1% [117].

Fluorescence detectors (FLD) measure the fluorescence of UV excited analytes, which results in a highly selective and sensitive detector. For many analytes, the sensitivity is 100-fold higher than for UV absorption. Highly fluorescent amino acid derivatization products are accessible with OPA (λ_{Ex}: 348, λ_{Em}: 450, LOD: < 1 pmol), FMOC-Cl (λ_{Ex}: 260, λ_{Em}: 313, LOD: low fmol), NBD-F (λ_{Ex}: 480, λ_{Em}: 530, LOD: ~ 10 fmol) and AQC (λ_{Ex}: 250, λ_{Em}: 395, LOD: 40-320 fmol) [118, 119]. Due to the superior selectivity, this technique is less sensitive to instrument (temperature and flow) and mobile phase (additives, modifier, gradient) alterations [24].

1.4.2 Charged Aerosol Detection

Some chromatographic applications require more selective detectors, while other prefer more universal detection. Charged aerosol detection (CAD) is an evaporative mass sensitive technique that offers universal detection of non-volatile and many semi-volatile analytes [114, 120-122].

The response is largely uniform regardless of molecular weight and structure, which again is related to mass and not chromophoric or fluorophoric properties of the analyte, nor the ability to be ionized, which translates into a complementary response compared to UV, FLD and mass spectrometry. In consequence, quantitative and sensitive detection of analytes, that may pass undetected using UV/VIS (e.g. free AAs salts and counterions (e.g. Cl$^-$) become feasible. Most importantly, it provides a good estimate of the amount of e.g. unknown peptide impurities and degradation products or compounds where calibration standards are not available. In order to calibrate over a high dynamic range (e.g. for impurity analysis) a logarithmic function can be used to calculate the response. The dynamic range is specified over four orders of magnitude from a single injection (mid-pg to µg quantities on column).
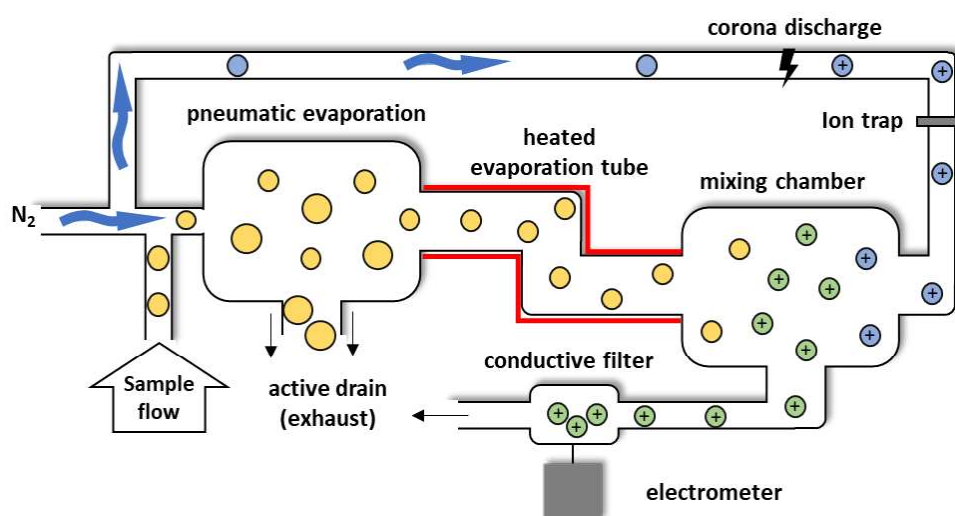

Figure 6: The operating principle of the charged aerosol detector (Corona Veo RS) [37].

The evaporation mechanism of the CAD (parabolic response) can be compared to ELSD (sigmoidal response) [123]. However, the prior is superior in terms of sensitivity, dynamic range (a parabolic response curve occupies a broader linear range than a sigmoidal one) and response uniformity. The operating mechanism (**Figure 6**) begins by nebulizing the LC eluent using a fraction (N$_2$ split) of the concentric nitrogen flow following through a drift tube, in which the solvent droplets are selected (heavy droplets are drained to the waste) and evaporated to dryness in the heated evaporation tube. Inside the mixing chamber, the other fraction of nitrogen stream, priorly charged by a high-voltage platinum wire (corona discharge) is introduced from the opposite direction, in order to transfer charge to the dried particle stream (note, the charge is retained on the surface of the particles without molecular ionization). Highly mobile charged particles are removed by a conductive filter and the remaining charged particles are finally detected by a sensitive electrometer. (Note, the ELSD on the other hand directs the stream through a detection cell and creates a signal proportional to the number of

photons scattered from the residual solid fraction [124].) The amount of charge is porportional to the area of the analyte particle, which is proportional to the injected mass and therefore the quantity of the analyte. When combining LC in gradient conditions with CAD, the evaporation process and response becomes dependent on the mobile phase composition at the particular position of the gradient. In this case a post-column inverse gradient should be considered in order to keep the mobile phase composition uniform at all time, which allows comparability of responses along the gradient [36, 37].

1.4.3 Mass spectrometry

1.4.3.1 Electrospray Ionization

The hyphenation of a chromatographic system to a mass spectrometer relies on the transfer of the ions from a liquid into a gaseous state, which is achieved by an ionization interface usually applied under atmospheric pressure. Amongst atmospheric pressure ionization techniques, electrospray ionization (ESI) stands out as the most popular one, next to APCI (atmospheric pressure chemical ionization) and APPI (atmospheric pressure photoionization). ESI is a soft ionization particularly useful to analyze large, easily ionizable non-volatiles like peptides and proteins [125].
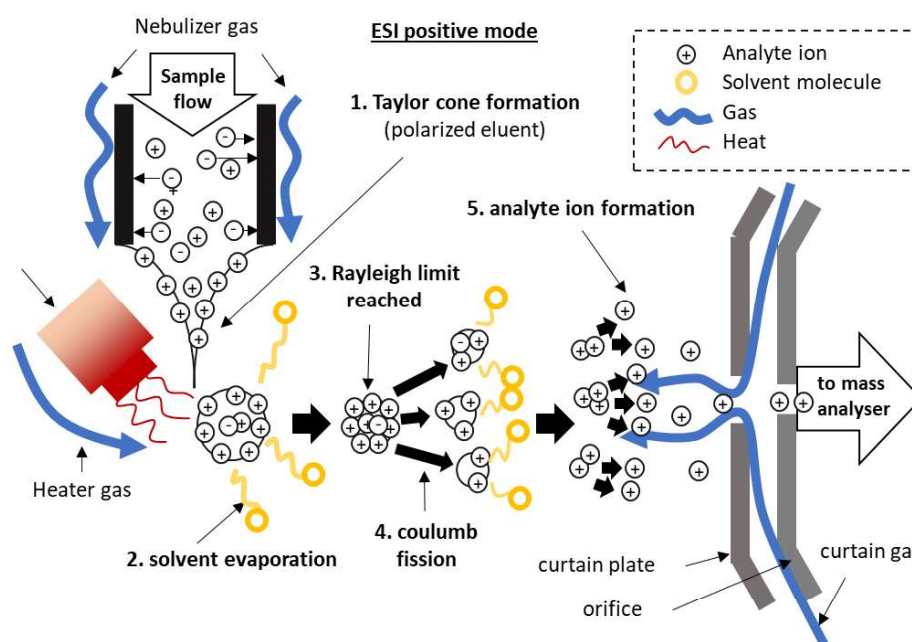

Figure 7: The working principle of electrospray ionization [126].

The first ESI interface was introduced by Fenn et al. in the 1980's [127, 128] and has since made several advancements. In principle, the ESI process (see Figure 7) can be described in three stages: (i) the formation of a charged aerosol by applying a strong electric field (3-6 kV [126]) to the liquid passing through a transfer capillary (ESI needle), (ii) the heat assisted

reduction of the droplet size by solvent evaporation and (iii) the release of the desolvated ions through Coulomb explosion [129].

At the needle tip, the electric field forces the separation of analytes according to their charge (polarization) within the solution, which results in the formation of the Taylor cone [130-132]. Highly charged droplets begin to disintegrate from the tip when the surface tension is surpassed by the electrostatic forces directing them toward the counter electrode. To further reduce the influence by surface tension of the solvent, the spray is pneumatically assisted by the concentrically enveloping nebulizer gas [126, 133]. The expanding aerosol is simultaneously subjected to a heated desolvation gas (inert, e.g. N_2) for thermally assisted solvent evaporation, resulting in a shrinkage of the droplets while the charge per unit volume increases. Once the Rayleigh-Limit [134] is reached, the droplets disintegrate (Coulomb fission) into smaller ones in a continuous repetitive process until fully desolvated ions are released [135]. The disintegration of the droplets may also occur before the Rayleigh limit because the strong electric field elongates the droplets to produce a new Taylor cone, which releases smaller droplets [136]. However, the released analyte ions are then directed through the curtain plate and orifice into the mass analyzer. The declustering potential (DP) is a voltage applied to the orifice in order to extract analyte ions from the spray and is especially used to reduce solvent clusters (or adducts) by regulating their collision with residual gas molecules. Further, a curtain gas is used to shield the ion path from unevaporated solvent droplets or ambient air, and the orthogonal setup between ESI needle and vacuum inlet prevents contamination by non-ionized molecules.

ESI assumes ion formation of analytes that are easily protonated or deprotonated in solution. However, the formation of multiply charged peptide ions has been proposed to occur through proton transfer reactions in the gaseous phase, e.g. from protonated solvent molecules (H_3O^+, NH_4^+ etc.) with lower proton affinity [129, 137]. The protonation occurs on available basic sidechain residues (Arg, Lys, His) until the charge is maximized [138]. Nevertheless, the charged state is still influenced by the solvent type and pH-value and the overall ESI spectrum further by chromatographic flowrate, nebulizer gas flow, heater gas temperature and DP. Solvents that are weakly volatile require increased nebulizer and heater gas setpoints. Volatile acids (e.g. $HCOOH$, CH_3COOH), bases (e.g. NH_4OH) and buffers (e.g. NH_4COOH, CH_3COONH_4) are frequently used to improve the ionization efficiency of analytes. The ionization efficiency can be impaired by ion suppressive (TFA) and non-volatile (phosphate) mobile phase additives, but also by co-eluting compounds that compete for ionization (ion suppression), known as the matrix effect, that may be enantioselective in case of enantiomer

separations, because coeluted interferences may be different for the two enantiomers with distinct retention times.

1.4.3.2 Mass analyzers

1.4.3.2.1 Triple Quadrupole Mass Spectrometry

In a quadrupole mass analyzer, the ions are passed through four perfectly parallel placed hyperbolic metal rods. The opposing rods form pairs of the same electric potential, and using a combination of radio frequency (RF) and direct current (DC) voltages, the trajectories for ions can be influenced. By calculating trajectories, the quadrupole can be set to only transmit ions of a certain *m/z* ratio and work as a mass filter [125].An exact mathematical description of the ion movement stability is given by Mathieu's differential equations (visualized by stability diagrams) [125]. Ion detection occurs by a continuous electron multiplier (CEM) and the electrical signal is converted by an analogue-to-digital converter [125].
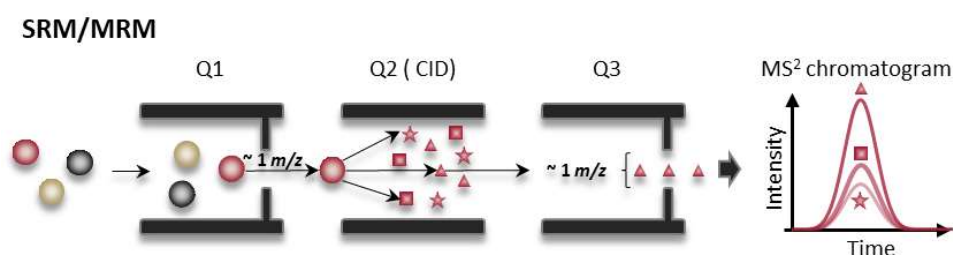

Figure 8: Schematic depiction of a triple quadrupole MS system operated in MRM mode, detecting three transitions from the same precursor. An MS^2 spectrum is obtained in full product ion scan mode.

In a triple quadrupole setup (**Figure 8**), three quadrupoles are used in tandem, where the outer quadrupoles are utilized as analyzers and the centered one for collision induced dissociation (CID). Different modes of operation are possible for the quadrupoles and can be combined for a multitude of experiments. Full scan and multiple ion experiments can be performed using either Q1 or Q3 as the mass filters (**Figure 8**). The benefit of a triple quadrupole however is the ability to filter a precursor ion with Q1, which is dissociated in Q2 to give a product ion that is filtered by Q3. This mode is termed selected or multiple reaction monitoring (SRM/MRM) and is the gold-standard for absolute quantification. If Q1 is operated in selected ion and Q3 in scan mode, or vice versa, then all products of a particular precursor or all precursors of a particular product can be searched in a product ion or precursor ion scan, respectively. In a neutral loss scan Q1 and Q3 are operated in scan mode at a fixed *m/z* difference over a certain mass range to observe a special neutral loss (e.g. loss of certain neutral structural elements, e.g. phosphocholine in phosphatidylcholines [119]).

1.4.3.2.2 Quadrupole Time of Flight Mass analyzer

In the following work a Sciex TripleTOF 5600 system was utilized, where the Q1 and Q2 operate as described above (Chapter 1.4.3.2.1), while Q3 is replaced with a time-of-flight (TOF) mass analyzer (**Figure 9**) adding the advantage of detecting all ions, at high resolution and high mass accuracy.
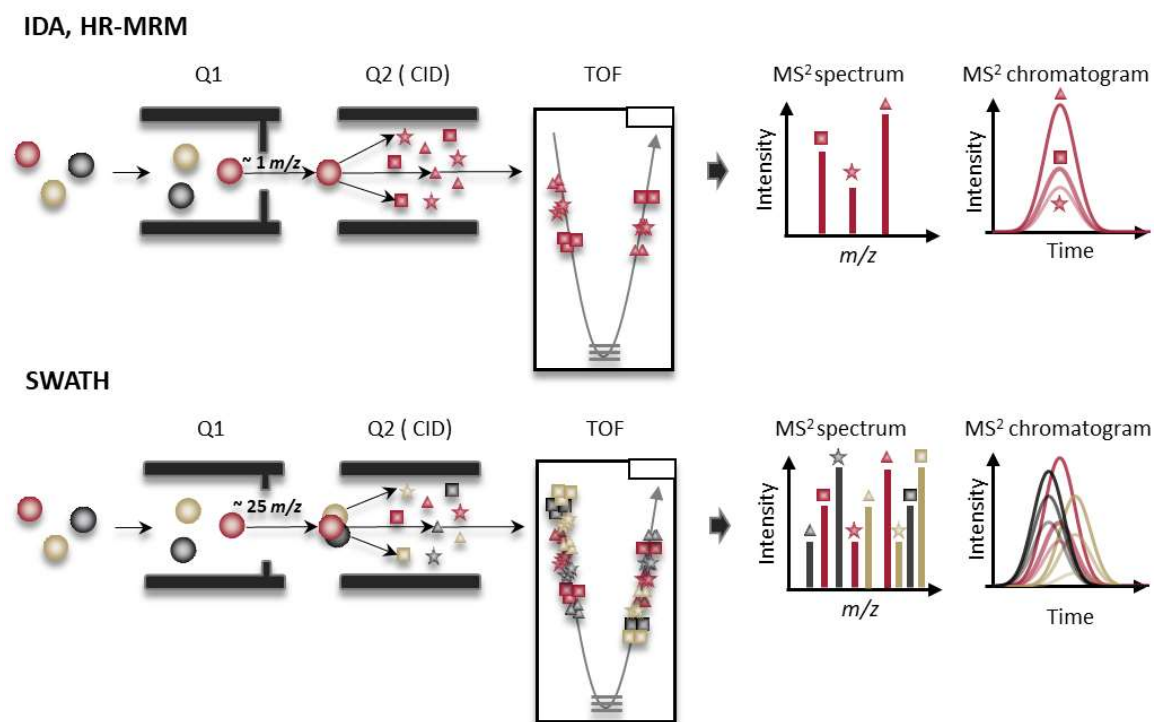

Figure 9: Quadrupole time-of-flight mass analyzer operated in IDA or HR-MRM and SWATH mode.

TOF analyzers are based on the migration of initially accelerated ions along a field free drift tube of defined length. Orthogonal pulsing provides all ions with the same kinetic energy, which then disperse according to their inertia [125, 139]. The light ones traverse the tube faster than the heavy ones. Using the knowledge of E_{kin}, time of flight and tube length, m/z is derived using physical equations. Consequently, the accessible *m/z* range is theoretically limitless. For a continuous ion beam, e.g., generated during hyphenation with chromatography by the Q1 in transmission mode, ion packages are continuously pulsed into the TOF in short intervals.

The simplest form of a TOF analyzer is the linear TOF. Scattering effects due to unequal kinetic energy distribution of identical ions pertain all directions and reduce the overall resolution in longitudinal direction. They are produced by confinements in the ion focusing process at the ion source or by collision with residual gas molecules in the vacuumed drift tube. The distance between the ion source and detector (drift tube length) is limited, which in turn compromises (time-of-flight dependent) resolution. A multi-channel plate equipped with a

time-to-digital converter (TDC, 4-channel 40 GHz) with a maximum time resolution of 25 ps is used to increase the detection sensitivity of scattered ions [125, 139, 140].

Modern TOF analyzers counter spatial ion dispersion by orthogonal acceleration, delayed pulse extraction, and by installing a reflector along the flight path (reTOF) [125]. With delayed pulse extraction, ions are priorly allowed to expand in a field-free zone after the collision cell, before they are extracted by a voltage pulse. In the orthogonal setup, ions which are further away from the detector and closer to the pulser, will receive higher acceleration and will be able to catch up with the ions initially further away from the pulser. Then, by directing the ion beam into a resistive network of ring electrodes (reflector) arranged successively with increasing potential, the ion beam is mirrored, resulting in refocusing of the longitudinally scattered ions [125].

1.4.3.2.2.1 Scan Modes

The central scan mode of the QTOF (Sciex TripleTOF 5600) is the high resolution TOF-MS survey scan or full MS scan, that is predicated on a low collision energy (CE) setting of the CID producing high resolution ($\geq 35000_{fwhm}$ for m/z 956 at a scan rate of 100 Hz [141]) spectra. The resulting accurate masses and isotopic patterns allow accurate estimation of potential sum formulas. Experiments performed on MS^2 level with an elevated CE setting define the scan mode. MS^2 data is optionally acquired in either high resolution ($\geq 25000_{fwhm}$ for m/z 186 at 100 Hz [141]) or high sensitivity ($\geq$3-fold increase, R $\geq 15000_{fwhm}$) mode. The sum of MS^1 and MS^2 experiment accumulation times plus system times (settling time, etc.) define the total cycle time. For a prior chromatographic separation of a sample, the total cycle time represents one data point on the time axis (and one or multiple datapoints on the m/z scale depending on the scan mode) and is therefore restrained by the peak width, which requires a minimum of 10 data points per peak to describe the peak accurately [142]. Accumulation time is very limited resource for 2D-LC experiments, where peak widths can be very narrow (e.g. 2-4s), due to very fast ^{2}D's. In contrast, dwell times should be increased for increased S/N and thus sensitivity for low abundant analytes. The scan types are generally divided into two distinct modes: data dependent (e.g. IDA and MRM-HR) and data independent acquisition (SWATH).

1.4.3.2.2.1.1 DDA - Data Dependent Acquisition

In a specific DDA mode termed IDA (Information Dependent Acquisition) by the manufacturer, a dynamic product ion scan (MS^2) is performed depending on the precursor ions (MS^1) detected by the full scan, which avails information about the compound fragmentation (**Figure 10B**) in an untargeted manner. The most abundant ions (user specified threshold) and CE (user-defined or automatic with collision energy spread or for peptides rolling collision which is based on charge state) are computed on the fly to trigger an instantaneous fragmentation

by adjusting the Q1 transmission window (*m/z* 0.5 – 1, typically *m/z* 0.7) in a subsequent MS^2 experiment (**Figure 10C-D**). IDA methods can be customized with an inclusion list for critical expected analytes (targeted) or an exclusion list for common undesired impurities. In conjunction with 2D-LC, data dependent MS methods are preferably combined with data dependent 2D-LC methods (**Figure 10A**), namely LC-LC and mLC-LC (Chapter 1.3.2).

By monitoring the fragmentation of only a few ions at a time span around their elution, it is possible to reduce the cycle time at optimized accumulation times, which is beneficial for fast chromatography [143] (e.g. 2D-LC). In scheduled HR-MRM, the targeted precursor ion list is augmented by the expected analyte retention time, availing their full fragmentation data at high resolution and mass accuracy [142, 144, 145]. Alternatively, static TOF-MS and product ion scan experiments (non-scheduled MRM) can be arranged within certain time periods to fragment only specified precursors eluting within predefined chromatographic windows. Source- and compound dependent parameters can be set independently for each period.

A simple but highly selective untargeted IDA experiment is restricted to peak integration on MS^1 level, since MS^2 spectra are not comprehensively triggered across the peaks to achieve sufficient data points. In contrast, scheduled and non-scheduled MRM both fully leverage the high-resolution data for pre-defined targets by enabling post-acquisition XICs generated on MS^2 level (**Figure 10E**). Further optional scan types involving IDA are neutral-loss-triggered IDA and mass-defect-triggered IDA [141], but they are of minor interest in this work.

1.4.3.2.2.1.2 DIA - Data Independent Acquisition

In DIA all ions are fragmented without preselection, resulting in a comprehensive approach. The QTOF system performs sequential window acquisition of all theoretical fragment ion spectra (SWATH) [146-150], where overlapping (1 Da) Q1 isolation windows are arranged stepwise to variable sizes (e.g. 25 Da) for sequential fragmentation to cover a broad range of ions (**Figure 10G**) [151]. The overlapping compensates the reduced transmission efficiency of the Q1 during window switching, in order to avoid precursor ion loss. Following, the resulting MS^2 spectra is a mixture of fragmented precursor ions of intermediate complexity (**Figure 10H-I**), that can be deconvoluted by matching precursor and product ion retention time (**Figure 10J**) [152]. For perfectly co-eluting peaks, smaller precursor isolation windows can be chosen for the *m/z* range of interest, which is however semi-targeted.

Comprehensive product ion analysis is ideally matched with comprehensive 2D-LC (sLCxLC and LCxLC) approaches (**Figure 10F**). Although the QTOF offers very high scan rates (100 Hz), the acquisition speed for stepping through all windows within reasonable cycle times in order to satisfy the speed of the ^{2}D remains challenging. However, fully comprehensive 2D-LC-QTOF approaches represent new area of endeavor and will likely require future

advancements in instrumentation, especially regarding data acquisition speed. Nevertheless, the produced untargeted data is both qualitative and quantitative on MS^1 and MS^2 level and ultimately open for retrospective targeted analysis.
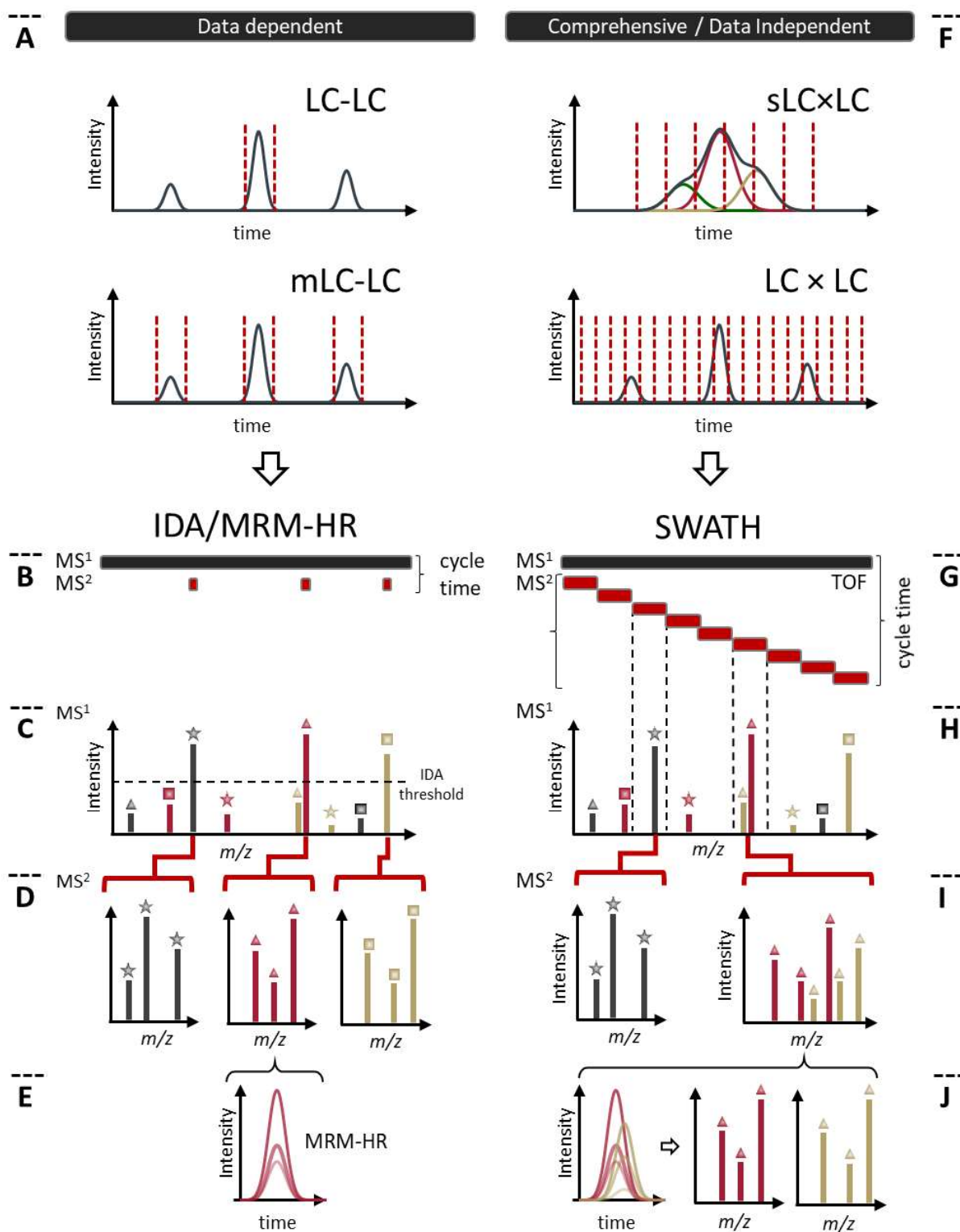

Figure 10: Data-dependent (LC-LC and mLC-LC) and data independent (sLC×LC, LC×LC) 2D-LC methods are hyphenated to data dependent and data independent MS (comprehensive, SWATH) methods, respectively.

1.5 Decision flow for peptide analysis

When a request for the analysis of a peptide is made, the following decision flow chart incorporating the above described platform methods is suggested (**Figure 11**). The first step is to control the purity by 1D-LC generic validated methods using different stationary phases (RPLC, Zwix(+/-), HILIC) and involving both UV and MS/MS (IDA, SWATH) detection (with respect to mobile phase compatibilities (non-volatile and ion suppressive additives) with ESI (Chapter 1.4.3.1). If the exact mass matches the target peptide, the peptide backbone should be sequenced (and if the structure is cyclic, an aliquot should be linearized for LC-MS/MS analysis to assure a complete sequencing), otherwise correctness of the sample should be verified [10].

In order to control the presence of API related co-eluting impurities (e.g. deamidation), a sLC×LC-MS/MS (SWATH) method (sRP×RP, sRP×HILIC, sRP×ZWIX(+/-)) should be deployed, where the generic ^{1}D conditions (0.1 % TFA) are maintained [87]. Alternatively, this method can be performed as the first step, since it provides the same 1D-UV information and additional (correlational) information with MS detection after the ^{2}D. If the degree of impurity is severely high, a preparative (analytical scale) step should be included using the most selective column. If the peptide sample is expected to contain a fatty acid sidechain (e.g. 3-hydroxy fatty acid), length and stereochemistry should be determined [14].

As the next step towards chiral impurity analysis or structure elucidation, a full amino acid analysis should be performed (bottom up approach). A high-throughput rapid enantioselective amino acid analysis (ReAAA) method was developed to provide a complete enantiomer resolved profile of all proteinogenic AAs (AQC derivatized) within 2.5 min, utilizing core-shell technology in a tandem column (QN-AX→ZWIX(+)) approach [15]. An AQC derivatized, racemized and characterized IS (^{13}C-^{15}N DL-AA mix) should be utilized, in order to obtain quantitative results and avoid enantioselective matrix effects [39, 50, 153].

Non-proteinogenic amino acids are commonly incorporated in non-ribosomal synthesized peptides (Chapter 1.1), including the isobars of Leu/Ile (Tle, Nle, alle) and Thr (Hse, aThr), that require full chromatographic resolution prior mass detection. So far, to our knowledge, no such ^{1}D method has been described. However, to tackle the issue, a mRP-QN-AX→ZWIX(+)-UV-FLD-ESI-QTOF-MS/MS method was developed [16]. For unknown peptide samples containing uncommon non-isobaric amino acids a comprehensive RP×QN-AX→ZWIX(+)-ESI-SWATH is envisioned. If the full AA profile, D/L ratio and sequence connectivity is obtained, the peptide can be verified as the last step.
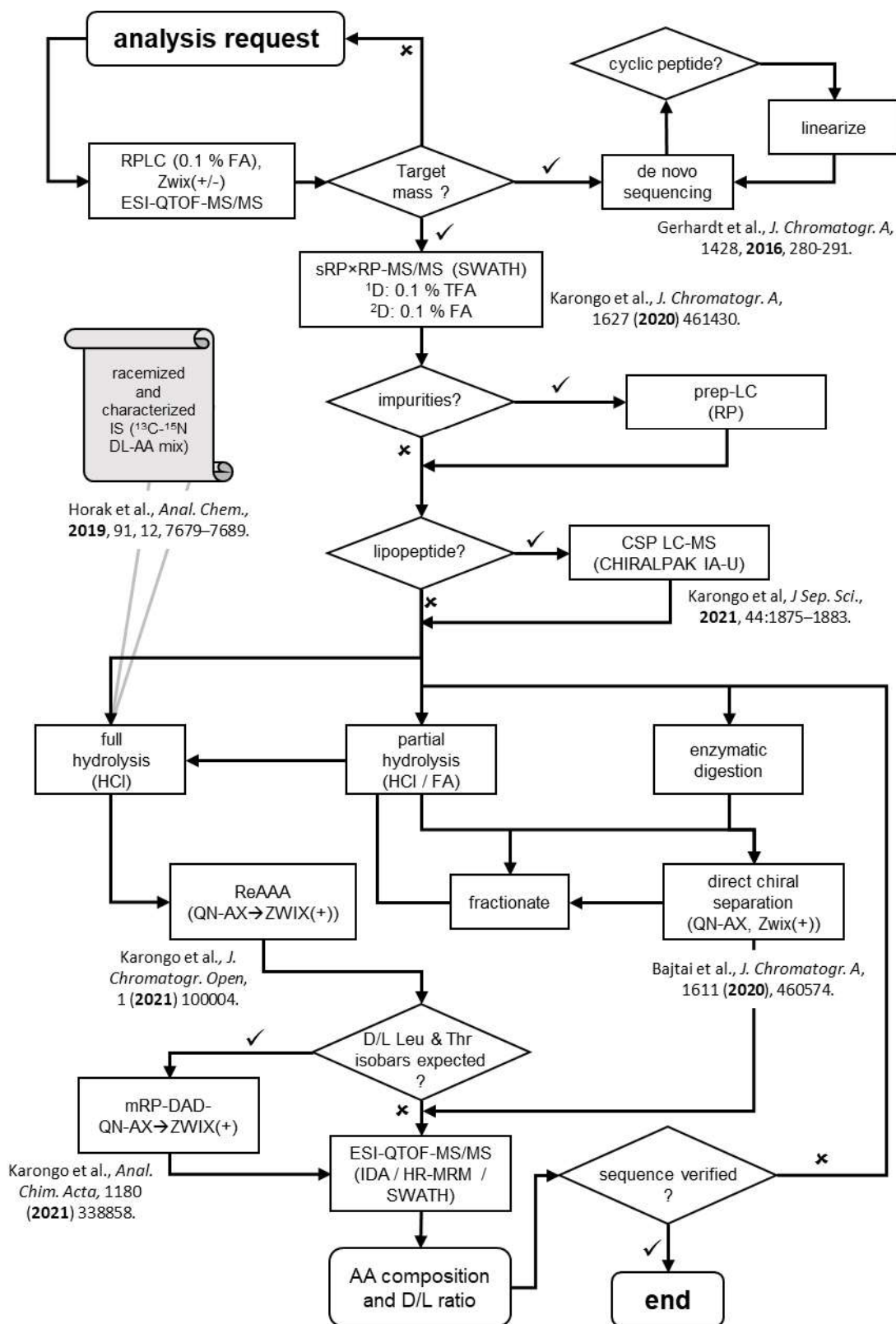
Figure 11: Decision flow chart for peptide analysis.

If the full peptide sequence cannot be obtained, alternative methods to verify the sequence should be considered. For example, since a full hydrolysis retains no information regarding the AA connectivity, situations can arise where di-, tri- or even oligopeptide building blocks

contain the same amino acids more than once in the peptide chain, but differing in stereochemistry. In that case, the assignment of D- and L-AAs to the respective building blocks is not possible. But, on a di-, tri-, or even oligopeptide level, if the CSP is selective enough [67, 70, 154]. These higher-level building blocks can be obtained by partial chemical hydrolysis (thermal or microwave assisted) or enzymatic digestion [10, 155]. For enzymatic digestion, immobilized enzyme reactors (IMER) could be incorporated in an online 2D/3D-LC setup [155-158]. As a result, the resolution of all isomers (LL-, DL-, LD- and DD-dipeptides) should be achieved and the full sequence verified. Enhanced detection methods should be included whenever possible (e.g. DAD, FLD, CAD, ESI-QTOF-MS/MS) and if necessary by spitting the flow.

1.6 Concluding Remarks and Outlook

The aim of the following work was to develop one- and multidimensional methods for the quality control of peptide APIs, comprising the elucidation of minor (< 0.1 %) peptide related impurities, the assessment of the stereointegrity (often not accessible by routine methods) on an intact (top down) and amino acid (bottom up) level and the utilization of these tools for the structure elucidation/verification of unknown peptides. The implemented strategies employ complementary phases (reversed phase, HILIC, chiral) and multiple detection (UV, FLD, CAD, MS) techniques.

- First, a Selective comprehensive 2D-LC (sRP×RP) to enhance generic 1D methods, in order to elucidate peptide related impurities. Orthogonal selectivity was achieved by maintaining acidic and basic conditions in the first and second dimension, respectively, in conjunction with multiple detection comprising a DAD in-line with a CAD, and a QTOF mass spectrometer with an electrospray ESI source [87].

- Second, a rapid enantioselective amino acid analysis (ReAAA) method for high throughput (2.5 min) analysis of proteinogenic AAs employing SPP (core-shell) particles [15].

- Third, a multiple-heart-cutting 2D-LC (mRP-chiral) fully automated platform method combining the chemoselectivity of reversed phase with the enantioselectivity of chiral ion exchangers in a targeted manner for all proteinogenic AAs considering the presence of the often interfering isobars of Leucine (Isoleucine, *allo*-Isoleucine, *tert*-Leucine, Norleucine) and Threonine (allo-Threonine, Homoserine) [16].

- Fourth, a direct enantioselective method for 3-hydroxy alkanoic acids originating from non-ribosomal lipopeptides, by an amylose tris(3,5-dimethylphenyl carbamate) based polysaccharide chiral selector, under generic ESI-MS compatible RP-UHPLC gradient elution conditions, was developed [14].

In the future, we envision a full comprehensive untargeted 2D-LC (RP×chrial) assay for the analysis of peptides containing uncommon or unknown AA, that further enables the quantification of AAs transferred into the ^{2}D. And a direct enantioselective dipeptide analysis method, that partially maintains the AA connectivity, for the localization of stereoconfigurational assignments of repeated AAs within a peptide sequence.

1.7 References

[1] T. Uhlig, T. Kyprianou, F.G. Martinelli, C.A. Oppici, D. Heiligers, D. Hills, X.R. Calvo, P. Verhaert, The emergence of peptides in the pharmaceutical business: From exploration to exploitation, *EuPA Open Proteomics* 4 (**2014**) 58-69.

[2] A.A. Zompra, A.S. Galanis, O. Werbitzky, F. Albericio, Manufacturing peptides as active pharmaceutical ingredients, *Future Medicinal Chemistry* 1(2) (**2009**) 361-377.

[3] M. D'Hondt, N. Bracke, L. Taevernier, B. Gevaert, F. Verbeke, E. Wynendaele, B. De Spiegeleer, Related impurities in peptide medicines, *J Pharm Biomed Anal* 101 (**2014**) 2-30.

[4] J.L. Lau, M.K. Dunn, Therapeutic peptides: Historical perspectives, current development trends, and future directions, *Biorg Med Chem* 26(10) (**2018**) 2700-2707.

[5] R.B. Merrifield, Solid Phase Peptide Synthesis. I. The Synthesis of a Tetrapeptide, *JACS* 85(14) (**1963**) 2149-2154.

[6] V. Vergote, C. Burvenich, C. Van de Wiele, B. De Spiegeleer, Quality specifications for peptide drugs: a regulatory-pharmaceutical approach, *J Pept Sci* 15(11) (**2009**) 697-710.

[7] A. Henninot, J.C. Collins, J.M. Nuss, The Current State of Peptide Drug Discovery: Back to the Future?, *J Med Chem* 61(4) (**2018**) 1382-1414.

[8] M. Erak, K. Bellmann-Sickert, S. Els-Heindl, A.G. Beck-Sickinger, Peptide chemistry toolbox – Transforming natural peptides into peptide therapeutics, *Biorg Med Chem* 26(10) (**2018**) 2759-2765.

[9] C. Zachow, G. Jahanshah, I. de Bruijn, C. Song, F. Ianni, Z. Pataj, H. Gerhardt, I. Pianet, M. Lämmerhofer, G. Berg, H. Gross, J.M. Raaijmakers, The Novel Lipopeptide Poaeamide of the Endophyte Pseudomonas poae RE*1-1-14 Is Involved in Pathogen Suppression and Root Colonization, *Molecular Plant-Microbe Interactions®* 28(7) (**2015**) 800-810.

[10] H. Gerhardt, A. Sievers-Engler, G. Jahanshah, Z. Pataj, F. Ianni, H. Gross, W. Lindner, M. Lämmerhofer, Methods for the comprehensive structural elucidation of constitution and stereochemistry of lipopeptides, *J Chromatogr A* 1428 (**2016**) 280-291.

[11] T. Schneider, A. Müller, H. Miess, H. Gross, Cyclic lipopeptides as antibacterial agents - potent antibiotic activity mediated by intriguing mode of actions, *Int J Med Microbiol* 304(1) (**2014**) 37-43.

[12] C. Ollivaux, D. Soyez, J.-Y. Toullec, Biogenesis of d-amino acid containing peptides/proteins: where, when and how?, *J Pept Sci* 20(8) (**2014**) 595-612.

[13] G. Jahanshah, Q. Yan, H. Gerhardt, Z. Pataj, M. Lämmerhofer, I. Pianet, M. Josten, H.-G. Sahl, M.W. Silby, J.E. Loper, H. Gross, Discovery of the Cyclic Lipopeptide Gacamide A by Genome Mining and Repair of the Defective GacA Regulator in Pseudomonas fluorescens Pf0-1, *J Nat Prod* 82(2) (**2019**) 301-308.

[14] R. Karongo, J. Jiao, H. Gross, M. Lammerhofer, Direct enantioselective gradient reversed-phase ultra-high performance liquid chromatography tandem mass spectrometry method for 3-hydroxy alkanoic acids in lipopeptides on an immobilized 1.6 mum amylose-based chiral stationary phase, *J Sep Sci* 44(9) (**2021**) 1875-1883.

[15] R. Karongo, M. Ge, J. Horak, H. Gross, M. Kohout, W. Lindner, M. Lämmerhofer, Rapid enantioselective amino acid analysis by ultra-high performance liquid chromatography-mass spectrometry combining 6-aminoquinolyl-N-hydroxysuccinimidyl carbamate derivatization with core-shell quinine carbamate anion exchanger separation, *Journal of Chromatography Open* 1 (**2021**) 100004.

[16] R. Karongo, M. Ge, C. Geibel, J. Horak, M. Lämmerhofer, Enantioselective multiple heart cutting online two-dimensional liquid chromatography-mass spectrometry of all proteinogenic amino acids with second dimension chiral separations in one-minute time scales on a chiral tandem column, *Anal Chim Acta* 1180 (**2021**).

[17] A. Szajek, I. Eggen, B. Gregg, A. Swietlow, H. Rode, M. Verlander, Control Strategies for Synthetic Therapeutic Peptide APIs Part II: Raw Material Considerations, *Pharm Technol* 38(4) (**2014**).

[18] A. Swietlow, H. Rode, A. Szajek, M. Verlander, I. Eggen, B. Gregg, Control Strategies for Synthetic Therapeutic Peptide APIs—Part I: Analytical Consideration, *Pharm Technol* 38(3) (**2014**).

[19] I. Eggen, B. Gregg, H. Rode, A. Swietlow, M. Verlander, A. Szajek, Control Strategies for Synthetic Therapeutic Peptide APIs Part III: Manufacturing Process Considerations, *Pharm Technol* 38(5) (**2014**).

[20] S. Ferre, V. Gonzalez-Ruiz, D. Guillarme, S. Rudaz, Analytical strategies for the determination of amino acids: Past, present and future trends, *J Chromatogr B Analyt Technol Biomed Life Sci* 1132 (**2019**) 121819.

[21] L.C. Wu, F. Chen, S.L. Lee, A. Raw, L.X. Yu, Building parity between brand and generic peptide products: Regulatory and scientific considerations for quality of synthetic peptides, *Int J Pharm* 518(1) (**2017**) 320-334.

[22] L.R. Snyder, J.W. Dolan, P.W. Carr, The hydrophobic-subtraction model of reversed-phase column selectivity, *J Chromatogr A* 1060(1-2) (**2004**) 77-116.

[23] L.R. Snyder, J.W. Dolan, J.R. Gant, Gradient elution in high-performance liquid chromatography: I. Theoretical basis for reversed-phase systems, *J Chromatogr A* 165(1) (**1979**) 3-30.

[24] J.J.K. Lloyd R. Snyder, John W. Dolan, Introduction to Modern Liquid Chromatography, 3 ed., John Wiley & Sons, Inc.**2010**.

[25] A.J. Alpert, Hydrophilic-interaction chromatography for the separation of peptides, nucleic acids and other polar compounds, *J Chromatogr A* 499 (**1990**) 177-196.

[26] B. Buszewski, S. Noga, Hydrophilic interaction liquid chromatography (HILIC)—a powerful separation technique, *Anal Bioanal Chem* 402(1) (**2012**) 231-247.

[27] H. Petrus, I. Knut, Hydrophilic interaction chromatography, *J Sep Sci* 29(12) (**2006**) 1784-1821.

[28] N.P. Dinh, T. Jonsson, K. Irgum, Water uptake on polar stationary phases under conditions for hydrophilic interaction chromatography and its relation to solute retention, *J Chromatogr A* 1320 (**2013**) 33-47.

[29] G. Kahsay, H. Song, A. Van Schepdael, D. Cabooter, E. Adams, Hydrophilic interaction chromatography (HILIC) in the analysis of antibiotics, *J Pharm Biomed Anal* 87 (**2014**) 142-154.

[30] A. Periat, I.S. Krull, D. Guillarme, Applications of hydrophilic interaction chromatography to amino acids, peptides, and proteins, *J Sep Sci* 38(3) (**2015**) 357-367.

[31] E. Largy, F. Cantais, G. Van Vyncht, A. Beck, A. Delobel, Orthogonal liquid chromatography–mass spectrometry methods for the comprehensive characterization of therapeutic glycoproteins, from released glycans to intact protein level, *J Chromatogr A* 1498 (**2017**) 128-146.

[32] D. Yeung, B. Mizero, D. Gussakovsky, N. Klaassen, Y. Lao, V. Spicer, O.V. Krokhin, Separation orthogonality in liquid chromatography-mass spectrometry for proteomic applications: comparison of 16 different two-dimensional combinations, *Anal Chem* (**2020**).

[33] K.M. Kalili, A. de Villiers, Systematic optimisation and evaluation of on-line, off-line and stop-flow comprehensive hydrophilic interaction chromatography×reversed phase liquid chromatographic analysis of procyanidins, Part I: Theoretical considerations, *J Chromatogr A* 1289 (**2013**) 58-68.

[34] R. Simon, Q. Enjalbert, J. Biarc, J. Lemoine, A. Salvador, Evaluation of hydrophilic interaction chromatography (HILIC) versus C18 reversed-phase chromatography for targeted quantification of peptides by mass spectrometry, *J Chromatogr A* 1264 (**2012**) 31-39.

[35] H.P. Nguyen, K.A. Schug, The advantages of ESI-MS detection in conjunction with HILIC mode separations: Fundamentals and applications, *J Sep Sci* 31(9) (**2008**) 1465-1480.

[36] M.P. Bruce Bailey, David Thomas, Chris Crafts, and Paul H. Gamache, Practical Use of CAD, Charged Aerosol Detection for Liquid Chromatography and Related Separation Techniques2017, pp. 163-189.

[37] T. Vehovec, A. Obreza, Review of operating principle and applications of the charged aerosol detector, *J Chromatogr A* 1217(10) (**2010**) 1549-1556.

[38] T. Zhang, E. Holder, P. Franco, M. Lämmerhofer, A. Sievers-Engler, H. Gerhardt, H. Gross, W. Lindner, Peptide Analysis: Zwitterionic Chiral Ion-Exchangers as Complementary Option to HILIC and to Reversed-Phase Chromatography, *LCGC Europe* 29(3) (**2016**) 112–128.

[39] J. Horak, M. Lämmerhofer, Derivatize, Racemize, and Analyze—an Easy and Simple Procedure for Chiral Amino Acid Standard Preparation for Enantioselective Metabolomics, *Anal Chem* 91(12) (**2019**) 7679-7689.

[40] J. Horak, M. Lämmerhofer, Stereoselective separation of underivatized and 6-aminoquinolyl-N-hydroxysuccinimidyl carbamate derivatized amino acids using zwitterionic quinine and quinidine type stationary phases by liquid chromatography–High resolution mass spectrometry, *Journal of Chromatography A* 1596 (**2019**) 69-78.

[41] Y. Zhang, D.-R. Wu, D.B. Wang-Iverson, A.A. Tymiak, Enantioselective chromatography in drug discovery, *Drug Discovery Today* 10(8) (**2005**) 571-577.

[42] B. Chankvetadze, Application of enantioselective separation techniques to bioanalysis of chiral drugs and their metabolites, *TrAC, Trends Anal Chem* 143 (**2021**) 116332.

[43] H. Hühnerfuss, M.R. Shah, Enantioselective chromatography—A powerful tool for the discrimination of biotic and abiotic transformation processes of chiral environmental pollutants, *J Chromatogr A* 1216(3) (**2009**) 481-502.

[44] G.K.E. Scriba, Chiral recognition in separation science – an update, *J Chromatogr A* 1467 (**2016**) 56-78.

[45] G.K.E. Scriba, Chiral Recognition Mechanisms in Analytical Separation Sciences, *Chromatographia* 75(15) (**2012**) 815-838.

[46] M. Lämmerhofer, W. Lindner, Liquid chromatographic enantiomer separation and chiral recognition by cinchona alkaloid-derived enantioselective separation materials, *Adv Chromatogr* 46 (**2008**) 1-107.

[47] N.J. Ayon, Features, roles and chiral analyses of proteinogenic amino acids, *AIMS Molecular Science* 7(3) (**2020**) 229-268.

[48] I. Ilisz, A. Péter, W. Lindner, State-of-the-art enantioseparations of natural and unnatural amino acids by high-performance liquid chromatography, *TrAC, Trends Anal Chem* 81 (**2016**) 11-22.

[49] O. Wahl, U. Holzgrabe, Amino acid analysis for pharmacopoeial purposes, *Talanta* 154 (**2016**) 150-163.

[50] J. Horak, M. Lammerhofer, Stereoselective separation of underivatized and 6-aminoquinolyl-N-hydroxysuccinimidyl carbamate derivatized amino acids using zwitterionic quinine and quinidine type stationary phases by liquid chromatography-High resolution mass spectrometry, *J Chromatogr A* (**2019**).

[51] M.J. Desai, D.W. Armstrong, Analysis of native amino acid and peptide enantiomers by high-performance liquid chromatography/atmospheric pressure chemical ionization mass spectrometry, *J Mass Spectrom* 39(2) (**2004**) 177-187.

[52] R. Berkecz, I. Ilisz, F. Fülöp, Z. Pataj, M.H. Hyun, A. Péter, High-performance liquid chromatographic enantioseparation of β-3-homo-amino acid stereoisomers on a (+)-(18-crown-6)-2,3,11,12-tetracarboxylic acid-based chiral stationary phase, *Journal of Chromatography A* 1189(1) (**2008**) 285-291.

[53] M.H. Hyun, Characterization of liquid chromatographic chiralseparation on chiral crown ether stationary phases, (**J. Sep. Sci. 2003, 26, 242–250**).

[54] B. Zhang, R. Soukup, D.W. Armstrong, Selective separations of peptides with sequence deletions, single amino acid polymorphisms, and/or epimeric centers using macrocyclic glycopeptide liquid chromatography stationary phases, *J Chromatogr A* 1053(1) (**2004**) 89-99.

[55] D.W. Armstrong, Y. Tang, S. Chen, Y. Zhou, C. Bagwill, J.-R. Chen, Macrocyclic Antibiotics as a New Class of Chiral Selectors for Liquid Chromatography, *Anal Chem* 66(9) (**1994**) 1473-1484.

[56] I. D'Acquarica, F. Gasparrini, D. Misiti, G. Zappia, C. Cimarelli, G. Palmieri, A. Carotti, S. Cellamare, C. Villani, Application of a new chiral stationary phase containing the glycopeptide antibiotic A-40,926 in the direct chromatographic resolution of β-amino acids, *Tetrahedron: Asymmetry* 11(11) (**2000**) 2375-2385.

[57] R. Berkecz, D. Tanács, A. Péter, I. Ilisz, Enantioselective Liquid Chromatographic Separations Using Macrocyclic Glycopeptide-Based Chiral Selectors, *Molecules* 26(11) (**2021**) 3380.

[58] M. Cebo, X. Fu, M. Gawaz, M. Chatterjee, M. Lämmerhofer, Enantioselective ultra-high performance liquid chromatography-tandem mass spectrometry method based on sub-2µm particle polysaccharide column for chiral separation of oxylipins and its application for the analysis of autoxidized fatty acids and platelet releasates, *J Chromatogr A* 1624 (**2020**) 461206.

[59] M. Lämmerhofer, Liquid chromatographic enantiomer separation with special focus on zwitterionic chiral ion-exchangers, *Anal Bioanal Chem* 406(25) (**2014**) 6095-6103.

[60] C.V. Hoffmann, R. Reischl, N.M. Maier, M. Lämmerhofer, W. Lindner, Stationary phase-related investigations of quinine-based zwitterionic chiral stationary phases operated in anion-, cation-, and zwitterion-exchange modes, *J Chromatogr A* 1216(7) (**2009**) 1147-1156.

[61] I. Ilisz, A. Bajtai, W. Lindner, A. Péter, Liquid chromatographic enantiomer separations applying chiral ion-exchangers based on Cinchona alkaloids, *J Pharm Biomed Anal* 159 (**2018**) 127-152.

[62] W. Stefanie, P. Reinhard, L. Wolfgang, Increments to chiral recognition facilitating enantiomer separations of chiral acids, bases, and ampholytes using Cinchona-based zwitterion exchanger chiral stationary phases, *J Sep Sci* 35(13) (**2012**) 1560-1572.

[63] R.J. Reischl, L. Hartmanova, M. Carrozzo, M. Huszar, P. Frühauf, W. Lindner, Chemoselective and enantioselective analysis of proteinogenic amino acids utilizing N-derivatization and 1-D enantioselective anion-exchange chromatography in combination with tandem mass spectrometric detection, *J Chromatogr A* 1218(46) (**2011**) 8379-8387.

[64] G. Lajkó, I. Ilisz, G. Tóth, F. Fülöp, W. Lindner, A. Péter, Application of Cinchona alkaloid-based zwitterionic chiral stationary phases in supercritical fluid chromatography for the enantioseparation of Nα-protected proteinogenic amino acids, *J Chromatogr A* 1415 (**2015**) 134-145.

[65] F. Ianni, R. Sardella, A. Lisanti, A. Gioiello, B.T. Cenci Goga, W. Lindner, B. Natalini, Achiral–chiral two-dimensional chromatography of free amino acids in milk: A promising tool for detecting different levels of mastitis in cows, *J Pharm Biomed Anal* 116 (**2015**) 40-46.

[66] R. Hellinger, J. Horak, W. Lindner, Enantioseparation of 6-aminoquinolyl-N-hydroxysuccinimidyl carbamate tagged amino acids and other zwitterionic compounds on cinchona-based chiral stationary phases, *Anal Bioanal Chem* 405(25) (**2013**) 8105-8120.

[67] R.J. Reischl, W. Lindner, The stereoselective separation of serine containing peptides by zwitterionic ion exchanger type chiral stationary phases and the study of serine racemization mechanisms by isotope exchange and tandem mass spectrometry, *J Pharm Biomed Anal* 116 (**2015**) 123-130.

[68] I. Federica, S. Roccaldo, C. Andrea, N. Benedetto, L. Wolfgang, L. Michael, Quinine-Based Zwitterionic Chiral Stationary Phase as a Complementary Tool for Peptide Analysis: Mobile Phase Effects on Enantio- and Stereoselectivity of Underivatized Oligopeptides, *Chirality* 28(1) (**2016**) 5-16.

[69] Z. Tong, H. Emilie, F. Pilar, L. Wolfgang, Zwitterionic chiral stationary phases based on cinchona and chiral sulfonic acids for the direct stereoselective separation of amino acids and other amphoteric compounds, *J Sep Sci* 37(11) (**2014**) 1237-1247.

[70] A. Bajtai, I. Ilisz, D.H.O. Howan, G.K. Tóth, G.K.E. Scriba, W. Lindner, A. Péter, Enantioselective resolution of biologically active dipeptide analogs by high-performance liquid chromatography applying Cinchona alkaloid-based ion-exchanger chiral stationary phases, *J Chromatogr A* 1611 (**2020**) 460574.

[71] C. Geibel, K. Dittrich, U. Woiwode, M. Kohout, T. Zhang, W. Lindner, M. Lammerhofer, Evaluation of superficially porous particle based zwitterionic chiral ion exchangers against fully porous particle benchmarks for enantioselective ultra-high performance liquid chromatography, *J Chromatogr A* (**2019**).

[72] C. Geibel, K. Dittrich, U. Woiwode, M. Kohout, T. Zhang, W. Lindner, M. Lämmerhofer, Evaluation of superficially porous particle based zwitterionic chiral ion exchangers against fully porous particle benchmarks for enantioselective ultra-high performance liquid chromatography, *Journal of Chromatography A* 1603 (**2019**) 130-140.

[73] C.V. Hoffmann, R. Reischl, N.M. Maier, M. Lämmerhofer, W. Lindner, Investigations of mobile phase contributions to enantioselective anion- and zwitterion-exchange modes on

quine-based zwitterionic chiral stationary phases, *J Chromatogr A* 1216(7) (**2009**) 1157-1166.

[74] S. Xia, D. Tao, H. Yuan, Y. Zhou, Z. Liang, L. Zhang, Y. Zhang, Nano-flow multidimensional liquid chromatography platform integrated with combination of protein and peptide separation for proteome analysis, *J Sep Sci* 35(14) (**2012**) 1764-1770.

[75] M. Lämmerhofer, R. Nogueira, W. Lindner, Multi-modal applicability of a reversed-phase/weak-anion exchange material in reversed-phase, anion-exchange, ion-exclusion, hydrophilic interaction and hydrophobic interaction chromatography modes, *Anal Bioanal Chem* 400(8) (**2011**) 2517-2530.

[76] D.R. Stoll, K. Shoykhet, P. Petersson, S. Buckenmaier, Active Solvent Modulation: A Valve-Based Approach To Improve Separation Compatibility in Two-Dimensional Liquid Chromatography, *Anal Chem* 89(17) (**2017**) 9260-9267.

[77] J.C. Giddings, Sample dimensionality: A predictor of order-disorder in component peak distribution in multidimensional separation, *J Chromatogr A* 703(1) (**1995**) 3-15.

[78] S.C. Rutan, J.M. Davis, P.W. Carr, Fractional coverage metrics based on ecological home range for calculation of the effective peak capacity in comprehensive two-dimensional separations, *J Chromatogr A* 1255 (**2012**) 267-276.

[79] F. Erni, R.W. Frei, Two-dimensional column liquid chromatographic technique for resolution of complex mixtures, *J Chromatogr A* 149 (**1978**) 561-569.

[80] J.C. Giddings, Maximum number of components resolvable by gel filtration and other elution chromatographic methods, *Anal Chem* 39(8) (**1967**) 1027-1028.

[81] J.M. Davis, J.C. Giddings, Statistical theory of component overlap in multicomponent chromatograms, *Anal Chem* 55(3) (**1983**) 418-424.

[82] G.J. C., Concepts and comparisons in multidimensional separation, *J High Resolut Chromatogr* 10(5) (**1987**) 319-323.

[83] J.M. Davis, D.R. Stoll, P.W. Carr, Effect of First-Dimension Undersampling on Effective Peak Capacity in Comprehensive Two-Dimensional Separations, *Anal Chem* 80(2) (**2008**) 461-473.

[84] R.E. Murphy, M.R. Schure, J.P. Foley, Effect of Sampling Rate on Resolution in Comprehensive Two-Dimensional Liquid Chromatography, *Anal Chem* 70(8) (**1998**) 1585-1594.

[85] S. Jaag, M. Shirokikh, M. Lämmerhofer, Charge variant analysis of protein-based biopharmaceuticals using two-dimensional liquid chromatography hyphenated to mass spectrometry, *J Chromatogr A* 1636 (**2021**) 461786.

[86] F. Li, X. Su, S. Bäurer, M. Lämmerhofer, Multiple heart-cutting mixed-mode chromatography-reversed-phase 2D-liquid chromatography method for separation and mass spectrometric characterization of synthetic oligonucleotides, *J Chromatogr A* 1625 (**2020**) 461338.

[87] R. Karongo, T. Ikegami, D.R. Stoll, M. Lämmerhofer, A selective comprehensive reversed-phase×reversed-phase 2D-liquid chromatography approach with multiple complementary detectors as advanced generic method for the quality control of synthetic and therapeutic peptides, *J Chromatogr A* 1627 (**2020**) 461430.

[88] M. Gilar, P. Olivova, A.E. Daly, J.C. Gebler, Orthogonality of Separation in Two-Dimensional Liquid Chromatography, *Anal Chem* 77(19) (**2005**) 6426-6434.

[89] M. Gilar, J. Fridrich, M.R. Schure, A. Jaworski, Comparison of Orthogonality Estimation Methods for the Two-Dimensional Separations of Peptides, *Anal Chem* 84(20) (**2012**) 8722-8732.

[90] P.J. Slonecker, X. Li, T.H. Ridgway, J.G. Dorsey, Informational Orthogonality of Two-Dimensional Chromatographic Separations, *Anal Chem* 68(4) (**1996**) 682-689.

[91] G. Semard, V. Peulon-Agasse, A. Bruchet, J.-P. Bouillon, P. Cardinaël, Convex hull: A new method to determine the separation space used and to optimize operating conditions for comprehensive two-dimensional gas chromatography, *J Chromatogr A* 1217(33) (**2010**) 5449-5454.

[92] M. Camenzuli, P.J. Schoenmakers, A new measure of orthogonality for multi-dimensional chromatography, *Anal Chim Acta* 838 (**2014**) 93-101.

[93] W. Nowik, S. Héron, M. Bonose, M. Nowik, A. Tchapla, Assessment of Two-Dimensional Separative Systems Using Nearest-Neighbor Distances Approach. Part 1: Orthogonality Aspects, *Anal Chem* 85(20) (**2013**) 9449-9458.

[94] M.R. Schure, J.M. Davis, Orthogonal separations: Comparison of orthogonality metrics by statistical analysis, *J Chromatogr A* 1414 (**2015**) 60-76.

[95] N.E. Watson, J.M. Davis, R.E. Synovec, Observations on "Orthogonality" in Comprehensive Two-Dimensional Separations, *Anal Chem* 79(20) (**2007**) 7924-7927.

[96] I. François, K. Sandra, P. Sandra, Comprehensive liquid chromatography: Fundamental aspects and practical considerations—A review, *Anal Chim Acta* 641(1) (**2009**) 14-31.

[97] D.R. Stoll, X. Li, X. Wang, P.W. Carr, S.E.G. Porter, S.C. Rutan, Fast, comprehensive two-dimensional liquid chromatography, *J Chromatogr A* 1168(1) (**2007**) 3-43.

[98] C.M. Willemse, M.A. Stander, J. Vestner, A.G.J. Tredoux, A. de Villiers, Comprehensive Two-Dimensional Hydrophilic Interaction Chromatography (HILIC) × Reversed-Phase Liquid Chromatography Coupled to High-Resolution Mass Spectrometry (RP-LC-UV-MS) Analysis of Anthocyanins and Derived Pigments in Red Wine, *Anal Chem* 87(24) (**2015**) 12006-12015.

[99] P. Donato, F. Rigano, F. Cacciola, M. Schure, S. Farnetti, M. Russo, P. Dugo, L. Mondello, Comprehensive two-dimensional liquid chromatography–tandem mass spectrometry for the simultaneous determination of wine polyphenols and target contaminants, *J Chromatogr A* 1458 (**2016**) 54-62.

[100] M.R. Filgueira, Y. Huang, K. Witt, C. Castells, P.W. Carr, Improving Peak Capacity in Fast Online Comprehensive Two-Dimensional Liquid Chromatography with Post-First-Dimension Flow Splitting, *Anal Chem* 83(24) (**2011**) 9531-9539.

[101] B.W.J. Pirok, A.F.G. Gargano, P.J. Schoenmakers, Optimizing separations in online comprehensive two-dimensional liquid chromatography, *J Sep Sci* 41(1) (**2018**) 68-98.

[102] D.R. Stoll, P.W. Carr, Two-Dimensional Liquid Chromatography: A State of the Art Tutorial, *Anal Chem* 89(1) (**2017**) 519-531.

[103] G.J. Opiteck, J.W. Jorgenson, R.J. Anderegg, Two-Dimensional SEC/RPLC Coupled to Mass Spectrometry for the Analysis of Peptides, *Anal Chem* 69(13) (**1997**) 2283-2291.

[104] S. Chapel, S. Heinisch, Strategies to circumvent the solvent strength mismatch problem in on-line comprehensive two-dimensional liquid chromatography, *J Sep Sci* n/a(n/a).

[105] M. Pursch, A. Wegener, S. Buckenmaier, Evaluation of active solvent modulation to enhance two-dimensional liquid chromatography for target analysis in polymeric matrices, *J Chromatogr A* 1562 (**2018**) 78-86.

[106] K. Zhu, M. Pursch, S. Eeltink, G. Desmet, Maximizing two-dimensional liquid chromatography peak capacity for the separation of complex industrial samples, *J Chromatogr A* 1609 (**2020**) 460457.

[107] P. W. Carr, D. Stoll, Primer: Two-Dimensional Liquid Chromatography - Principles, Practical Implementation and Applications, Agilent Technologies**2015**.

[108] M. Sarrut, A. D'Attoma, S. Heinisch, Optimization of conditions in on-line comprehensive two-dimensional reversed phase liquid chromatography. Experimental comparison with one-dimensional reversed phase liquid chromatography for the separation of peptides, *J Chromatogr A* 1421 (**2015**) 48-59.

[109] D.R. Stoll, R.W. Sajulga, B.N. Voigt, E.J. Larson, L.N. Jeong, S.C. Rutan, Simulation of elution profiles in liquid chromatography − II: Investigation of injection volume overload under gradient elution conditions applied to second dimension separations in two-dimensional liquid chromatography, *J Chromatogr A* 1523 (**2017**) 162-172.

[110] G. Leme, B. Madigan, J. Eikens, D.C. Harmes, D. Richardson, P. Carr, D. Stoll, In situ measurement of pH in liquid chromatography systems using a colorimetric approach, *Analytical Methods* 11(3) (**2019**) 381-386.

[111] G. Vivó-Truyols, S. van der Wal, P.J. Schoenmakers, Comprehensive Study on the Optimization of Online Two-Dimensional Liquid Chromatographic Systems Considering Losses in Theoretical Peak Capacity in First- and Second-Dimensions: A Pareto-Optimality Approach, *Anal Chem* 82(20) (**2010**) 8525-8536.

[112] P.J. Schoenmakers, G. Vivó-Truyols, W.M.C. Decrop, A protocol for designing comprehensive two-dimensional liquid chromatography separation systems, *J Chromatogr A* 1120(1) (**2006**) 282-290.

[113] C. Seidl, D.S. Bell, D.R. Stoll, A study of the re-equilibration of hydrophilic interaction columns with a focus on viability for use in two-dimensional liquid chromatography, *J Chromatogr A* 1604 (**2019**) 460484.

[114] K. Zhang, K.L. Kurita, C. Venkatramani, D. Russell, Seeking universal detectors for analytical characterizations, *J Pharm Biomed Anal* 162 (**2019**) 192-204.

[115] S. Bäurer, M. Ferri, A. Carotti, S. Neubauer, R. Sardella, M. Lämmerhofer, Mixed-mode chromatography characteristics of chiralpak ZWIX(+) and ZWIX(−) and elucidation of their chromatographic orthogonality for LC × LC application, *Anal Chim Acta* 1093 (**2020**) 168-179.

[116] C.G. Horvath, S.R. Lipsky, Use of Liquid Ion Exchange Chromatography for the Separation of Organic Compounds, *Nature* 211(5050) (**1966**) 748-749.

[117] H.R. Keller, D.L. Massart, Peak purity control in liquid chromatography with photodiode-array detection by a fixed size moving window evolving factor analysis, *Anal Chim Acta* 246(2) (**1991**) 379-390.

[118] E.P. 10.0, 2.2.56. Amino Acid Analysis, 2010, pp. 100-106.

[119] Y.-S. Sung, A. Berthod, D. Roy, D.W. Armstrong, A Closer Examination of 6-Aminoquinolyl-N-Hydroxysuccinimidyl Carbamate Amino Acid Derivatization in HPLC with Multiple Detection Modes, *Chromatographia* 84(8) (**2021**) 719-727.

[120] K. Zhang, L. Dai, N.P. Chetwyn, Simultaneous determination of positive and negative pharmaceutical counterions using mixed-mode chromatography coupled with charged aerosol detector, *J Chromatogr A* 1217(37) (**2010**) 5776-84.

[121] R. Pawellek, T. Muellner, P. Gamache, U. Holzgrabe, Power function setting in charged aerosol detection for the linearization of detector response − optimization strategies and their application, *J Chromatogr A* 1637 (**2021**) 461844.

[122] R. Pawellek, U. Holzgrabe, Performance of ion pairing chromatography and hydrophilic interaction liquid chromatography coupled to charged aerosol detection for the analysis of underivatized amino acids, *J Chromatogr A* 1659 (**2021**) 462613.

[123] K. Takahashi, S. Kinugasa, M. Senda, K. Kimizuka, K. Fukushima, T. Matsumoto, Y. Shibata, J. Christensen, Quantitative comparison of a corona-charged aerosol detector and an evaporative light-scattering detector for the analysis of a synthetic polymer by supercritical fluid chromatography, *Journal of chromatography. A* 1193(1-2) (**2008**) 151-155.

[124] T. Vehovec, A. Obreza, Review of operating principle and applications of the charged aerosol detector, *Journal of Chromatography A* 1217 (**2010**) 1549-1556.

[125] J.H. Gross, Massenspektrometrie - Ein Lehrbuch, 1 ed., Springer Spektrum**2013**.

[126] N.B. Cech, C.G. Enke, Practical implications of some recent studies in electrospray ionization fundamentals, *Mass Spectrom Rev* 20(6) (**2001**) 362-387.

[127] J.B. Fenn, M. Mann, C.K. Meng, S.F. Wong, C.M. Whitehouse, Electrospray Ionization for Mass Spectrometry of Large Biomolecules, *Science* 246(4926) (**1989**) 64-71.

[128] C.M. Whitehouse, R.N. Dreyer, M. Yamashita, J.B. Fenn, Electrospray interface for liquid chromatographs and mass spectrometers, *Anal Chem* 57(3) (**1985**) 675-679.

[129] P. Kebarle, U.H. Verkerk, Electrospray: From ions in solution to ions in the gas phase, what we know now, *Mass Spectrom Rev* 28(6) (**2009**) 898-917.

[130] J. Zeleny, Instability of Electrified Liquid Surfaces, *Physical Review* 10(1) (**1917**) 1-6.

[131] G.I. Taylor, Disintegration of water drops in an electric field, *Proceedings of the Royal Society of London. Series A. Mathematical and Physical Sciences* 280(1382) (**1964**) 383-397.

[132] M.S. Wilm, M. Mann, Electrospray and Taylor-Cone theory, Dole's beam of macromolecules at last?, *Int J Mass Spectrom Ion Processes* 136(2) (**1994**) 167-180.

[133] M.G. Ikonomou, A.T. Blades, P. Kebarle, Electrospray-ion spray: a comparison of mechanisms and performance, *Anal Chem* 63(18) (**1991**) 1989-1998.

[134] L. Rayleigh, XX. On the equilibrium of liquid conducting masses charged with electricity, *The London, Edinburgh, and Dublin Philosophical Magazine and Journal of Science* 14(87) (**1882**) 184-186.

[135] E.d. Hoffmann, J.J. Charette, V. Stroobant, J. Trottier, Mass Spectrometry: Principles and Applications, 1997.

[136] A. Gomez, K. Tang, Charge and fission of droplets in electrostatic sprays, *Phys Fluids* 6 (**1994**) 404-414.

[137] J. Fernandez de la Mora, Electrospray ionization of large multiply charged species proceeds via Dole's charged residue mechanism, *Anal Chim Acta* 406(1) (**2000**) 93-104.

[138] J.A. Loo, C.G. Edmonds, H.R. Udseth, R.D. Smith, Effect of reducing disulfide-containing proteins on electrospray ionization mass spectra, *Anal Chem* 62(7) (**1990**) 693-698.

[139] I.V. Chernushevich, A.V. Loboda, B.A. Thomson, An introduction to quadrupole–time-of-flight mass spectrometry, *J Mass Spectrom* 36(8) (**2001**) 849-865.

[140] D.W. Koppenaal, Charles J. Barinaga, M.B. Denton, R.P. Sperline, G.M. Hieftje, G.D. Schilling, F.J. Andrade, J.H. Barnes, MS Detectors, *Anal Chem* 77(21) (**2005**) 418 A-427 A.

[141] G.L. Andrews, B.L. Simons, J.B. Young, A.M. Hawkridge, D.C. Muddiman, Performance Characteristics of a New Hybrid Quadrupole Time-of-Flight Tandem Mass Spectrometer (TripleTOF 5600), *Anal Chem* 83(13) (**2011**) 5442-5446.

[142] N. Hermes, K.S. Jewell, A. Wick, T.A. Ternes, Quantification of more than 150 micropollutants including transformation products in aqueous samples by liquid chromatography-tandem mass spectrometry using scheduled multiple reaction monitoring, *J Chromatogr A* 1531 (**2018**) 64-73.

[143] B. Drotleff, M. Hallschmid, M. Lämmerhofer, Quantification of steroid hormones in plasma using a surrogate calibrant approach and UHPLC-ESI-QTOF-MS/MS with SWATH-acquisition combined with untargeted profiling, *Anal Chim Acta* 1022 (**2018**) 70-80.

[144] P. Picotti, B. Bodenmiller, L.N. Mueller, B. Domon, R. Aebersold, Full Dynamic Range Proteome Analysis of S. cerevisiae by Targeted Proteomics, *Cell* 138(4) (**2009**) 795-806.

[145] S. Ghaemmaghami, W.-K. Huh, K. Bower, R.W. Howson, A. Belle, N. Dephoure, E.K. O'Shea, J.S. Weissman, Global analysis of protein expression in yeast, *Nature* 425(6959) (**2003**) 737-741.

[146] M. Raetz, R. Bonner, G. Hopfgartner, SWATH-MS for metabolomics and lipidomics: critical aspects of qualitative and quantitative analysis, *Metabolomics* 16(6) (**2020**) 71.

[147] C. Ludwig, L. Gillet, G. Rosenberger, S. Amon, B.C. Collins, R. Aebersold, Data-independent acquisition-based SWATH-MS for quantitative proteomics: a tutorial, *Mol Syst Biol* 14(8) (**2018**) e8126.

[148] C. Messner, V. Demichev, N. Bloomfield, G. Ivosev, F. Wasim, A. Zelezniak, K. Lilley, S. Tate, M. Ralser, ScanningSWATH enables ultra-fast proteomics using high-flow chromatography and minute-scale gradients, *bioRxiv* (**2019**) 656793.

[149] K. Frederick, P. Ciborowski, 9 - SWATH-MS: Data Acquisition and Analysis, in: P. Ciborowski, J. Silberring (Eds.), Proteomic Profiling and Analytical Chemistry (Second Edition), Elsevier, Boston, 2016, pp. 161-173.

[150] R. Bonner, G. Hopfgartner, SWATH acquisition mode for drug metabolism and metabolomics investigations, *Bioanalysis* 8(16) (**2016**) 1735-1750.

[151] Y. Zhang, A. Bilbao, T. Bruderer, J. Luban, C. Strambio-De-Castillia, F. Lisacek, G. Hopfgartner, E. Varesio, The Use of Variable Q1 Isolation Windows Improves Selectivity in LC–SWATH–MS Acquisition, *Journal of Proteome Research* 14(10) (**2015**) 4359-4371.

[152] H. Tsugawa, T. Cajka, T. Kind, Y. Ma, B. Higgins, K. Ikeda, M. Kanazawa, J. VanderGheynst, O. Fiehn, M. Arita, MS-DIAL: data-independent MS/MS deconvolution for comprehensive metabolome analysis, *Nat Methods* 12(6) (**2015**) 523-526.

[153] J. Horak, M. Lämmerhofer, Racemization without deamidation: Effect of racemization conditions on 6-aminoquinolyl-N-hydroxysuccinimidyl carbamate tagged amino acids, *J Chromatogr A* 1604 (**2019**) 460492.

[154] T. Upmanis, H. Kažoka, P. Arsenyan, A study of tetrapeptide enantiomeric separation on crown ether based chiral stationary phases, *J Chromatogr A* 1622 (**2020**) 461152.

[155] S. Moore, S. Hess, J. Jorgenson, Characterization of an immobilized enzyme reactor for on-line protein digestion, *J Chromatogr A* 1476 (**2016**) 1-8.

[156] L.M.H. Reinders, M.D. Klassen, T. Teutenberg, M. Jaeger, T.C. Schmidt, Development of a multidimensional online method for the characterization and quantification of monoclonal

antibodies using immobilized flow-through enzyme reactors, *Anal Bioanal Chem* 413(28) (**2021**) 7119-7128.

[157] C. Gstöttner, D. Klemm, M. Haberger, A. Bathke, H. Wegele, C. Bell, R. Kopf, Fast and Automated Characterization of Antibody Variants with 4D HPLC/MS, *Anal Chem* 90(3) (**2018**) 2119-2125.

[158] S. Pot, C. Gstöttner, K. Heinrich, S. Hoelterhoff, I. Grunert, M. Leiss, A. Bathke, E. Domínguez-Vega, Fast analysis of antibody-derived therapeutics by automated multidimensional liquid chromatography – mass spectrometry, *Anal Chim Acta* (**2021**) 339015.

2. List of Figures

3. List of Tables

4. Results and Discussion

4.1 Publication I

A selective comprehensive reversed-phase × reversed-phase 2D-liquid chromatography approach with multiple complementary detectors as advanced generic method for the quality control of synthetic and therapeutic peptides

Ryan Karongo[a], Tohru Ikegami[a,b], Dwight R. Stoll[c], Michael Lämmerhofer[a,*]

[a]Institute of Pharmaceutical Sciences, Pharmaceutical (Bio-) Analysis, University of Tübingen, Auf der Morgenstelle 8, 72076 Tübingen, Germany

[b]Kyoto Institute of Technology, Department of Materials Synthesis, Faculty of Molecular Chemistry and Engineering, Matsugasaki, Sakyo-ku, Kyoto 606-8585, Japan

[c]Department of Chemistry, Gustavus Adolphus College, 800 West College Avenue, Saint Peter, MN 56082, USA

A selective comprehensive reversed-phase×reversed-phase 2D-liquid chromatography approach with multiple complementary detectors as advanced generic method for the quality control of synthetic and therapeutic peptides

Ryan Karongo[a], Tohru Ikegami[a,b], Dwight R. Stoll[c], Michael Lämmerhofer[a,*]

[a] Institute of Pharmaceutical Sciences, Pharmaceutical (Bio-) Analysis, University of Tübingen, Auf der Morgenstelle 8, 72076 Tübingen, Germany
[b] Kyoto Institute of Technology, Department of Materials Synthesis, Faculty of Molecular Chemistry and Engineering, Matsugasaki, Sakyo-ku, Kyoto 606-8585, Japan
[c] Department of Chemistry, Gustavus Adolphus College, 800 West College Avenue, Saint Peter, MN 56082, USA

ABSTRACT

There is a huge, still increasing market for synthetic and therapeutic peptides. Their quality control is commonly based on a generic reversed-phase liquid chromatography (RPLC) method with C18 stationary phase and acetonitrile gradient with 0.1% trifluoroacetic acid in the mobile phase. It performs exceptionally well for a wide variety of impurities, yet structurally closely related impurities with similar sequences, not resolved in preparative RPLC, may easily coelute in the corresponding QC run as well. To address this problem an advanced generic 2D-LC impurity profiling method was developed in this work. It employs a selective comprehensive (high resolution sampling) RP×RP 2D-LC separation using a 100×2.1 mm ID column with the common acidic generic gradient in the first dimension, while RPLC under basic pH on a short 30×3 mm ID column is used in the second dimension. Recording data with a UV detector at 215 nm after ^{1}D separation provides the common generic 1D chromatogram. However, after the ^{2}D separation a flow splitter enabled recording of the signals of complementary detectors comprising a diode array detector (DAD) in-line with a charged aerosol detector (CAD) and a quadrupole-time-of-flight (QTOF) mass spectrometer (MS) with an electrospray ionization (ESI) source. Generic conditions of this 2D-LC method have been established through optimization of ^{2}D stationary and mobile phase considering different pH values and buffer concentrations. The orthogonal separation principle has been documented by a number of therapeutic peptides including Exenatide, Octreotide, Cyclosporine A and Oxytocin as well as some other proprietary synthetic peptides. The information density can be further enhanced by using the QTOF-MS detector by data independent acquisition with SWATH. Through this sequential window acquisition of all theoretical fragment ion mass spectra it became possible to collect MS/MS data comprehensively in the high-resolution sampling window, thus enabling the extraction of 2D-EICs from fragment ions and the generation of 2D-contour plots of all product ions. Using Oxytocin as an example for an important therapeutic peptide, the ability of this advanced generic sRP-UV×RP-DAD-CAD-ESI-QTOF-MS/MS method with SWATH for peptide quality control is discussed.

© 2020 Elsevier B.V. All rights reserved.

1. Introduction

The number of therapeutic peptide regulatory approvals is steadily increasing and hence the global peptide drug market is continuously growing [1–3]. The majority of peptide therapeutics on the market are of synthetic origin. Modern solid and liquid phase peptide synthesis protocols give access to practically any of these peptide sequences with reasonable yields. Nevertheless, raw products contain impurities from side reactions, deletions as well as incomplete protection/deprotection of reactive groups, and so forth. Consequently, purification of raw peptide products remains an essential step for the production of pharmaceutical grade therapeutic peptides. The state-of-the-art for this purpose is preparative reversed-phase HPLC (RPLC) with trifluoroacetic acid (TFA) as ion paring agent [1,4]. The ion-pairing capacity of TFA masks the cationic groups of peptide analytes, and its acidic nature

* Corresponding author.
 E-mail address: michael.laemmerhofer@uni-tuebingen.de (M. Lämmerhofer).

suppresses ionization of carboxylic groups, resulting in excellent separations. For quality control, the corresponding analytical scale RPLC method is employed. Consequently, there is a certain risk that structurally similar impurities co-eluted with the main peak during preparative LC are not detected in the QC run because they are hidden beneath the target peptide peak. This represents a serious threat in QC of peptide therapeutics by 1D-LC.

To deal with this problem, complementary analytical approaches have been suggested for peptide quality control. They include liquid chromatography with stationary phases having orthogonal selectivities such as hydrophilic interaction chromatography (HILIC) phases [5] mixed-bed or mixed-mode stationary phases [5–9], chiral stationary phases [10–15], but also RPLC with complementary selectivity [16]. Nevertheless, method development on mixed-mode and chiral columns, while offering high flexibility and good potential of orthogonal selectivity, is naturally more complex compared to optimizing RPLC separations [17].

Regardless of the extraordinary performance one-dimensional separation methods exhibit, their power to resolve and monitor co-eluting impurities from their active pharmaceutical ingredient (API) is limited and the resolving power can be greatly improved by the addition of a complementary second dimension (^{2}D). Two-dimensional liquid chromatography (2D-LC) surpasses 1D-LC in multiple aspects, such as peak capacity, resolving power and especially productivity (peaks separated per unit time) [18–20]. For the separation of tryptic peptides, which usually adopt different charges, it seems obvious to combine RP with strong cation-exchange (SCX) in order to separate them according to their charge in ^{1}D followed by hydrophobic separation with RP-LC in the ^{2}D [21]. In fact, this is the state of the art in bottom up proteomics [22–25]. Combination of RP with HILIC and anion-exchange are other options to achieve selectivity complementarity and their peptide separation orthogonality to RP has been evaluated for 16 different 2D-LC- ESI-MS systems, including SCX [26]. Furthermore, it was shown that good orthogonality for separating tryptic digests can also be achieved, when operating two RP separation dimensions at low (e.g. 0.2% formic acid, pH 2.6) and high pH (e.g. 20 mM ammonium formate buffer, pH 10) [21,24,27–34] Generally, RP×RP methods with different mobile phase pH values in the two dimensions have been popular for pharmaceutical quality assurance / quality control (QA/QC) of therapeutic proteins after tryptic digestion at the peptide level [30]. In this context, a high sequence coverage (ideally 100%) as well as the absence of unexpected peptides are quality attributes. For synthetic therapeutic peptides, regulatory agencies require the determination of impurities with similar structures down to the 0.1–0.05% level [4,35,36]. Full comprehensive 2D-LC [21] is not required for this purpose. However, the overall assay specificity may benefit from a second dimension separation with a complementary selectivity principle and adopting a heart cutting or multiple heart cutting technology [37–39] may be suitable. Indeed, the 2D-LC impurity profiling of Naproxen, for instance, successfully allowed the quantification of impurities present at 0.05% relative to the API concentration [40].

The implementation of 2D-LC in the field of synthetic (therapeutic) peptides and particularly the development of a generic 2D-LC method replacing the generic 1D counterpart would address an urgent demand from the QA/QC viewpoint and is the objective of this report. The strategy implemented in the current work is called selective comprehensive (also named High Resolution Sampling, HiRes) 2D-LC, wherein specific ^{1}D peaks of particular interest are sampled comprehensively. We illustrate its potential on a series of therapeutic test peptides, propose optimized stationary and mobile phase conditions, and hyphenate the selective comprehensive 2D-LC with various orthogonal detection modalities including UV (diode array detector, DAD), charged aerosol detection (CAD) and

quadrupole-time of flight mass spectrometry (QTOF-MS) in data-dependent (DDA) and data independent acquisition (DIA) modes.

2. Experimental

2.1. Materials

Oxytocin was purchased from Carbosynth (Compton, United Kingdom), Exenatide from Hangzhou MolCore BioPharmatech (Hangzhou, China), Octreotide from AvaChem Scientific (San Antonio, TX, USA) and Cyclosporin A from Sigma-Aldrich (Schnelldorf, Germany). Proprietary peptides 1–3 were provided as gifts. An Agilent ZORBAX Rapid Resolution High Definition SB-C18 column (100 mm x 2.1 mm, 1.8 μm) was used in ^{1}D, while a YMC-Triart C18 ExRS column (30×3 mm, 1.9 μm) was used in the ^{2}D. Trifluoroacetic acid (TFA, ≥99.5%) was obtained from AppliChem (Darmstadt, Germany), formic acid (FA) from Carl Roth (Karlsruhe, Germany), ammonium hydroxide solution (NH$_4$OH, 25–30% NH$_3$), ammonium bicarbonate (NH$_4$HCO$_3$, ≥99.5%), ammonium formate (NH$_4$FA, ≥99.0%) and ammonium acetate (NH$_4$Ac, ≥98%) from Sigma-Aldrich. Acetonitrile (ACN) and methanol (MeOH) in Ultra LC-MS grade were purchased from Carl Roth, while ultrapure water was obtained by Elga PureLab Ultra purification system (Celle, Germany).

2.2. Instrumentation

An Agilent 1290 Infinity II 2D-LC Solution from Agilent Technologies (Waldbronn, Germany) was used for High Resolution (HiRes) sampling 2D-LC (Fig. S1). The ^{1}D LC consisted of a quaternary low pressure gradient UHPLC pump (Flexible Pump, G7104A), a Multisampler (G7167B), a Multicolumn Thermostat (G7116B), a Variable wavelength detector (G7114B) with 14 μL flow cell (G1314–60,186) and a pressure release kit (G4236–60,010) between UV-detector and 2D-interface. The ^{2}D was composed of a binary high-pressure gradient UHPLC pump (High Speed Pump, G7120A), a valve drive (G1170A) with a 5 pos/10 port 2D-LC active solvent modulation (ASM) valve (G4243A) connected to two 6 pos/14 port valve heads (#5067–4142) carrying six 40 μL loops each, a Multicolumn Thermostat (G7116B), and a diode array detector (G7117B) with 1 μL flow cell (#G4212–60,008). Experiments utilizing active solvent modulation (ASM) were performed with the ASM factor 5 (split ratio 1:4) restriction capillary (85×0.12 mm, 0.96 μL). Dwell volumes were determined using a zero dead volume union connector in place of the column. The measured volumes were 550 μL in the first and 120 μL in the second at a flow rate of 0.20 mL/min. The acquisition rates were set at 10 Hz and 40 Hz in the first and second dimension, respectively. The 2D-chromatographic data were processed with Open Lab CDS Rev. C.01.07 SR4 (Agilent Technologies). Contour plots were created with GC Image LCxLC–HRMS V2.7 Edition Software (GC Image, Lincoln, NE, USA).

For the enhanced detection setup, a QuickSplit Flow Splitter from ERC (Riemerling, Germany) was installed prior to the detectors in the ^{2}D at a ratio of 1:5, whereby the high flow was directed to the DAD (G7117B) connected in series to a Corona Veo Charged Aerosol Detector (Thermo Fischer Scientific, Germering, Germany) and the low flow to a TripleTOF 5600+ QTOF mass spectrometer (Sciex, Darmstadt, Germany) using the contact closure connection for peripheral devices (Suppl. Fig. S2). QTOF-MS measurements were performed using a Duospray ion source (electrospray ionization interface) in positive ion mode. The following MS instrument parameters were used: curtain gas (CUR) 35 psi, ion source gas (nebulizing gas; GS1) 50 psi, heater gas (drying gas; GS2) 40 psi, ion spray voltage floating (ISVF) 5000 V, source temperature (TEM) 600 °C and a declustering potential (DP) 100 V. Data acquisition was performed either in information-dependent
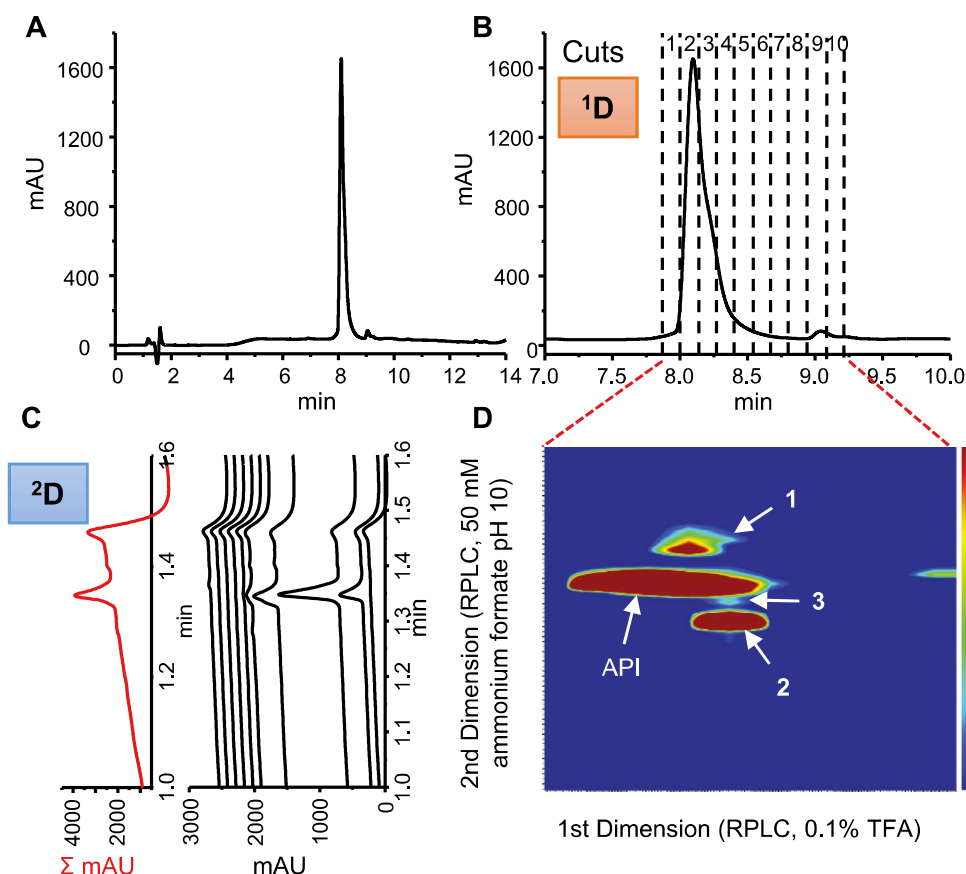
Fig. 1. From generic 1D-RPLC towards advanced 2D generic synthetic peptide impurity profiling. **A**: Generic one dimensional RPLC impurity profile of a synthetic model peptide (Peptide 1), which represents the state-of-the-art in QC of synthetic peptides. **B**: Zoom in indicates the co-eluting impurity as a shoulder of the main peak. The entirety of the peak from ¹RPLC (at acidic pH) is quantitatively transferred by 10 consecutive cuts (fractions as indicated by the vertical dashed lines) into the second dimension (²RPLC at pH 10), in which each cut (fraction) is analyzed successively as depicted in **C. D** Contour plot obtained by reconstitution of the 10 ²D chromatograms using LC-Image software indicating the comprehensive two-dimensional impurity profile including the impurities co-eluted in the first dimension (¹RPLC, 0.1% TFA). The impurities resulting from the **API** depicted in **D** correspond to the cleavage product (**1**) and the respective deamidation products of API (**2**) and the cleavage product (**3**), respectively.

acquisition (IDA) mode or in data independent acquisition (DIA) mode with SWATH (sequential windowed acquisition of all theoretical fragment ion mass spectra). The mass range of the TOF-MS full scan comprised m/z 100–2000 with an accumulation time of 50 ms and a collision energy (CE) of 10 V. MS/MS in IDA & SWATH were performed with rolling CE and a spread (CES) of 15 V. SWATH was applied using 30 windows of 30 Da within a range of 230 – 1070 Da and an accumulation time of 12 ms per window (i.e. for each MS/MS experiment), while 15 ms were used as accumulation time in IDA for each MS/MS experiment. For IDA, the top 20 ions of the full scan with $m/z > 200$ and intensity > 100 cps were selected for MS/MS. Data Acquisition was performed with Analyst TF 1.7 software (Sciex) and analysis with the LC-Image software. Furthermore, in IDA mode the number of MS cycles per 2D-LC run depended on the number of triggered MS^2 measurements. Therefore, the length of the MS chromatograms for the ²D measurements were not uniform. To deal with this, the development of an LC-Image software update was initiated for IDA applications that allows nearest neighbor alignment of the generated raw data (.wiff) according to the 2D-LC sampling information (.drvml). In SWATH acquisition the nearest neighbor alignment is not necessary due to the uniformity of MS data string lengths.

2.3. Chromatographic conditions

Chromatographic conditions are specified in the respective figure captions or otherwise in the supplementary Table S1.

3. Results and discussion

3.1. Advanced generic sRP×RP 2D-LC impurity profiling method: a proof of principle

A selective comprehensive RP×RP 2D-LC method was devised as a more powerful tool for comprehensive impurity profiling of therapeutic peptides. The basic idea was to keep the current generic 1D-RPLC peptide impurity profiling method available and it was therefore fixed as the ¹D separation. Since we have installed a UV detector after the ¹D separation, the common 1D RPLC chromatogram remains available. The ²D separation had to be developed with the aim to provide complementary retention and selectivity as well as CAD and MS compatibility. Complementarity of the ²D was achieved by adjusting distinct ionization of the zwitterionic peptides through altered pH resulting in different RP-LC separation selectivity [24,41,42].

As a proof of principle, Fig. 1A depicts the ¹D separation of a synthetic peptide, detected with UV at 215 nm, on a C18 column (Zorbax SB C18, 100×2.1 mm, 1.8 μm) operated with 0.1% TFA in water and acetonitrile in gradient elution mode. It is evident that only a single minor impurity peak, eluted after the target peptide, was obtained by the common generic method. However, upon zooming in a shoulder on the main peak can be seen (Fig. 1B). The resolution of this co-eluting compound requires complementary selectivity. Thus, a series of multiple adjacent heart-cuts have been made to comprehensively sample the entire effluent contain-
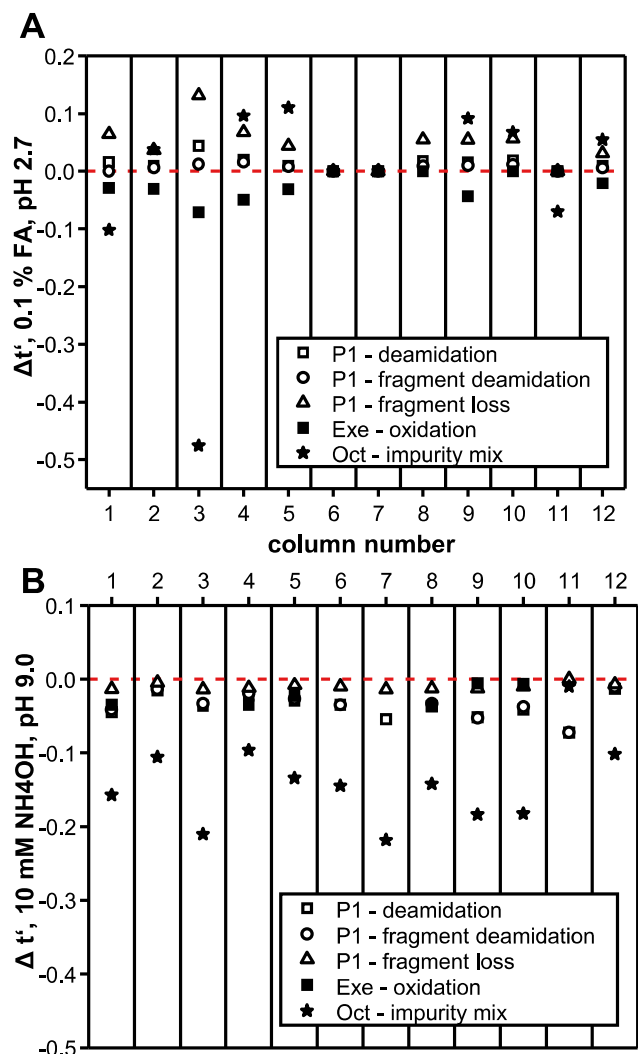
Fig. 2. Differential normalized migration times ($\Delta t'$) between peptide impurities and parent target peptides on a variety of different reversed phase columns under acidic conditions (**A**) and basic eluent (**B**). Columns: **1**: YMC-Triart C18 ExRS (30×3.0 mm, 1.9 μm), **2**: YMC-Triart C8 (50×2.1 mm, 1.9 μm), **3**: Agilent Zorbax Bonus RP (30×3.0 mm, 1.8 μm), **4**: Agilent Poroshell HPH C18 (50×3.0, 1.9 μm), **5**: Waters Cortecs C18 (50×2.0, 1.0 mm, 2.7 μm), **6**: Kinetex EVO C18 (20×2.1 mm, 2.6 μm), **7**: Synergi Fusion-RP (50×2.0 mm, 4.0 μm), **8**: Agilent Zorbax Eclipse Plus C18 (50×3.0 mm 1.8 μm), **9**: Kinetex C18 (50×4.6 mm, 2.6 μm), **10**: Kinetex C8 (50×2.1 mm, 2.6 μm), **11**: Kinetex PFP (100×3.0 mm, 2.6 μm), **12**: InfinityLab Poroshell 120EC C18 (150×3.0 mm, 2.7 μm). Test peptides: Peptide 1, Exenatide and Octreotide and their corresponding impurities. Normalized retention times were applied to subtract the impurities' retention time from the parent compounds' retention time. The same set of columns was operated at both low (0.1% FA, pH 2.7) and high (10 mM NH$_4$OH, pH 9.0) pH. A sign reversal implies a reversed elution order and thus outlines a significant shift in selectivity. Method transfers were executed for each column proceeding from column no. **1** according to 1 μL injection volume, 0.5 mL/min flow rate and the following gradient: 0 min (10%B) – 1 min (10%B) – 10 min (100%B) – 13 min (100%B) – 13.10 min (10%B) – 16 min (10%B).

ing the peak of interest (Fig. 1B). The cuts were sampled into two loop decks, each equipped with six 40 μL loops. The loops were filled to 40% only and a cocurrent loop filling/analyzing mode was selected (i.e. the sample loop was unloaded in the same direction as it was filled). The 10 fractions from the first dimension where then analyzed subsequently (in the reversed order as they were sampled into the loops) by the ^{2}D-RPLC method on a YMC-Triart C18 ExRS at pH 10. The ^{2}D chromatograms of the 10 fractions are shown in Fig. 1C. The interpretation of the individual chromatograms is inconvenient and thus a sum chromatogram can be reconstituted (red trace in Fig. 1C). Here, it becomes already visible

that some impurities are present. A more illustrative way of representation of the 2D chromatogram is by a contour plot (Fig. 1D). As we can see in Fig. 1D, three impurities were detected by sRP×RP-2D-LC-UV of which only one was found by ^{1}D RPLC (for relative quantification see Suppl. Fig S8).

A full comprehensive analysis, which necessitates that ^{2}D cycle time is matching the ^{1}D sampling time, is not required for this application. The selected high resolution sampling has, since fractions can be stored in loops until the ^{2}D separation system is available, the advantage of being less demanding in terms of speed and ^{2}D cycle time. On the other hand, in contrast to heart-cutting 2D-LC, the entirety of a peak gets quantitatively transferred and analyzed in selective comprehensive mode [33,43]. Therefore, selective comprehensive 2D-LC is fully sufficient and the perfect 2D-LC analysis modality in order to discriminate and quantitate impurities that tend to co-elute with the main compound. Little extra information would be gained by a full comprehensive RP×RP 2D-LC approach; it might be of interest only in cases in which peak purity information of impurity peaks is required. In Fig. 1D, the impurity peak eluted at ^1t_R = 9.1 min/^2t_R= 1.35 min can be recognized as pure according to 2D-LC.

In the current example, a time-based sampling strategy was selected, i.e. fractionation in ^{1}D was devised based on a prior 1D-RPLC run. Peak-based sampling, in which sample collection is triggered upon signal rise over a certain set threshold, is an alternative strategy avoiding the additional 1D-RPLC run for designing the fractionation. By developing a 2D-LC method, in which the ^{2}D separation is fast enough, the total run time of the 2D-LC method does not exceed the runtime of the corresponding 1D method and thus, in terms of time, the increased peak production rate and enhanced amount of information acquired is gained for free [28].

3.2. Optimization of the ^{2}D stationary phase

Coupling RP in ^{1}D and ^{2}D differing in pH has the advantage of nearly optimal mobile phase compatibility. Ideally, the more retentive phase system is selected for the ^{2}D as it allows more efficient refocusing. Thus, the choice of the stationary phase in ^{2}D is a crucial method parameter. There are also other requirements that have to be fulfilled. First, for a generic method gradient elution is preferred over isocratic in order to avoid wrap arounds of highly hydrophobic sample components. Adequate post gradient re-equilibration is required in order to maintain reproducibility, however, at the same time the overall ^{2}D cycle time should be minimized. Further, a broad versatility and applicability, as well as high efficiencies and good stability, are desirable if the second dimension is to be operated at extreme conditions including flow rate, pressure, temperatures and pH values. RPLC is superior in this regard over other separation modes, such as HILIC and ion exchange, of which the re-equilibration volumes are usually much higher. Another aspect is the consideration of column dimensions. In order to achieve fast separations in the ^{2}D and keep the total run time short, very short and very efficient columns with relatively wide inner diameter are necessary [44]. In the following, a selection of reversed phase columns (see Suppl. Table S2) was evaluated for their applicability at high pH conditions in the ^{2}D.

The prime criterion for this evaluation was on their orthogonality to the ^{1}D separation, as induced by a different mobile phase pH but efficiently supported by complementary stationary phase selectivity. A small set of therapeutic peptides and their impurities were utilized for this study. The retention times of the peptide API and their impurities were normalized according to Eq. 1:

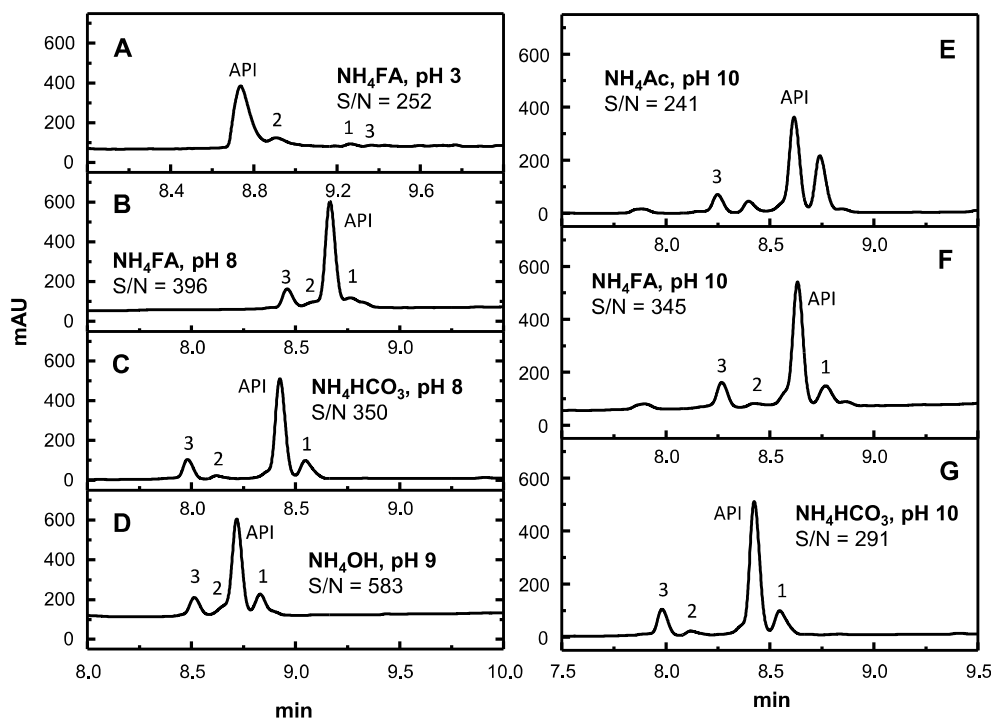$$t' = \frac{t_R - t_{begin}}{t_{end} - t_{begin}}$$

Fig. 3. Comparison of different combinations of buffer and pH values designated for the second dimension of the generic 2D-LC peptide separation, exemplified by chromatograms for the separation of Peptide 1 (peak annotation according to Fig. 1). All buffer concentrations were maintained at 10 mM within their buffering ranges: HCOOH: pH 2.5 – 5.0 (pKa 3.8, buffer capacity β = 5.4 mM), CH$_3$COOH: 3.5 – 6.0 (pKa 4.8, β = 13.36), NH$_4$FA: pH 8.2 – 10.2 (pKa 9.2 of ammonium, β = 1.21 mM (pH 8) & 19.99 (pH 10)), NH$_4$Ac: pH: 8.2 – 10.2 (pKa 9.2 of ammonium, β = 13.36 (pH 10)), NH$_4$HCO$_3$: pH 9.0 – 11.5 (pKa 10.3, β = 1.48 mM) and NH$_4$OH: pH 8.0 – 10.5 (pKa 9.2, β = 5.42). Chromatographic conditions were applied as specified in Fig. 2 for YMC-Triart C18 ExRS.

With t_{begin} and t_{end} defining the beginning and the end of the gradient slope. The linear velocity of the mobile phase was kept constant at 2.95 mm/s for all separations and other method parameters, such as injection volume, were adjusted by method transfer protocols based on an initially defined method on the YMC-Triart C18 ExRS (30×3.0 mm, 1.9 μm) column [45] (for details see Suppl. Table S2). Differential normalized migration times ($\Delta t'$) between peptide API and its impurities were then calculated, which were above zero (impurity eluted after parent peptide), or below zero (impurity eluted before API). Eluents with 0.1% FA (low pH as ^{1}D mobile phase condition) and 10 mM NH$_4$OH (pH 9 as preliminary ^{2}D eluent) were selected for this screening (note, FA was used here in ^{1}D in replacement of TFA for its better compatibility with ESI-MS for identification of impurity peaks). pH 9 is high enough to be orthogonal to 0.1% FA and low enough that a wider range of RP columns can sustain such conditions. Fig. 2 shows the results of $\Delta t'$ values for acidic and basic eluents for three therapeutic peptides (Peptide 1, P1, Exenatide, Exe, and Octreotide, Oct) and their impurities (for details see Suppl. Table S3).

Peptide 1, Exenatide and Octreotide have p*I* values of 7.52, 9.44 and 6.21, respectively. Therefore, at pH 9 Peptide1 and Octreotide are net negatively charged, whilst Exenatide is net positively charged. Good selectivities between target peptide and impurities under acidic conditions were observed for YMC-Triart C18 ExRS (No. 1), Bonus RP (No. 3), HPH C18 (No. 4), Cortecs C18 (No. 5), and Kinetex C 18 (No. 9) (Fig. 2A). In general, selectivities between target peptide and impurities are worse at pH 9, except for Octreotide, as can be seen by a narrower spread close to the 0-line (Fig. 2B). However, the elution pattern is quite complementary as indicated by elution order reversals for many cases (see the change of many $\Delta t'$ values from positive in Fig. 2A to negative in Fig. 2B). Good potential as ^{2}D column due to reasonable selectivities between parent peptides and impurities is exhibited by the columns

YMC-Triart C18 ExRS (No. 1), HPH C18 (No. 4) and Synergi C 18 (No. 7).

Overall, the YMC Triart C18 ExRS column exhibited an overall superior performance at high pH and is able to cover a wide range of molecular sizes, endowing it with a favorable versatility for a generic peptide separation method. It also provides favorable pH stability (up to pH 12) and therefore adds more flexibility to adjust complementary selectivities in the alkaline pH range (note, HPH C18 could be a good replacement column for YMC Triart C18 ExRS for its favorable pH stability and good chromatographic performance). Complementarity plots with normalized retention times of peptide and impurities for the ^{1}D (Zorbax SB C18 at pH 2.0) and selected ^{2}D (YMC Triart C18 ExRS at pH 8.0) are shown in Fig. S3.

3.3. Optimization of ^{2}D mobile phase

As pointed out above, the eluent pH has a significant effect on solute retention of ionizable compounds, in particular of zwitterionic compounds like peptides. It is a prime experimental variable to fine-tune selectivity in RPLC. Therefore, a selection of buffer systems was examined for their suitability in the ^{2}D at ± 1 pH units around their optimal buffering capacity. The mobile phase pH was adjusted with the pH electrode in the aqueous mobile phase A, then equimolar amounts were used to prepare the organic phase (mobile phase B). The addition of organic solvent may shift the pH of the final mobile phase, but this shift is minor unless the organic content is very high. Only ammonium salts of volatile acids were used to prepare buffers in order to preserve CAD and MS-compatibility of the ^{2}D. With respect to organic modifier, both ACN and MeOH were compared in preliminary experiments, however, MeOH was finally preferred in the ^{2}D for several reasons: as a weaker solvent, analytes transferred from ^{1}D to ^{2}D can be retained and thus refocused more efficiently at the column head at the beginning of the gradient. Furthermore, since ACN is already
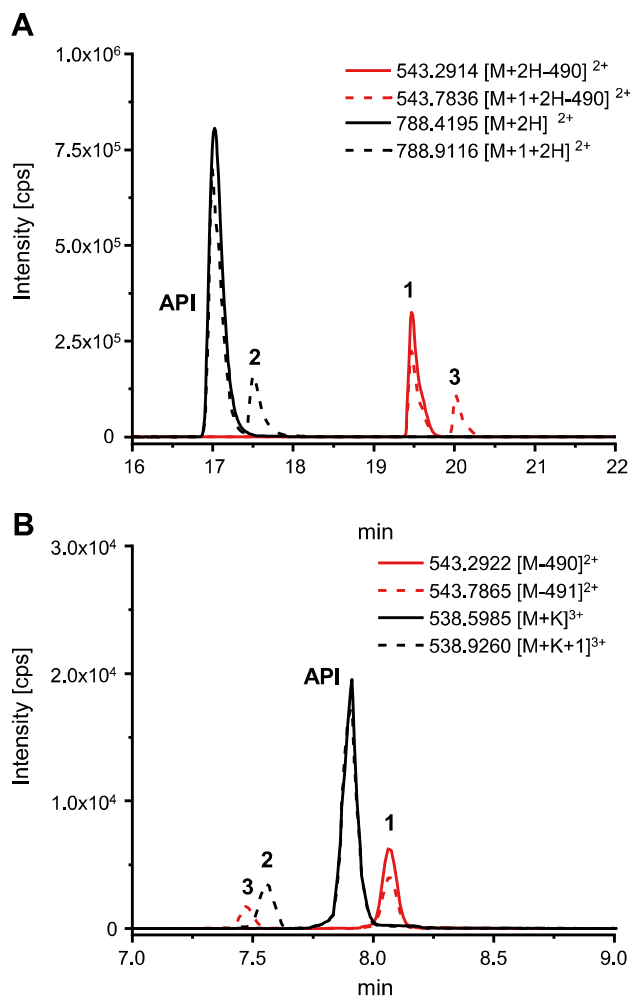
Fig. 4. 1D Extracted ion chromatograms of the synthetic model peptide (Peptide 1) at a) low pH and b) high pH. Conditions: a) Zorbax SBRP (100 mm x 2.1 mm i.d., 1.8 μm); flow rate, 0.259 mL/min; injection volume, 1.0 μL; gradient: 0 min (10%B) – 6.34 min (10%B) – 34.76 min (100%B) – 44.24 min (100%B) – 44.55 min (10%B) – 55 min (10%B). Mobile phase A and B were 0.1% FA in H_2O and ACN, respectively. b) YMC-Triart C18 ExRS (30 mm x 3.0 mm i.d., 1.9 μm); flow rate, 0.5 mL/min; injection volume, 1.6 μL; gradient: 0 min (10%B) – 1 min (10%B) – 10 min (100%B) – 13 min (100%B) – 13.10 min (10%B) – 16 min (10%B). Mobile phase A was 10 mM NH_4HCO_3 in H_2O adjusted to pH 8 with NH_4OH, while mobile phase B was prepared with equivalent amounts of NH_4HCO_3 and NH_4OH in H_2O/MeOH (5:95, (v/v)). The Peaks represent the **API**, the cleavage product (**1**) and the respective deamidation products of API (**2**) and cleavage product (**3**).

used in ^{1}D, MeOH is supposed to reveal better mobile phase complementarity owing to its distinct solvation properties Fig. 3 shows the resulting chromatograms for proprietary Peptide 1 using multiple buffer systems in MeOH. The main impurity of peptide 1 is the deamidation of a Gln-side chain. At pH 3 (Fig. 3A) the impurity with Glu-side chain is eluted after the main peptide. At high pH (Fig. 3B-3G), more peaks become detectable compared to low pH with NH_4FA pH 3 which clearly indicates orthogonal selectivity between low and high pH (see Fig. 4 as well as Suppl. Figs S3 and S4 for further examples). The complementary selectivities at pH 3 and 8 may partly also originate from residual silanols on the silica-supported RP stationary phases: their dissociation is largely suppressed under acidic conditions, whereas at basic pH they are dissociated. Secondary interactions at pH 10 may evolve as repulsive electrostatic interactions for peptides above their pI thereby significantly modulating selectivities as compared to low pH.

Besides selectivity aspects, selection of a suitable buffer is also of importance from two other viewpoints. First, some peptides such as proprietary Peptide 1 which carries several acidic and basic

ionizable moieties, are troublesome and are prone to peak splitting if inappropriate conditions are chosen. As can be seen from Fig. 3E, Peptide 1 shows a peak splitting under conditions of ammonium acetate buffer pH 10. Both the main peptide peak (API) as well as the prior eluted impurity peak (2) are split into two peaks. On the contrary, this phenomena is mitigated for the corresponding NH_4FA buffer pH 10 (Fig. 3F). Hence, it is not pH related but originates from other effects. A reasonable buffering capacity of the ^{2}D eluent appears to be of utmost importance because the transferred fractions (0.1% TFA) are strongly acidic and need to be buffered properly to avoid peak shape problems in the ^{2}D [46,47]. Second, for impurity profiling using UV detection it is mandatory to have an eluent with high UV transparency at low wavelength (like 215 nm). The generic peptide eluent with 0.1% TFA is advantageous in this respect. Buffers containing UV absorbing anion like NH_4FA, NH_4Ac, NH_4HCO_3 have elevated noise levels leading to reduced detection sensitivities (because of lower S/N). Hence, NH_4OH by itself which does not contain a UV-absorbing anion might be first choice in this regard.

3.4. Selective comprehensive 2D-LC

To this point in the work, ^{1}D and ^{2}D separations have been developed individually. However, their online hyphenation is constrained by additional considerations. Consequently, 2D-LC method development must encounter multiple key decisions, some of which follow principles valid for 1D-LC while others are specific for 2D-LC [18]. Besides individual optimization of phase systems and gradient profiles of both dimensions, 2D-LC method development must take into account orthogonality of ^{1}D and ^{2}D phase systems [25,48], sampling frequency, and in particular mobile phase compatibilities [19], which increases the overall complexity of 2D method development.

For selective comprehensive 2D-LC, to some extent, the same principles apply as for full comprehensive 2D-LC. A peak from the first dimension (or actually a region of the ^{1}D chromatogram) is quantitatively transferred into the second dimension by a series of consecutive multiple heart cuts. To avoid remixing of peaks separated in ^{1}D and preserve the resolution of ^{1}D, undersampling has to be precluded also in sLCxLC. It can be minimized, if the targeted peak is approximately sampled at least four times across its 8σ peak width [49]. However, since we want to detect small impurity peaks coeluted with an overloaded and tailing main peak, more than 4 fractions may be desirable. For example, in Fig. 1 10 fractions were collected between 7.87 and 9.25 min with a sampling time of 8 s. At a ^{1}D flow rate of 200 μL/min this corresponds to around 270 μL total sample volume (or 27 μL per cut). The first 5 cuts totally cover the entire target peptide peak and thus allow a comprehensive transfer and separation in the ^{2}D without significant remixing and resolution loss, respectively. After capturing the fractions in the 40 μL loops, they are temporarily stored and serially injected into the ^{2}D. The analysis of the fractions stored in the decks occurs in the reversed order of their filling in order to avoid carryover and minimize valve switches. Once all sample loops are filled, any consequent sampling becomes impossible until the loops have been emptied. Thus, fast runs in ^{2}D are advantageous as loops become available quickly for collecting further fractions. It means, all sample loops can be reused multiple times during one run, which yields a high storage capacity. While this may seem complicated, the process of parking and analyzing cuts is fully automated.

Effective sLC×LC, like other 2D-LC modalities, requires orthogonal retention characteristics in ^{1}D and ^{2}D. In principle this is straightforward to achieve by theory, especially for peptides, via distinct phase systems in ^{1}D and ^{2}D, as pointed out above. However, one has to consider that extremely large sample volumes are injected into the ^{2}D ($^2V_{inj}$ ~40 μL). This corresponds to about
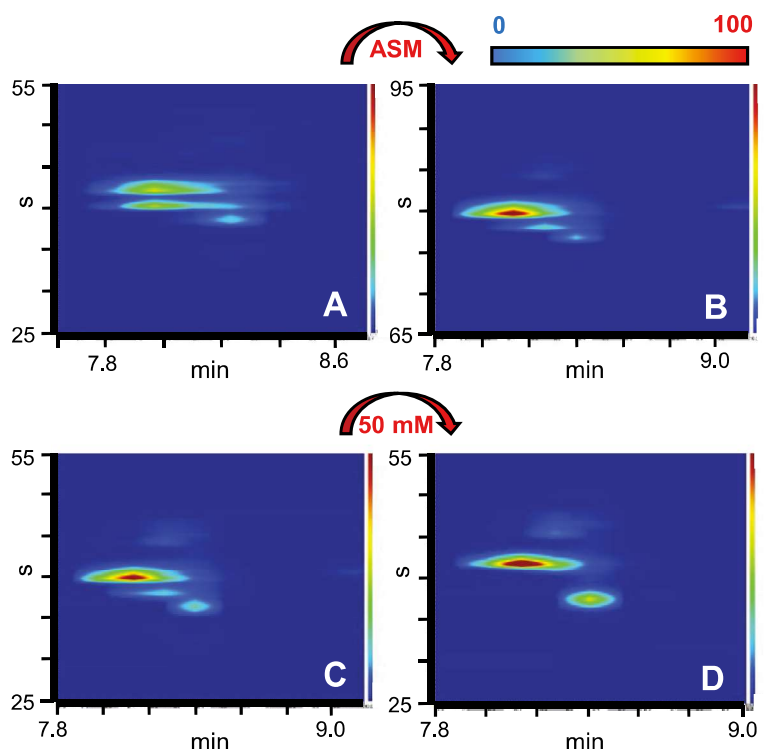
Fig. 5. Solvent compatibility mismatch in sRP×RP 2D-LC and possibilities to overcome this problem: (A) Peak splitting for Peptide 1 induced by pH mismatch in ^{2}D. (B) Its mitigation due to the use of active solvent modulation ASM. (C) Effect of acid additive in ^{1}D on peak splitting (0.1% TFA in ^{1}D as compared to 0.1% FA in (a). (D) Mitigation of peak splitting by use of high buffer concentration in the ^{2}D. Conditions: **A** - ^{1}D: 0.1% FA & ^{2}D: 10 mM NH$_4$FA; **B** - ^{1}D: 0.1% FA and ^{2}D: 10 mM NH$_4$FA; **C** - ^{1}D: 0.1% TFA & ^{2}D: 10 mM NH$_4$FA; **D** - ^{1}D: 0.1% TFA and ^{2}D: 50 mM NH$_4$FA. The mobile phase mismatch is more severe with FA than with TFA. .
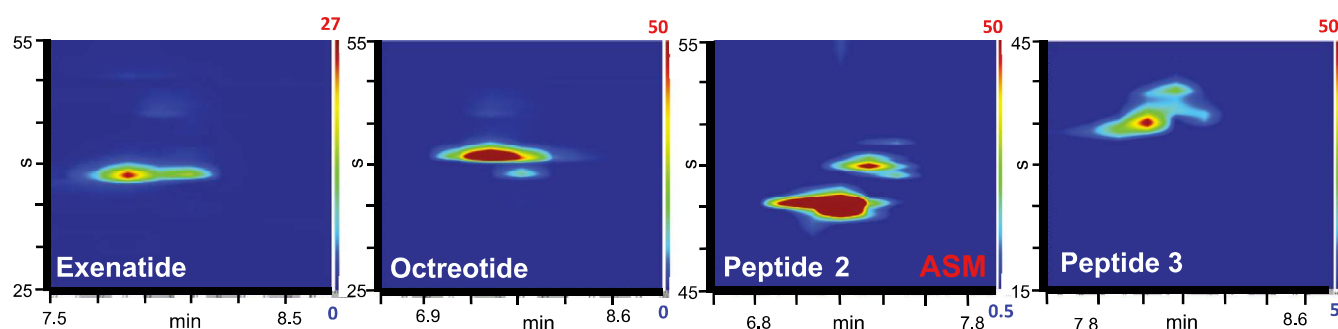

Fig. 6. Two-dimensional contour plots for four different therapeutic peptides generated with generic sRP×RP 2D-LC method presenting their impurity profiles (UV detection). A generic RP method was applied in the ^{1}D containing 0.1% TFA in both MP-A (H$_2$O) and MP-B (ACN). The ^{2}D is operated at pH 10 containing 10 mM NH$_4$FA in both MP-A (H$_2$O) and MP-B (95% MeOH in H$_2$O).

28% of the ^{2}D column void volume. In the example shown in Fig. 1, around 67% of the 40 µL loop are filled with ^{1}D mobile phase. It might easily lead to solvent incompatibility issues even in (s)RP×RP, which are detrimental to ^{2}D chromatographic performance. When the ^{1}D solvent strength exceeds that of the ^{2}D eluent, sample components, especially weakly retained ones in the ^{2}D column, may easily traverse the ^{2}D column with little or no retention and separation (breakthrough) or as splitted zones (peak splitting). To avoid or minimize eluent mismatch effects either ^{2}D column inner diameter should be increased (so that the sampled volume in ^{1}D represents maximal 15% of the column volume of ^{2}D), mobile phases adjusted, or active solvent modulation applied. Fig. 5. depicts the effects of peak splitting resulting from pH mismatches between the dimensions, where the pH of the solvent plug containing the sampled analyte does not fully equilibrate with the surrounding medium [47]. It is most severe, when FA (Fig. 5A) is used in the ^{1}D rather than TFA (Fig. 5C). Likely because TFA is

much more efficient as an ion pairing agent to increase the hydrophobicity of the peptide. Thus, the resulting retention at the entrance of the column of the ^{2}D is stronger, which in turn reduces the initial band broadening. One possibility to solve this problem is to utilize the on-column re-focusing effect by diluting the sample with weak solvent prior to the introduction into the ^{2}D column. For the ^{2}D separation it was shown that up to 90% of the native column efficiency was regained by diluting the ^{1}D effluent three- to four-fold [50]. This concept of focusing is particularly useful where large volumes are injected and has been successfully demonstrated most recently by the use of an ASM valve [51]. However, it is recommended to use the more retentive column in the second dimension to generally achieve the focusing effect to a certain extent. Fig. 5B shows the effect of using an ASM valve. By diluting the solvent plug with mobile phase containing the targeted pH reduces the peak splitting as compared to standard operation without the ASM valve shown in Fig. 5A. Besides
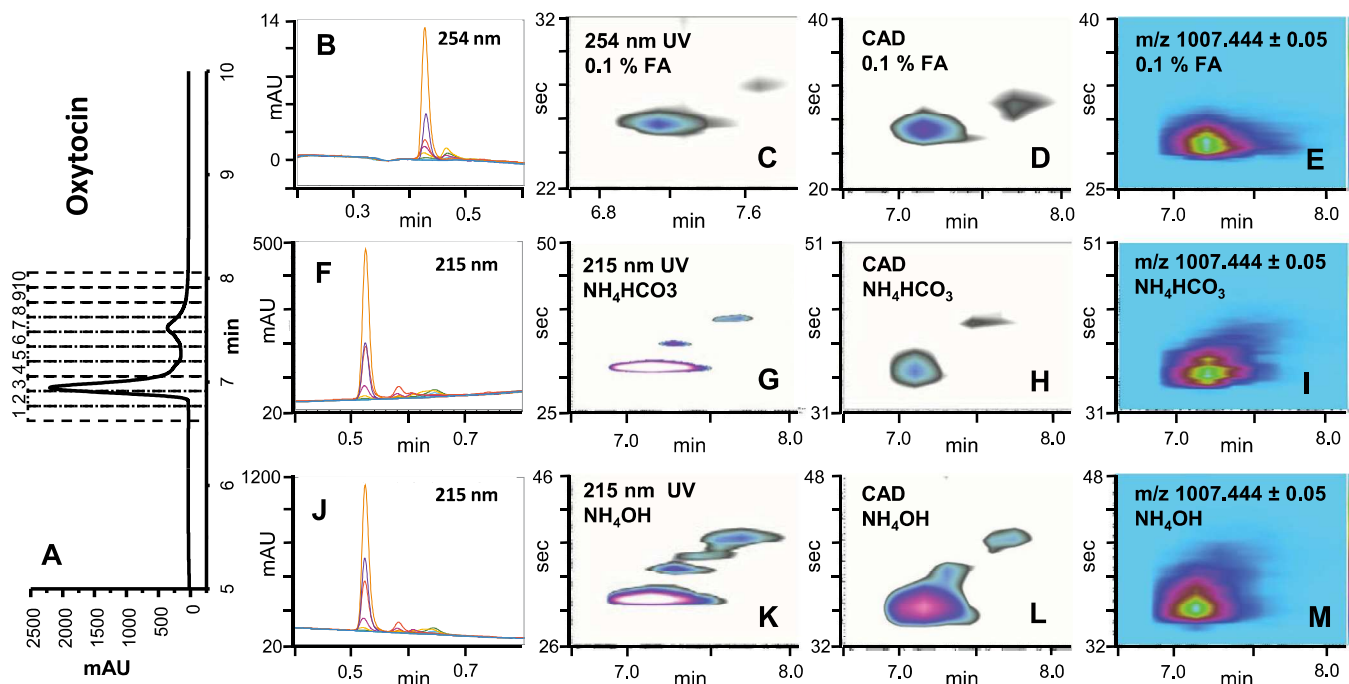
Fig. 7. The 2D-LC impurity profiles of Oxytocin under different ^{2}D mobile phase conditions with multiple complementary detectors utilizing UV (DAD), Charged Aerosol Detection (CAD) and ESI-QTOF MS through a split arrangement as depicted in Suppl. Fig. S2. The ^{1}D separation was performed with 0.1% TFA as additive. The separation in the ^{2}D was executed with ^{2}D mobile phases adjusted to low (0.1% FA) and high pH (NH$_4$HCO$_3$ at pH 8 and NH$_4$OH at pH 9).

ASM valve, the pH mismatch-induced peak splitting (Fig. 5C) can also be efficiently mitigated by using higher buffer concentrations in ^{2}D eluent (Fig. 5D). The advanced generic conditions suggested comprise 0.1% TFA in the ^{1}D (Zorbax SB C18, 100×2.1 mm, 1.8 μm) and 10 mM NH$_4$OH in the ^{2}D (YMC Triart C18 ExRS, 30×3.0 mm, 1.8 μm). For standard peptides, ASM is not needed for the generic sRP×RP 2D-LC method. However, for peptides with multiple ionizable groups (e.g. peptides used for imaging that have chelating moieties) use of ASM is highly recommended to avoid peak splitting.

The established generic sRP×RP 2D-LC method was applied to a set of four further peptides (Fig. 6). It can be seen in the contour plots that in all (except for Exenatide) additional peaks were detected by 2D-LC which were co-eluted in the ^{1}D. The presented examples of impurity profiling of therapeutic peptides convincingly demonstrate that the generic 1D-RPLC is at high risk to overlook impurities in QC of therapeutic peptides while the advanced generic sRP×RP 2D-LC impurity profiling method provides more reliable analysis that all impurities are detected.

3.5. Enhancing comprehensiveness by hyphenation with multiple complementary detectors

QC laboratories typically employ liquid chromatographic methods with UV detection. For peptides and their impurities this is usually adequate due to the chromophoric properties of the amide bond that allows essentially generic detection at 215 nm. Due to the ability to record multiple wavelengths and even a full spectrum, the use of a DAD provides additional capabilities such as to derive information on the presence of aromatic amino acids in peptide impurities and also demonstrates outstanding selectivity for different compounds. However, any impurities and/or degradants that lack a chromophore may not be detectable, and at low wavelengths baseline drifts and disturbances may be observed due to the absorbance of mobile phases and additives. With a dynamic range of four orders of magnitude the CAD further allows an

impurity profiling in the concentration range of 0.1% to 0.5% relative to the API, which is in compliance with regulatory thresholds (e.g. ICH). Further, the suggested 2D-LC setup is generic, and therefore the selective comprehensive sampling area in the ^{1}D chromatogram is variable, which is useful to evaluate non co-eluting (in regard to API) impurities when necessary (e.g. for the less UV detectable short chained peptides) and/or inorganic impurities or counterions. Consequently, the aim was to establish a more advanced impurity profiling setup in which the new sRP×RP 2D-LC system is combined with complementary detection principles, viz. UV (DAD), CAD (for non-chromophoric non-volatile impurities, and ESI-QTOF-MS (for structural information). The experimental setup with the multi-detector configuration is schematically depicted in Suppl. Fig. S3. The effluent from the ^{2}D column was divided by a flow splitter in the ratio 5:1 whereby the smaller flow was directed to the QTOF instrument. The larger volumetric flow was directed to the DAD detector and CAD that was coupled in-line with UV.

The great utility of such an advanced generic impurity profiling setup, is depicted in Fig. 7 for Oxytocin. In ^{1}D, there is at least one major side product eluting after the Oxytocin peak and a shoulder at the tailing edge of the latter that can be observed (see Fig.7A). selective comprehensive sampling enabled fractionation of the entire critical chromatographic region, i.e. both the target peptide and also the impurity peak, comprehensively into the ^{2}D. Three different buffer systems were applied in the ^{2}D (0.1% FA, 10 mM NH$_4$HCO$_3$ and 10 mM NH$_4$OH). When using 0.1% FA as ^{2}D mobile phase, there is little orthogonality but there is enhanced separation of the impurity peak in the 2D-setup (see Fig. 7B-E). However, there is also a minor deamidated species present in this sample, which is neither detectable in the 1D-LC chromatogram nor the sRP×RP 2D-LC with acidic ^{2}D separation (using 0.1% FA). The deamidated species is only resolved when high pH is applied in the ^{2}D. For example, with NH$_4$HCO$_3$ buffer at least one additional peak was detected (see Fig. 7F-I). However, due to the high background in the CAD signal when using NH$_4$HCO$_3$ the minor impurity peaks disappear in the corresponding contour plot. NH$_4$OH
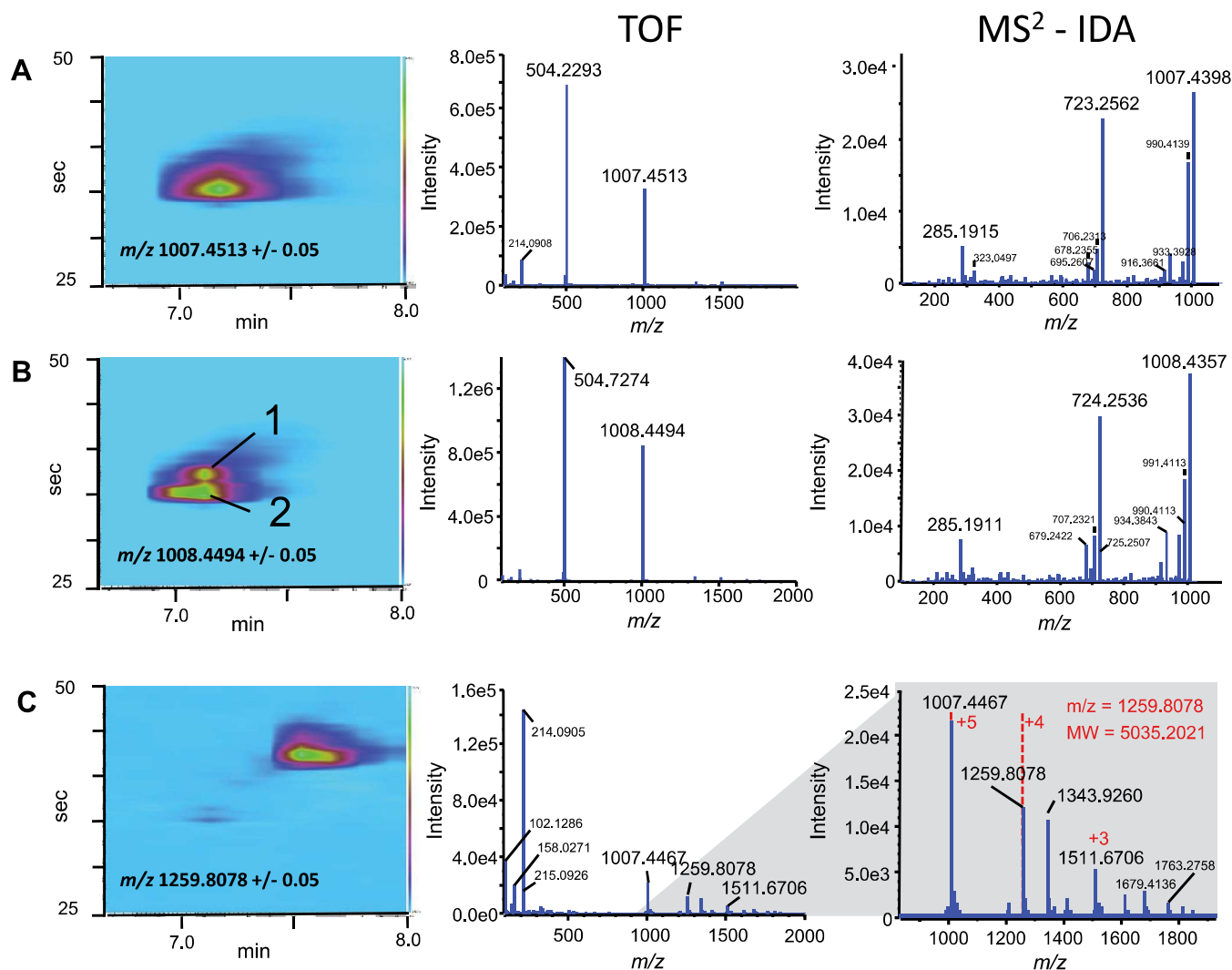
Fig. 8. EICs of Oxytocin (upper row), deamidation product (middle row) and oligomers (bottom row) are depicted as 2D profiles. The corresponding MS spectra (middle column) and the MS² fragmentation pattern (right column of upper and middle row) are used for identification and verification, respectively. The deconvoluted mass is shown for the oligomeric impurity of high molecular mass (right column bottom row). B: 1, deamidation impurity of API, 2, API (Oxytocin).

appears to be superior, both for CAD, but also UV detection due to absence of a chromophoric anion (see Fig. 7J-M). Indeed, peaks were more intensive in the corresponding UV contour plot as compared to the NH_4HCO_3 2D chromatogram.

Comprehensive characterization of a peptide API requires adequate tests for verification of the identity in addition to testing for impurities. This can be accomplished by the QTOF detector in our multi-detector setup. It allows determination of the accurate mass of the peptides and impurities and records MS/MS spectra that may also provide sequence information. As pointed out above, flow splitting is required because CAD and MS are both destructive detection methods. Splitting of the flow has the advantage that low flow rates can be used entering the ESI source and thus improve the ionization efficiency, while at the same time the higher flow is introduced to the UV-CAD flow path securing sufficient sensitivity for the detection of impurities. Extracted ion chromatograms (EICs) of Oxytocin and impurities are shown in Fig. 7 (E, I & M) and 8. The MS data allowed the identification of the spots in the UV and CAD contour plots. Fig. 8 illustrates the contour plots and corresponding MS as well as MS/MS spectra of the target peptide (Fig. 8A), deamidation impurity (Fig. 8B) and another impurity peak (oligomer) (Fig. 8C). Both MS and MS/MS data of the main peak clearly identify it as Oxytocin (Fig. 8A). The

main fragment of Oxytocin with m/z 723.2562, which is also commonly used as the characteristic product ion in quantitative single-reaction-monitoring assays, is clearly detectable in the IDA spectrum and results from side chain cleavage of Pro-Leu-Gly-NH_2 (see Suppl. Fig. S5). The second spot in the UV and CAD contour plot of Fig. 7, bottom (NH_4OH as ²D eluent) could be identified as deamidation product of Oxytocin. The respective EIC contour plot of m/z 1008.4494 in Fig. 8B shows two peaks because the singly charged deamidation product is not sufficiently resolved at TOF mass resolution from the $M + 1$ isotope peak of singly charged Oxytocin. So the peak at $^1t_R/^2t_R$ of 7.1 min/35 s corresponds to Oxytocin and the second peak at 7.1 min/38 s represents its degradation product, i.e. deamidated Oxytocin. This is confirmed by the MS/MS spectrum of this peak shown in Fig. 8B which lacks the corresponding characteristic Oxytocin fragment with m/z 723.2562, but shows instead the fragment with m/z 724.2536, indicating deamidated Oxytocin of one of the cyclic amide residues. The sRP×RP chromatogram shows another peak in the UV and CAD contour plot of Fig. 7. It is separated from the target peptide in both ¹D and ²D and has higher mass than oxytocin. The EIC contour plot of m/z 1259.4469 is shown in Fig. 8C along with MS spectra. Based on MS data, this impurity peak turns out to correspond to oligomeric forms of Oxytocin (tetrameric $m/z = 1344.2621$, pentameric
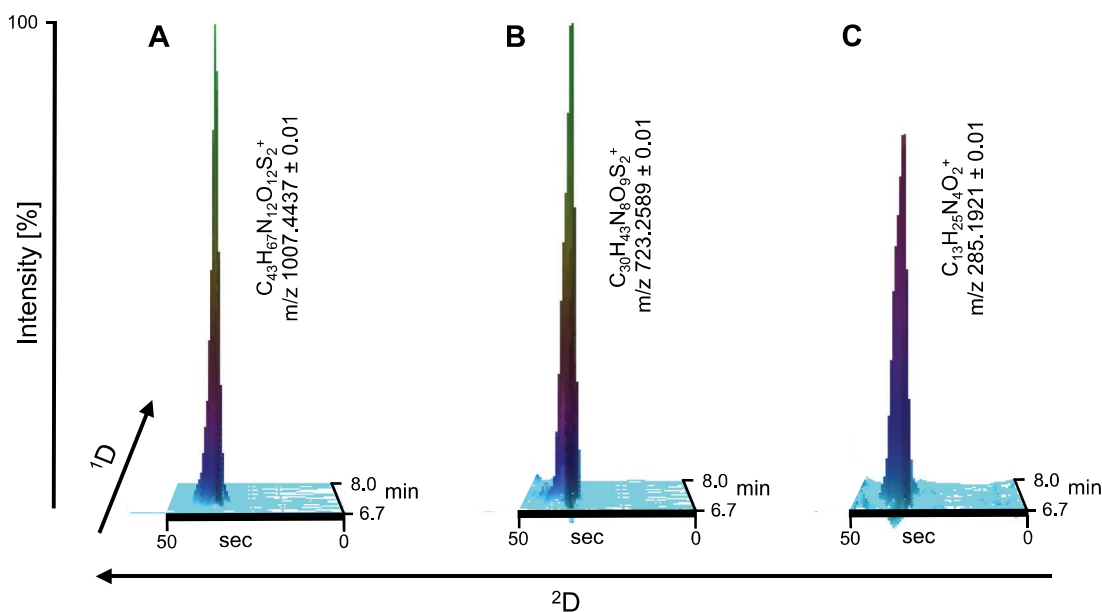
Fig. 9. 3D contour plots from SWATH data. Shown are extracted ion chromatograms from SWATH window 27 (see Table S4 for SWATH design). (a) EIC of Oxytocin (m/z 1007.4437 ± 0.01), (b) EIC of the main product ion from MS^2 of m/z 723.2589 ± 0.01 (cyclic peptide fragment without exocyclic peptide chain) and (c) EIC of fragment ion with m/z 285.1921 ± 0.01 (exocyclic peptide chain).

m/z 1259.4469, hexameric m/z = 1511.6706) (see also Suppl. Fig. S6).

A point to be considered is the difference in ionization efficiency between acidic and alkaline mobile phase, and thus the sensitivity of ESI-MS detection after the alkaline ^{2}D separation. Commonly, peptides do ionize well in acidic mobile phases in positive ion mode. It was less clear whether alkaline conditions give better sensitivity in positive or negative ion mode. For this reason, a preliminary study on the ionization efficiencies with acidic (0.1% FA) and alkaline (10 mM NH$_4$OH, pH 9) mobile phase was conducted with some model peptides (oxytocin, octreotide). Dilution series were prepared and analyzed with the two eluents by 1D-LC. Suppl. Fig. S7 illustrates the comparison of the slopes between acidic and alkaline eluents in positive and negative ion modes as measure for the instrumental detection sensitivities. It is evident that in general acidic conditions afford higher detection sensitivities both in positive and negative ion mode. However, the sensitivity was still quite acceptable under alkaline conditions (see Suppl. Fig. S7).

3.6. 2D-LC with SWATH-MS

The information density and comprehensiveness of the established peptide impurity profiling method can be further increased, when the QTOF-MS detector is operated in the data-independent acquisition mode. With IDA as described above, only the most abundant precursors from the MS full scan are selected for triggering MS/MS spectra with narrow (unit mass) precursor isolation width. Thus, MS/MS spectra are available for identification, but no MS/MS chromatograms can be extracted from the selective comprehensive 2D-LC-MS data. With DIA such as SWATH, MS/MS data are collected comprehensively in the chromatographic window acquired with selective comprehensive 2D-LC. Accordingly, contour plots and 2D-chromatograms can be created with both precursor and product ions, which may be, in some cases, more selective or more sensitive. To indicate the general ability of such 2D-LC SWATH-MS, the developed sRPxRP 2D-LC separation was combined with SWATH acquisition and used for the analysis of Oxytocin (for details of SWATH design see Experimental and Suppl. Table S4).

Fig. 9 depicts 3D chromatograms of precursor (Fig. 9A) and product ions (Fig. 9B and 9C). The product ion with m/z 723.2589 used to reconstruct the EIC of Fig. 9B corresponds to the characteristic cyclic peptide fragment resulting from peptide bond cleavage at the Pro-residue (see Suppl. Fig. S5). The product ion with m/z 285.1921 used for the EIC of Fig. 9C corresponds to the exocyclic peptide chain. Likewise, product ion EICs can be constructed for the peptide impurities providing support of their structure and presence in the peptide product. In this example there is no additional information gained from MS/MS chromatograms, however in other cases it may be a useful tool to solve specific selectivity problems.

In this proof of principle study we could document that expanded information on the quality of therapeutic peptides can be derived with the proposed advanced generic sRP-UV×RP-DAD-CAD-ESI-QTOF-MS/MS impurity profiling setup with SWATH.

4. Conclusion

Moving from a generic 1D-RPLC-UV towards an advanced generic sRP×RP 2D-LC method hyphenated online with UV-DAD, CAD and ESI-QTOF-MS/MS with SWATH as complementary detection schemes greatly increases the information content of analyses aimed at characterization of purified therapeutic peptides. It may allow for detection of critical impurities which tend to co-elute with the target peptide and remain undetected by 1D-RPLC. This 2D-LC setup uses the common generic RPLC method in the first dimension including a UV detector for acquiring a chromatogram that is comparable to what is the state of art until now. Only the main peak, or a region of the ^{1}D chromatogram that contains the main peptide peak, is transferred into the second dimension and separated by orthogonal conditions. High pH RPLC turned out to be advantageous due to high orthogonality to generic peptide separation under acidic conditions. Reasonable buffering capacity, and acceptable UV transparency for detection at 215 nm was achieved with 10 mM NH$_4$OH (pH 9). Also its volatility and ESI-MS compatibility is secured. The complementary detectors reduced the risk that relevant peptide-related and other impurities are overlooked. MS provides accurate mass and MS/MS sequence information. The

resultant advanced generic 2D-LC system can therefore be classified as multi-attribute method providing information on critical quality attributes of therapeutic peptides such as identity and peptide related impurities, as well as other impurities. If the first and second dimension separations are performed individually in two independent runs, the correspondence between them is lost and it is unclear whether impurities were hidden beneath the main peptide peak. The generic first dimension conditions are also not ideal for ESI-MS hyphenation, while this problem is circumvented by the ESI-MS compatible conditions of the ^{2}D separation in the 2D-LC setup. Using a short column filled with sub-2 μm particles in ^{2}D enables the 2D-LC analysis at no extra time. For quantification, fully resolved impurity peaks and quantification by UV at 215 nm is more reliable than quantification of an impurity co-eluted with the main peptide by ESI-MS. Overall, the quality of released synthetic peptides often deserves improvements and better QC methods could certainly contribute to this important endeavor.

Declaration of Competing Interest

The authors declare no conflict of interests.

CRediT authorship contribution statement

Ryan Karongo: Investigation, Methodology, Formal analysis, Data curation, Visualization, Writing - original draft, Writing - review & editing. **Tohru Ikegami:** Supervision, Writing - review & editing, Funding acquisition. **Dwight R. Stoll:** Writing - review & editing, Funding acquisition. **Michael Lämmerhofer:** Conceptualization, Methodology, Supervision, Writing - review & editing, Resources, Funding acquisition.

Acknowledgements

Supplementary materials

Supplementary material associated with this article can be found, in the online version, at doi:10.1016/j.chroma.2020.461430.

References

[1] M. D'Hondt, N. Bracke, L. Taevernier, B. Gevaert, F. Verbeke, E. Wynendaele, B. De Spiegeleer, Related impurities in peptide medicines, J, Pharm. Biomed. Anal. 101 (2014) 2–30, doi:10.1016/j.jpba.2014.06.012.

[2] K. Fosgerau, T. Hoffmann, Peptide therapeutics: current status and future directions, Drug Discov. Today 20 (2015) 122–128, doi:10.1016/j.drudis.2014.10.003.

[3] J.L. Lau, M.K. Dunn, Therapeutic peptides: historical perspectives, current development trends, and future directions, Biorg. Med. Chem. 26 (2018) 2700–2707, doi:10.1016/j.bmc.2017.06.052.

[4] A. Swietlow, H. Rode, A. Szajek, M. Verlander, I. Eggen, B. Gregg, Control strategies for synthetic therapeutic peptide APIs—Part I: analytical consideration, Pharm. Technol. 38 (2014).

[5] C.T. Mant, L.H. Kondejewski, P.J. Cachia, O.D. Monera, R.S. Hodges, Analysis of synthetic peptides by high-performance liquid chromatography, in: Methods Enzymol., Academic Press, 1997, pp. 426–469.

[6] J.R. Litowski, P.D. Semchuk, C.T. Mant, R.S. Hodges, Hydrophilic interaction/cation-exchange chromatography for the purification of synthetic peptides from closely related impurities: serine side-chain acetylated peptides, J. Pept. Res. 54 (1999) 1–11, doi:10.1034/j.1399-3011.1999.00066.x.

[7] W.S. Hancock, J.T. Sparrow, Use of mixed-mode, high-performance liquid chromatography for the separation of peptide and protein mixtures, J. Chromatogr. A 206 (1981) 71–82, doi:10.1016/S0021-9673(00)82606-0.

[8] M. Lämmerhofer, R. Nogueira, W. Lindner, Multi-modal applicability of a reversed-phase/weak-anion exchange material in reversed-phase, anion-exchange, ion-exclusion, hydrophilic interaction and hydrophobic interaction chromatography modes, Anal. Bioanal. Chem. 400 (2011) 2517–2530, doi:10.1007/s00216-011-4755-3.

[9] R. Nogueira, M. Lämmerhofer, W. Lindner, Alternative high-performance liquid chromatographic peptide separation and purification concept using a new mixed-mode reversed-phase/weak anion-exchange type stationary phase, J. Chromatogr. A 1089 (2005) 158–169, doi:10.1016/j.chroma.2005.06.093.

[10] B. Zhang, R. Soukup, D.W. Armstrong, Selective separations of peptides with sequence deletions, single amino acid polymorphisms, and/or epimeric centers using macrocyclic glycopeptide liquid chromatography stationary phases, J. Chromatogr. A 1053 (2004) 89–99, doi:10.1016/j.chroma.2004.06.117.

[11] A. Bajtai, I. Ilisz, D.H.O. Howan, G.K. Tóth, G.K.E. Scriba, W. Lindner, A. Péter, Enantioselective resolution of biologically active dipeptide analogs by high-performance liquid chromatography applying Cinchona alkaloid-based ion-exchanger chiral stationary phases, J. Chromatogr. A 1611 (2020) 460574, doi:10.1016/j.chroma.2019.460574.

[12] I. Federica, S. Roccaldo, C. Andrea, N. Benedetto, L. Wolfgang, L. Michael, Quinine-based zwitterionic chiral stationary phase as a complementary tool for peptide analysis: mobile phase effects on enantio- and stereoselectivity of underivatized oligopeptides, Chirality 28 (2016) 5–16, doi:10.1002/chir.22541.

[13] T. Zhang, E. Holder, P. Franco, M. Lämmerhofer, A. Sievers-Engler, H. Gerhardt, H. Gross, W. Lindner, Peptide analysis: zwitterionic chiral ion-exchangers as complementary option to HILIC and to reversed-phase chromatography, LCGC Eur. 29 (2016) 112–128.

[14] C.V. Hoffmann, R. Reischl, N.M. Maier, M. Lämmerhofer, W. Lindner, Stationary phase-related investigations of quinine-based zwitterionic chiral stationary phases operated in anion-, cation-, and zwitterion-exchange modes, J. Chromatogr. A 1216 (2009) 1147–1156, doi:10.1016/j.chroma.2008.12.045.

[15] Z. Tong, H. Emilie, F. Pilar, L. Wolfgang, Zwitterionic chiral stationary phases based on cinchona and chiral sulfonic acids for the direct stereoselective separation of amino acids and other amphoteric compounds, J. Sep. Sci. 37 (2014) 1237–1247, doi:10.1002/jssc.201400149.

[16] P.W.R. Harris, J.T. Lee, M.A. Brimble, A slow gradient approach for the purification of synthetic polypeptides by reversed phase high performance liquid chromatography, J. Pept. Sci. 18 (2012) 549–555, doi:10.1002/psc.2432.

[17] K. Zhang, X. Liu, Mixed-mode chromatography in pharmaceutical and biopharmaceutical applications, J. Pharm. Biomed. Anal. 128 (2016) 73–88, doi:10.1016/j.jpba.2016.05.007.

[18] D.R. Stoll, P.W. Carr, Two-dimensional liquid chromatography: a state of the art tutorial, Anal. Chem. 89 (2017) 519–531, doi:10.1021/acs.analchem.6b03506.

[19] B.W.J. Pirok, A.F.G. Gargano, P.J. Schoenmakers, Optimizing separations in online comprehensive two-dimensional liquid chromatography, J. Sep. Sci. 41 (2018) 68–98, doi:10.1002/jssc.201700863.

[20] P. Dugo, F. Cacciola, T. Kumm, G. Dugo, L. Mondello, Comprehensive multidimensional liquid chromatography: theory and applications, J. Chromatogr. A 1184 (2008) 353–368, doi:10.1016/j.chroma.2007.06.074.

[21] G. Vanhoenacker, I. Vandenheede, F. David, P. Sandra, K. Sandra, Comprehensive two-dimensional liquid chromatography of therapeutic monoclonal antibody digests, Anal. Bioanal. Chem. 407 (2015) 355–366, doi:10.1007/s00216-014-8299-1.

[22] D.A. Wolters, M.P. Washburn, J.R. Yates, An automated multidimensional protein identification technology for shotgun proteomics, Anal. Chem. 73 (2001) 5683–5690, doi:10.1021/ac010617e.

[23] M.P. Washburn, D. Wolters, J.R. Yates, Large-scale analysis of the yeast proteome by multidimensional protein identification technology, Nat. Biotechnol. 19 (2001) 242–247, doi:10.1038/85686.

[24] M. Gilar, P. Olivova, A.E. Daly, J.C. Gebler, Two-dimensional separation of peptides using RP-RP-HPLC system with different pH in first and second separation dimensions, J. Sep. Sci. 28 (2005) 1694–1703, doi:10.1002/jssc.200500116.

[25] M. Gilar, P. Olivova, A.E. Daly, J.C. Gebler, Orthogonality of separation in two-dimensional liquid chromatography, Anal. Chem. 77 (2005) 6426–6434, doi:10.1021/ac050923i.

[26] D. Yeung, B. Mizero, D. Gussakovsky, N. Klaassen, Y. Lao, V. Spicer, O.V. Krokhin, Separation orthogonality in liquid chromatography-mass spectrometry for proteomic applications: comparison of 16 different two-dimensional combinations, Anal. Chem. (2020), doi:10.1021/acs.analchem.9b05407.

[27] D. Stoll, J. Danforth, K. Zhang, A. Beck, Characterization of therapeutic antibodies and related products by two-dimensional liquid chromatography coupled with UV absorbance and mass spectrometric detection, J. Chromatogr. B 1032 (2016) 51–60, doi:10.1016/j.jchromb.2016.05.029.

[28] M. Sarrut, G. Crétier, S. Heinisch, Theoretical and practical interest in UHPLC technology for 2D-LC, TrAC, Trends Anal. Chem. 63 (2014) 104–112, doi:10.1016/j.trac.2014.08.005.

[29] M. Sarrut, F. Rouvière, S. Heinisch, Theoretical and experimental comparison of one dimensional versus on-line comprehensive two dimensional liquid chromatography for optimized sub-hour separations of complex peptide samples, J. Chromatogr. A 1498 (2017) 183–195, doi:10.1016/j.chroma.2017.01.054.

[30] K. Sandra, P. Sandra, The opportunities of 2D-LC in the analysis of monoclonal antibodies, Bioanalysis 7 (2015) 2843–2847, doi:10.4155/bio.15.210.

[31] M. Alvarez, G. Tremintin, J. Wang, M. Eng, Y.-.H. Kao, J. Jeong, V.T. Ling, O.V. Borisov, On-line characterization of monoclonal antibody variants by liq-

uid chromatography–mass spectrometry operating in a two-dimensional format, Anal. Biochem. 419 (2011) 17–25, doi:10.1016/j.ab.2011.07.033.

[32] D.R. Stoll, D.C. Harmes, J. Danforth, E. Wagner, D. Guillarme, S. Fekete, A. Beck, Direct identification of rituximab main isoforms and subunit analysis by on-line selective comprehensive two-dimensional liquid chromatography–mass spectrometry, Anal. Chem. 87 (2015) 8307–8315, doi:10.1021/acs.analchem.5b01578.

[33] I. François, D. Cabooter, K. Sandra, F. Lynen, G. Desmet, P. Sandra, Tryptic digest analysis by comprehensive reversed phase×two reversed phase liquid chromatography (RP-LC×2RP-LC) at different pH's, J. Sep. Sci. 32 (2009) 1137–1144, doi:10.1002/jssc.200800578.

[34] P. Donato, F. Cacciola, E. Sommella, C. Fanali, L. Dugo, M. Dachà, P. Campiglia, E. Novellino, P. Dugo, L. Mondello, Online comprehensive RPLC × RPLC with mass spectrometry detection for the analysis of proteome samples, Anal. Chem. 83 (2011) 2485–2491, doi:10.1021/ac102656b.

[35] I. Eggen, B. Gregg, H. Rode, A. Swietlow, M. Verlander, A. Szajek, Control strategies for synthetic therapeutic peptide APIs Part III: manufacturing process considerations, Pharm. Technol. (2014) 38.

[36] A. Szajek, I. Eggen, B. Gregg, A. Swietlow, H. Rode, M. Verlander, Control strategies for synthetic therapeutic peptide APIs Part II: raw material considerations, Pharm. Technol. (2014) 38.

[37] M. Pursch, S. Buckenmaier, Loop-based multiple heart-cutting two-dimensional liquid chromatography for target analysis in complex matrices, Anal. Chem. 87 (2015) 5310–5317, doi:10.1021/acs.analchem.5b00492.

[38] M. Pursch, P. Lewer, S. Buckenmaier, Resolving co-elution problems of components in complex mixtures by multiple heart-cutting 2D-LC, Chromatographia 80 (2017) 31–38, doi:10.1007/s10337-016-3214-x.

[39] P. Petersson, K. Haselmann, S. Buckenmaier, Multiple heart-cutting two dimensional liquid chromatography mass spectrometry: towards real time determination of related impurities of bio-pharmaceuticals in salt based separation methods, J. Chromatogr. A 1468 (2016) 95–101, doi:10.1016/j.chroma.2016.09.023.

[40] D.R. Stoll, E.S. Talus, D.C. Harmes, K. Zhang, Evaluation of detection sensitivity in comprehensive two-dimensional liquid chromatography separations of an active pharmaceutical ingredient and its degradants, Anal. Bioanal. Chem. 407 (2015) 265–277, doi:10.1007/s00216-014-8036-9.

[41] Z. Wang, H. Ma, K. Smith, S. Wu, Two-dimensional separation using high-pH and low-pH reversed phase liquid chromatography for top-down proteomics, Int. J. Mass Spectrom. 427 (2018) 43–51, doi:10.1016/j.ijms.2017.09.001.

[42] H. Toll, H. Oberacher, R. Swart, C.G. Huber, Separation, detection, and identification of peptides by ion-pair reversed-phase high-performance liquid chromatography-electrospray ionization mass spectrometry at high and low pH, J. Chromatogr. A 1079 (2005) 274–286, doi:10.1016/j.chroma.2005.03.121.

[43] I. François, K. Sandra, P. Sandra, Comprehensive liquid chromatography: fundamental aspects and practical considerations—a review, Anal. Chim. Acta 641 (2009) 14–31, doi:10.1016/j.aca.2009.03.041.

[44] M. Sarrut, A. D'Attoma, S. Heinisch, Optimization of conditions in on-line comprehensive two-dimensional reversed phase liquid chromatography. Experimental comparison with one-dimensional reversed phase liquid chromatography for the separation of peptides, J. Chromatogr. A 1421 (2015) 48–59, doi:10.1016/j.chroma.2015.08.052.

[45] D. Guillarme, D.T. Nguyen, S. Rudaz, J.L. Veuthey, Method transfer for fast liquid chromatography in pharmaceutical analysis: application to short columns packed with small particle. Part II: gradient experiments, Eur. J. Pharm. Biopharm. 68 (2008) 430–440, doi:10.1016/j.ejpb.2007.06.018.

[46] D.R. Stoll, D.C. Harmes, Effects of pH mismatch between the two dimensions of reversed-phase×reversed-phase two-dimensional separations on second dimension separation quality for ionogenic compounds—I. Carboxylic acids, J. Chromatogr. A 1383 (2015) 25–34, doi:10.1016/j.chroma.2014.12.054.

[47] G. Leme, B. Madigan, J. Eikens, D.C. Harmes, D. Richardson, P. Carr, D. Stoll, In situ measurement of pH in liquid chromatography systems using a colorimetric approach, Anal. Methods 11 (2019) 381–386, doi:10.1039/C8AY02496K.

[48] M. Gilar, J. Fridrich, M.R. Schure, A. Jaworski, Comparison of orthogonality estimation methods for the two-dimensional separations of peptides, Anal. Chem. 84 (2012) 8722–8732, doi:10.1021/ac3020214.

[49] R.E. Murphy, M.R. Schure, J.P. Foley, Effect of sampling rate on resolution in comprehensive two-dimensional liquid chromatography, Anal. Chem. 70 (1998) 1585–1594, doi:10.1021/ac971184b.

[50] S.R. Groskreutz, M.M. Swenson, L.B. Secor, D.R. Stoll, Selective comprehensive multi-dimensional separation for resolution enhancement in high performance liquid chromatography. Part I: principles and instrumentation, J. Chromatogr. A 1228 (2012) 31–40, doi:10.1016/j.chroma.2011.06.035.

[51] D.R. Stoll, K. Shoykhet, P. Petersson, S. Buckenmaier, Active solvent modulation: a valve-based approach to improve separation compatibility in two-dimensional liquid chromatography, Anal. Chem. 89 (2017) 9260–9267, doi:10.1021/acs.analchem.7b02046.
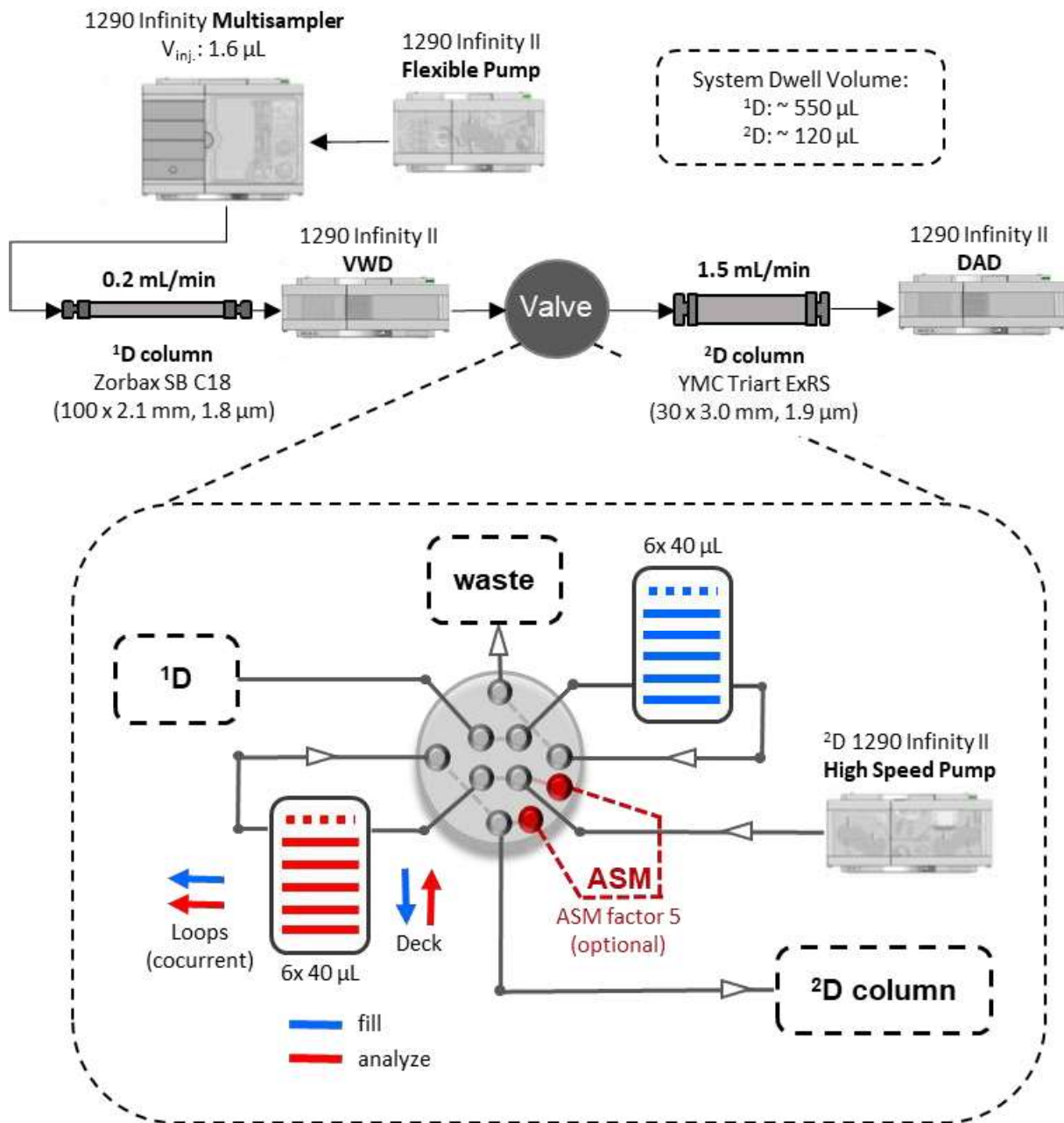
4.1.1 Supporting Information

Fig. S 1: 2D-LC Setup.
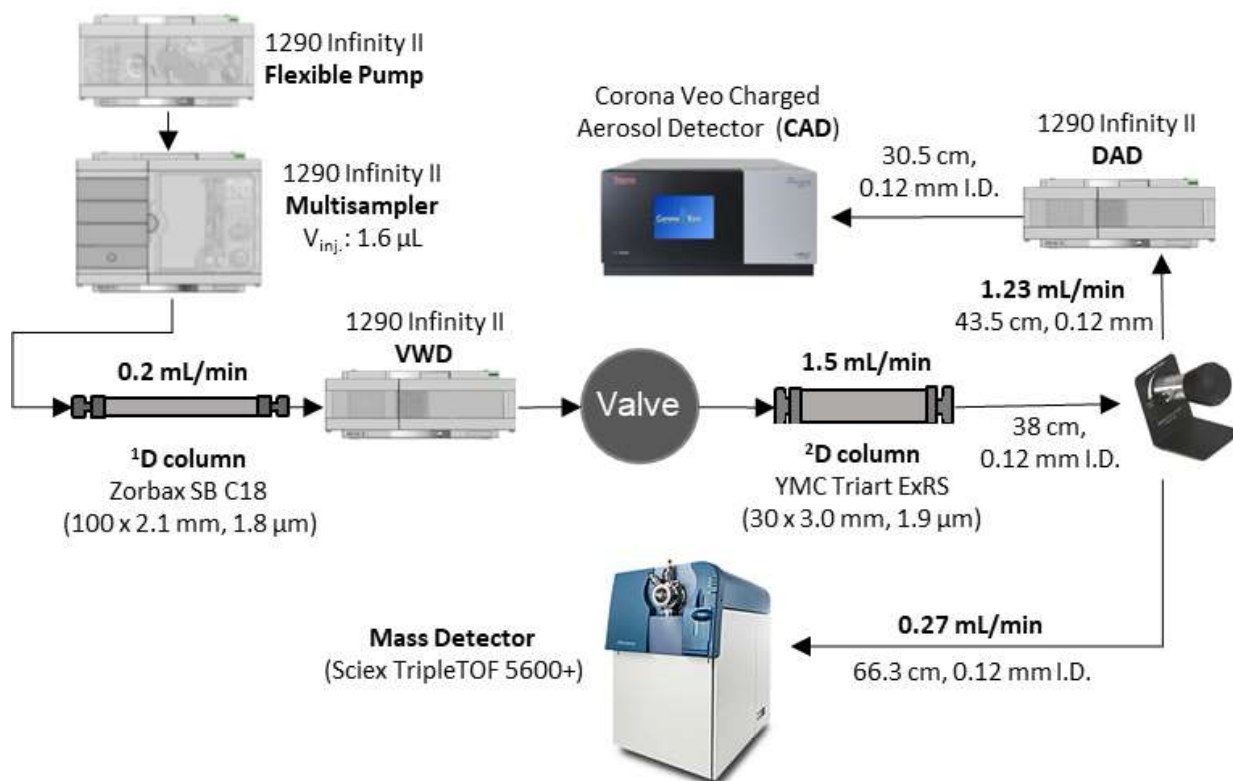
Fig. S 2: 2D-LC Setup with enhanced detection (note, some further reductions of extra-column system volumes after ^{2}D column could be beneficial in terms of separation performance, however, at expense of back pressure).

Fig. S 3: Complementarity plot of the ^{1}D column against the most favorable column for the ^{2}D for a set of therapeutic peptides using normalized retention values. Closed symbols, respective peptide API and corresponding open symbols impurity derived from this API.
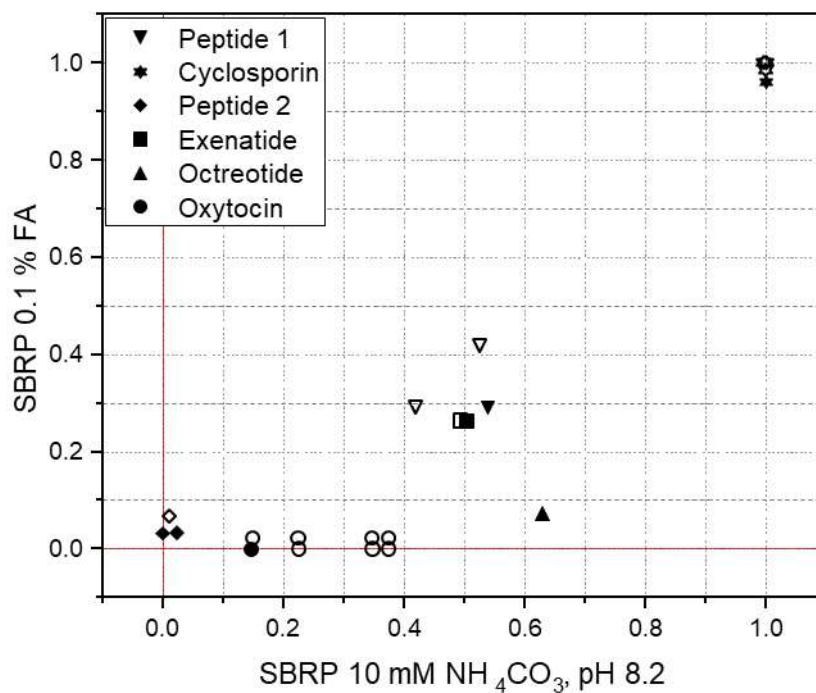
Fig. S 1: Orthogonality plot of normalized peptide retention obtained from two distinct mobile phases (acidic and alkaline) on the same column. Column: Agilent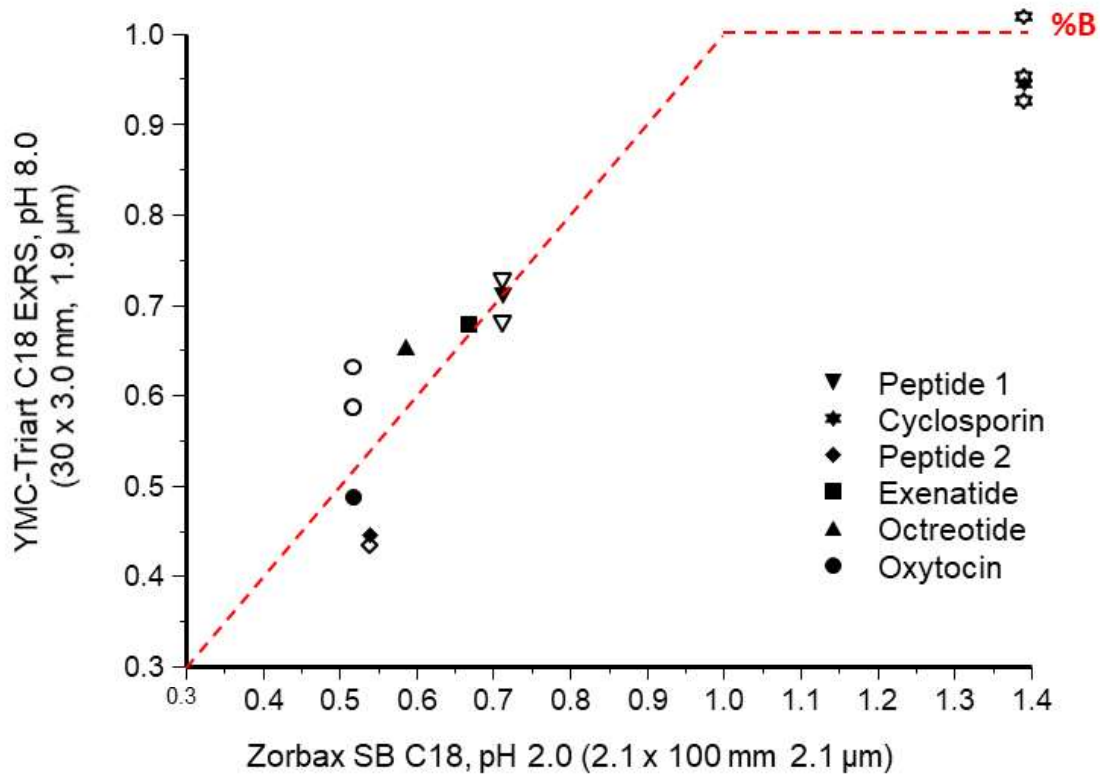 Zorbax SB-C18 (100 x 2.1 mm, 1.8 μm); mobile phase systems: system 1, 0.1 % FA in A (H_2O) and B (ACN), system 2, 10 mM NH_4HCO_3 in A (H_2O) and B (5 % H_2O in MeOH). The minimal and maximal retained compounds define the normalization borders of 0 and 1, respectively. The plot includes several synthetic peptides, and retention times were tracked using LC-MS measurements. Closed symbols, respective peptide API and corresponding open symbols impurity derived from this API.

**Table S 1:** Chromatographic 2D Conditions and mobile phases.

Column	Zorbax SB C18 (100 x 2.1 mm, 1.8 µm)	YMC Triart C18 ExRS (30 x 3.0 mm, 1.9 µm)
Flow rate [mL/min]	0.2 mL/min	1.5 mL/min
Inj. Vol. [µL]	2.8 µL	26.8 µL
Modulation time	-	8s
Temperature	30 °C	40 °C
Gradient	0 min 10 %B	0 min 10 %B
	1 min 10 %B	0.7 min 100 % B
	9 min 100 % B	0.71 min 10 %B
	11 min 100 %B	1 min 100 %B
	11.10 min 10 %B	
	15 min 10 %B	

Additive		TFA	HCOOH/ HCOO⁻	CH_3HCOOH/ CH_3HCOO^-	CO_3^{2-}	NH_4OH/NH_4^+	Buffer Capacity [β]
	[1]**TFA**	0.1 % (v/v) (12.98 mM)	-	-	-	-	
	[1]**FA**	-	0.1 % (v/v) (26.50 mM)	-	-	-	
	[2]**NH₄FA (pH 3)**	-	10 mM	-	-	0.77 mM	5.41 mM
	[2]**NH₄FA (pH 8)**	-	10 mM	-	-	10 mM + 0.51 mM	1.21 mM
Mobile phase A	[2]**NH₄FA (pH 10)**	-	10 mM	-	-	10 mM + 46.23 mM	19.99 mM
	[2]**NH₄Ac (pH 10)**	-	-	10 mM	-	10 mM + 33.34 mM	13.36 mM
	[2]**NH₄HCO₃ (pH 8)**	-	-	-	10 mM	-	1.48 mM
	[2]**NH₄HCO₃ (pH 10)**	-	-	-	10 mM	10 mM + 43.66 mM	27.90 mM
	[2]**NH₄OH (pH 9)**	-	+ 6.36 mM	-	-	10 mM	5.42 mM
Mobile phase B	equimolar in ACN ([1]D) or 5% H_2O in MeOH ([2]D)						

Table S 2: Method transfers were applied for the following columns preceding from the method parameters defined for column no.1.

No.	Column	Particle Size [μm]	Column Length [mm]	Column I.D. [mm]	Flow rate [mL/min]	V inj. [μL]	%B 10	%B 10	%B 100	%B 100	%B 10	%B 10
1	YMC-Triart C18 ExRS (30 x 3.0 mm, 1.9 μm)	1.9	30	3	0.5	1	0	1	10	13	13.1	16
2	YMC-Triart C8 (50 x 2.1 mm, 1.9 μm)	1.9	50	2.1	0.245	0.8	0	1.26	16.26	21.26	21.42	26.26
3	Agilent Zorbax Bonus RP (30 x 3.0 mm, 1.8 μm)	1.8	50	2.1	0.259	0.8	0	1.19	15.4	20.14	20.29	24.87
4	Agilent Poroshell HPH C18 (50 x 3.0, 1.9 μm)	1.9	50	3	0.5	1.7	0	2.4	17.4	22.4	22.57	27.4
5	Waters Cortecs C18 (50 x 2.0, 1.0 mm, 2.7 μm)	2.7	50	2.1	0.12	0.8	0	1.78	23.1	30.2	30.44	37.31
6	Phenomenex Kinetex EVO C18 (20 x 2.1 mm, 2.6 μm)	2.6	20	2.1	0.179	0.3	0	0	8.21	10.95	11.04	13.68
7	Phenomenex Synergi Fusion-RP (50 x 2.0 mm, 4.0 μm)	4	50	2	0.106	0.7	0	2.16	33.74	44.26	44.61	54.79
8	Agilent Zorbax Eclipse Plus C18 (50 x 3.0 mm 1.8 μm)	1.8	50	3	0.528	1.7	0	2.27	16.48	21.22	21.38	25.96
9	Phenomenex Kinetex C18 (50 x 4.6 mm, 2.6 μm)	2.6	100	3	0.365	3.3	0	8.07	49.13	62.81	63.27	76.49
10	Phenomenex Kinetex C8 (50 x 2.1 mm, 2.6 μm)	2.6	50	2.1	0.179	0.8	0	1.72	22.24	29.09	29.31	35.93
11	Phenomenex Kinetex PFP (100 x 3.0 mm, 2.6 μm)	2.6	100	3	0.365	3.3	0	8.07	49.13	62.81	63.27	76.49
12	InfinityLab Poroshell 120EC C18 (150 x 3.0 mm, 2.7 μm)	2.7	150	3	0.352	5	0	13.36	77.31	98.62	99.33	119.94

Table S 3: Compound retention times were normalized according to the resulting gradient time after column transfer. Delta values resulting from retention times between the APIs and their corresponding impurities were calculated and tabulated for a set of 15 reversed phase columns at different pH's (pH 2.7, 6.8 and 9). All columns were employed considering their pH stability. Missing values originate from co-eluting compounds or not acquired data due to pH instability of the columns.

| Column No.	Δt' (NB - deamidation) pH 2.7	pH 6.8	pH9	Δt' (Fragment - deamidation) pH 2.7	pH 6.8	pH9	Δt' (Fragment loss) pH 2.7	pH 6.8	pH9	Δt' (Exe - oxidation) pH 2.7	pH 6.8	pH9	Δt' (Oct - oxidation) pH 2.7	pH 6.8	pH9
1	0.016	0.021	-0.05	0.000	-	-0.041	0.064	-	-0.013	-0.029	-	-0.035	0.102	-0.067	-0.157
2	0.009	-0.005	-0.015	0.006	-	-0.013	0.037	-	-0.005	-0.030	-0.017	-	0.038	-0.037	-0.106
3	0.044	0.036	-0.036	0.012	-0.036	-0.033	0.132	0.054	-0.014	-0.071	-0.045	-	-0.476	0.091	-0.210
4	0.020	0.006	-0.022	0.016	-0.025	-0.019	0.068	0.014	-0.012	-0.050	0.000	-0.035	0.096	-0.056	0.096
5	0.010	-0.005	-0.029	0.008	-	-0.027	0.044	-	-0.008	-0.031	0.015	-0.023	0.110	-0.055	-0.134
6	-	0.000	-0.035	-	-	-0.035	-	-	-0.010	-	-	-	-	-0.075	-0.145
7	-	0.000	-0.054	-	-	-	-	-	-0.014	-	0.014	-	-	-0.059	-0.218
8	0.017	0.000	-0.037	0.009	-	-0.033	0.055	-	-0.013	0.000	-1,032	-0.036	0.099	-0.068	-0.142
9	0.015	0.000	-0.052	0.010	-0.020	-0.053	0.054	0.013	-0.013	0.043	0.026	-0.005	0.091	-0.071	-0.18
10	0.019	-0.003	-0.041	0.012	-	-0.037	0.057	-	-0.010	0.000	-	-0.007	0.068	-0.083	-0.183
11	0.000	-0.027	-0.072	0.000	-0.055	-0.072	0.000	0.019	0.000	0.000	-	-	-0.070	-0.174	-0.010
12	0.010	0.002	-0.013	0.006	-0.013	-0.011	0.031	0.008	-0.007	-0.021	-0.012	-	0.054	-0.038	-0.102
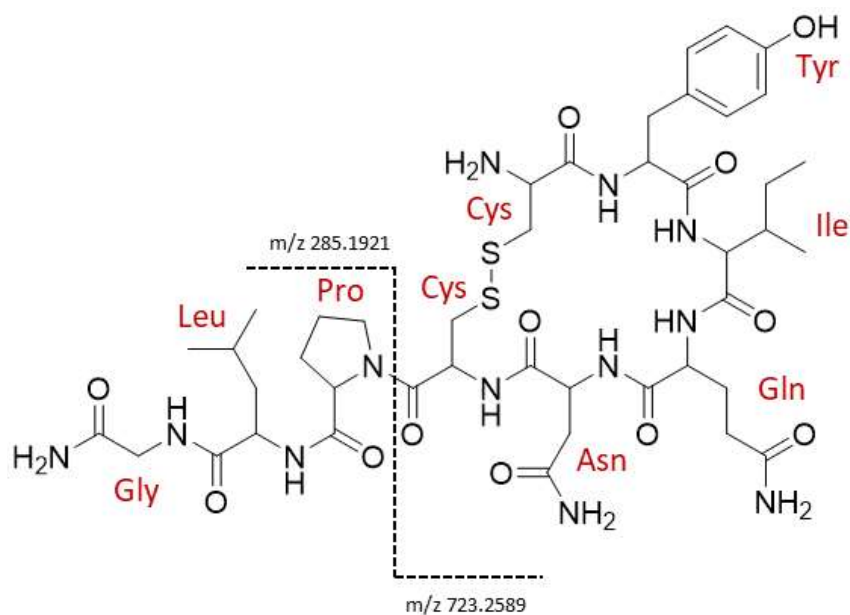
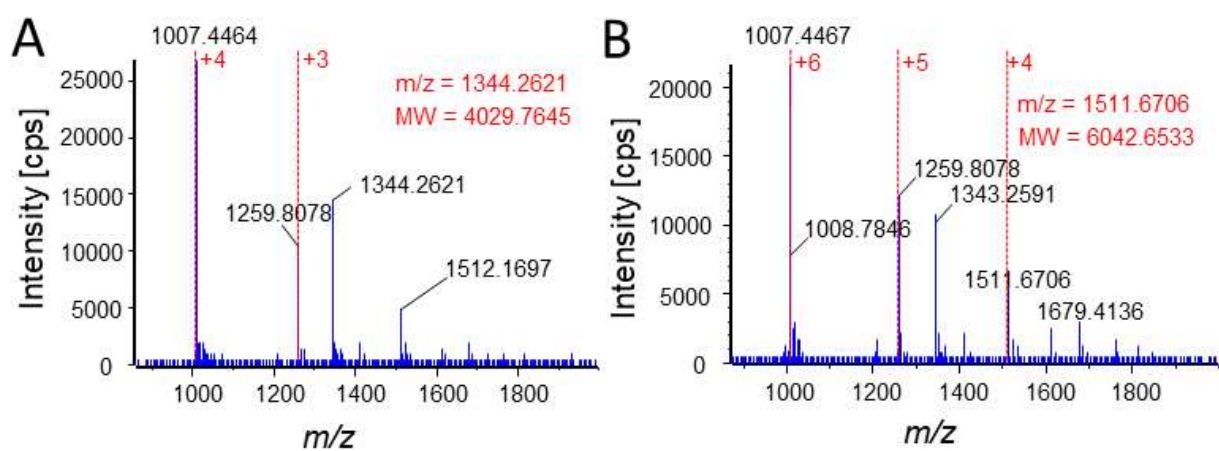**Fig. S5:** Structure and primary MS fragmentation of Oxytocin.

Fig. S6: MS/MS (IDA) spectra of impurity peak from ^{1}D/^{2}D retention time 7.6 min / 42.5 s (see Fig. 8 of main document): **A**: tetrameric form, **B**: hexameric form.
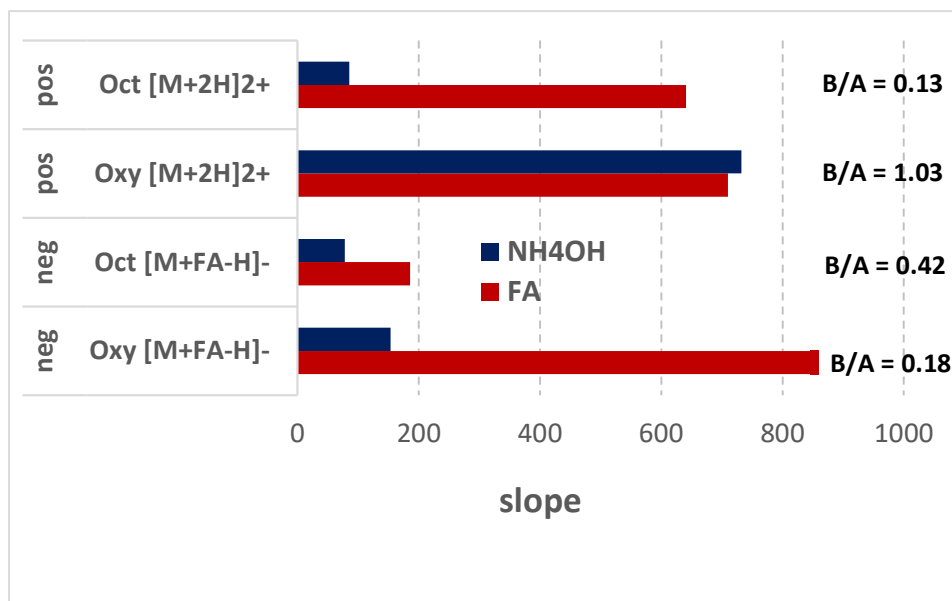
Fig. S7: A peptide mix containing oxytocin and octreotide were analysed in IDA mode at five times ten-fold dilution (beginning with 99.27 pmol and 69.66 pmol for Oxytocin and Octreotide, respectively) in positive and negative ion mode at low (0.1 % FA) and high pH (10 mM NH_4OH, pH 9.0). The calibration curve was determined and the slope plotted. Higher slopes correspond to a higher ionization efficiency. Relative ionization efficiencies in basic (B) and acidic conditions (A) are depicted as B/A ratios of respective slopes of calibration functions.

Table S4: Design of the SWATH experiment for ESI+.

| Experiment	MS Type	Min m/z	Max m/z	Accumulation Time (ms)	CE (V)	CES (V)
0	SCAN	100	2000	50	10	-
1	SWATH	200	230	12	9.848	15
2	SWATH	229	260	12	11.676	15
3	SWATH	259	290	12	13.555	15
4	SWATH	289	320	12	15.433	15
5	SWATH	319	350	12	17.311	15
6	SWATH	349	380	12	19.188	15
7	SWATH	379	410	12	21.065	15
8	SWATH	409	440	12	22.941	15
9	SWATH	439	470	12	24.818	15
10	SWATH	469	500	12	26.694	15
11	SWATH	499	530	12	28.570	15
12	SWATH	529	560	12	30.446	15
13	SWATH	559	590	12	32.322	15
14	SWATH	589	620	12	34.198	15
15	SWATH	619	650	12	36.073	15
16	SWATH	649	680	12	37.949	15
17	SWATH	679	710	12	39.825	15
18	SWATH	709	740	12	41.700	15
19	SWATH	739	770	12	43.576	15
20	SWATH	769	800	12	45.451	15
21	SWATH	799	830	12	47.327	15
22	SWATH	829	860	12	49.202	15
23	SWATH	859	890	12	51.077	15
24	SWATH	889	920	12	52.953	15
25	SWATH	919	950	12	54.828	15
26	SWATH	949	980	12	56.703	15
27	SWATH	979	1010	12	58.579	15
28	SWATH	1009	1040	12	60.454	15
29	SWATH	1039	1070	12	62.329	15
30	SWATH	1069	1100	12	64.204	15
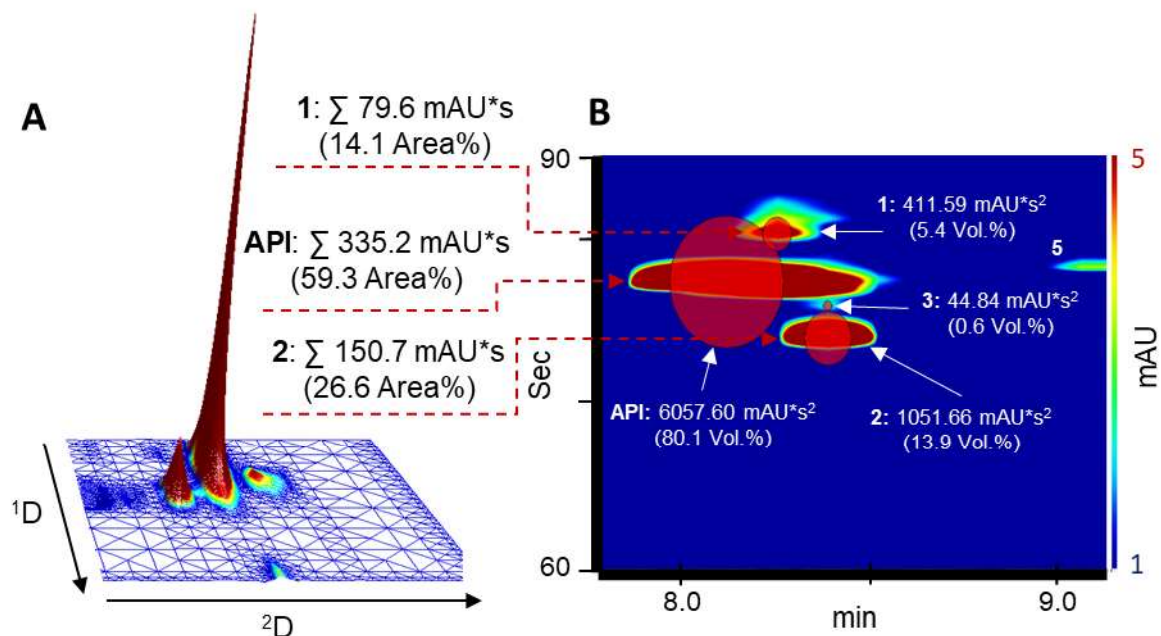
Fig. S8: Relative quantification was performed on the 2D-separation shown in Fig. 1 of main document, depicted in full scale 3D plot (**A**) and as a 2D contour plot (**B**). **A**: Areas (mAU*s) represent the sum of ^{2}D chromatograms (as calculated by vendor software), while volumes (mAU*s^2) result from blob detection applied on the contour plot ((as determined by LC Image software). Note, in **B** the signal maximum is reduced to 5 mAU in order to emphasize minor impurities.

4.2 Publication II

Direct enantioselective gradient reversed-phase ultra-high performance liquid chromatography tandem mass spectrometry method for 3-hydroxy alkanoic acids in lipopeptides on an immobilized 1.6 μm amylose-based chiral stationary phase

Ryan Karongo[1], Junjing Jiao[2], Harald Gross[2], Michael Lämmerhofer[1,*]

[1]Institute of Pharmaceutical Sciences, Pharmaceutical (Bio-)Analysis, Eberhard Karls University of Tübingen, Auf der Morgenstelle 8, Tübingen 72076, Germany

[2]Institute of Pharmaceutical Sciences, Pharmaceutical Biology, Eberhard Karls University of Tübingen, Auf der Morgenstelle 8, Tübingen 72076, Germany

RESEARCH ARTICLE

JOURNAL OF
SEPARATION SCIENCE

Direct enantioselective gradient reversed-phase ultra-high performance liquid chromatography tandem mass spectrometry method for 3-hydroxy alkanoic acids in lipopeptides on an immobilized 1.6 μm amylose-based chiral stationary phase

Ryan Karongo[1] | Junjing Jiao[2] | Harald Gross[2] | Michael Lämmerhofer[1] 📷

[1] Institute of Pharmaceutical Sciences, Pharmaceutical (Bio-)Analysis, Eberhard Karls University of Tübingen, Auf der Morgenstelle 8, Tübingen 72076, Germany

[2] Institute of Pharmaceutical Sciences, Pharmaceutical Biology, Eberhard Karls University of Tübingen, Auf der Morgenstelle 8, Tübingen 72076, Germany

Correspondence
Dr. Michael Lämmerhofer, Pharmaceutical (Bio-)Analysis, Institute of Pharmaceutical Sciences, University of Tübingen, Auf der Morgenstelle 8, 72076 Tübingen, Germany.
Email: michael.laemmerhofer@uni-tuebingen.de

3-Hydroxy fatty acids are important chiral building blocks of lipopeptides and metabolic intermediates of fatty acid oxidation, respectively. The analysis of the stereochemistry of such biomolecules has significant practical impact to elucidate and assign the enzymatic specificity of the biosynthesis machinery. In this work, a new mass spectrometry compatible direct chiral ultra high performance liquid chromatography separation method for 3-hydroxy fatty acids without derivatization is presented. The application of amylose tris(3,5-dimethylphenyl carbamate) based polysaccharide chiral stationary phase immobilized on 1.6 μm silica particles (CHIRALPAK IA-U) allows the enantioseparation of 3-hydroxy fatty acids under generic electrospray ionization mass spectrometry friendly reversed phase gradient elution conditions. Adequate separation factors were achieved with both acetonitrile and methanol as organic modifiers, covering hydrocarbon chain lengths between C_6 and C_{14}. Elution orders were derived from rhamnolipid (R-95) of which enantiomerically pure or enriched (R)-3-hydroxy fatty acids were recovered after ester hydrolysis. The S-configured acids consistently eluted before the respective R-enantiomers. The method was successfully applied for the elucidation of the absolute configuration of 3-hydroxy fatty acids originating from a novel lipopeptide with unknown structure. The work furthermore demonstrates that gradient elution is a viable option also in enantioselective (ultra)high performance liquid chromatography, even for analytes with modest separation factors, although less commonly exploited.

KEYWORDS
3-hydroxy fatty acids, chiral stationary phases, enantioselective lipidomics, non-ribosomal peptide synthetase, polysaccharide selectors

---

Article Related Abbreviations: 3-OH-FA, 3-hydroxy fatty acid; CSP, chiral stationary phase; NRPS, non-ribosomal peptide synthetase

1 | INTRODUCTION

Lipopeptides are amphiphilic compounds containing either a linear or cyclic peptide headgroup attached to a linear, branched, or even cyclic lipid moiety of varying length (typically C_6-C_{18}) [1,2]. In fact, they have emerged as a new class of antibiotics against drug resistant bacteria, due to their efficacy and biodegradability [3, 4]. More than once, genome sequence research has led to the identification of lipopeptides by encoding orphan gene clusters, which are a potential source for novel compounds and potential bioactive agents [5–7]. Isolation and identification of these compounds, synthesized by nonribosomal peptide synthetases (NRPSs) [5, 8, 9], is therefore paramount for their accessibility and applicability as drugs as well as for their biological testing.

Even though signature sequences within the adenylation domains of NRPSs are adequate to specify the amino acid composition of the oligopeptide, complementary methods are required for experimental verification (Marfey's, Edman, NMR, MS/MS sequencing). Full structural characterization requires to address the stereochemistry of the constituent amino acids and of the, often substituted fatty acid side chain(s). Accessing information regarding the absolute configuration at the chiral center of the fatty acid side chain substituents, which is commonly a 3-hydroxy fatty acid (3-OH-FA) [5, 6], by enantioselective LC is still a challenge [10–15].

Polysaccharide-based chiral stationary phases (CSPs) appreciate tremendous popularity, which is mainly attributed to their wide range of versatility [16–18]. Traditionally theses phases were predominantly used in normal phase mode, but actually have multimodal applicability. Their recent immobilization (instead of coating) on 1.6 μm particles has afforded their implementation for fast and efficient UHPLC separations [19, 20]. Their compatibility with virtually all mobile phases comprising supercritical fluid, polar organic, hydrophilic interaction, and RP elution modes is maintained and selectivity with non-standard solvents often enhanced or complementary, making these CSPs rather universal [10, 17, 18, 21-23]. The most prominent derivatives are based on amylose and cellulose aryl esters and carbamates with methyl, chloro, or mixed methyl/chloro substituents [24]. Through these structural variations a large number of broadly selective chiral columns are obtained. Changes in enantioselectivity can often be achieved by replacing one with the other. Enantioselectivity can be tuned by the backbone stereochemistry of the polysaccharide, the functional group by which the aryl moiety is attached and by substituents on the aromatic ring which influence the electron density in the aromatic moiety and hydrogen donor-acceptor properties of the functional (ester, carbamate) group [22,

25]. The carbamate functionality additionally allows some flexibility of the aromatic moiety to maximize π–π interactions. Overall, a combination of electrostatic interactions, steric discrimination and the docking into chiral (binding) cavities governs the chiral recognition process [10, 26, 27].

The direct separation of hydroxylated aliphatic acids on polysaccharide based CSPs has been reported for polyunsaturated oxygenated fatty acids [14, 19] as well as 3-hydroxyalkanoic acids after pre-column derivatization with 3,5-dimethylphenylisocyanate [28]. The latter, based on 3,5-dimethylphenyl carbamate derivative of cellulose coated silica, resolved a homologous series of 3-OH-FAs ($R < S$) ranging from C_6 to C_{16}, albeit requiring runtimes over 100 min due to loss of resolution with gradient elution and relatively large particle sizes (5 μm) [28]. Up to date the successful direct enantioresolution for underivatized 3-hydroxy alkanoic acids employing these polysaccharide phases was not reported, although other approaches based on derivatization [29] or utilizing ion-exchange CSPs were successfully implemented for such aliphatic alkanoic acids [30–32].

To our knowledge, we herein report the first direct UHPLC enantioseparation of 3-hydroxy alkanoic acids on an amylose tris(3,5-dimethylphenyl carbamate) based polysaccharide CSP immobilized on 1.6 μm silica particles (CHIRALPAK IA-U) for UHPLC-ESI-MS/MS applications. RP type gradient elution allowed to analyze a homologous series in one run within about 20 min and revealed perfect ESI-MS compatibility. Subsequently, the new method was employed for the enantioselective analysis of 3-hydroxy fatty acids released from a recently discovered novel class of lipopeptides. Assignment of absolute configurations of the 3-hydroxy fatty acid side chain of the lipopeptide was realized by use of rhamnolipid (R-95) hydrolysate as enantiomer standard.

2 | MATERIALS AND METHODS

2.1 | Materials

The standards 3-hydroxybutyric acid (3-OH-FA (4:0)) sodium salt, (±)−3-hydroxyhexanoic acid (3-OH-FA (6:0)), (±)−3-hydroxyoctanoic acid (3-OH-FA (8:0)), (±)−3-hydroxydecanoic acid (3-OH-FA (10:0)), (±)−3-hydroxydodecanoic acid (3-OH-FA (12:0)), (±)−3-hydroxy myristic acid (3-OH-FA (14:0)), and rhamnolipid (R-95), di-rhamnolipid dominant (Rha), were obtained from Sigma Aldrich (Steinheim, Germany). Solvents and additives used for MS-detection were of LC-MS grade. Methanol (MeOH), acetonitrile (ACN), and acetic acid (AcOH) were obtained from Carl Roth (Karlsruhe, Germany).

TABLE 1 Optimized parameters for ESI MS/MS selected reaction monitoring transitions

Name	Q1	Q3	Dwell time (ms)	CE	DP
3-OH-FA (4:0)	103	59.1	50	−15	−80
3-OH-FA (6:0)	131.1	59.1	50	−15	−80
3-OH-FA (8:0)	159.1	59.1	50	−15	−80
3-OH-FA (10:0)	187.1	59.1	50	−20	−80
3-OH-FA (12:0)	215.2	59.1	50	−20	−80
3-OH-FA (14:0)	243.2	59.1	50	−20	−80
3-OH-FA (12:0) [M+1-H]⁻	132.1	59.1	50	−15	−80
3-OH-FA (14:0) [M+1-H]⁻	160.1	59.1	50	−15	−80

2.2 | Sample preparation of standards

Due to differing solubility in water, as a consequence of varying chain length, 3-OH-FA (4:0), 3-OH-FA (6:0), and 3-OH-FA (8:0) were dissolved in H_2O, while 3-OH-FA (10:0), 3-OH-FA (12:0), and 3-OH-FA (14:0) were dissolved in MeOH/H_2O (6:4, v/v), both at a concentration of 2 µg/mL.

2.3 | Rhamnolipid hydrolysis

For acidic hydrolysis, 5 mg of rhamnolipid (R-95) was suspended in 0.5 mL 2.7 M H_2SO_4 in a screw-capped glass vial. A volume of 0.5 mL of $CHCl_3$ was added and the obtained biphasic system was heated at 110°C for 140 min. The chloroform layer containing the fatty acid was collected, evaporated to dryness, and subsequently, solubilized in 1 mL MeOH.

For alkaline hydrolysis, a stock solution of 5 mg of rhamnolipid (R-95) in 0.5 mL MeOH (10 mg/mL) was prepared. Stock solution (50 µL) and a methanolic solution of 2N NaOH (50 µL) were each added to 900 µL of a solution of THF/MeOH (9:1, v/v) and stirred for 2 h at room temperature (≈25°C). The solvents were then removed under vacuum, the residue diluted with 200 µL of water and acidified with 0.1 M HCl to pH 2–3. The solution was then extracted thrice with 200 µL ethyl acetate, the combined organic layers evaporated to dryness and reconstituted with 100 µL MeOH/H_2O (3:7, v/v). The solution was diluted tenfold (H_2O) for LC-MS analysis.

2.4 | Lipopeptide hydrolysis

The lipopeptide was first dissolved in MeOH to obtain the stock solution (10 mg/mL). An aliquot of 50 µL (corresponding to 500 µg) was added up to 1 mL with a solution of 6 M deuterated hydrochloric acid (DCl/D_2O, 1:1, v/v) in a screw-capped glass vial and heated for 24 h at 110°C.

The hydrochloric acid was evaporated in an EZ-2 high performance evaporator from GeneVac (Ipswich, UK). The residue was extracted with 200 µL of a mixture of water and chloroform in a ratio of 1:1 (v/v). The chloroform layer containing the 3-hydroxyalkanoic acid was evaporated to dryness using the Genevac, and the residue reconstituted with 100 µL MeOH. The solution was dissolved tenfold with H_2O for RP and MeOH for HILIC measurements. The aqueous layer was likewise evaporated to dryness and used for amino acid analysis (reported elsewhere).

2.5 | Instrumentation

Chiral chromatographic separation was performed on an Agilent 1290 Infinity UHPLC system (Waldbronn, Germany) equipped with a binary pump (G4220A), a column thermostat (G1316A), and a PAL autosampler (CTC Analytics AG, Switzerland). The separations were performed on a CHIRALPAK IA-U column (100 × 3.0 mm, 1.6 µm). The mobile phases comprised water (MP-A) and acetonitrile (MP-B), both containing 0.1% (v/v) acetic acid. The following gradient was applied if not otherwise stated: 0–2 min 10% MP-B, 2–20 min 10–100% MP-B, 20–22 min 100% MP-B, 22-22.1 min 100–10% MP-B, and 22.1-25 min 10% MP-B. The flow rate was 300 µL/min, the column temperature 40°C, and the injection volume 10 µL.

MS detection was performed on an AB SCIEX API 4000 MS/MS mass spectrometer equipped with a TurboIon-Spray (SCIEX, Ontario, Canada) in selected reaction monitoring (SRM) mode. The parameters of the selected reaction monitoring transitions, including dwell time, collision energy, and delustering potential (DP), were optimized for each compound individually and are displayed in Table 1. The total cycle time was 385 ms. All measurements were run in negative polarity mode. The cell exit potential was set to −15 V, the entrance potential to −10 V, the ion source voltage to −4500 V, the temperature to 400°C, the nebulizer gas and heater gas pressures to 30 psi, the curtain gas

to 35 psi, and the collisionally activated dissociation gas to 6 psi. PeakView 2.2 software was used for data analysis.

3 | RESULTS AND DISCUSSION

3.1 | Generation of enantiomeric standards by rhamnolipid hydrolysis

The full structural characterization of chiral building blocks from natural products requires besides the determination of the chemical composition also their stereochemical analysis. What lipopeptides are concerned, the amino acid sequence and their configuration as well as fatty acid carbon chain length, hydroxyl substitution and stereochemistry are structural variables which need to be clarified. Herein we use the coupling of MS with enantioselective UHPLC as a powerful tool for the structural analysis of the 3-hydroxyalkanoic acid side chains of lipopeptides. MS provides the fatty acid information, while the stereoconfiguration of the 3-hydroxyl group can be derived from known elution orders on an enantioselective chiral column.

For enantioselective analysis, enantiomeric elution orders are usually derived by comparison with enantiomerically pure (internal) standards with known configuration. However, due to their unavailability for the full series of 3-hydroxyalkanoic acids, they were generated as enantiomerically enriched references by hydrolysis of the glycolipid rhamnolipid (R-95) which is a bacterial surfactant produced by *Pseudomonas aeruginosa* [33]. This sample was reported to contain the corresponding abundant C_{10} and C_{12} (R)—3-hydroxy fatty acids (corresponding to $(3R)$-OH-FAs) [34, 35].

According to literature, rhamnolipid hydrolysis is performed under acidic conditions [36], probably due to a desired release of further lipid sub classes, such as the recently discovered fatty acid esters of hydroxy fatty acids [37]. However, for pure 3-hydroxy fatty acid hydrolysis the reaction kinetics governing ester hydrolysis of fatty acyl esters is substantially faster than the corresponding acidic approach [38, 39]. Two methods of hydrolysis were therefore compared, acidic with H_2SO_4 and basic (saponification) using NaOH. Although only the ester bonded fatty acid chain is cleaved with alkaline conditions (Figure 1A), the yield was found to be >100 and >1000 times higher, for 3-OH-FA (10:0) and 3-OH-FA (12:0), respectively, and therefore quantitative. Nevertheless, acidic hydrolysis should be preferred for glycoside bond cleavages, e.g. for releasing the di-rhamnose moiety. The results in Figure 1B clearly document that alkaline ester hydrolysis is more efficient for release of 3-OH-FAs from rhamnolipid than acidic hydrolysis (*cf.* black vs. red traces). Furthermore, the results in Figure 1B confirm the presence of 3-OH-FA
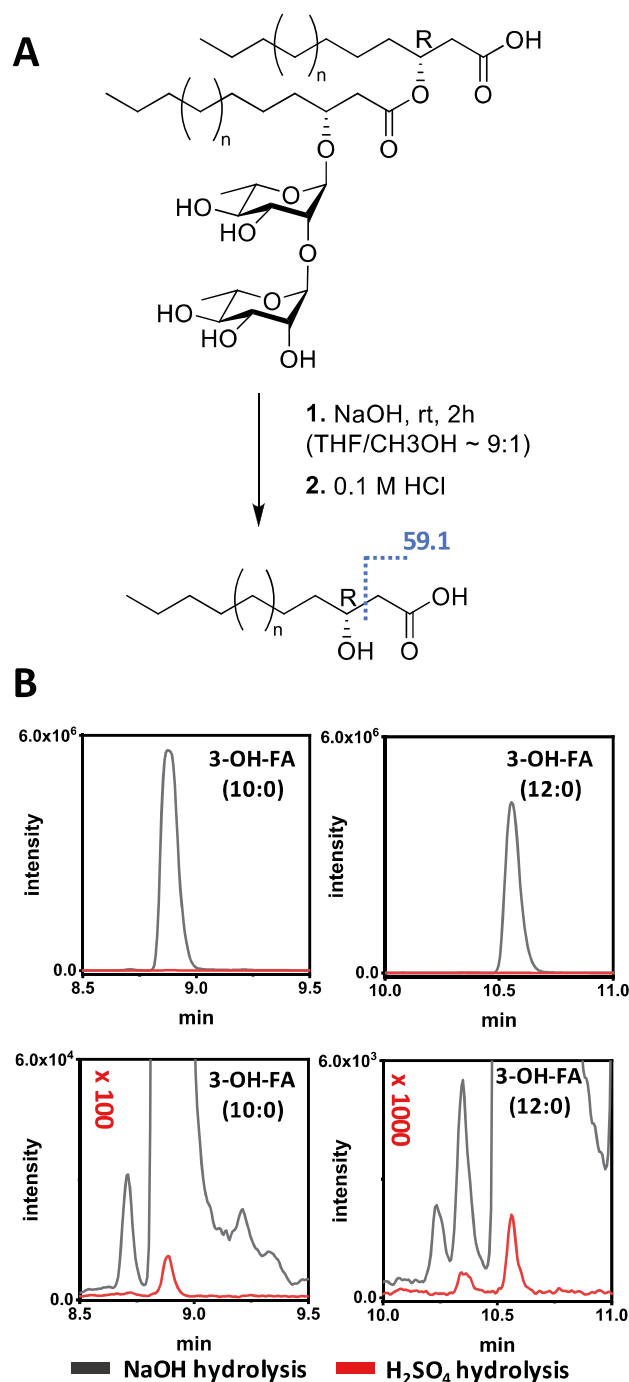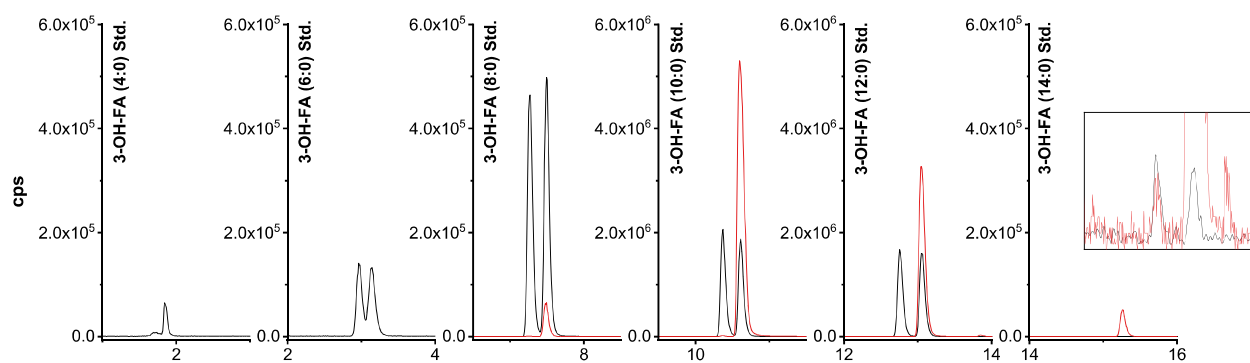

FIGURE 1 Generation of enantiomeric standards of 3-hydroxy fatty acids from rhamnolipid (R-95). (**A**) Ester hydrolysis of rhamnolipid releases 3-OH-fatty acids. Selected reaction monitoring transitions exploit the cleavage of acetate (*m/z* 59.1 in MS²). (**B**) Results are shown for hydrolysis under basic (black trace) and acidic (red trace) conditions for 3-hydroxy decanoic acid (3-OH-FA (10:0), upper left) and 3-hydroxy dodecanoic acid (3-OH-FA (8:0), upper right), as well as the corresponding zoom below for better visualization. Column: CHIRALPAK IA-U (100 × 3.0 mm, 1.6 μm). Gradient: 0–2 min 10% MP-B, 2–20 min 10–100% MP-B, 20–22 min 100% MP-B, 22–22.1 min 100–10% MP-B and 22.1-25 min 10% MP-B (MP-B: ACN (0.1% AcOH))
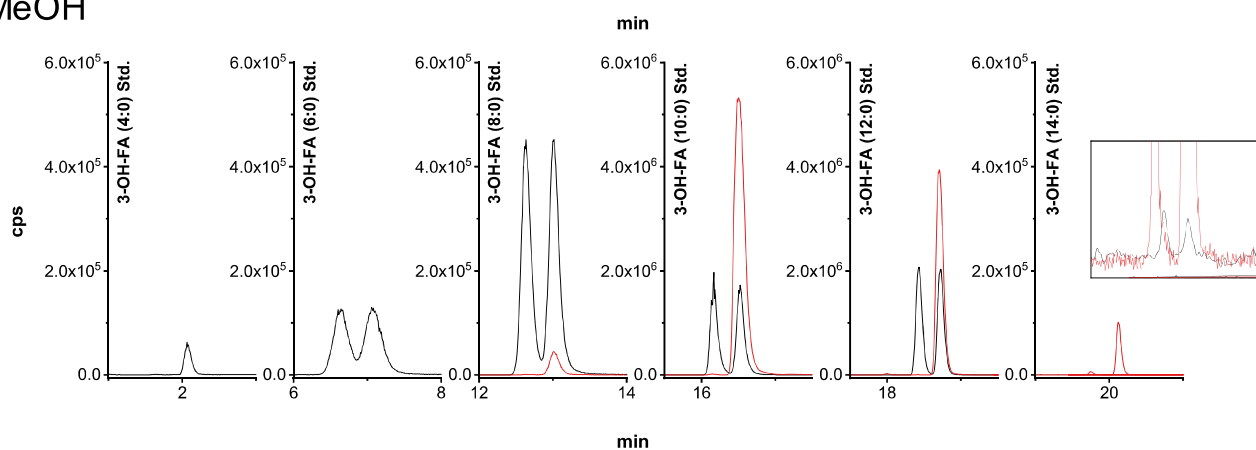
FIGURE 2 Separation of a homologous series of 3-hydroxy alkanoic acids originating from commercial standards (black trace) and rhamnolipid (R-95) hydrolysates (red trace). Both acetonitrile (ACN) and methanol (MeOH) were used as organic modifiers (MP-B, 0.1% AcOH, v/v) in a RP gradient containing water as MP-A (0.1% AcOH, v/v)

(10:0) and 3-OH-FA (12:0). Besides, we found 3-OH-FA (8:0) and 3-OH-FA (14:0) at lower concentration levels. From these results we can conclude that the rhamnolipid (R-95) should be a useful standard for pinpointing the elution orders for wider series of 3-OH-FAs and for supporting the identification of the stereochemistry of 3-OH-FA building blocks in lipopeptides. An alkaline hydrolysis protocol is recommended for this purpose prior to analysis.

3.2 | Enantioseparation of 3-hydroxy fatty acid homologues

Chiral recognition processes and hence column selection are usually hardly predictable, especially for polysaccharide-based chiral selectors and CSPs. Recently, 3-hydroxyalkanoic acids were resolved into enantiomers on cellulose tris(3,5-dimethylphenyl carbamate) coated CSP after precolumn derivatization with 3,5-dimethylphenyl isocyanate, generating carbamate derivatives [23]. The goal in the present work, however, was to avoid a derivatization step. Polysaccharide phases exhibited also enantioselectivity for hydroxylated

polyunsaturated fatty acids and oxylipins [19]. This was, however, not demonstrated yet for non-derivatized 3-hydroxyalkanoic acids.

In our recent work, CHIRALPAK IA-U was, to some degree, successfully applied for the structurally similar oxylipins [19] and was therefore tested first. Operated in RP elution mode, a separation of the hydroxy fatty acids according to increasing carbon number and hydrophobicity including their enantioseparation becomes feasible in a single run. At the same time, the mobile phase volatility assures ESI-MS compatibility. Therefore, a straightforward linear gradient from 10 to 100% organic modifier was applied for the separation of the homologous series of racemic 3-OH-FA standards (Figure 2, black traces). Both ACN and MeOH were applied as organic modifiers (MP-B, 0.1% AcOH) and water as MP-A (0.1% AcOH), resulting in a successful enantioseparation for all 3-OH-FAs (C_6, C_8, C_{10}, C_{12}, C_{14}), except for 3-hydroxybutyric acid (C_4). The corresponding chromatographic data are reported in Table 2. It can be seen that separation factors in gradient elution mode (ratio of net retention factors of the two enantiomers) are very similar for both organic modifiers, ACN and MeOH, ranging typically between 1.02 and 1.15. However,

TABLE 2 Chromatographic parameters obtained by chiral LC-MS 3-hydroxy fatty acids

	ACN				MeOH			
Sample	$t_R(S)$ (min)	$t_R(R)$ (min)	α*	R_S	$t_R(S)$ (min)	$t_R(R)$ (min)	α*	R_S
3-OH-FA (4:0)	1.85	–	–	–	2.07	–	–	–
3-OH-FA (6:0)	2.97	3.14	1.15	1.05	6.64	7.08	1.09	1.09
3-OH-FA (8:0)	7.27	7.50	1.04	1.80	12.64	13.01	1.03	1.53
3-OH-FA (10:0)	10.37	10.62	1.03	1.86	16.17	16.52	1.02	2.03
3-OH-FA (12:0)	12.76	13.06	1.03	2.17	18.43	18.73	1.02	1.78
3-OH-FA (14:0)	14.85	15.29	1.03	3.25	19.86	20.15	1.02	2.16
Lipopeptide hydrolysate	7.28	7.50	1.04	1.86	12.63	13.00	1.03	1.46
3-OH-FA (8:0)#	–	7.49	–	–	–	13.02	–	–
3-OH-FA (10:0)#	–	10.61	–	–	–	16.51	–	–
3-OH-FA (12:0)#	–	13.05	–	–	–	18.71	–	–
3-OH-FA (14:0)#	–	15.26	–	–	–	20.13	–	–
3-OH-FA (6:0), isocratic 10%B	3.09	3.27	1.14	1.01	8.00	9.08	1.18	1.75
3-OH-FA (6:0), isocratic 12.5%B	2.62	2.73	1.14	0.72	–	–	–	–
3-OH-FA (6:0), isocratic 15%B	2.39	2.47	1.14	0.54	–	–	–	–
3-OH-FA (6:0), isocratic 30%B	–	–	–	–	3.44	3.72	1.17	1.05

*Calculated for gradient conditions, except where stated otherwise.
#Obtained from rhamnolipid hydrolysis.
$t_0 = 1.85$.

peak shapes are narrower for ACN than for MeOH, which are in agreement with the findings for oxylipin separations on CHIRALPAK IA-U [19], most probably due to its lower viscosity and better mass transfer properties. The separation clearly benefits from the high efficiency of the 1.6 μm CSP which allows baseline resolutions in spite of modest separation factors. Resolution values increased with carbon chain length and were between 1.05 and 3.25 with ACN and between 1.09 and 2.16 for MeOH (Table 2). Early eluted 3-OH-FA (6:0) was not fully baseline separated in gradient elution mode (Rs ~ 1.1). Assuming that through the gradient the separation factor could be compromised, a series of experiments under isocratic conditions was devised. The results corroborated that under isoeluotropic conditions no significant improvement in Rs can be achieved upon switching from gradient to isocratic separations (see Figure 3 and Table 2). In order to achieve full baseline separation for 3-OH-FA (6:0), conditions with significantly longer retention need to be adjusted, at expense of analysis times. 3-OH-FA (4:0) was not retained, therefore no enantioselectivity was observed. Some further optimizations under isocratic elution conditions were undertaken for 3-OH-FA (4:0). Minor changes in mobile phase composition and temperature were examined under isocratic elution for ACN (5, 10, 12.5, 15, 20, 25, 30, and 35% organic modifier) and MeOH (5, 10, 30, and 60% organic modifier) between 20 and 40°C (at 10% organic modifier in intervals of 5°C), but retention was not increased significantly to allow sufficient interaction with the CSP (data not shown). Since it

was not contained in our sample, no further attempts were made to separate 3-OH-FA (4:0) enantiomers.

Finally, gradient elution with ACN was deemed favorable for fast separations producing narrower peaks, which is beneficial regarding detection sensitivities. Enantioseparation factors large enough to conclude of the absolute configurations of the hydroxyl fatty acid side chains were obtained for all test compounds, except 3-OH-FA (4:0), within a runtime of 20 min. It was found highly adequate for the present application and similar ones because lipopeptides typically exhibit fatty acid chain lengths varying from C_6 to C_{18} [1]. Fortunately, successful separation conditions for derivatized and underivatized enantiomers of 3-OH-FA (4:0) have been reported for anion exchange-type quinine- and quinidine-derived CSPs [31, 32], which provides a good alternative for this analyte if it becomes relevant.

3.3 | Determination of elution orders

The identity of enantiomers is fully characterized only once the absolute configuration is known. Rhamnolipid (R-95) is known to contain 3-hydroxyfatty acids in *R*-configuration [40]. For rhamnolipid, alkaline hydrolysate, peak abundances for *R*-3-OH-FA (10:0) and *R*-3-OH-FA (12:0) are significantly higher (note, scale is ×10⁶ cps), while minor concentrations of *R*-3-OH-FA (8:0) and *R*-3-OH-FA (14:0) are present as well and can be used as
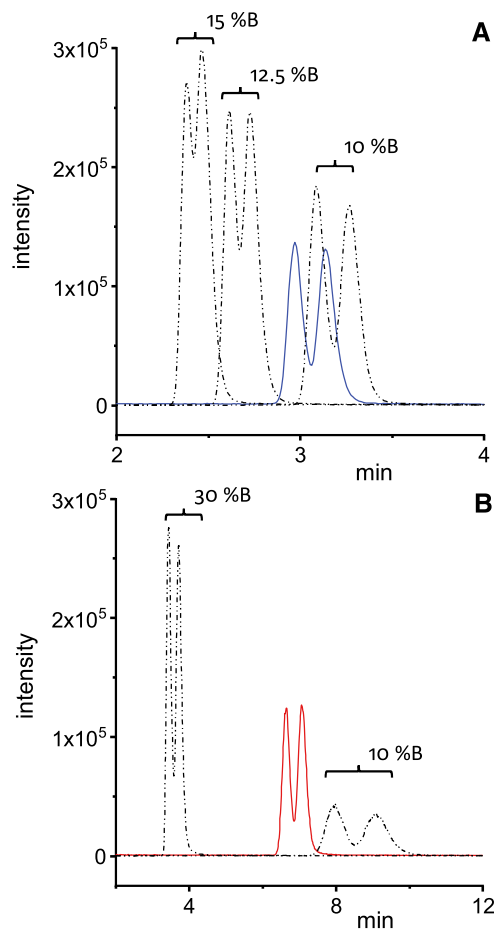
FIGURE 3 Comparison of chromatographic profiles using acetonitrile (**A**) and methanol (**B**) as organic modifiers (MP-B) in gradient (blue and red trace) vs. isocratic (black dotted traces) elution. Gradient elution: 0–2 min 10% MP-B, 2–20 min 10–100% MP-B, 20–22 min 100% MP-B, 22-22.1 min 100–10% MP-B and 22.1-25 min 10% MP-B. Isocratic elution: organic modifier percentage according to the label

FIGURE 4 Enantioseparation of 3-OH-FA released from lipopeptide hydrolysis (black trace) and rhamnolipid (R-95, red trace) on CHIRALPAK IA-U (100 × 3.0 mm, 1.6 μm)

standards to assign the elution order (Figure 2). The corresponding extracted ion traces of the rhamnolipid hydrolysate are shown in red in Figure 2. The concluded elution order is consistently *S*-enantiomer eluting before *R*-enantiomer (*S* < *R*) throughout the homologous series. This trend can be extrapolated with a certain degree of confidence to 3-OH-FA (6:0). With this information at hand, the configuration of the 3-hydroxyfatty acid from a lipopeptide sample can be unequivocally derived based on the elution order in relation to racemic standards.

3.4 | Applicability: Side chain elucidation of a novel lipopeptide

The applicability of the new method was then demonstrated on a real lipopeptide sample with unknown
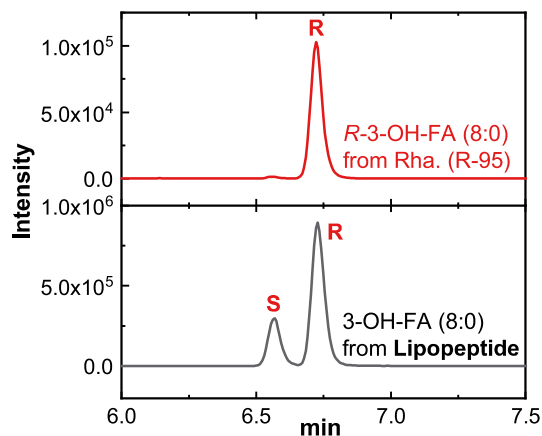
structure. In order to access the stereoconfiguration of the lipopeptide side chain of this research sample from a genome-driven drug discovery study for which the structure, including stereochemistry of the constituents, has to be fully elucidated, it has to be released from the oligopeptide. Total acidic hydrolysis with HCl is the most efficient and method of first choice [36]. Structure elucidation of the compounds was accomplished by a combination of achiral LC-ESI-HR-MS and multidimensional NMR experiments, inferring the FA sidechain constituting of 3-OH-FA (8:0). However, the stereoconfiguration of the fatty acid sidechain remained inaccessible using the above-mentioned approaches.

Consequently, the cyclic lipopeptide was hydrolyzed to release the corresponding 3-OH-FA, its identity and stereoconfiguration was confirmed and concluded, respectively, by enantioselective UHPLC using the method described above employing CHIRALPAK IA-U as the chiral column prior ESI-MS detection. Using the same method for the racemic 3-OH-FA standard, fatty acids hydrolyzed from the rhamnolipid were analyzed alongside that released from the cyclic lipopeptide (Figure 4). Significant, but minor amounts of the *S* isomer were found in the sample in addition to the predominantly *R* configured isomer. According to our knowledge, natural lipopeptides containing fatty acid side chains of both configurations have not been reported, which is why the occurrence of the *S* isomer likely occurred due to racemization. However, the large excess of the *R*-enantiomer confirms that the NRPS biosynthesis generates the *R*-configuration of the 3-OH-FA in the lipopeptide of the research sample. This finding is in agreement with our results for the FA moiety of poaeamide [36, 41]. However, it has to be emphasized that the *S*-configuration has also been reported for 3-OH-FAs in lipopeptides, e.g. one related to orfamide A [5]. It

clearly demonstrates that the stereochemistry cannot be simply assumed, but must be experimentally derived. The proposed method is relatively generic and straightforward to apply.

4 | CONCLUDING REMARKS

A direct simple enantioselective UHPLC-ESI-MS/MS assay was established for the experimental assignment of both the carbon chain length and stereochemistry of 3-hydroxy fatty acids ranging from hexanoic to myristic acid. The analysis can be performed without sample derivatization using amylose tris(3,5-dimethylphenyl carbamate) based polysaccharide CSP immobilized on 1.6 μm silica particles (CHIRALPAK IA-U). The elution order was consistently $S < R$ for all reference compounds found in rhamnolipid (R-95). Enantioselectivity may also be expected for the corresponding 3-hydroxy alkanoic acids with carbon chain length $> C_{14}$ since resolution improved with carbon chain length from C_6 to C_{14}. In contrast, for short chain 3-OH-FAs ($< C_6$) a different selector e.g. quinine or quinidine carbamate is a viable option [30–32]. In general, the CHIRALPAK IA-U column has great potential to resolve hydroxy fatty acid enantiomers emerging as secondary metabolites from different natural sources, such as rhamnolipids [35], and biomarkers of inflammatory processes derived from polyunsaturated fatty acids [19]. Gradient elution outperformed isocratic separation as it allows to analyze the full series in a single run within 20 min and at no significant expense for separation factors.

CONFLICT OF INTEREST
The authors have declared no conflict of interest.

ORCID
Michael Lämmerhofer https://orcid.org/0000-0002-1318-0974

REFERENCES
1. Götze S, Stallforth P. Structure elucidation of bacterial nonribosomal lipopeptides. Org Biomol Chem. 2020;18:1710–27.
2. Youssef NH, Duncan KE, McInerney MJ. Importance of 3-hydroxy fatty acid composition of lipopeptides for biosurfactant activity. Appl Environ Microbiol. 2005;71:7690–5.
3. Nemati R, Dietz C, Anstadt E, Clark R, Smith M, Nichols F, Yao X. Simultaneous determination of absolute configuration and quantity of lipopeptides using chiral liquid chromatography/mass spectrometry and diastereomeric internal standards. Anal Chem. 2017;89:3583–9.
4. Schneider T, Müller A, Miess H, Gross H. Cyclic lipopeptides as antibacterial agents - potent antibiotic activity mediated by intriguing mode of actions. Int J Med Microbiol. 2014;304:37–43.
5. Gross H, Stockwell VO, Henkels MD, Nowak-Thompson B, Loper JE, Gerwick WH. The genomisotopic approach: a systematic method to isolate products of orphan biosynthetic gene clusters. Chem Biol. 2007;14:53–63.
6. Kirchner N, Cano-Prieto C, Schulz-Fincke A-C, Gütschow M, Ortlieb N, Moschny J, Niedermeyer THJ, Horak J, Lämmerhofer M, van der Voort M, Raaijmakers JM, Gross H. Discovery of Thanafactin A, a linear, proline-containing octalipopeptide from pseudomonas sp. SH-C52, motivated by genome mining. J Nat Prod. 2021;84:101–9.
7. Jahanshah G, Yan Q, Gerhardt H, Pataj Z, Lämmerhofer M, Pianet I, Josten M, Sahl H-G, Silby MW, Loper JE, Gross H. Discovery of the cyclic lipopeptide gacamide a by genome mining and repair of the defective GacA regulator in Pseudomonas fluorescens Pf0-1. J Nat Prod. 2019;82:301–8.
8. Raaijmakers JM, de Bruijn I, de Kock MJD. Cyclic lipopeptide production by plant-associated Pseudomonas spp.: diversity, activity, biosynthesis, and regulation. Mol Plant-Microbe Interact 2006;19:699–710.
9. Nybroe O, Sørensen J, in: Ramos, J.-L. (Ed.), Pseudomonas: Volume 3 Biosynthesis of Macromolecules and Molecular Metabolism. Boston, MA: Springer US; 2004: 147–72.
10. Lämmerhofer M. Chiral recognition by enantioselective liquid chromatography: Mechanisms and modern chiral stationary phases. J Chromatogr A. 2010;1217:814–56.
11. Ilisz I, Bajtai A, Lindner W, Péter A. Liquid chromatographic enantiomer separations applying chiral ion-exchangers based on Cinchona alkaloids. J Pharm Biomed Anal. 2018;159:127–52.
12. Scriba GKE. Chiral recognition mechanisms in analytical separation sciences. Chromatographia. 2012;75:815–38.
13. Sardella R, Ianni F, Lisanti A, Marinozzi M, Scorzoni S, Natalini B. The effect of mobile phase composition in the enantioseparation of pharmaceutically relevant compounds with polysaccharide-based stationary phases. Biomed Chromatogr. 2014;28:159–67.
14. Ianni F, Saluti G, Galarini R, Fiorito S, Sardella R, Natalini B. Enantioselective high-performance liquid chromatography analysis of oxygenated polyunsaturated fatty acids. Free Radicals Biol Med. 2019;144:35–54.
15. Scriba GKE. Chiral recognition in separation science – an update. J Chromatogr A 2016;1467:56–78.
16. Jakubec P, Douša M, Nováková L. Supercritical fluid chromatography in chiral separations: evaluation of equivalency of polysaccharide stationary phases. J Sep Sci. 2020;43:2675–89.
17. Zhang T, Nguyen D, Franco P. Enantiomer resolution screening strategy using multiple immobilised polysaccharide-based chiral stationary phases. J Chromatogr A2008;1191:214–22.
18. Thunberg L, Hashemi J, Andersson S. Comparative study of coated and immobilized polysaccharide-based chiral stationary phases and their applicability in the resolution of enantiomers. J Chromatogr B Analyt Technol Biomed Life Sci. 2008;875:72–80.

19. Cebo M, Fu X, Gawaz M, Chatterjee M, Lämmerhofer M. Enantioselective ultra-high performance liquid chromatography-tandem mass spectrometry method based on sub-2μm particle polysaccharide column for chiral separation of oxylipins and its application for the analysis of autoxidized fatty acids and platelet releasates. J Chromatogr A 2020;1624:461206.

20. Berger TA. Preliminary kinetic evaluation of an immobilized polysaccharide sub-2mum column using a low dispersion supercritical fluid chromatograph. J Chromatogr A 2017;1510:82–8.

21. Ikai T, Okamoto Y. Structure control of polysaccharide derivatives for efficient separation of enantiomers by chromatography. Chem Rev. 2009;109:6077–101.

22. Chankvetadze B. Recent developments on polysaccharide-based chiral stationary phases for liquid-phase separation of enantiomers. J Chromatogr A 2012;1269:26–51.

23. Colombo M, Ferretti R, Zanitti L, Cirilli R. Direct separation of the enantiomers of ramosetron on a chlorinated cellulose-based chiral stationary phase in hydrophilic interaction liquid chromatography mode. J Sep Sci. 2020;43:2589–93.

24. Matarashvili I, Chelidze A, Dolidze G, Kobidze G, Zaqashvili N, Dadianidze A, Bacskay I, Felinger A, Farkas T, Chankvetadze B. Separation of enantiomers of chiral basic drugs with amylose- and cellulose- phenylcarbamate-based chiral columns in acetonitrile and aqueous-acetonitrile in high-performance liquid chromatography with a focus on substituent electron-donor and electron-acceptor effects. J Chromatogr A 2020;1624:461218.

25. Chankvetadze B. Recent trends in preparation, investigation and application of polysaccharide-based chiral stationary phases for separation of enantiomers in high-performance liquid chromatography. TrAC, Trends Anal Chem. 2020;122:115709.

26. Scriba GK, Chiral Separations. Boston, MA: Springer; 2019: 1–33.

27. Scriba GKE. Chiral recognition in separation sciences. Part I: Polysaccharide and cyclodextrin selectors. TrAC, Trends Anal Chem. 2019;120:115639.

28. Abdel-Mawgoud AM, Lépine F, Déziel E. A chiral high-performance liquid chromatography–tandem mass spectrometry method for the stereospecific analysis of enoyl-coenzyme A hydratases/isomerases. J Chromatogr A 2013;1306:37–43.

29. Tsai Y-C, Liao T-H, Lee J-A. Identification of l-3-hydroxybutyrate as an original ketone body in rat serum by column-switching high-performance liquid chromatography and fluorescence derivatization. Anal Biochem. 2003;319:34–41.

30. Liu S-L, Oyama T, Miyoshi Y, Sheu S-Y, Mita M, Ide T, Lindner W, Hamase K, Lee J-A. Establishment of a two-dimensional chiral HPLC system for the simultaneous detection of lactate and 3-hydroxybutyrate enantiomers in human clinical samples. J Pharm Biomed Anal. 2015;116:80–5.

31. Ianni F, Pataj Z, Gross H, Sardella R, Natalini B, Lindner W, Lämmerhofer M. Direct enantioseparation of underivatized aliphatic 3-hydroxyalkanoic acids with a quinine-based zwitterionic chiral stationary phase. J Chromatogr A 2014;1363:101–8.

32. Calderón C, Lämmerhofer M. Chiral separation of short chain aliphatic hydroxycarboxylic acids on cinchonan carbamate-based weak chiral anion exchangers and zwitterionic chiral ion exchangers. J Chromatogr A 2017;1487:194–200.

33. Varjani SJ, Upasani VN. Critical review on biosurfactant analysis, purification and characterization using rhamnolipid as a model biosurfactant. Bioresour Technol. 2017;232:389–97.

34. Tiso T, Zauter R, Tulke H, Leuchtle B, Li W-J, Behrens B, Wittgens A, Rosenau F, Hayen H, Blank LM. Designer rhamnolipids by reduction of congener diversity: production and characterization. Microb Cell Fact. 2017;16:225.

35. Behrens B, Engelen J, Tiso T, Blank LM, Hayen H. Characterization of rhamnolipids by liquid chromatography/mass spectrometry after solid-phase extraction. Anal Bioanal Chem. 2016;408:2505–14.

36. Gerhardt H, Sievers-Engler A, Jahanshah G, Pataj Z, Ianni F, Gross H, Lindner W, Lämmerhofer M. Methods for the comprehensive structural elucidation of constitution and stereochemistry of lipopeptides. J Chromatogr A 2016;1428:280–91.

37. Ma Y, Kind T, Vaniya A, Gennity I, Fahrmann JF, Fiehn O. An in silico MS/MS library for automatic annotation of novel FAHFA lipids. J Cheminf. 2015;7:53.

38. Ault A. Telling it like it is: teaching mechanisms in organic chemistry. J Chem Educ. 2010;87:937–41.

39. Theodorou V, Skobridis K, Tzakos AG, Raoussis V. A simple method for the alkaline hydrolysis of esters. Tetrahedron Lett. 2007;48:8230–3.

40. Déziel E, Lépine F, Milot S, Villemur R. Mass spectrometry monitoring of rhamnolipids from a growing culture of Pseudomonas aeruginosa strain 57RP. Biochim Biophys Acta, Mol Cell Biol Lipids. 2000;1485:145–52.

41. Zachow C, Jahanshah G, de Bruijn I, Song C, Ianni F, Pataj Z, Gerhardt H, Pianet I, Lämmerhofer M, Berg G, Gross H, Raaijmakers JM. The novel lipopeptide poaeamide of the endophyte Pseudomonas poae RE*1-1-14 is involved in pathogen suppression and root colonization. Mol. Plant-Microbe Interact 2015;28:800–10.

4.3 Publication III

Enantioselective multiple heart cutting online two-dimensional liquid chromatography-mass spectrometry of all proteinogenic amino acids with second dimension chiral separations in one-minute time scales on a chiral tandem column
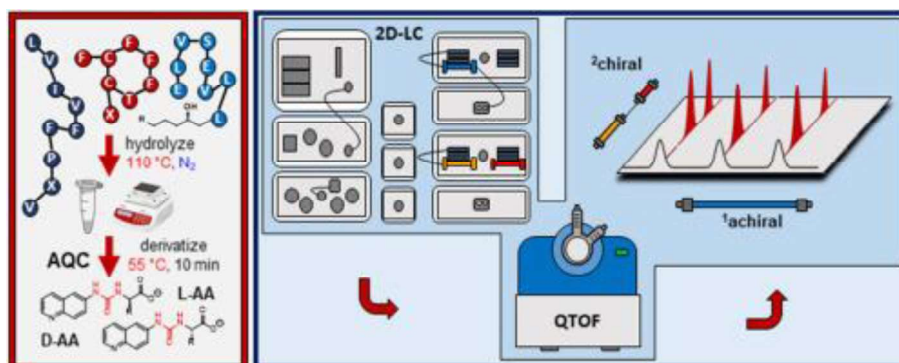
Ryan Karongo[a], Min Ge[a], Christian Geibel[a], Jeannie Horak[a,b,**], Michael Lämmerhofer[a,*]

[a]Institute of Pharmaceutical Sciences, Pharmaceutical (Bio-)Analysis, University of Tübingen, Auf der Morgenstelle 8, 72076, Tübingen, Germany

[b]Division of Metabolic and Nutritional Medicine, Dr. von Hauner Children's Hospital, Ludwig-Maximilians-University Munich Medical Center, Lindwurmstraße 4, 80337, Munich, Germany

Graphical Abstract

Enantioselective multiple heart cutting online two-dimensional liquid chromatography-mass spectrometry of all proteinogenic amino acids with second dimension chiral separations in one-minute time scales on a chiral tandem column

Ryan Karongo [a], Min Ge [a], Christian Geibel [a], Jeannie Horak [a, b, **], Michael Lämmerhofer [a, *]

[a] Institute of Pharmaceutical Sciences, Pharmaceutical (Bio-)Analysis, University of Tübingen, Auf der Morgenstelle 8, 72076, Tübingen, Germany
[b] Division of Metabolic and Nutritional Medicine, Dr. von Hauner Children's Hospital, Ludwig-Maximilians-University Munich Medical Center, Lindwurmstraße 4, 80337, Munich, Germany

HIGHLIGHTS

- Multiple heart cutting 2D LC-MS for enantioselective amino acid (AA) analysis (AQC derivatized).
- [1]D achiral RP separation of proteinogenic AAs and isobaric analogues of (alle, Nle, Tle; Hse, aThr).
- [2]D chiral separations of 24 amino acids achieved on a chiral tandem column in 68 s.
- Use of time-based sampling, smart peak parking and shifted gradient tool for efficient analysis.
- Fastest 2D-LC separation for enantioselective amino acid analysis to date (in total 45 min).

GRAPHICAL ABSTRACT
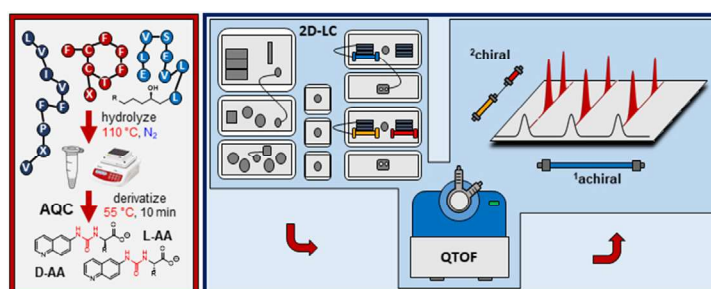
ARTICLE INFO

ABSTRACT

In this work, we present a unique, robust and fully automated analytical platform technology for the enantioselective amino acid analysis using a multiple heart cutting RPLC-enantio/stereoselective HPLC-ESI-QTOF-MS method. This 2D-LC method allows the full enantioselective separation of 20 proteinogenic AAs plus 5 isobaric analogues, namely *allo*-Threonine (aThr), homoserine (Hse), *allo*-isoleucine (alle), *tert*-Leucine (Tle) and Norleucine (Nle), after pre-column derivatization with 6-aminoquinolyl-*N*-hydroxysuccinimidyl carbamate (AQC; AccQ). This N-terminal AA-derivatization method introduces on the one hand beneficial chromatographic properties for [1]D RP-LC (stronger retention) and [2]D chiral separation (better chiral recognition), and on the other hand favorable detection properties with its chromophoric, fluorophoric, and easily ionizable quinoline mass tag. The entire separation occurs within a total 2DLC run time of 45 min, which includes the [1]D-RP run and the 68 s [2]D chiral separations of 30 heart-cuts (from the [1]D-RP-run) on a chiral quinine carbamate (core-shell QNAX/fully porous ZWIX) tandem column. This relatively short overall run time was only possible by utilizing the highly efficient "smart peak parking" algorithm for the heart cuts and the resulting optimized analysis order thereof. [1]D

* Corresponding author. Pharmaceutical (Bio-)Analysis, Institute of Pharmaceutical Sciences, University of Tübingen, Auf der Morgenstelle 8, 72076, Tübingen, Germany.
** Corresponding author. Division of Metabolic and Nutritional Medicine, Dr. von Hauner Children's Hospital Ludwig-Maximilians-University, Munich Medical Center, Lindwurmstraße 4, 80337, Munich, Germany.
E-mail addresses: Jeannie.Horak@med.uni-muenchen.de (J. Horak), michael.laemmerhofer@uni-tuebingen.de (M. Lämmerhofer).

6-Aminoquinolyl-*N*-Hydroxysuccinimidyl carbamate

retention time precisions of <0.21% RSD were a requirement for the time-based sampling mode and finally led to a robust, fully automated enantioselective amino acid analysis platform.

This achiral-chiral 2DLC method was applied for the amino acid stereoconfiguration assignment of three peptides (aureobasidin A, a lipopeptide research sample, and octreotide) using an L-[u-^{13}C^{15}N] labelled internal AA standard mix spiked to each sample. The isotopically labelled L-AA standard allowed an easy and straightforward identification and configuration assignment, as well as the relative quantification of amino acids within the investigated peptides, allowing the direct determination of the number of respective amino acids and their chirality within a peptide.

Abbreviations

aThr	*allo*-Threonine
Hse	homoserine
aIle	*allo*-isoleucine
Nle	norleucine
Tle	*tert*-leucine
AQC;AccQ	aminoquinolyl-*N*-hydroxysuccinimidyl carbamate
AA	amino acid
OPA	*ortho*-phthaldialdehyde
MHC	multiple heart-cutting
mLC-LC	multiple heart-cutting two-dimensional liquid chromatography
IDA	information dependent acquisition
FLD	fluorescence detection
CSP	chiral stationary phase
QN-AX	quinine-carbamate-based anion-exchanger CSP
ZWIX	zwitterionic quinine-carbamate-based CSP
WAX	weak anion exchange
SCX	strong cation exchange
SPP	superficially porous particles (core-shell)
FPP	fully porous particles

1. Introduction

For many decades, homochirality (L-configuration of amino acids) had been considered the norm in nature, but with the gradual discoveries of D-AAs in various biological matrices, as free D-AAs as well as incorporated in peptides, awareness has been aroused towards their stereochemical consequences in bioactivity. Therefore, the interest in determining D-amino acids in biochemical environments such as tissues and physiological fluids is continuously increasing, especially since they have been related to various diseases, e.g. D-Asp and D-Ser in age related disorders such as cataract [1], multiple sclerosis [2] and Alzheimer's disease [3]. On the other hand, peptides are increasingly emerging as therapeutical agents, whereby the enantiomeric purity of each amino acid within the peptide is crucial, especially for those derived from synthesis [4]. On the other hand, non-ribosomal peptides produced by microorganisms, such as lipopeptides, are raising great interest as potential novel bioactive peptides. Their structure often contains D-amino acid enantiomers and frequently non-proteinogenic AAs such as aIle, aThr, and Hse, amongst many others [5].

For a long time, direct enantioselective gas chromatography on Chirasil Val using *N*- and *C*-terminal amino acid derivatization [5–8] or indirect chiral liquid chromatography (LC) on reversed phase columns using chiral derivatizing agents such as *ortho*-phthaldialdehyde (OPA) and chiral thiols [9] or Marfey's reagent [10–12] have been employed as first choice for chiral separation [13]. In the last decades, however, direct LC approaches using chiral stationary phases have become more popular for the analysis of complex amino acid enantiomer mixtures [11], allowing chiral separation of underivatized AAs [17] as well as achiral precolumn derivatization followed by mass spectrometric detection [14–17]. Common examples for achiral precolumn derivatization supporting chiral separation comprise 6-aminoquinolyl-*N*-hydroxysuccinimidyl carbamate (AQC) [18,19], 1-fluoro-2,4-dinitrobenzene (DNB-F, Sanger's reagent) [20], 4-fluoro-7-nitro-2,1,3-benzoxadiazol (NBD) [21], dansyl chloride (Dns) [22,23] and 9-fluorenylmethyl-chloroformate (Fmoc-Cl) [24–26]. Innovative approaches to analyze AAs comprise SFC [27], ion mobility mass spectrometry [28,29] and 2D-LC [25,30–33].

Many of these one-dimensional methods can separate the majority of amino acid enantiomers, but fail for the one or the other amino acid. One particular problem is the separation of the isobaric amino acids with isomeric side chains (e.g. Leu, Ile, aIle) or the secondary amino acids (like Pro). 2D-LC with achiral pre-separation can resolve some of these selectivity issues in complex samples and issues with interferences and matrix effects [30]. Although technically still challenging, the recent decade has experienced a great technological leap in multidimensional chromatography and

brought about commercially available, highly robust 2D-LC systems. This has triggered various endeavors to improve peak capacity, selectivity, resolving power, separation time etc. by establishing 2D-LC methods, despite the complex method development necessary to combine chromatographic parameters across multi-dimensional systems [30,34–39].

A special mode in 2D-LC analysis is multiple heart-cutting (MHC), in which multiple peaks or fractions thereof which contain the analyte/s of interest are transferred from the first dimension (^{1}D) to the second dimension (^{2}D) and then separated by a second complementary chromatographic principle [40,41]. Desirably, 2D-LC methods should exhibit a maximum extent of orthogonality between both dimensions, which is achievable when each of them targets a specific sample dimensionality (e.g. hydrophobicity in the ^{1}D and chirality in the ^{2}D, or vice versa).

MHC for AAs has been applied by Ianni et al. [22], Ishii et al. [21] and Woiwode et al. [42] using an achiral (RPLC) - chiral 2D-LC system after pre-column derivatization with either dansyl chloride, NBD-F and Sangers reagent, respectively. These reagents not only increase detectability, but also the RPLC retention of otherwise very hydrophilic amino acids. While tagging can improve electrospray ionization efficiency and detection sensitivity, even with HRMS the chromatographic resolution of isobaric amino acids is mandatory, especially the leucine analogues with alle being especially problematic. Woiwode et al. were able to separate all proteinogenic amino acids in one run (130 min) except for the isobaric analogues of Leu, which were only partially resolved, but enough to get clean cuts [42]. Hamase and coworkers usually select a set of biologically relevant amino acids, and their 2DLC as well as 3DLC separations have usually long analysis times (>2 h) [21,30].

The present study is focused on the establishment of a robust, fully automated online MHC achiral-chiral 2D-LC method using RPLC in the ^{1}D and cinchona alkaloid-derived ion-exchange type chiral stationary phases [43] in the ^{2}D for the analysis of AQC-derivatized AAs, which can accomplish the full separation in less than an hour. Chemoselective derivatization is a common strategy in amino acid analysis, for both achiral and chiral approaches. The advantages for the current chiral separation are manifold. It increases retention and selectivity of polar amino acids in RPLC, provides them with favorable functional groups tunable for effective chiral recognition process of the utilized chiral stationary phase (CSP), drives the relative enantiomer affinity towards the chiral selector and thus determines the elution order, and last but not least allows the introduction of chromophoric, fluorophoric, electrochemical and better ionizable mass tags for sensitive UV, fluorescence, electrochemical or MS detection.

Numerous derivatization reagents have been successfully tested and employed for the LC enantiomer separation on cinchonan carbamate based CSPs [44], including arylhalides such as Sanger's reagent [20,45], NBD-F [46–48], chloroformates or corresponding OSu derivatives such as FMOC-Cl/-OSu [25,49], acyl chlorides like benzoylchlorides [50,51], and AQC [19,52]. Precolumn derivatization of amino acids with 6-aminoquinolyl-*N*-hydroxysuccinimidyl carbamate (AQC) followed by reversed phase HPLC separation with fluorometric detection is a method suggested by pharmacopeias which makes it an attractive choice for ^{1}D separation. AQC combines favorable detection characteristics, possessing a strong quinoline chromophore for UV detection, which is also a fluorophore allowing highly sensitive fluorescence detection (FLD) (λ_{Ex} 250, λ_{Em} 395 nm) reaching LODs at the fmol level [12], but

representing also a favorable mass tag with excellent ionization efficiencies in positive ion mode for the negatively charged AQC-amino acid derivatives. Its fast reaction kinetics allows derivatization at 55 °C in 10 min. Moreover, D/L mixtures of [u-^{13}C^{15}N] amino acid internal standards are accessible by a simple protocol from commercially available L-[u-^{13}C^{15}N]-AA IS mix [18]. The stable isotope labelled D/L-internal standard mixture facilitates identification and allows corrections for (enantioselective) matrix effects when utilizing MS detection. Thus, in the current study, a standard mix of all proteinogenic amino acids, including the five isobaric analogues Hse, aThr, Tle, alle and Nle was prepared for method development and was additionally spiked with an L-[u-^{13}C^{15}N] amino acid IS standard mixture for ʟ-enantiomer identification.

Particular focus was set on the resolution of all AAs with emphasis on the isobaric analogues (Thr, aThr, Hse and Leu, Ile, aIle, Tle, Nle) for which neither MS nor the ^{2}D chiral separation has enough selectivity. Furthermore, for time-based sampling procedure excellent run-to-run repeatabilities are required for the ^{1}D RPLC separation and method optimization was carried out in consideration of this demand. An additional challenge was the complete enantioselective separation of all 24 chiral AA pairs within a reasonable timeframe on one chiral column in the ^{2}D to accommodate the complete analysis of all heart cuts. By the virtue of mass spectrometric detection, the separation of non-isobaric AAs in the ^{1}D was not critical. Chiral separation of all amino acids was finally achieved by a tandem setup with a core-shell *tert*-butyl carbamate modified quinine based chiral stationary phase (QN-AX) followed by a short zwitterionic quinine type stationary phase (Chiralpak ZWIX(+)) [15,53,54]. The applicability of the automated 2D-LC setup is demonstrated by the amino acid configuration determination of three peptides.

2. Materials and methods

2.1. Materials

Acetonitrile, methanol and formic acid (FA) purchased from Carl Roth (Karlsruhe, Germany) were of ultra-LC−MS grade quality. All amino acids (AAs), ammonium formate (NH$_4$FA), hydrochloric acid (HCl), dithiothreitol (DTT), deuterium oxide, deuterium chloride, boric acid, sodium hydroxide, iodoacetamide (IAA) were provided by Sigma Aldrich, Schnelldorf (Germany). A solution of uniformly labelled [u-^{13}C^{15}N] ʟ-amino acid metabolomics standard mix (2.5 mM in 0.1 M HCl) which contained all labelled proteinogenic amino acids with exception of asparagine, glutamine and tryptophan was acquired from Euroisotop GmbH (Saarbrücken, Germany) and was used as internal standard. Single L- or ᴅʟ-amino acid stock solutions (50 mM in 0.1 M HCl) were used to prepare a 2.5 mM stock solution. All amino acid standard solutions were stored at −20 °C prior to use. Water was purified using a Water Purelab Analytics Purification System from ELGA (Celle, Germany). 6-Aminoquinolyl-*N*-hydroxysuccinimidyl carbamate (AQC, AccQ) was purchased from Synchem (Felsberg/Altenburg, Germany). Derivatization reactions were performed in 1.5 mL Crystal Clear microcentrifuge tubes from Starlab (Hamburg, Germany) using a Thermo-Shaker PHMT Gant-bio for 1.5 mL micro-centrifugation tubes (PSC24 N) from Grant Instruments Ltd. (Shepreth, England).

For achiral chromatographic separations a ZORBAX SB-C18 (1 × 50 mm, 3.5 μm) from Agilent Technologies (Waldbronn, Germany), an Acquity UPLC BEH C18 (1 × 150 mm, 1.7 μm) and an

XBridge BEH C18 (1 × 150 mm, 3.5 μm), both from Waters (Eschborn, Germany), were used. For preliminary MHC-2D-LC experiments, a core-shell QN-AX column (3 × 50 mm, 2.7 μm, 160 Å) [54] was tested.

For the final optimized method, however, a self-made chiral QNAX-ZWIX tandem column consisting of a core-shell QN-AX column (3 × 50 mm, 2.7 μm, 160 Å) [54] coupled to an in-house packed Chiralpak ZWIX(+) FPP (3 × 20 mm, 3.0 μm) [53,55] column using a short stainless steel capillary (0.12 mm id, 75 mm) was employed.

2.2. Sample preparation

For peptide hydrolysis the sample was dissolved in 1 mL of 6 M DCl in D_2O (1 mg mL^{-1}). The glass vial was sealed under nitrogen and heat-treated at 110 °C for 16 h. Subsequently, the sample was evaporated to dryness, the residue re-dissolved to the original volume (1 mL) with 0.4 M borate buffer (pH 8.8), vortexed, and centrifuged for 60 s at 13,200 rpm. The supernatant was used for AQC derivatization of the liberated amino acids.

Non-isotopically labelled AA stock solutions (L-[u-$^{12}C^{14}N$]-amino acids) as standard mixtures were prepared at a concentration of 2.5 mM in 0.1 M HCl containing all proteinogenic amino acids and additionally Hse, aThr, alle, Tle and Nle as isobaric analogues.

2.2.1. Alkylation
Cysteine-containing mixtures were prepared according to the following protocol [14,18]. Iodoacetamide (IAA) and dithiothreitol (DTT) were freshly prepared at a concentration of 10 mM in ultrapure water shortly before use and kept on ice. Solutions of 10 μL AA mix (2.5 mM), 5 μL DTT and 10 μL L-[u-$^{13}C^{15}N$]-AA IS (0.25 mM) were added to a solution of 40 μL 0.4 M sodium borate buffer (pH 8.8) in a 1.5 mL microcentrifuge tube. The reaction solution was placed on a thermoshaker (Grand Instruments) and allowed to react at 800 rpm and 55 °C for 10 min. After short centrifugation (13200 rpm, 4 °C, 1 min), 10 μL IAA was added followed by heating (55 °C) and shaking (800 rpm) for 10 min. After centrifugation, 5 μL DTT were added followed by yet another step of heating and shaking. Subsequently, 40 μL of this solution was filled up to 50 μL with ultrapure water (0.25 mM AA mix-IAA). For direct MS measurements, the solution was further diluted 1:10 with 0.4 M sodium borate buffer (pH 8.8) prior to derivatization with AQC reagent.

2.2.2. Derivatization
The derivatization reagent AQC was prepared at a concentration of 3 mg mL^{-1} in dry acetonitrile (AQC: 10.5 mM), stored at −20 °C and shortly ultrasonicated before use. If not otherwise stated 10 μL sample solution (0.25 mM AA mix or hydrolyzed sample) was added to 80 μL 0.4 M sodium borate buffer (pH 8.8), followed by the addition of 10 μL AQC reagent solution. This reaction solution was immediately heated to 55 °C for 10 min at 800 rpm. After centrifugation the sample was ready to use. According to the European Pharmacopoeia 10.0 peak areas for AQC-amino acids remain unchanged for at least a week at room temperature. Nevertheless, the samples were constantly cooled in the autosampler at 4 °C and were only utilized for a week, then freshly prepared.

2.3. Instrumentation

An Agilent 1290 Infinity II 2D-LC Solution from Agilent Technologies (Waldbronn, Germany) was used for multiple heart-cutting 2D-LC (Suppl. Fig. S1). The ^{1}D LC consisted of a quaternary low pressure gradient UHPLC pump (Flexible Pump, G7104A), a Multisampler (G7167B), a Multicolumn Thermostat (G7116B), a

diode array detector (G7117B) with 1 μL flow cell (#G4212-60008) and a pressure release kit (G4236-60010) between UV-detector and 2D-interface. The ^{2}D comprised a binary high-pressure gradient UHPLC pump (High Speed Pump, G7120A), a valve drive (G1170A) with a 5 position/10 port 2D-LC active solvent modulation (ASM) valve (5067−4266) connected to two 6 position/14 port valve heads (5067−4142) carrying six 40 μL loops each and a multicolumn thermostat (G7116B). Experiments utilizing active solvent modulation (ASM) were performed with the ASM factor 5 (split ratio 1:4) restriction capillary (85 × 0.12 mm, 0.96 μL). For enhanced detection, a QuickSplit Flow Splitter from ERC (Riemerling, Germany) was installed prior to the detectors in the ^{2}D at a ratio of 1:5, whereby the high flow was directed to a variable wavelength detector (VWD) (G7114B) with a 2 μL (initially 14 μL) flow cell (G1314-60187) connected in series with a fluorescence detector (FLD) (G1321A) with an 8 μL flow cell (standard FLD cell) and the low flow to a TripleTOF 5600+ QTOF mass spectrometer from Sciex (Concord, Ontario, Canada) using a contact closure connection for peripheral devices. The acquisition rates were set to 10 Hz in the ^{1}D for the DAD, and 20 and 18.52 Hz for VWD and FLD detectors in the ^{2}D, respectively. Dwell volumes were determined using a zero dead volume union connector in place of the column. The measured dwell volumes were 550 μL in the ^{1}D and 120 μL in the ^{2}D at a flow rate of 0.20 mL min^{-1}. The 2D-chromatographic data were processed with Open Lab CDS Rev. C.01.07 SR4 from Agilent Technologies (Waldbronn, Germany) and DryLab 4 software (Molnár-Institute, Germany).

The optimization of the ^{2}D chiral separation was performed on an Agilent 1290 UHPLC system with a 1290 binary pump (G4220A), a 1290 thermostated column oven (G1316C), a Sciex calibrant delivery system (CDS) for calibration (Waldbronn, Germany) and a CTC-PAL HTS autosampler from CTC Analytics (Zwingen, Switzerland).

QTOF-MS measurements were performed using a Duospray ion source operated in positive electrospray ionization mode. The following MS instrument parameters were used: curtain gas (CUR) 40 psi, ion source gas (nebulizing gas; GS1) 60 psi, heater gas (drying gas; GS2) 60 psi, ion spray voltage floating (ISVF) 5500 V, source temperature (TEM) 400 °C and declustering potential (DP) 100 V. Data acquisition was performed in information-dependent acquisition (IDA) in high sensitivity mode with an inclusion list comprising the m/z ratios of the precursor ions of all single and double derivatized amino acid compounds (Table S2). The mass range of the TOF-MS full scan comprised m/z 30−2000 with an accumulation time of 250 ms and a collision energy (CE) of 10 V. MS/MS in IDA (top 4) was performed with 45 V CE and 15 V CE spread (CES) and an accumulation time of 100 ms. Mass calibration was conducted with a calibrant delivery system (Sciex, Darmstadt, Germany) through the APCI inlet using the positive calibration solution for the SCIEX X500 System. Data acquisition and analysis was performed with Analyst TF 1.7 and PeakView software (Sciex), respectively. Chromatographic conditions are specified in the respective figure captions.

3. Results and discussion

3.1. Optimization of ^{1}D for AA analysis

Several critical factors need to be considered for the ^{1}D method development, including sufficient resolution between critical peaks that cannot be resolved in the ^{2}D or by MS detection, mobile phase compatibility between ^{1}D and ^{2}D, run-to-run repeatability, and gradient-dwell volume as well as extra-column peak broadening effects. The AQC amino acid method stated in the European Pharmacopoeia (Ph. Eur.) 10th Edition exhibits full resolution of amino

acids including Ile and Leu. However, other isobaric amino acids often present in microbial lipopeptides like aIle, aThr, Hse are not considered. Their simultaneous achiral separation in the presence of all the other proteinogenic amino acids pose a major challenge for the ¹D RPLC-UV or -FLD method.

Initially three distinct mobile phase compositions were investigated on a Zorbax SB-RP (50 × 1.0 mm, 3.5 μm) containing water with 10 mM NH₄FA or 10 mM NH₄FA and 10 mM FA or 0.05% (v/v) FA as mobile phase A (MP-A) and ACN as MP-B (Fig. S2). Despite an efficient separation of most amino acids, the critical isobaric pair of Ile and aIle was not even partially separated. Consequently, the column was replaced by an Acquity UPLC BEH C18 (1 × 150 mm, 1.7 μm) column. Acidic analytes like AQC-amino acids exhibit stronger retention and good peak shapes with 0.1% TFA as additive. However, TFA was avoided for incompatibility reasons with the ²D as it represents a strong counterion for the anion exchange selector in the ²D chiral separation with quinine-type CSPs. Therefore, FA at 0.05% (v/v) as a weaker acid and counterion was deemed

appropriate for the compatibility between the ¹D and ²D. Furthermore, it was found that methanol improved the peak shapes for the early eluting amino acids, while ACN was more beneficial for the late eluting AAs. Consequently, a low percentage (1%, v/v) of MeOH was added to the aqueous MP-A, while ACN without additives was used as MP-B. As a result, all isobaric amino acids, namely Thr, aThr and Hse as well as Ile, aIle, Leu, Nle and Tle could be resolved from each other (Fig. S3). A further improvement of resolution and peak shape was achieved by elevating the temperature from 30 to 50 °C, especially for Met (9) and Tyr (12), Ile (8) and aIle (23), respectively
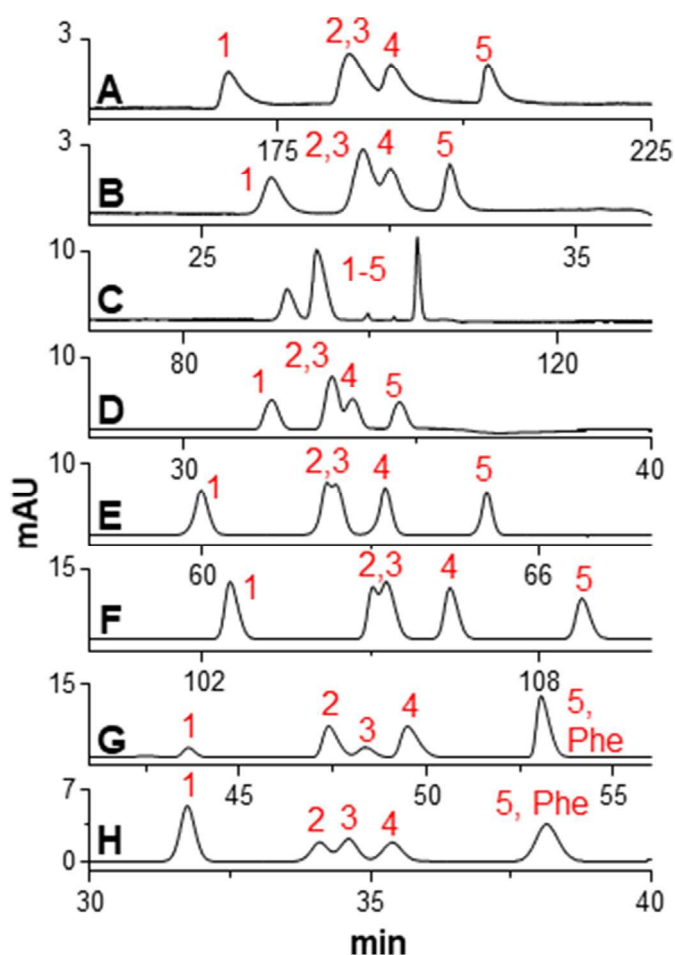

Fig. 1. Chromatographic separation of *tert*-Leucine (1), Isoleucine (2), *allo*-Isoleucine (3), Leucine (4), Norleucine (5) recorded on a variety of columns in under reversed phase conditions using **MP-A:** 0.05% FA + 1% MeOH in water and **MP-B:** 0.05% FA in ACN. Columns: **A:** COSMOSIL Cholester (250 × 4.6 mm, 2.6 μm), **B:** Cortecs C18+ (50 × 2.1 mm, 2.7 μm), **C:** COSMOCORE PBr (150 × 2.1 mm, 2.6 μm), **D:** Gemini C18 (100 × 1.0 mm, 3 μm), **E:** Kinetex C18 (100 × 3.0 mm, 2.6 μm), **F:** Poroshell EC C18 (150 × 3.0 mm, 2.7 μm), **G:** Acquity BEH C18 (150 × 1.0 mm, 1.7 μm), **H:** XBridge C18 (150 × 1.0 mm, 3.5 μm). Method transfers were executed for each column proceeding from the Acquity BEH C18 according to 0.5 μL injection volume, 0.15 mL min⁻¹ flow rate and the following gradient: 0−2.15 min − 0 %B, 2.15−24.65 min − 0-7.5 %B, 24.65−35.90 min − 7.5 %B, 35.90−47.15 min − 7.5−15 %B, 47.15−48.65 min − 15−50 % B, 48.65−51 min − 50 %B, 51−51.10 min − 50-0 %B, 50−65 min − 0 %B.
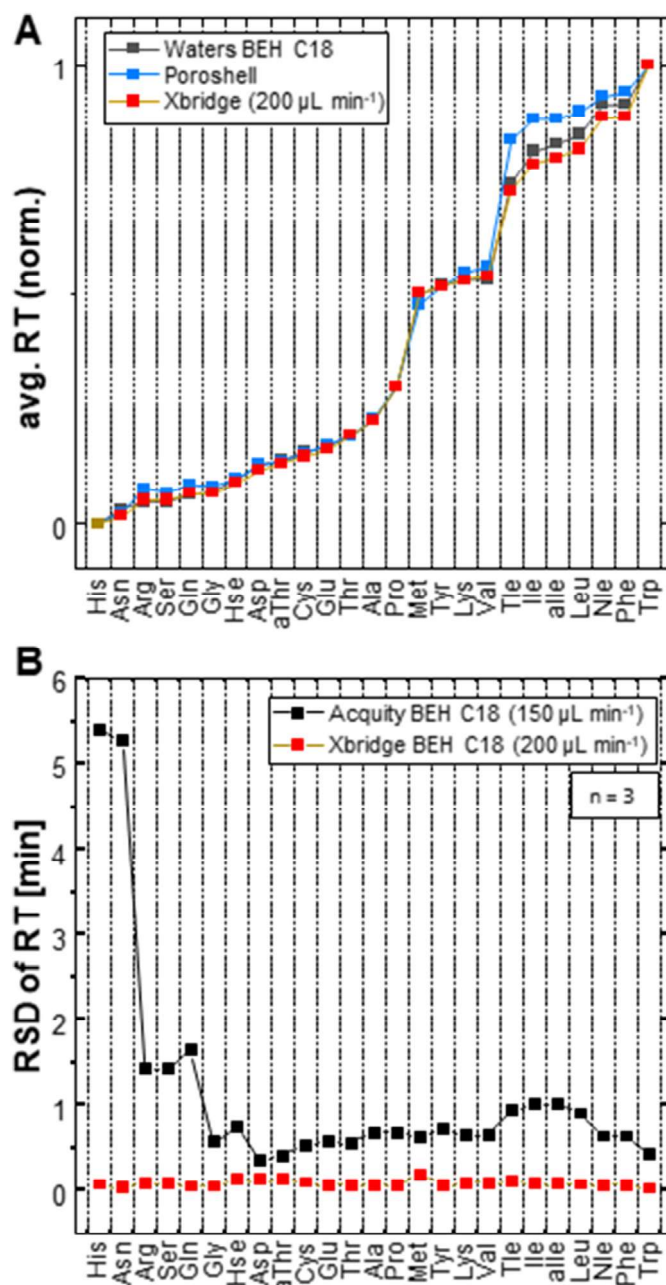

Fig. 2. A) Normalized retention times for 25 amino acids between the first and last eluting compounds were recorded on the following stationary phases: Acquity BEH C18 (150 × 1.0 mm, 1.7 μm), XBridge BEH C18 (150 × 1.0 mm, 3.5 μm) and Poroshell EC C18 (150 × 3.0 mm, 2.7 μm) according to the method conditions described in Fig. 1. B) RSDs (n = 3) of 25 AAs were calculated on the Acquity BEH C18 (150 × 1.0 mm, 1.7 μm) and XBridge BEH C18 (150 × 1.0 mm, 3.5 μm) at 150 μL min⁻¹ and 200 μL min⁻¹, respectively.

(Fig. S4). Although a flow rate of 0.07 mL min^{-1} was applied for method development, it was increased to 0.15 mL min^{-1} in order to stabilize run-to-run repeatability and reduce relative standard deviations of retention times across consecutive chromatograms (Fig. S5), which is a critical factor for time-based MHC 2D-LC. However, this improvement of repeatability was achieved at the expense of resolution for the early eluting AA pairs Arg/Ser, Gln/Gly, Val/Lys. Nle and Phe could not be resolved whichever flow rate was used. Since they are not isobaric they can be distinguished by MS detection. Finally, a DryLab optimization was performed to finalize method development for the ^{1}D resulting in a step gradient (step gradient 2, Fig. S6), which was used for further experiments [56].

In order to establish a successful time-based multiple heart-cutting method, the ^{1}D retention times have to be highly reproducible with a run-to-run repeatability of <0.5% RSD. The necessity of a time-based method will be discussed in chapter 3.4. The Acquity UPLC BEH (150 × 1.0 mm, 1.7 μm) column proved the necessary selectivity to successfully separate the isobaric compounds Tle, Ile, aIle, Leu and Nle, as shown above. However, the high backpressure generated by the 150 mm long column packed with 1.7 μm particles limited the working range of the flow rate to approximately 150 μL min^{-1}. This is still outside the flow rate for which the specifications of the ^{1}D quaternary pump confirm adequate gradient precision (≤0.07% RSD or 0.01 min for 0.2−5.0 mL min^{-1}). The resulting relative standard deviations for retention times, mainly originating from the low flow and low amounts of MP-B, were less than 5%. Yet, these slight retention time shifts frequently resulted in heart cuts beside the peak, which is a serious problem in terms of method ruggedness. Multiple optimization approaches considering re-equilibration time, the volatile additive MeOH, the dwell volume (exchange of quaternary for a binary pump) to improve the precision were undertaken without success. Increasing the flow rate was not possible due to the limiting backpressures imposed by the sub-2 μm column. Therefore, multiple other reversed phase columns were screened regarding their ability to separate the mentioned isobaric compounds. With a few exceptions, namely the Agilent Poroshell EC (150 × 3 mm, 2.7 μm) and the Waters XBridge BEH C18 (150 × 1.0 mm, 3.5 μm), with the latter having the same column chemistry as the Waters Acquity UPLC BEH C18, the majority of columns did not separate Ile, aIle and Leu (Fig. 1).

Since RP chromatography follows the linear solvent strength theory, the normalized retention times between the first and last eluting compounds allowed for a good comparison of selectivities between these columns. Indeed, they differed mainly for the late eluting isobaric compounds between the Poroshell EC C18 and the BEH C18 columns (Fig. 2A). Therefore, the XBridge BEH C18 (3.5 μm) was finally selected, because it allowed a significant reduction of the operating column backpressure and thus operation at an increased flow rate. When it was used at a flow rate of 200 μL min^{-1}, ^{1}D retention time precisions were below 0.25% RSD for all amino acids, which seems to be robust enough for reliable time-based multiple heart cutting 2DLC (Fig. 2B).

It should be noted that even higher ^{1}D flowrates are disadvantageous, since decreased ^{1}D retention times means that the ^{2}D runs must become faster.

3.2. Optimization of ^{2}D for AA analysis

The ^{2}D separation is facing some requirements which are challenging to achieve. First of all, the ^{2}D method must be capable to separate the enantiomers of all 19 chiral proteinogenic amino acids as well as the additionally relevant isobaric amino acids (aThr, Hse, aIle, Nle, Tle) on the same column and ideally with the same mobile phase. Second, the separation must be reasonably fast so that

always at least one of the 10 sampling loops of the MHC valve is available for peak storage when a new compound elutes in the ^{1}D. This is particularly challenging in the beginning of the ^{1}D chromatogram. In general, in heart cutting mode the speed of the ^{2}D is less restrictive, but determines the number of cuts that can be made per unit time. The goal here was to finish the entire 2D separation in maximum 60 min. With a panel of 25 targeted amino acids it means that the ^{2}D run time must be no longer than approximately 2 min. Unfortunately, the current software version does not allow to adjust analysis times individually for each ^{2}D run. Hence, the strongest retained analyte dictates the acceptable ^{2}D run time. Furthermore, mobile phase compatibility between ^{1}D and ^{2}D may be an issue. In chiral separation, selectivity may easily be lost if the optimal mobile phase is not employed. Furthermore, like in other modes of chromatography, peak distortion may occur due to mobile phase mismatch (the ^{1}D mobile phase represents the sample diluent for ^{2}D injection). For the currently evaluated QN-AX cinchonan carbamate CSP, ionic strength and possibly the water content of the ^{1}D eluent were envisioned to be critical factors in terms of compatibility. So finally, the selection of the ^{2}D phase system may be also driven by compatibility with the mobile phase of the ^{1}D.

Recent studies have shown that superficially porous particle (SPP) based CSPs outperform corresponding sub-2 μm fully porous particle CSPs in terms of speed of chiral separations [54]. This can be explained by a lower total surface area per column, and also lower total porosity and column void volume, respectively. For this reason, initial experiments were employed on QN-AX SPP-based CSP, which consisted of a solid core (1.7 μm Ø) and a porous shell (0.5 μm) with 160 Å. This favorable particle morphology resulted in a gain in efficiency due to an overall improvement of the A, B and C terms in the van Deemter equation at reduced backpressures compared to sub-2 μm particle columns favorable for high speed separations at a sub-minute time scale [53,57].

The QN-AX CSP operates by an anion-exchange principle and tolerates a higher water content in the transferred fractions as long as ionic strength is lower than in the ^{2}D eluent. The main driving force for retention is the ionic interaction between the weak anion-exchange site of the quinuclidine ring and the acidic functional group of the analyte, while additional interactions such as hydrogen-bonding between the carbamate moiety of the CSP and urea group of the AQC-tag, π-π stacking between aromatic moieties of selector and selectand, van der Waals interaction and steric hindrance caused by the *tert*-butyl motif of the selector influence both retention and chiral recognition. A prototype QN-AX core-shell CSP (3 × 50 mm, 2.7 μm) was investigated more extensively after providing more promising results in a preliminary test. Initial tests revealed that Asp, Arg, His are the critical amino acids besides the isobaric compounds of Thr and Leu, which are already separated in the ^{1}D. Preliminary optimization was only performed with these amino acids, focusing on factors such as buffer concentration, water content, and gradient elution in the polar organic mode. The analyte retention obeys the stoichiometric displacement model and can be steered by the amount and ratio of acidic and basic additives [58,59]. With the mobile phase generally constituted of x mM NH$_4$FA + x mM FA + 0.5% H$_2$O in MeOH (x = 1, 2.5, 5, 10 & 50), enantioseparation increased with decreasing molarities of additives, especially for the isobaric analogues of Leu and Thr. Low molarities provided a handicap for the acidic amino acids (Glu and Asp), since retention times were too high (up to 40 min). At 50 mM they were well resolved within a short time, but enantiomers of isobaric compounds of Leu were insufficiently separated. Furthermore, Arg was unfortunately not resolved under either condition. Considering the amount of water in the mobile phase, an improved resolution of Arg and His was observed at a low water content.

Since a certain water content is inevitably introduced to the ^{2}D depending on the elution time in the ^{1}D, it was further investigated by injecting 20 μL of diluted aqueous sample into different mobile phases whether the water content would be tolerated. Unfortunately, no reasonable mobile phase conditions, which tolerated a transfer of the aqueous sample from ^{1}D to ^{2}D without loss of resolution were found for AQC-DL-Arg. Subsequently, flow rate and temperature were evaluated, resulting in 50 mM NH$_4$FA + 50 mM FA + 0.5% H$_2$O in MeOH, 1 mL min^{-1}, 30 °C as the final condition, with which all DL-enantiomers were separated within 1.5 min, except for Asp which required 2.5 min and no separation was achievable for Arg. The latter were finally resolved with a QN-AX/ZWIX tandem column approach (*vide infra*).

3.3. Establishing the MHC 2D-LC-QTOF MS method

The current multiple heart-cutting 2D-LC method utilized an interface with a central 2D-LC ASM valve head connected to two loop decks each carrying 6 sample storage loops á 40 μL (for details see suppl. Fig. S1). Five of the six loops of each loop deck could be used for sample storage while one loop was always reserved for the

^{1}D mobile phase flow-through and ^{2}D eluent, respectively. Hence, in total 10 loops were simultaneously available for fraction collection. Heart cuts taken from the first dimension were analyzed as quickly as possible in an automated manner. The system was also optimized to minimize detrimental extra-column effects. In order to prevent a loss of resolution in the ^{1}D, the standard ^{1}VWD with 14 μL flow cell was exchanged for a DAD with 1 μL cell, which had a beneficial effect on Rs in the ^{1}D (see Suppl. S8). In addition, the flow path through the ^{1}D and ^{2}D column compartment was optimized by removal of the ^{2}D UV detector, which resulted in a significantly improved ^{2}D resolution (see suppl Figs. S7 and S8).

In the normal MHC mode, the first fraction was collected in loop 1 of deck A and immediately analyzed. The next cuts were stored in deck B, until the ^{2}D was available for the analysis of the collected fractions (see Fig. S9b for a typical sampling table). In this sampling mode, the loops were filled in a consecutive order and analyzed in the reversed order, followed by a loop and transfer capillary flush to avoid carryover and contamination. During challenging separations with more than 20 cuts, it may happen that not all peaks from the ^{1}D are collected with this sampling mode, e.g. the last peak in suppl. Fig. S9b could not be parked. A "smart peak parking" algorithm,
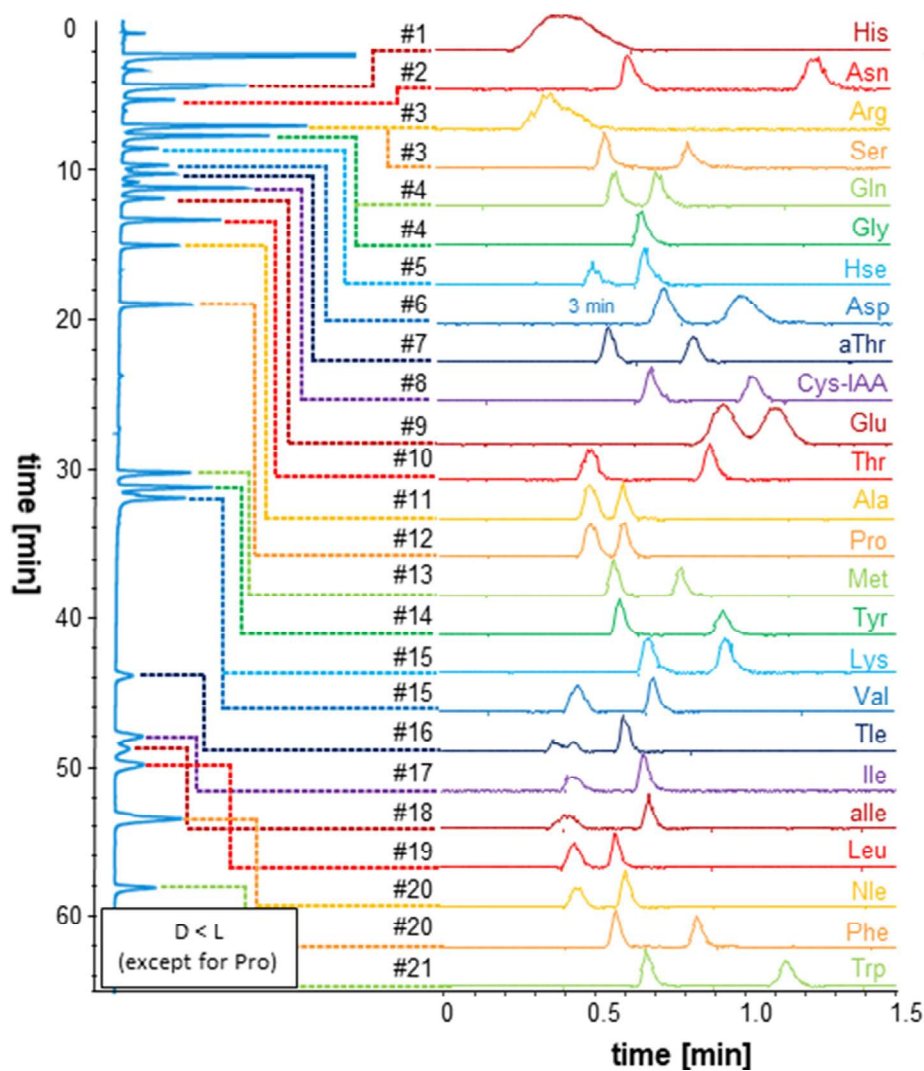

Fig. 3. Multiple heart cut 2D-LC analysis of 25 amino acids. Sample: 0.25 mM AA mix (25-DL-AA, 17 L-[u-^{13}C^{15}N]-AA and Cys-IAA-AQC). **^{1}Column:** BEH-C18 (1 × 150 mm, 1.7 μm); **^{1}MP-A:** 0.05% FA + 1% MeOH in water; **^{1}MP-B:** 0.05% FA in ACN; **^{1}Gradient:** 0−30 min 0−7.5% B, 30−45 min 7.5−7.5% B, 45−60 min 7.5−15% B; **^{1}F:** 0.15 mL min^{-1}; **^{1}T:** 50 °C, **^{1}Inj. vol.:** 0.5 μL, **^{2}Column:** QNAX core-shell (3 × 50 mm, 2.7 μm); **^{2}MP-A1** (isocratic): 50 mM NH$_4$FA + 50 mM FA + 0.5% H$_2$O in MeOH; **^{2}F:** 1 mL min^{-1}; **^{2}T:** 30 °C; smart peak parking.

however, does not follow the consecutive analysis order, but further optimizes the sampling and analysis procedure across both sampling decks, thereby maximizing the amount of attainable cuts (see suppl. Fig. S9a for an example and Table S5 for the final method).

Multiple heart-cutting can be performed in two sampling modes, either "time-based" or "peak-based". A time-based method places manually defined heart-cuts according to a sampling table,

which is usually constructed in accordance to a ^{1}D reference chromatogram. A peak-based method on the other hand does not need a prior run as it utilizes a predefined upslope or threshold (or a combination of both) of a peak eluting from the ^{1}D to automatically trigger a heart cut, which requires a detector in the ^{1}D. Each mode has its advantages and limitations. Peak based methods better cope with slight retention time shifts in the ^{1}D which do not
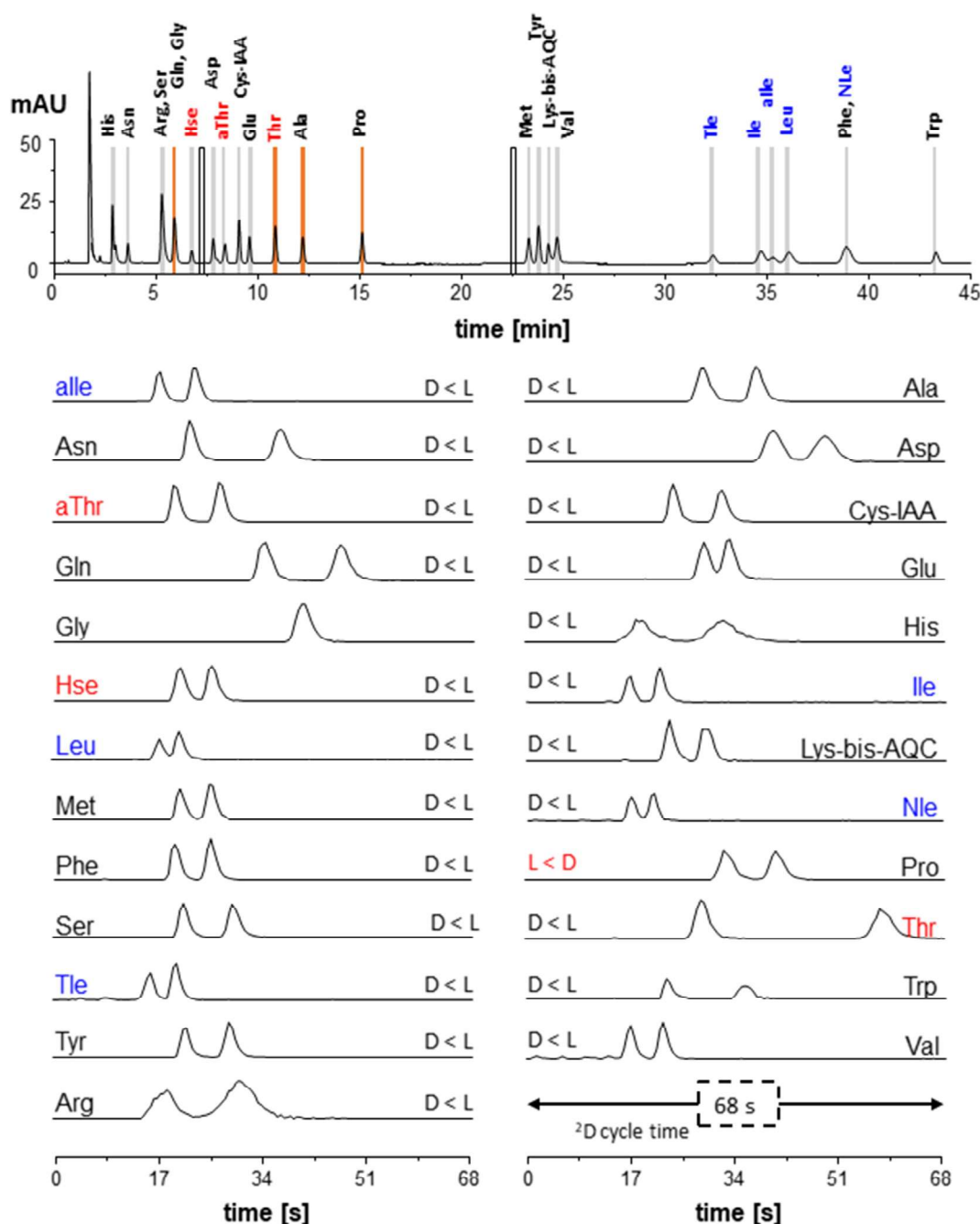

Fig. 4. A multiple heart cut 2D-LC analysis of 25 amino acids with tandem column in ^{2}D. The sample contained 0.25 mM AA mix (25-DL AA, 17 L-[u-^{13}C^{15}N]-AA and Cys-IAA-AQC) separated according to the following conditions. ^{1}**Column:** XBridge (150 × 1.0 mm, 3.5 μm); ^{1}**MP-A:** 0.05% FA + 1% MeOH in water; ^{1}**MP-B:** 0.05% FA in ACN; ^{1}**Gradient:** 0−2.15 min − 0 %B, 2.15−24.65 min − 0-7.5 %B, 24.65−35.90 min − 7.5 %B, 35.90−47.15 min − 7.5−15 %B, 47.15−48.65 min − 15−50 %B, 48.65−51 min − 50 %B, 51−51.10 min − 50-0 %B, 50−65 min − 0 %B; ^{1}**F:** 0.15 mL min^{-1}; ^{1}**T:** 50 °C, ^{1}**Inj. vol.:** 0.5 μL, ^{2}**Column (tandem):** QNAX core-shell (3 × 50 mm, 2.7 μm)→Chiralpak ZWIX(+) FPP (3 × 20 mm, 3.0 μm).; ^{2}**MP-A1** (isocratic)**:** 50 mM NH$_4$FA + 50 mM FA + 0.5% H$_2$O in MeOH (grey cuts) or ^{2}**MP-B1** (isocratic)**:** 10 mM NH$_4$FA + 10 mM FA + 0.5% H$_2$O in MeOH (orange cuts); ^{2}**F:** 2 mL min^{-1}; ^{2}**T:** 30 °C; smart peak parking utilizing dummy cuts (white cuts) for equilibration of ^{2}D. (For interpretation of the references to colour in this figure legend, the reader is referred to the Web version of this article.)

affect proper fraction transfer into the ^{2}D. On the other hand, peaks that are not baseline resolved may not be recognized as separate peaks. If a sample contains several unexpected components and all loops are already occupied, the relevant peaks will be skipped when they elute.

In contrast to peak-based sampling, a time-based method requires a highly reproducible ^{1}D retention time, otherwise the cut will be made "off-target". As pointed out above, in this sampling mode the advanced feature "smart peak parking" is available. It is more efficient and actually required to manage highly complex ^{1}D chromatograms as the example in Fig. S9 shows. The resulting seemingly random parking and analysis order is recorded in a sampling table, which contains the sampling time of each loop and the subsequent analysis time in the ^{2}D.

Fig. 3 shows the enantioselective multiple heart-cut 2D-LC-analysis of the 25 precolumn-derivatized AQC amino acids. The sampling time in the ^{1}D was 0.2 min for all peaks. Since some critical amino acids required a low molarity of the buffer additives in the ^{2}D, as outlined above, a "shifted step gradient" method was established in the ^{2}D, utilizing the sampling table shown in Table S3. In fact, all separations were performed in isocratic mode (50 mM) except cuts # 4,11 and 13, which were performed with a 10 mM buffer concentration (see caption of Fig. 3). Single dummy cuts on blank ^{1}D baseline without an analyte peak were utilized before the peak was analyzed with altered conditions to assure sufficient column equilibration. The critical peak pair Ile and aIle, which would otherwise co-elute in the ^{2}D, were resolved in the ^{1}D. To make sure that pure fractions of these AAs are sampled, the cuts were taken at the ascending and descending parts of the Ile and aIle peaks. Thus, by comparing the EICs of Leu and aIle with the isotopic labelled standards of AQC-L-[u-^{13}C^{15}N]-Leu and -Ile, the peak purity of the sampled Ile and aIle was confirmed (Figs. S10 and S11). This kind of flexibility cannot be realized with a peak-based method. The elution order was D < L except for Pro. Asp eluted after 3 min only, and eluted in the next chromatogram ("wrap-

around") which is uncritical with MS detection. All amino acids were well resolved in enantiomer pairs, with the exception of His and Arg, which exhibit repulsive forces between their cationic side chains and the positively charged anion exchange site of the QN-AX selector.

To alleviate this problem, a tandem column approach was evaluated [15,60–62]. The 50 × 3 mm 2.7 μm QN-AX core-shell column (first column) was coupled in-line with an in-house packed 3 × 20 mm, 3.0 μm fully porous particle Chiralpak ZWIX(+) column as the second column and used for the ^{2}D. The corresponding MHC 2D-LC enantioseparation is depicted in Fig. 4. The additional cation exchange site of the ZWIX selector provides an additional retention increment for the amino acids with cationic side chains (Arg, His) which are the most strongly retained amino acids on this column; hence their enantiomers can be well resolved. The amino acids with acidic side chains are less retained on the ZWIX column due to repulsive electrostatic interaction between their carboxylate side chain and the SCX moiety. The retention factors of the two columns in the tandem column approach is additive and due to the same stereoconfiguration of their quinine-derived selectors their relative enantiomer affinities and elution orders are the same in the two columns, allowing a full separation of all amino acids. To compensate for the longer run times with the tandem column, the flow rate was increased from 1 to 2 mL min^{-1}. The isobaric amino acids are depicted in blue and red. The increased ^{1}F reduced the total analysis time to 45 min (plus 15 min re-equilibration of the ^{1}D). Accompanied by an increased ^{2}F, the ^{2}D cycle time could be reduced to 68 s, without re-equilibration necessary due to the isocratic nature of the method. For Thr, Ala, Pro and Gly a lower ionic strength eluent (indicated in Fig. 4 by orange heart cuts) was used (employing 10 mM NH$_4$FA + 10 mM FA + 0.5% H$_2$O in MeOH instead of 50 mM NH$_4$FA + 50 mM FA + 0.5% H$_2$O in MeOH), which in accordance to the stoichiometric displacement model enables stronger retention in ion-exchange mode. The blank heartcuts were placed as dummy cuts to equilibrate the ^{2}D column when the

Table 1
Chromatographic parameters for AQC-derivatized AAs obtained by multiple heart cutting RPLC-chiral HPLC-ESI-QTOF-MS. ^{2}Mobile phase (isocratic)**:** 50 mM NH$_4$FA + 50 mM FA + 0.5% H$_2$O.

AA-AQC	Cut #	^{1}D RT [min]	^{1}RSD (%)	^{2}D RT D-AAs [min]	^{2}RSD [%] D-AAs	^{2}D RT L-AAs [min]	^{2}RSD [%] L-AAs	Elution order	$^2\alpha_{DL}$	$^2R_{DL}$
His	1	2.847	0.084	0.313	0.206	0.537	0.131	D < L	3.054	1.950
Asn	2	3.626	0.047	0.372	0.960	0.618	0.317	D < L	2.462	3.943
Arg	3	5.262	0.091	0.301	0.388	1.509	0.187	D < L	13.395	9.315
Ser	3	5.262	0.091	0.353	0.192	0.489	0.000	D < L	1.910	2.533
Gln[a]	4	5.896	0.060	0.574	0.000	0.783	0.166	D < L	1.564	2.812
Gly[a]	4	5.896	0.060	0.680	0.038	—	—	—	—	—
Hse	5	6.762	0.141	0.322	0.098	0.401	0.056	D < L	1.671	1.537
Asp	7	7.361	0.140	0.665	0.085	0.806	0.049	D < L	1.306	1.391
aThr	8	8.348	0.149	0.335	0.042	0.457	0.042	D < L	1.929	2.420
Cys-IAA	9	9.058	0.108	0.401	0.275	0.533	0.062	D < L	1.672	2.488
Glu	10	9.574	0.078	0.485	0.059	0.552	0.000	D < L	1.238	1.100
Thr[a]	11	10.863	0.077	0.478	0.195	0.969	0.031	D < L	2.789	5.997
Ala[a]	12	12.215	0.079	0.481	0.088	0.628	0.033	D < L	1.531	2.232
Pro[a]	13	15.105	0.070	0.681	0.141	0.544	0.035	L < D	1.403	1.881
Met	15	23.317	0.204	0.341	0.398	0.427	0.442	D < L	1.629	1.740
Tyr	16	23.795	0.078	0.356	0.095	0.477	0.024	D < L	1.796	2.436
Lys-bis-AQC	17	24.277	0.102	0.388	0.362	0.488	0.341	D < L	1.543	1.730
Val	18	24.707	0.097	0.280	0.357	0.369	0.388	D < L	2.168	1.912
Tle	21	32.359	0.122	0.262	0.044	0.332	0.033	D < L	2.208	1.465
Ile	23	34.688	0.097	0.282	0.015	0.365	0.015	D < L	2.062	1.852
aIle	25	35.261	0.089	0.292	0.016	0.389	0.032	D < L	2.108	2.013
Leu	26	36.056	0.084	0.289	0.023	0.343	0.000	D < L	1.635	1.160
Phe	28	38.916	0.074	0.332	0.014	0.429	0.000	D < L	1.755	1.967
Nle	28	38.916	0.074	0.287	0.014	0.346	0.038	D < L	1.707	1.306
Trp	30	43.267	0.036	0.376	0.035	0.585	0.034	D < L	2.212	3.385

^a ^{2}Mobile phase (isocratic)**:** 10 mM NH$_4$FA + 10 mM FA + 0.5% H$_2$O.
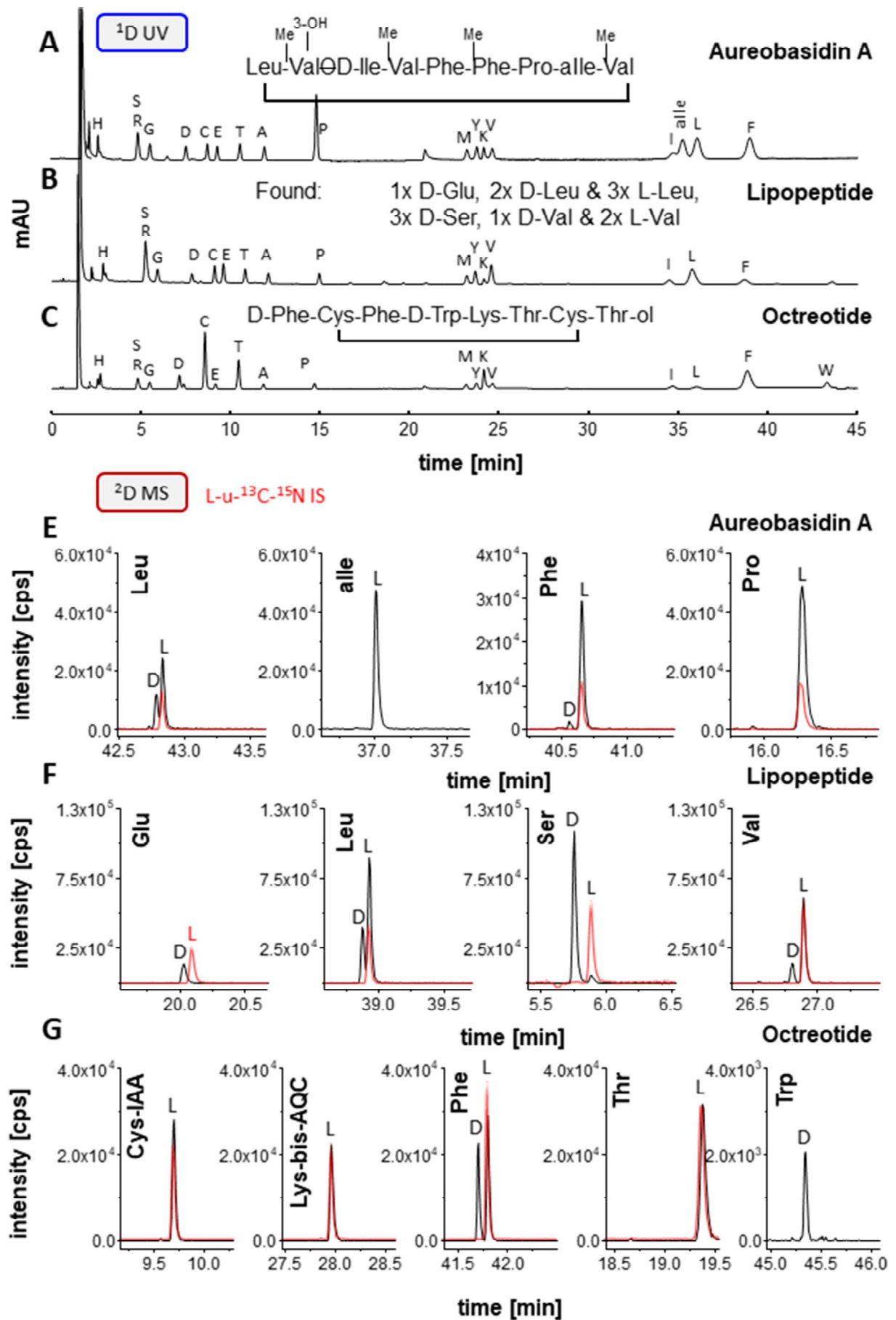
Fig. 5. Applied multiple heart cutting 2D-LC for Aureobasidin A, a lipopeptide research sample and Octreotide. The corresponding [1]D UV chromatograms (**A**, **B**, **C**) and the corresponding [2]D XICs of the identified AAs (**D**, **E**, **F**) are depicted, respectively. All proteinogenic AAs (except Trp, Gln and Asn) were included as L-[u-[13]C[15]N] internal standard for reference.

mobile phase conditions change (note, the analysis order of the dummy cuts does not correspond to the position in the [1]D chromatogram due to the smart peak parking algorithm). The full sampling table of this optimized method can be found in Suppl. Table S3. Table 1 summarizes the chromatographic data of the [1]D and [2]D along with run-to-run repeatability (n = 3). It can be seen that the precision of [1]D retention time was always <0.21% RSD and that of the [2]D typically <0.4% RSD. All amino acids are fully baseline resolved (except Leu and Glu with Rs 1.1) which indicates the practical suitability for applications in AA stereoconfiguration determination of peptide hydrolysates. Although being not of relevance in the current application, LODs were estimated to be around 1.11 nM (which corresponds to 0.111 pmol injected on-column in the [1]D or 0.055 pmol per enantiomer peak in the [2]D).

Comparable 2D-LC methods perform inferior in either analysis time, maximum number of surveilled amino acids or both. Hamase et al. typically utilize more than 2 h for selected amino acids at a time, nonetheless with the advantage of quantitative sampling and an increased avoidance of matrix interferences from real samples [21,30,63]. Similarly, in an achiral-chiral approach Woiwode et al. [42] and Ianni et al. [22] were unable to resolve the isobaric compounds Ile, Leu, and aIle in the achiral dimension, with analysis times of >115 min for 16 AAs and 130 min for 22 AAs, respectively. In a 1D approach, Kimura et al. [15] and Horak et al. [14] managed the separation of all proteinogenic amino acids (including aIle and aThr) within 60 min on a coupled QN-AX/ZWIX(+) and ZWIX(+) CSP, respectively, unfortunately without the resolution of D-Ile and D-aIle, which is the main drawback. Amino acid enantioseparation using GC−MS on Chirasil L-Val as the state of the art remains a valuable alternative, whereby enantiomers of Leu, Ile and aIle can be well resolved but other amino acids are problematic such as Arg, His and Cys [5,64].

3.4. Application for the elucidation of absolute configurations in peptides

The assignment of the absolute configurations of the amino acid constituents is an integral part of the structure elucidation of novel peptides from the natural pool as well as in quality control of the stereointegrity of therapeutic and synthetic peptides, respectively. For this purpose, peptide hydrolysis was performed according to the European Pharmacopoeia 10.0 in order to release the free amino acids for subsequent enantioselective MHC 2D-LC amino acid analysis.

3.4.1. Aureobasidin

Aureobasidin A, a cyclic depsipeptide with antifungal activity, was chosen as an exemplary L-aIle containing peptide (Fig. S12). Besides, the peptide hydrolysate should contain a number of proteinogenic amino acids (L-Leu, L-Pro, and L-Phe) as well as special amino and hydroxy acids (N-methyl-L-valine, N-methyl-L-phenyl-alanine, 2-(R)-hydroxy-3-(R)-methylpentanoic acid, β-hydroxy-N-methyl-L-valine) (which were not in the focus herein) [65,66]. The experimental results (Fig. 5E) indeed reveal the presence of L-aIle L-Leu, L-Pro, and L-Phe. However, also D-Leu and a small quantity of D-Phe were found which might result from peptide impurities in aureobasidin A (see Fig. S12) [66]. Note, only the targeted 25 amino acids were transferred from the [1]D to the [2]D for MS detection, therefore N-methylated and hydroxylated AAs were not analyzed. These uncommon amino acids, however, could be targeted in an adjusted MHC method.

3.4.2. Lipopeptide

Lipopeptides are produced by certain bacteria strains that frequently contain a significant percentage of D-amino acids (which

protect them from enzymatic digestion) and very often non-proteinogenic AAs such as aIle. The optimized enantioselective MHC-2DLC amino acid analysis method was implemented for the qualitative analysis of a novel lipopeptide following acidic hydrolysis.

According to genome sequencing and NMR data [67], the cyclic peptide moiety contained Glu, Leu, Ser, Val, but their ratio and stereoconfiguration was unknown. The [1]D UV chromatogram of the sample including internal standards is shown in Fig. 5B. It turned out that no aIle was present in this lipopeptide, however, a number of D-amino acids were confirmed. The L-configured isotopically labelled internal standards allowed a clear identification between the D- and L-isomers, and the area ratios allowed the determination of the number of the respective amino acid in the peptide. From the chromatogram shown in Fig. 5F it can be seen that the analyzed lipopeptide research sample is constituted of 1x D-Glu, 2x D-Leu, 3x L-Leu, 3x D-Ser, 1x D-Val and 2x L-Val. However, the actual peptide sequence within the cyclic peptide has yet to be elucidated, by utilizing a different approach that preserves the amino acid connectivity [5].

3.4.3. Octreotide

A further example was the analysis of the hydrolysate from the cyclic therapeutic peptide Octreotide, which is a synthetic analog of the peptide hormone somatostatin. Its C-terminal Thr is reduced to an alcohol and the ring closure is obtained by a disulfide bridge between two Cys residues. The synthetic peptide contains two D-amino acids, i.e. one D-Trp and one D-Phe. The EICs of all expected amino acids Cys-IAA, Lys-bis-AQC, Phe, Thr and Trp are shown in Fig. 5G. It becomes evident that the current Octreotide sample has correct stereochemical integrity. Trp was present only in D-form, Phe as 1:1 mixture of D and L, while the other amino acids (Cys, Lys, Thr) were present in L-form only. The configuration of threaninol must be analyzed by a different method.

4. Conclusion

A targeted enantioselective MHC 2D-LC-ESI-QTOF-MS amino acid analysis method was established for the simultaneous enantioseparation of all proteinogenic amino acids, including the side chain isomeric analogues of Leu (aIle, Nle, Tle), and Thr (aThr, Hse) (in total 25 components), within a total runtime of 45 min (including re-equilibration 65 min). The [1]D achiral RPLC separation resolved the majority of amino acids from each other and from their isomeric analogues which could not be separated simultaneously by the [2]D chiral separation. Particularly challenging was the separation of aIle and Ile, besides Leu, in the [1]D, but was finally accomplished on an XBridge BEH C18 column. Complete enantioseparation of all 24 chiral amino acids was achieved by constructing a robust [1]D achiral separation (RSD of retention times < 0.21%, n = 3) utilizing a tandem column approach with a 2.7 μm QNAX core-shell column (5 cm long) and a short 3 μm FFP ZWIX(+) column (2 cm long) in the [2]D for fast enantiomer separation of the AQC-amino acids in less than 68 s. The AQC tag not only provided a chromophor and fluorophor, but also an easily ionizable mass tag allowing highly selective and sensitive MS detection. The achiral pre-separation not only ensured proper separation of the isobaric amino acids, but may be beneficial if a more complex matrix is present, reducing bias from matrix effects. The automated MHC 2D-LC setup can be applied for the quality control of the integrity of the stereochemistry of amino acid constituents in therapeutic peptides and structural elucidation of the configurations in natural (lipo-/cyclo-)peptides. Similar MHC-2D-LC methods can be developed with little adaptations for other analytes and could be particularly valuable for chiral drugs with multiple chiral centers.

CRediT authorship contribution statement

Ryan Karongo: Investigation, Methodology, Formal analysis, Data curation, Visualization, Writing − original draft, Writing − review & editing. **Min Ge:** Investigation, Methodology, Formal analysis, Data curation, Writing − review & editing. **Christian Geibel:** Investigation, Writing − review & editing. **Jeannie Horak:** Conceptualization, Methodology, Supervision, Writing − review & editing. **Michael Lämmerhofer:** Conceptualization, Methodology, Supervision, Writing − review & editing, Resources, Funding acquisition.

Declaration of competing interest

The authors declare that they have no known competing financial interests or personal relationships that could have appeared to influence the work reported in this paper.

Acknowledgements

Appendix A. Supplementary data

Supplementary data to this article can be found online at https://doi.org/10.1016/j.aca.2021.338858.

References

[1] P.M. Masters, J.L. Bada, J. Samuel Zigler, Aspartic acid racemisation in the human lens during ageing and in cataract formation, Nature 268 (5615) (1977) 71−73.

[2] M.G. Friedrich, S.E. Hancock, M.J. Raftery, R.J.W. Truscott, Isoaspartic acid is present at specific sites in myelin basic protein from multiple sclerosis patients: could this represent a trigger for disease onset? Acta Neuropathologica Communications 4 (1) (2016) 83.

[3] T.R. Lambeth, D.L. Riggs, L.E. Talbert, J. Tang, E. Coburn, A.S. Kang, J. Noll, C. Augello, B.D. Ford, R.R. Julian, Spontaneous isomerization of long-lived proteins provides a molecular mechanism for the lysosomal failure observed in Alzheimer's disease, ACS Cent. Sci. 5 (8) (2019) 1387−1395.

[4] M. D'Hondt, N. Bracke, L. Taevernier, B. Gevaert, F. Verbeke, E. Wynendaele, B. De Spiegeleer, Related impurities in peptide medicines, J. Pharmaceut. Biomed. Anal. 101 (2014) 2−30.

[5] H. Gerhardt, A. Sievers-Engler, G. Jahanshah, Z. Pataj, F. Ianni, H. Gross, W. Lindner, M. Lämmerhofer, Methods for the comprehensive structural elucidation of constitution and stereochemistry of lipopeptides, J. Chromatogr. A 1428 (2016) 280−291.

[6] E. Bayer, H. Allmendinger, G. Enderle, B. Koppenhoefer, Anwendung von d-Chirasil-Val bei der gas-chromatographischen Analytik von Enantiomeren, Fresenius' Z. für Anal. Chem. 321 (4) (1985) 321−324.

[7] V. Schurig, Separation of enantiomers by gas chromatography, J. Chromatogr. A 906 (1) (2001) 275−299.

[8] B. Koppenhoefer, V. Muschalek, M. Hummel, E. Bayer, Determination of the enhancement of the enantiomeric purity during recrystallization of amino acids, J. Chromatogr. A 477 (1) (1989) 139−145.

[9] Z. Dai, Z. Wu, S. Jia, G. Wu, Analysis of amino acid composition in proteins of animal tissues and foods as pre-column o-phthaldialdehyde derivatives by HPLC with fluorescence detection, J. Chromatogr. B 964 (2014) 116−127.

[10] S. Sethi, J. Martens, R. Bhushan, Assessment and application of Marfey's reagent and analogs in enantioseparation: a decade's perspective, Biomed. Chromatogr. 35 (1) (2021), e4990.

[11] I. Ilisz, A. Péter, W. Lindner, State-of-the-art enantioseparations of natural and unnatural amino acids by high-performance liquid chromatography, Trac. Trends Anal. Chem. 81 (2016) 11−22.

[12] S. Ferre, V. Gonzalez-Ruiz, D. Guillarme, S. Rudaz, Analytical strategies for the determination of amino acids: past, present and future trends, J Chromatogr B Analyt Technol Biomed Life Sci 1132 (2019) 121819.

[13] S. Tanwar, R. Bhushan, Enantioresolution of amino acids: a decade's perspective, prospects and challenges, Chromatographia 78 (17) (2015) 1113−1134.

[14] J. Horak, M. Lämmerhofer, Stereoselective separation of underivatized and 6-aminoquinolyl-N-hydroxysuccinimidyl carbamate derivatized amino acids

using zwitterionic quinine and quinidine type stationary phases by liquid chromatography-High resolution mass spectrometry, J. Chromatogr. A 1596 (2019) 69−78, https://doi.org/10.1016/j.chroma.2019.02.060.

[15] R. Kimura, H. Tsujimura, M. Tsuchiya, S. Soga, N. Ota, A. Tanaka, H. Kim, Development of a cognitive function marker based on D-amino acid proportions using new chiral tandem LC-MS/MS systems, Sci. Rep. 10 (1) (2020) 804.

[16] S. Du, Y. Wang, C.A. Weatherly, K. Holden, D.W. Armstrong, Variations of l- and d-amino acid levels in the brain of wild-type and mutant mice lacking d-amino acid oxidase activity, Anal. Bioanal. Chem. 410 (12) (2018) 2971−2979.

[17] K. Yoshikawa, M. Furuno, N. Tanaka, E. Fukusaki, Fast enantiomeric separation of amino acids using liquid chromatography/mass spectrometry on a chiral crown ether stationary phase, J. Biosci. Bioeng. 130 (4) (2020) 437−442.

[18] J. Horak, M. Lämmerhofer, Derivatize, racemize, and analyze—an easy and simple procedure for chiral amino acid standard preparation for enantioselective metabolomics, Anal. Chem. 91 (12) (2019) 7679−7689, https://doi.org/10.1021/acs.analchem.9b00666.

[19] R. Hellinger, J. Horak, W. Lindner, Enantioseparation of 6-aminoquinolyl-N-hydroxysuccinimidyl carbamate tagged amino acids and other zwitterionic compounds on cinchona-based chiral stationary phases, Anal. Bioanal. Chem. 405 (25) (2013) 8105−8120.

[20] A. Acquaviva, G. Siano, P. Quintas, M.R. Filgueira, C.B. Castells, Chiral x Achiral Multidimensional Liquid Chromatography. Application to the enantioseparation of dintitrophenyl amino acids in honey samples and their fingerprint classification, J. Chromatogr. A 1614 (2019), 460729.

[21] C. Ishii, T. Akita, M. Mita, T. Ide, K. Hamase, Development of an online two-dimensional high-performance liquid chromatographic system in combination with tandem mass spectrometric detection for enantiomeric analysis of free amino acids in human physiological fluid, J. Chromatogr. A 1570 (2018) 91−98.

[22] F. Ianni, R. Sardella, A. Lisanti, A. Gioiello, B.T. Cenci Goga, W. Lindner, B. Natalini, Achiral−chiral two-dimensional chromatography of free amino acids in milk: a promising tool for detecting different levels of mastitis in cows, J. Pharmaceut. Biomed. Anal. 116 (2015) 40−46.

[23] X. Yao, T.T.Y. Tan, Y. Wang, Thiol−ene click chemistry derived cationic cyclodextrin chiral stationary phase and its enhanced separation performance in liquid chromatography, J. Chromatogr. A 1326 (2014) 80−88.

[24] I. Molnár-Perl, Advancement in the derivatizations of the amino groups with the o-phthaldehyde-thiol and with the 9-fluorenylmethyloxycarbonyl chloride reagents, J. Chromatogr. B 879 (17) (2011) 1241−1269.

[25] U. Woiwode, R.J. Reischl, S. Buckenmaier, W. Lindner, M. Lämmerhofer, Imaging peptide and protein chirality via amino acid analysis by chiral × chiral two-dimensional correlation liquid chromatography, Anal. Chem. 90 (13) (2018) 7963−7971, https://doi.org/10.1021/acs.analchem.8b00676.

[26] G. Mazzoccanti, S. Manetto, A. Ricci, W. Cabri, A. Orlandin, M. Catani, S. Felletti, A. Cavazzini, M. Ye, H. Ritchie, C. Villani, F. Gasparrini, High−throughput enantioseparation of Nα−fluorenylmethoxycarbonyl proteinogenic amino acids through fast chiral chromatography on zwitterionic-teicoplanin stationary phases, J. Chromatogr. A 1624 (2020) 461235.

[27] E.L. Regalado, C.J. Welch, Separation of achiral analytes using supercritical fluid chromatography with chiral stationary phases, Trac. Trends Anal. Chem. 67 (2015) 74−81.

[28] J.M. Will, A. Behrens, M. Macke, C.D. Quarles, U. Karst, Automated chiral analysis of amino acids based on chiral derivatization and trapped ion mobility−mass spectrometry, Anal. Chem. 93 (2) (2021) 878−885.

[29] R. Pérez-Míguez, B. Bruyneel, M. Castro-Puyana, M.L. Marina, G.W. Somsen, E. Domínguez-Vega, Chiral discrimination of DL-amino acids by trapped ion mobility spectrometry after derivatization with (+)-1-(9-Fluorenyl)ethyl chloroformate, Anal. Chem. 91 (5) (2019) 3277−3285.

[30] C. Ishii, A. Furusho, C.-L. Hsieh, K. Hamase, Multi-dimensional high-performance liquid chromatographic determination of chiral amino acids and related compounds in real world samples, Chromatography 41 (1) (2020) 1−17.

[31] Y. Miyoshi, K. Hamase, Y. Tojo, M. Mita, R. Konno, K. Zaitsu, Determination of d-serine and d-alanine in the tissues and physiological fluids of mice with various d-amino-acid oxidase activities using two-dimensional high-performance liquid chromatography with fluorescence detection, J. Chromatogr. B 877 (24) (2009) 2506−2512.

[32] K.J. Adams, B. Pratt, N. Bose, L.G. Dubois, L. St John-Williams, K.M. Perrott, K. Ky, P. Kapahi, V. Sharma, M.J. MacCoss, M.A. Moseley, C.A. Colton, B.X. MacLean, B. Schilling, J.W. Thompson, Skyline for small molecules: a unifying software package for quantitative metabolomics, J. Proteome Res. 19 (4) (2020) 1447−1458.

[33] J. Lin, C. Tsang, R. Lieu, K. Zhang, Method screening strategies of stereoisomers of compounds with multiple chiral centers and a single chiral center, J. Chromatogr. A 1624 (2020) 461244.

[34] M.P. Dwight Stoll, Stephan Buckenmaier, 2D-LC - A Tutorial Focusing on Best Practices, HPLC Milano, 2019.

[35] D.R. Stoll, P.W. Carr, Two-dimensional liquid chromatography: a state of the art tutorial, Anal. Chem. 89 (1) (2017) 519−531.

[36] P. Dugo, F. Cacciola, T. Kumm, G. Dugo, L. Mondello, Comprehensive multi-dimensional liquid chromatography: theory and applications, J. Chromatogr. A 1184 (1) (2008) 353−368.

[37] A.F.G. Gargano, M. Duffin, P. Navarro, P.J. Schoenmakers, Reducing dilution and analysis time in online comprehensive two-dimensional liquid

chromatography by active modulation, Anal. Chem. 88 (3) (2016) 1785—1793.

[38] B.W.J. Pirok, D.R. Stoll, P.J. Schoenmakers, Recent developments in two-dimensional liquid chromatography: fundamental improvements for practical applications, Anal. Chem. 91 (1) (2019) 240—263.

[39] H. Wang, H.R. Lhotka, R. Bennett, M. Potapenko, C.J. Pickens, B.F. Mann, I.A.H. Ahmad, E.L. Regalado, Introducing online multicolumn two-dimensional liquid chromatography screening for facile selection of stationary and mobile phase conditions in both dimensions, J. Chromatogr. A 1622 (2020) 460895.

[40] M. Pursch, S. Buckenmaier, Loop-based multiple heart-cutting two-dimensional liquid chromatography for target analysis in complex matrices, Anal. Chem. 87 (10) (2015) 5310—5317.

[41] M. Pursch, P. Lewer, S. Buckenmaier, Resolving Co-elution problems of components in complex mixtures by multiple heart-cutting 2D-LC, Chromatographia 80 (1) (2017) 31—38.

[42] U. Woiwode, S. Neubauer, W. Lindner, S. Buckenmaier, M. Lämmerhofer, Enantioselective multiple heartcut two-dimensional ultra-high-performance liquid chromatography method with a Coreshell chiral stationary phase in the second dimension for analysis of all proteinogenic amino acids in a single run, J. Chromatogr. A 1562 (2018) 69—77.

[43] N. Grecsó, M. Kohout, A. Carotti, R. Sardella, B. Natalini, F. Fülöp, W. Lindner, A. Péter, I. Ilisz, Mechanistic considerations of enantiorecognition on novel Cinchona alkaloid-based zwitterionic chiral stationary phases from the aspect of the separation of trans-paroxetine enantiomers as model compounds, J. Pharmaceut. Biomed. Anal. 124 (2016) 164—173.

[44] I. Ilisz, A. Bajtai, W. Lindner, A. Péter, Liquid chromatographic enantiomer separations applying chiral ion-exchangers based on Cinchona alkaloids, J. Pharmaceut. Biomed. Anal. 159 (2018) 127—152.

[45] U. Woiwode, M. Ferri, N.M. Maier, W. Lindner, M. Lämmerhofer, Complementary enantioselectivity profiles of chiral cinchonan carbamate selectors with distinct carbamate residues and their implementation in enantioselective two-dimensional high-performance liquid chromatography of amino acids, J. Chromatogr. A 1558 (2018) 29—36.

[46] K. Hamase, A. Morikawa, T. Ohgusu, W. Lindner, K. Zaitsu, Comprehensive analysis of branched aliphatic d-amino acids in mammals using an integrated multi-loop two-dimensional column-switching high-performance liquid chromatographic system combining reversed-phase and enantioselective columns, J. Chromatogr. A 1143 (1) (2007) 105—111.

[47] Y. Tojo, K. Hamase, M. Nakata, A. Morikawa, M. Mita, Y. Ashida, W. Lindner, K. Zaitsu, Automated and simultaneous two-dimensional micro-high-performance liquid chromatographic determination of proline and hydroxyproline enantiomers in mammals, J. Chromatogr. B 875 (1) (2008) 174—179.

[48] H. Han, Y. Miyoshi, K. Ueno, C. Okamura, Y. Tojo, M. Mita, W. Lindner, K. Zaitsu, K. Hamase, Simultaneous determination of d-aspartic acid and d-glutamic acid in rat tissues and physiological fluids using a multi-loop two-dimensional HPLC procedure, J. Chromatogr. B 879 (29) (2011) 3196—3202.

[49] G. Lajkó, I. Ilisz, G. Tóth, F. Fülöp, W. Lindner, A. Péter, Application of Cinchona alkaloid-based zwitterionic chiral stationary phases in supercritical fluid chromatography for the enantioseparation of Nα-protected proteinogenic amino acids, J. Chromatogr. A 1415 (2015) 134—145.

[50] P.A. Levkin, N.M. Maier, V. Schurig, W. Lindner, Strong detrimental effect of a minute enantiomeric impurity of a chiral selector on the enantioselectivity factor, Angew. Chem. Int. Ed. 49 (42) (2010) 7742—7744.

[51] M. Wolter, M. Lämmerhofer, In-situ functionalized monolithic polysiloxane-polymethacrylate composite materials from polythiol-ene double click reaction in capillary column format for enantioselective nano-high-performance liquid chromatography, J. Chromatogr. A 1497 (2017) 172—179.

[52] S. Karakawa, K. Shimbo, N. Yamada, T. Mizukoshi, H. Miyano, M. Mita, W. Lindner, K. Hamase, Simultaneous analysis of d-alanine, d-aspartic acid, and d-serine using chiral high-performance liquid chromatography-tandem mass spectrometry and its application to the rat plasma and tissues, J. Pharmaceut. Biomed. Anal. 115 (2015) 123—129.

[53] C. Geibel, K. Dittrich, U. Woiwode, M. Kohout, T. Zhang, W. Lindner, M. Lammerhofer, Evaluation of superficially porous particle based zwitterionic chiral ion exchangers against fully porous particle benchmarks for enantioselective ultra-high performance liquid chromatography, J. Chromatogr. A 1603 (2019) 130—140, https://doi.org/10.1016/j.chroma.2019.06.026.

[54] K. Schmitt, U. Woiwode, M. Kohout, T. Zhang, W. Lindner, M. Lämmerhofer, Comparison of small size fully porous particles and superficially porous particles of chiral anion-exchange type stationary phases in ultra-high performance liquid chromatography: effect of particle and pore size on chromatographic efficiency and kinetic performance, J. Chromatogr. A 1569 (2018) 149—159, https://doi.org/10.1016/j.chroma.2018.07.056.

[55] C.V. Hoffmann, R. Pell, M. Lämmerhofer, W. Lindner, Synergistic effects on enantioselectivity of zwitterionic chiral stationary phases for separations of chiral acids, bases, and amino acids by HPLC, Anal. Chem. 80 (22) (2008) 8780—8789.

[56] I. Molnar, Computerized design of separation strategies by reversed-phase liquid chromatography: development of DryLab software, J. Chromatogr. A 965 (1) (2002) 175—194.

[57] R. Hayes, A. Ahmed, T. Edge, H. Zhang, Core—shell particles: preparation, fundamentals and applications in high performance liquid chromatography, J. Chromatogr. A 1357 (2014) 36—52.

[58] M. Lämmerhofer, W. Lindner, Liquid chromatographic enantiomer separation and chiral recognition by cinchona alkaloid-derived enantioselective separation materials, Adv. Chromatogr. 46 (2008) 1—107.

[59] M. Lämmerhofer, Chiral recognition by enantioselective liquid chromatography: mechanisms and modern chiral stationary phases, J. Chromatogr. A 1217 (6) (2010) 814—856.

[60] I. D'Acquarica, F. Gasparrini, B. Giannoli, E. Badaloni, B. Galletti, F. Giorgi, M.O. Tinti, A. Vigevani, Enantio- and chemo-selective HPLC separations by chiral—achiral tandem-columns approach: the combination of CHIROBIOTIC TAG™ and SCX columns for the analysis of propionyl carnitine and related impurities, J. Chromatogr. A 1061 (2) (2004) 167—173.

[61] R. Sardella, M. Lämmerhofer, B. Natalini, W. Lindner, In-line coupling of a reversed-phase column to cope with limited chemoselectivity of a quinine carbamate-based anion-exchange type chiral stationary phase, J. Separ. Sci. 31 (10) (2008) 1702—1711.

[62] R.S. Hegade, M. De Beer, F. Lynen, Chiral stationary phase optimized selectivity liquid chromatography: a strategy for the separation of chiral isomers, J. Chromatogr. A 1515 (2017) 109—117.

[63] C. Ishii, T. Akita, M. Nagano, M. Mita, K. Hamase, Determination of chiral amino acids in various fermented products using a two-dimensional HPLC-MS/MS system, Chromatography 40 (2) (2019) 83—87.

[64] J. Horak, H. Gerhardt, J. Theiner, W. Lindner, Correlation between amino acid racemization and processing conditions for various wheat products, oil seed press cakes and lignin samples, Food Bioprod. Process. 92 (4) (2014) 355—368.

[65] K.T. Katsushige Ikail, Kazuro Shiomi, Makoto Moriguchi, Yoshihisa Umeda, Junko Yamamoto, Ikunoshin Kato, Hiroshi Naganawa, Structure of aureobasidin A, J. Antibiot. 44 (9) (1991) 925—933.

[66] Y. In, T. Ishida, K. Takesako, Unique molecular conformation of aureobasidin A, a highly amide N-methylated cyclic depsipeptide with potent antifungal activity: X-ray crystal structure and molecular modeling studies, J. Pept. Res. 53 (5) (1999) 492—500.

[67] H. Gross, V.O. Stockwell, M.D. Henkels, B. Nowak-Thompson, J.E. Loper, W.H. Gerwick, The genomisotopic approach: a systematic method to isolate products of orphan biosynthetic gene clusters, Chem. Biol. 14 (1) (2007) 53—63.
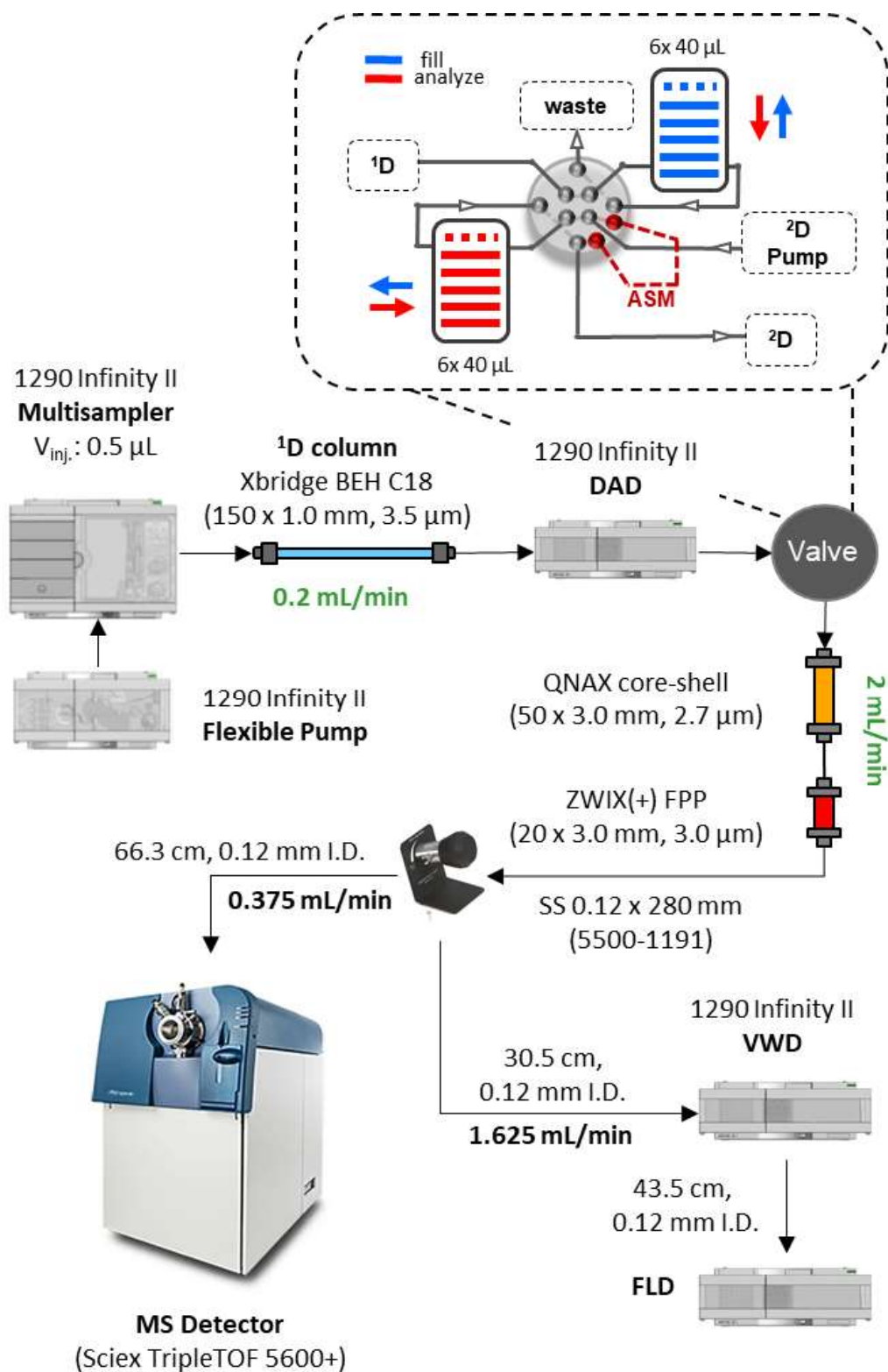
4.3.1 Supporting Information


Figure S 1: Final 2D-LC Setup.

Table S 4: Labels of 20 proteinogenic amino acids (1-20) and 5 isobaric amino acids (21-25).

1. Glycine (Gly)	11. Phenylalanine (Phe)	21. Homoserine (Hse)
2. Alanine (Ala)	12. Tyrosine (Tyr)	22. allo-Threonine (aThr)
3. Serine (Ser)	13. Tryptophan (Trp)	23. allo-Isoleucine (alle)
4. Threonine (Thr)	14. Aspartic Acid (Asp)	24. tert-Leucine (Tle)
5. Cysteine (Cys)	15. Glutamic Acid (Glu)	25. Norleucine (Nle)
6. Valine (Val)	16. Asparagine (Asn)	
7. Leucine (Leu)	17. Glutamine (Gln)	
8. Isoleucine (Ile)	18. Histidine (His)	
9. Methionine (Met)	19. Lysine (Lys)	
10. Proline (Pro)	20. Arginine (Arg)	

If not otherwise stated, the above shown numbers beside the amino acids will be used instead of the three-letter-code to label chromatographic peaks.

4.3.1.1 Optimization of ¹D

(a) Mobile phase: A: 10 mM Ammonium formate in water (pH:6.271); B: ACN
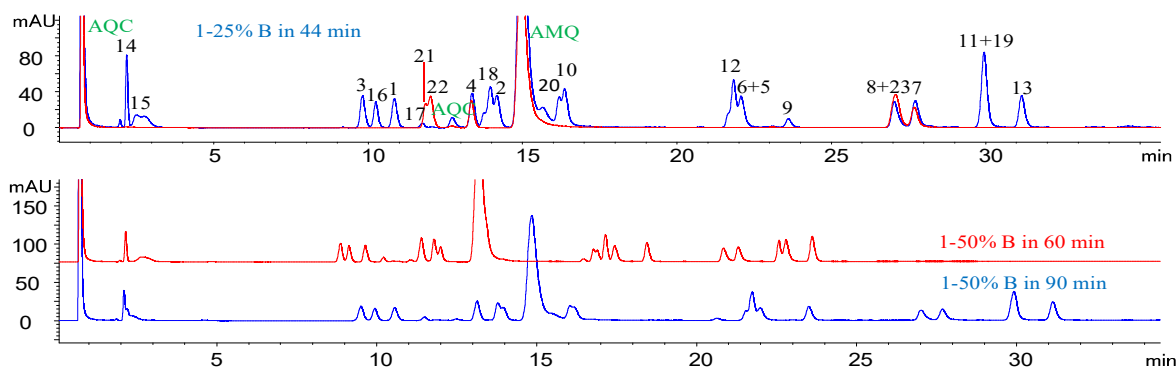
(b) Mobile phase: A: 0.05% FA in water (pH:2.734); B: ACN
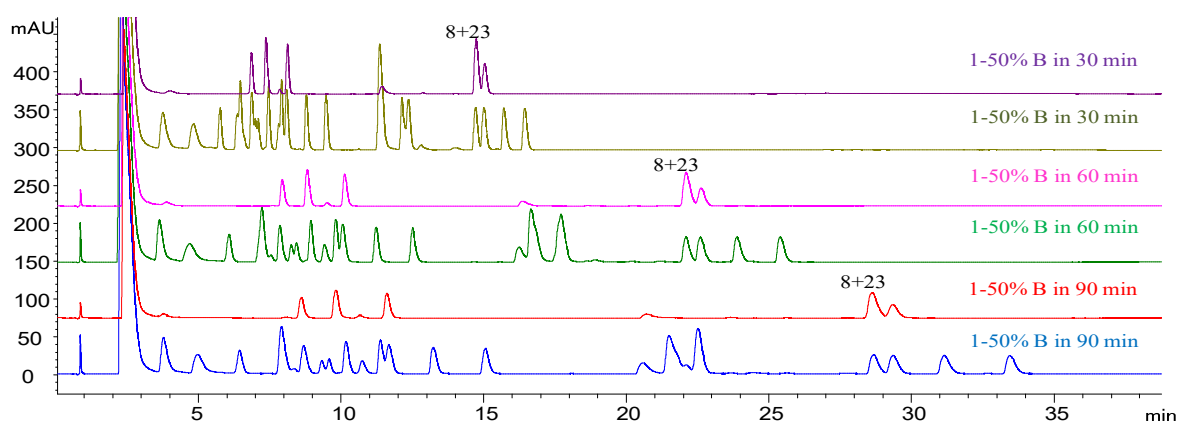
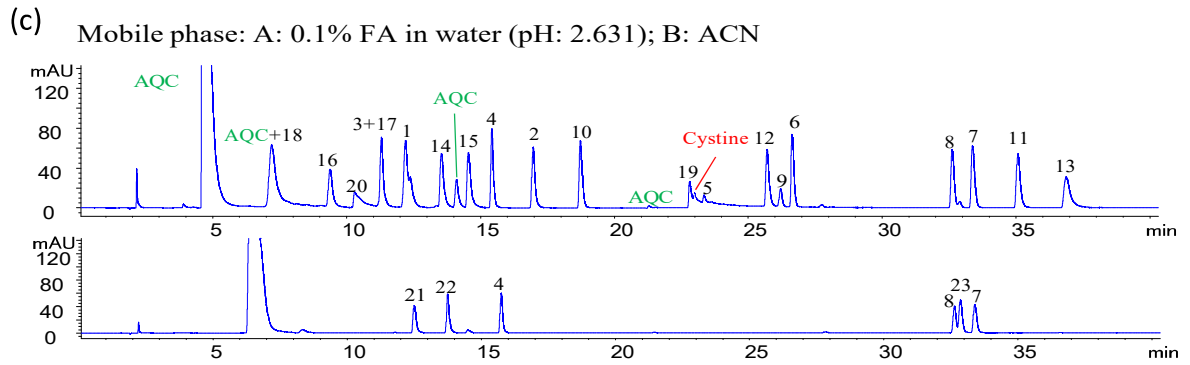(c) Mobile phase: A: 10 mM NH4FA + 10 mM FA in water (pH:3.677); B: ACN
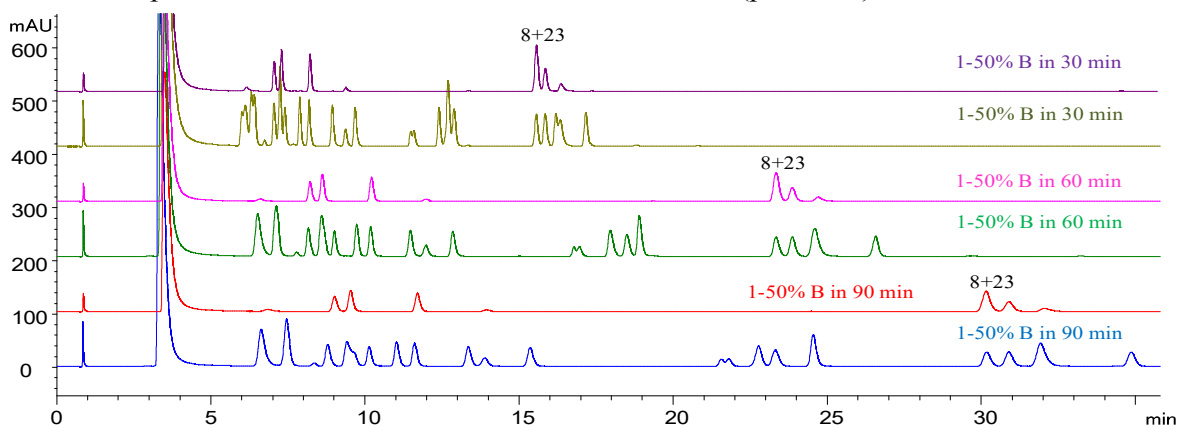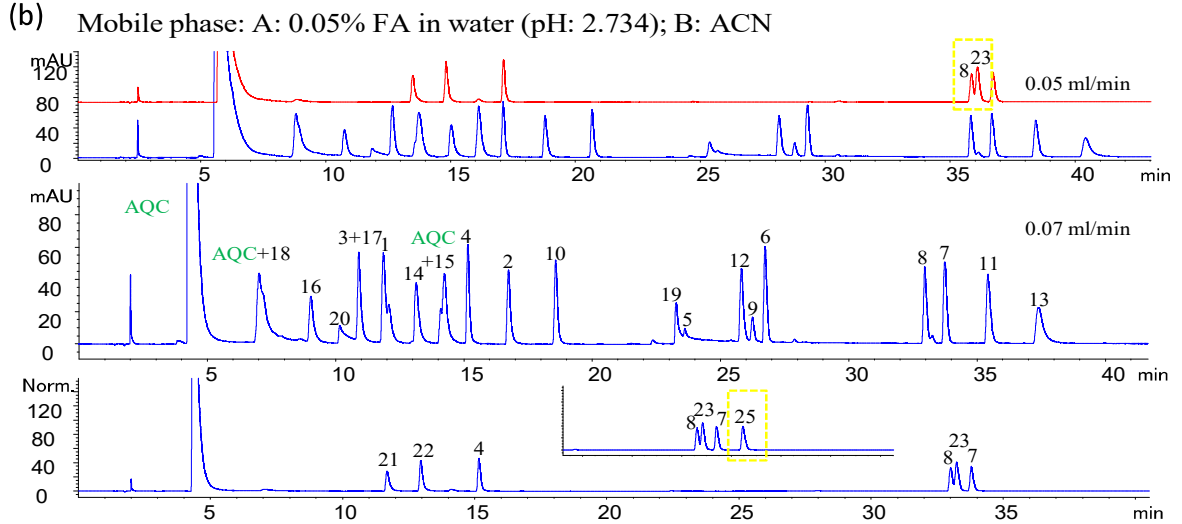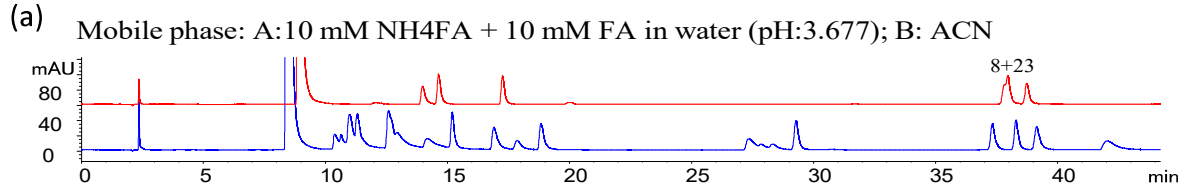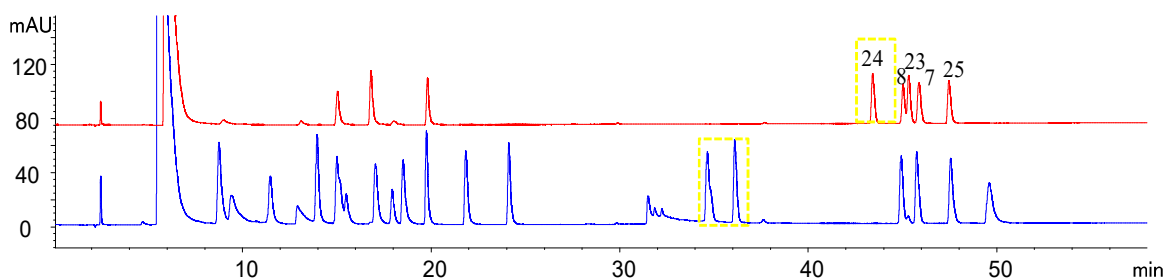

Figure S 2: Amino acid mixture separation on a ZORBAX SB-C18 (1 x 50 mm, 3.5 μm) column with different mobile phases and gradient methods (a, b, c). Injection volume: 0.5 μL; flow rate: 0.05 mL min⁻¹; temperature: 30 °C; sample: 0.25 mM AQC-AA mix (20 AAs) and 0.25 mM isobaric AA mix (Thr, aThr, Hse, Leu, Ile, alle) for peak assignment.
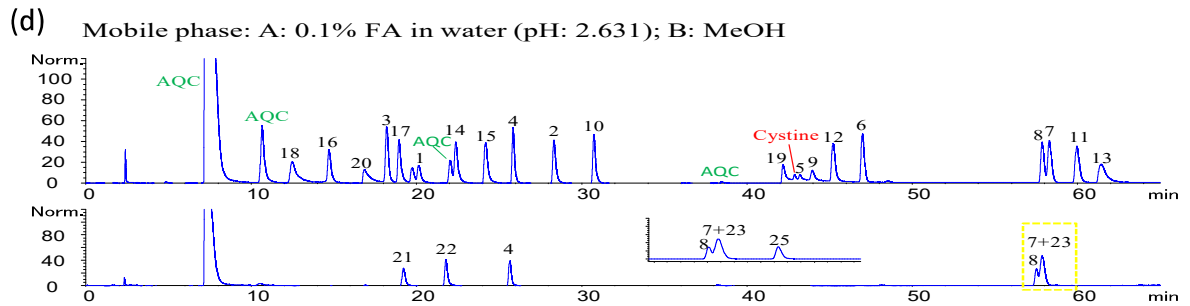
(a) Mobile phase: A:10 mM NH4FA + 10 mM FA in water (pH:3.677); B: ACN

(b) Mobile phase: A: 0.05% FA in water (pH: 2.734); B: ACN

(c) Mobile phase: A: 0.1% FA in water (pH: 2.631); B: ACN

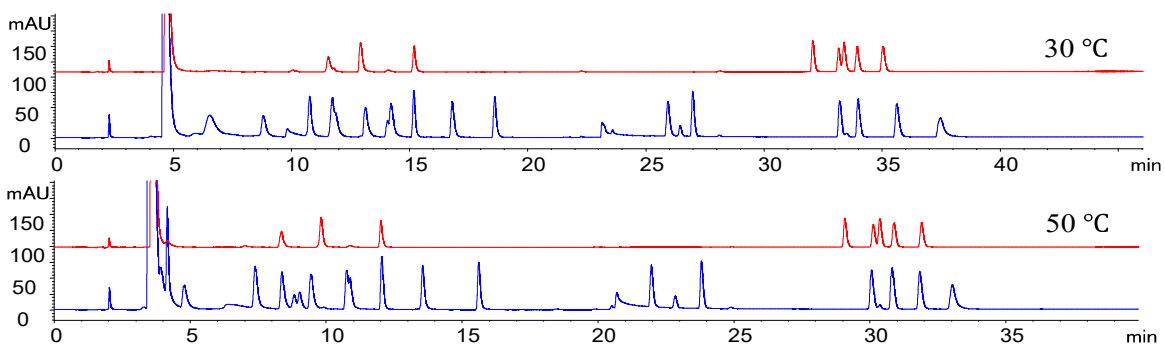(d) Mobile phase: A: 0.1% FA in water (pH: 2.631); B: MeOH

Figure S 3: Amino acid mixture separation on a BEH-C18 (1 x 150 mm, 1.7 µm) column with different mobile phases and different conditions (flow rates and temperature). The flow rate without special marking was 0.07 mL min^{-1} and temperature was 30 °C; Injection volume: 0.5 µL; sample: 0.25 mM AQC-AA mix (20 AAs), 0.25 mM isobaric AA mix (Thr, aThr, Hse, Leu, Ile, alle; Tle and Nle was added in Figure e-f), 0.25 mM single AA for peak assignment. (isobaric AAs are shown in red, while the proteinogenic AAs are shown in blue).
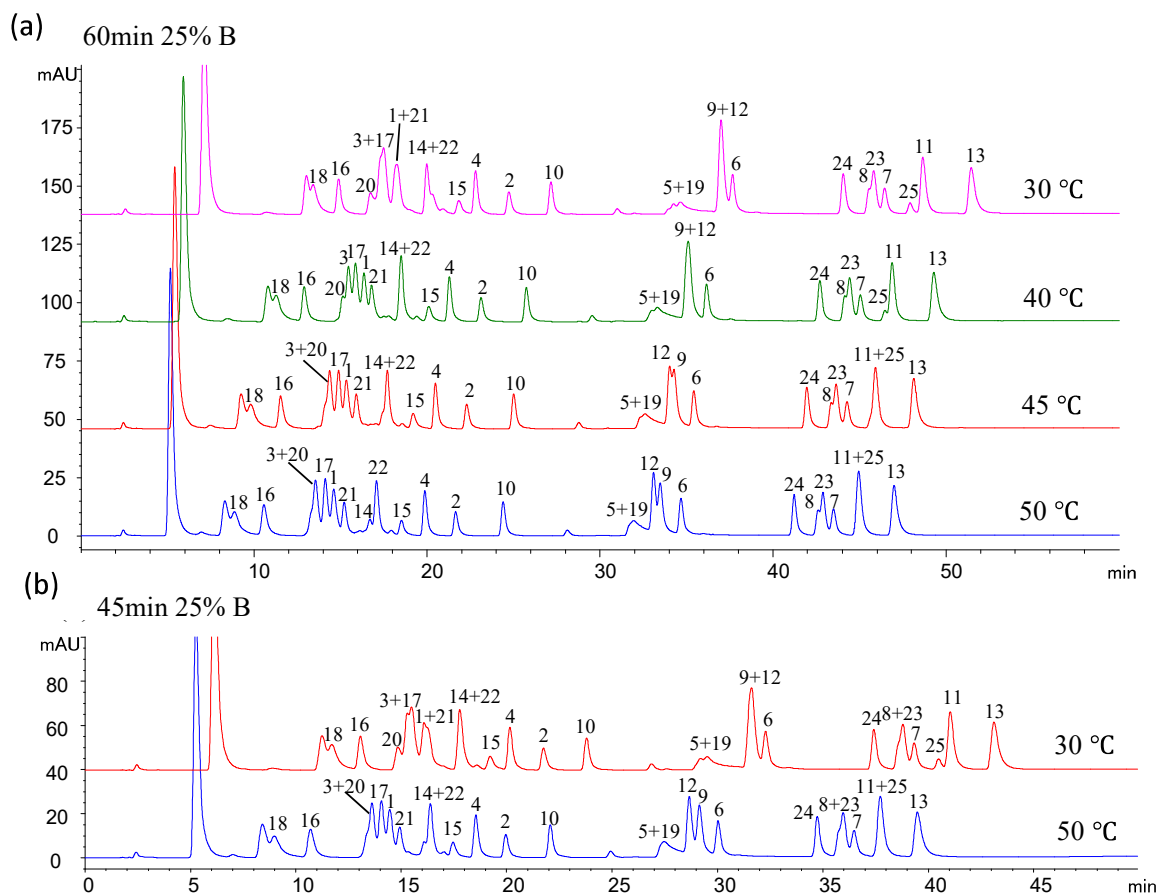
Figure S 4: Influence of the column temperature on the first-dimension separation on a BEH-C18 (1 x 150 mm, 1.7 μm) column using 2D-LC. Injection volume: 0.5 μL; flow rate: 0.07 mL min^{-1}; sample: 0.25 mM AQC-AA mix (25); mobile phase: A: 0.05% FA + 1% MeOH in water; B: 0.05% FA in ACN.
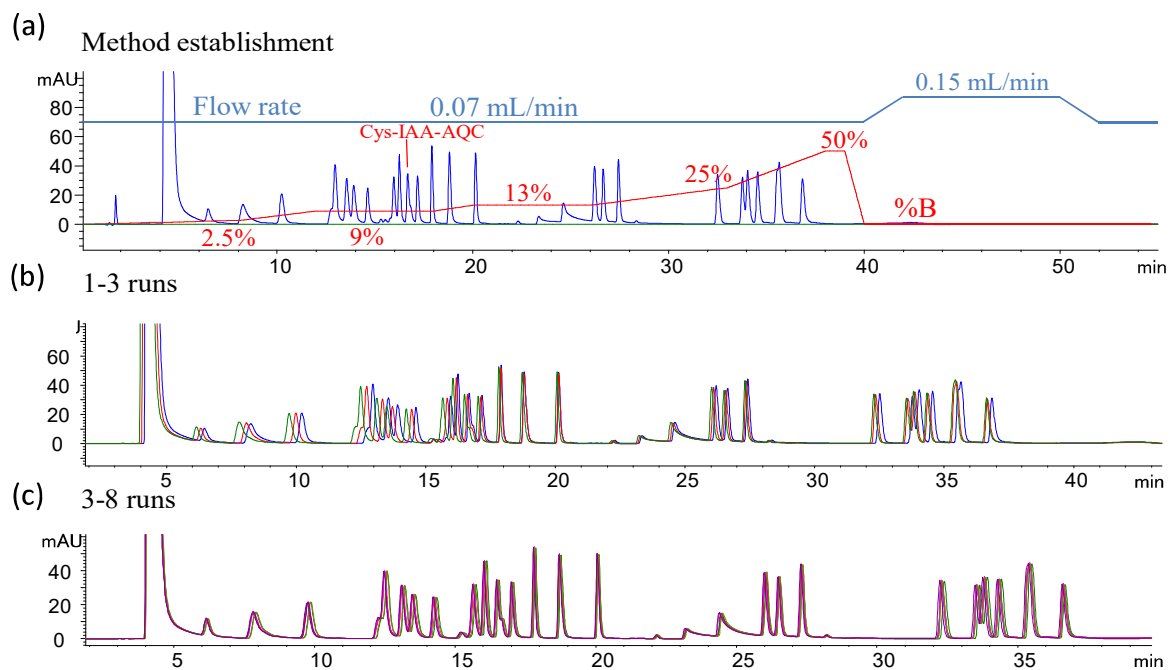
Figure S 5: Reproducibility of the first dimension separation on a 2D-LC system. Column: BEH-C18 (1 x 150 mm, 1.7 μm); mobile phase: A: 0.05% FA + 1% MeOH in water; B: 0.05% FA in ACN; sample: 0.25 mM AQC-AA mix (25 AAs); injection volume: 0.5 μL; flow rate: 0.07 mL min^{-1}; temperature: 50 °C.
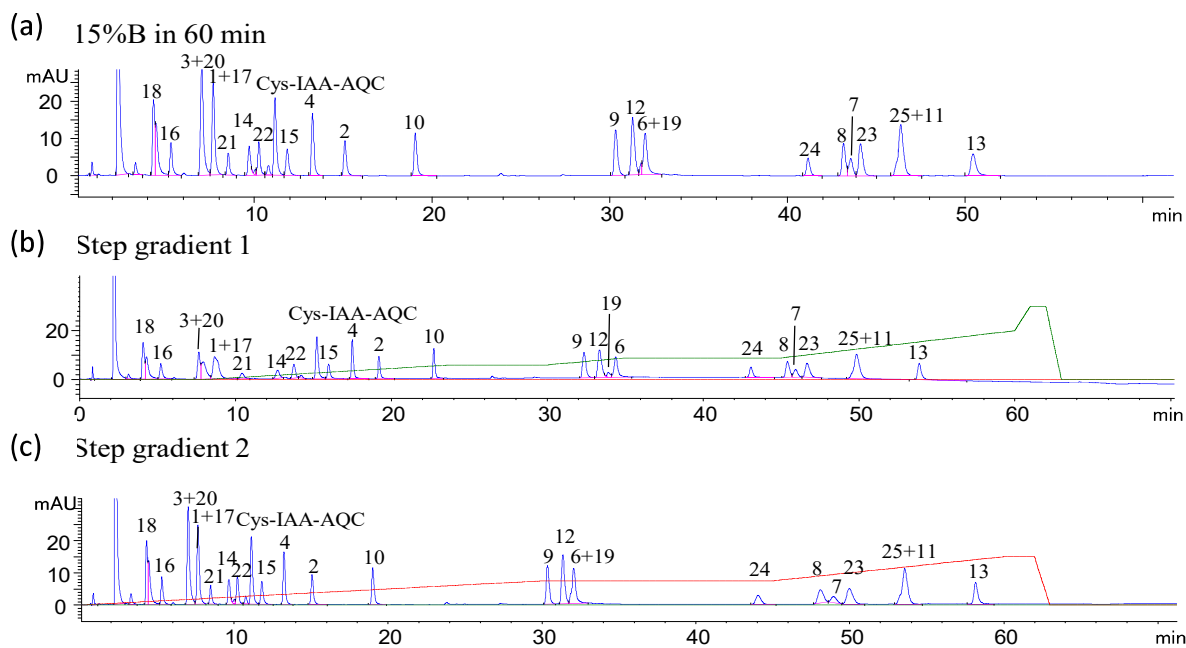
Figure S 6: Optimization of the ^{1}D measurement with flow rate 0.15 mL min^{-1} on a BEH-C18 (1 x 150 mm, 1.7 µm) column using a 2D-LC system. Mobile phase: A: 0.05% FA + 1% MeOH in water; B: 0.05% FA in ACN; sample: 0.25 mM AQC-AA mix (24 AQC-AA and Cys-IAA-AQC); injection volume: 0.5 µL; temperature: 50 °C.
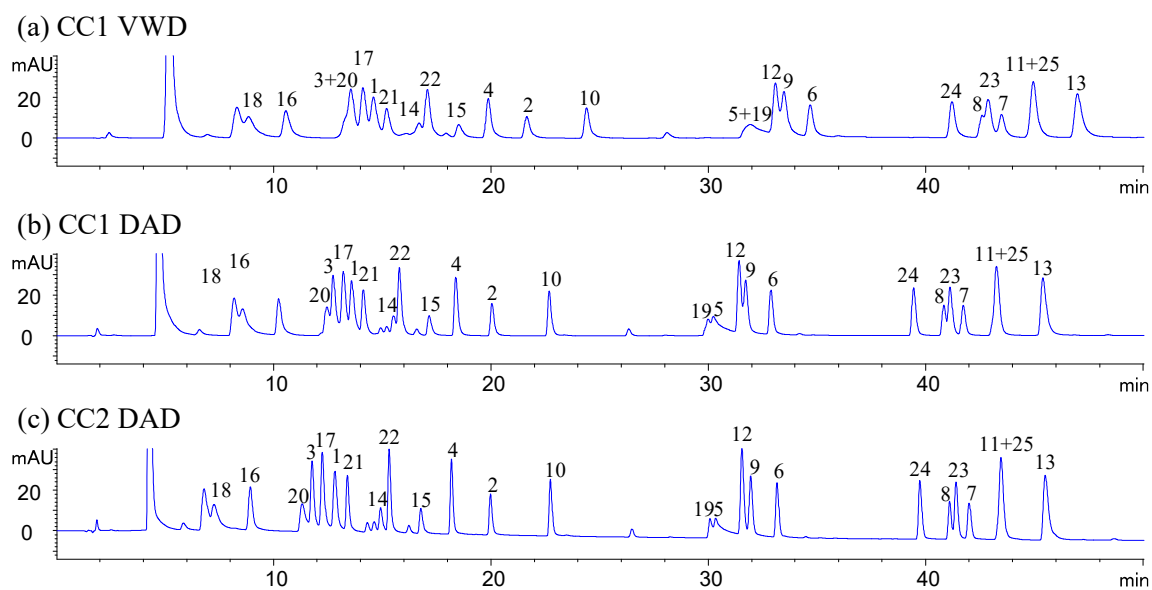
Figure S 7: Influence of the size of the UV-flow cell on peak resolution in the first dimension of a 2D-LC analysis. Column: BEH-C18 (1x150 mm, 1.7 µm); mobile phase: A: 0.05% FA + 1% MeOH in water; B: 0.05% FA in ACN. sample: 0.25 mM AQC-AA mix (25); injection volume: 0.5 µL; flow rate: 0.07 mL min⁻¹; temperature: 50 °C.

4.3.1.2 Optimization of ^{2}D

Table S 5: The [M+H]$^+$ values of amino acids used in MS data analysis.

Name	chemical Formula ([u-^{12}C^{14}N]-AA / [u-^{13}C^{15}N]-AA)	exact mass	precursor ion (*m/z*) [M+H]+
Asp - AQC	C4H7NO4C10H6N2O	303.08552	304.0928
Glu - AQC	C5H9NO4C10H6N2O	317.10117	318.1085
Asn - AQC	C4H8N2O3C10H6N2O	302.10151	303.1088
Ser - AQC	C3H7NO3C10H6N2O	275.09061	276.0979
Gln - AQC	C5H10N2O3C10H6N2O	316.11716	317.1244
His - AQC	C6H9N3O2C10H6N2O	325.11749	326.1248
Gly - AQC	C2H5NO2C10H6N2O	245.08004	246.0873
Thr - AQC	C4H9NO3C10H6N2O	289.10626	290.1135
Ala - AQC	C3H7NO2C10H6N2O	259.09569	260.1030
Arg - AQC	C6H14N4O2C10H6N2O	344.15969	345.1670
Tyr - AQC	C9H11NO3C10H6N2O	351.12191	352.1292
Cystine-bis-AQC	C6H12N2O4S2C10H6N2OC10H6N2O	580.11988	581.1272
Val - AQC	C5H11NO2C10H6N2O	287.12699	288.1343
Met - AQC	C5H11NO2SC10H6N2O	319.09906	320.1063
Trp - AQC	C11H12N2O2C10H6N2O	374.13789	375.1452
Phe - AQC	C9H11NO2C10H6N2O	335.12699	336.1343
Ile - AQC	C6H13NO2C10H6N2O	301.14264	302.1499
Leu - AQC	C6H13NO2C10H6N2O	301.14264	302.1499
Lys - AQC	C6H14N2O2C10H6N2O	316.15354	317.1608
Lys-bis-AQC	C6H14N2O2C10H6N2OC10H6N2O	486.20155	487.2088
Pro - AQC	C5H9NO2C10H6N2O	285.11134	286.1186
Cys - AQC	C3H7NO2SC10H6N2O	291.06776	292.0750
Cys-bis-AQC	C3H7NO2SC10H6N2OC10H6N2O	461.11578	462.1231
Cys - IAA-AQC	C5H10N2O3SC10H6N2O	348.08923	349.0965
13C, 15N - Asp - AQC	(13C)4H7(15N)O4C10H6N2O	308.09598	309.1033
13C, 15N - Glu - AQC	(13C)5H9(15N)O4C10H6N2O	323.11498	324.1223
13C, 15N - Asn - AQC	(13C)4H8(15N)2O3C10H6N2O	308.10899	309.1163
13C, 15N - Ser - AQC	(13C)3H7(15N)O3C10H6N2O	279.09771	280.1050

13C, 15N - Gln - AQC	(13C)5H10(15N)2O3C10H6N2O	323.128	324.1353
13C, 15N - His - AQC	(13C)6H9(15N)3O2C10H6N2O	334.12872	335.1360
13C, 15N - Gly - AQC	(13C)2H5(15N)O2C10H6N2O	248.08379	249.0911
13C, 15N - Thr - AQC	(13C)4H9(15N)O3C10H6N2O	294.11671	295.1240
13C, 15N - Ala - AQC	(13C)3H7(15N)O2C10H6N2O	263.10279	264.1101
13C, 15N - Arg - AQC	(13C)6H14(15N)4O2C10H6N2O	354.16796	355.1752
13C, 15N - Tyr - AQC	(13C)9H11(15N)O3C10H6N2O	361.14913	362.1564
13C, 15N - Cystine-bis-AQC	(13C)6H12(15N)2O4S2C10H6N2OC10H6N2O	588.13408	589.1414
13C, 15N - Val - AQC	(13C)5H11(15N)O2C10H6N2O	293.1408	294.1481
13C, 15N - Met - AQC	(13C)5H11(15N)O2SC10H6N2O	325.11287	326.1202
13C, 15N - Trp - AQC	(13C)11H12(15N)2O2C10H6N2O	387.16886	388.1761
13C, 15N - Phe - AQC	(13C)9H11(15N)O2C10H6N2O	345.15422	346.1615
13C, 15N - Ile - AQC	(13C)6H13(15N)O2C10H6N2O	308.15981	309.1671
13C, 15N - Leu - AQC	(13C)6H13(15N)O2C10H6N2O	308.15981	309.1671
13C, 15N - Lys - AQC	(13C)6H14(15N)2O2C10H6N2O	324.16774	325.1750
13C, 15N - Lys-bis-AQC	(13C)6H14(15N)2O2C10H6N2OC10H6N2O	494.21575	495.2230
13C, 15N - Pro - AQC	(13C)5H9(15N)O2C10H6N2O	291.12515	292.1324
13C, 15N - Cys - AQC	(13C)3H7(15N)O2SC10H6N2O	295.07486	296.0821
13C, 15N - Cys-bis-AQC	(13C)3H7(15N)O2SC10H6N2OC10H6N2O	465.12288	466.1302
13C, 15N -Cys - IAA-AQC	(13C)3C2H10(15N)NO3SC10H6N2O	352.09633	353.1036

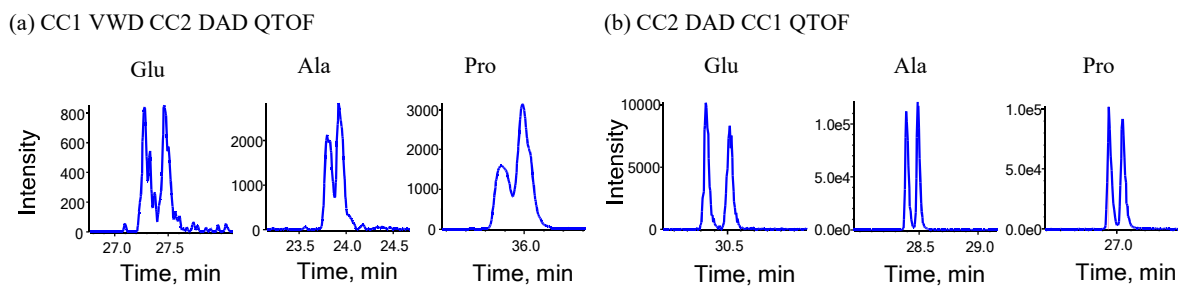### 4.3.1.3   Establishing the MHC 2D-LC-QTOF-ESI-MS Method

Figure S 8: Influence of the size of the UV-flow cell on 2D-LC analysis results. a) CC1→^{1}D-VWD→ASM→CC2→2D-DAD→ESI-QTOF-MS;   b)   CC2→2D-DAD→ASM→CC1→ESI-QTOF-MS. sample: 0.25 mM AA mix (20 DL-AA and 17 [u-^{13}C^{15}N]-L-AA). ^{1}D-Column: BEH-C18 (1 x 150 mm, 1.7 µm); mobile phase: A: 0.05% FA + 1% MeOH in water; B: 0.05% FA in ACN; linear gradient (15% B in 60 min); 0.07 mL min^{-1}; 30°C, Injection volume: 0.5 µL. ^{2}D-column: QNAX core shell (3 x 50 mm, 2.7 µm); mobile phase: 50 mM NH$_4$FA + 50 mM FA + 0.5% H$_2$O in MeOH (a) and 50 mM NH$_4$FA + 50 mM FA in MeOH (b); 1 mL min^{-1}; 30 °C. Smart peak parking, No ASM valve.

(a) Smart peak parking
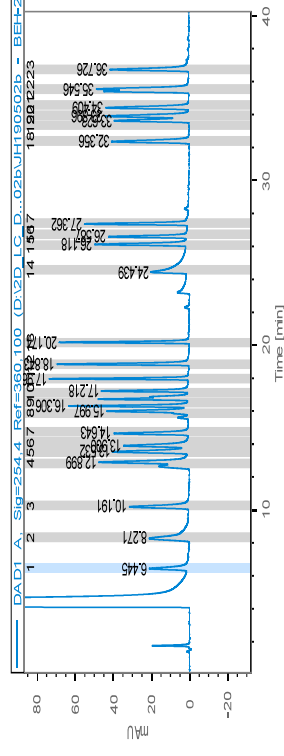
Sampling table (1D)
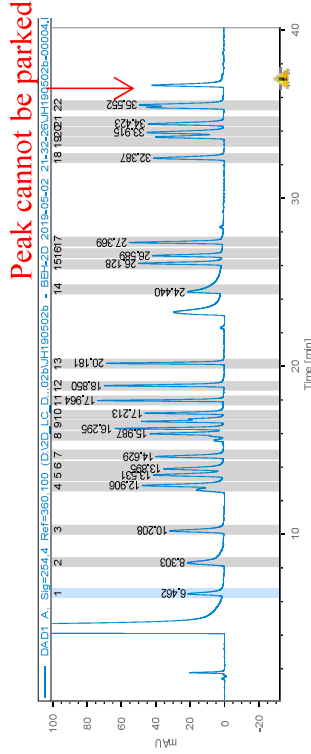
Cut #	1D Cut start	Sampling time	Mode	2D Run start [min]	Deck	Loop	1D Ret. time [min]
1	6.19	0.57	Time	10.16	A	1	6.445
2	8.06	0.57	Time	8.66	A	2	8.271
3	9.99	0.57	Time	14.64	B	1	10.191
4	12.55	0.56	Time	13.14	B	2	12.899
5	13.23	0.57	Time	22.83	A	1	13.532
6	13.80	0.57	Time	21.33	A	2	13.900
7	14.47	0.56	Time	19.83	A	3	14.643
8	15.59	0.57	Time	18.33	A	4	15.997
9	16.24	0.56	Time	16.83	A	5	16.306
10	16.84	0.56	Time	30.89	B	1	17.218
11	17.68	0.57	Time	29.39	B	2	17.962
12	18.56	0.56	Time	27.89	B	3	18.843
13	19.88	0.56	Time	26.39	B	4	20.174
14	24.29	0.57	Time	24.89	B	5	24.439
15	25.78	0.57	Time	37.21	A	1	26.118
16	26.45	0.57	Time	35.71	A	2	26.587
17	27.13	0.57	Time	34.21	A	3	27.362
18	32.11	0.57	Time	32.71	A	4	32.356
19	33.08	0.56	Time	46.21	B	1	33.623
20	33.69	0.56	Time	44.71	B	2	33.896
21	34.30	0.57	Time	43.21	B	3	34.409
22	35.26	0.57	Time	41.71	B	4	35.546
23	36.45	0.56	Time	40.21	B	5	36.726

(b) No smart peak parking

Peak cannot be parked

Sampling table (1D)

Cut #	1D Cut start	Sampling time	Mode	2D Run start [min]	Deck	Loop	1D Ret. time [min]
1	6.19	0.57	Time	6.79	A	1	6.462
2	8.06	0.57	Time	8.66	B	1	8.303
3	9.99	0.57	Time	10.59	A	1	10.208
4	12.55	0.56	Time	13.14	B	1	12.906
5	13.23	0.57	Time	18.06	A	1	13.531
6	13.80	0.57	Time	16.56	A	2	13.895
7	14.47	0.56	Time	15.06	A	3	14.629
8	15.59	0.57	Time	27.06	B	1	15.987
9	16.24	0.56	Time	25.56	B	2	16.295
10	16.84	0.56	Time	24.06	B	3	17.213
11	17.68	0.57	Time	22.56	B	4	17.964
12	18.56	0.56	Time	21.06	B	5	18.850
13	19.88	0.57	Time	36.06	A	1	20.181
14	24.29	0.57	Time	34.56	A	2	24.440
15	25.78	0.57	Time	33.06	A	3	26.128
16	26.45	0.57	Time	31.56	A	4	26.589
17	27.13	0.57	Time	30.06	A	5	27.369
18	32.11	0.57	Time	45.06	B	1	32.387
19	33.08	0.56	Time	43.56	B	2	33.915
20	33.69	0.56	Time	42.06	B	3	33.915
21	34.30	0.57	Time	40.56	B	4	34.423
22	35.26	0.57	Time	39.06	B	5	35.552

Figure S 9: Influence of smart loop filling on 2D-LC analysis results. Sample: 0.25 mM AA mix (25 DL-AA and 17 [u-^{13}C^{15}N]-L-AA, Cys-IAA-AQC). ^{1}D-column: BEH-C18 (1 x 150 mm, 1.7 μm); mobile phase: A: 0.05% FA + 1% MeOH in water; mobile phase B: 0.05% FA in ACN; step gradient (Table 5); 0.07 mL min^{-1}; 50 °C, injection volume: 0.5 μL. ^{2}D-column: QNAX core shell (3 x 50 mm, 2.7 μm); mobile phase: 50 mM NH$_4$FA + 50 mM FA + 0.5% H$_2$O in MeOH; 1 mL min^{-1}, 30 °C. No ASM valve.
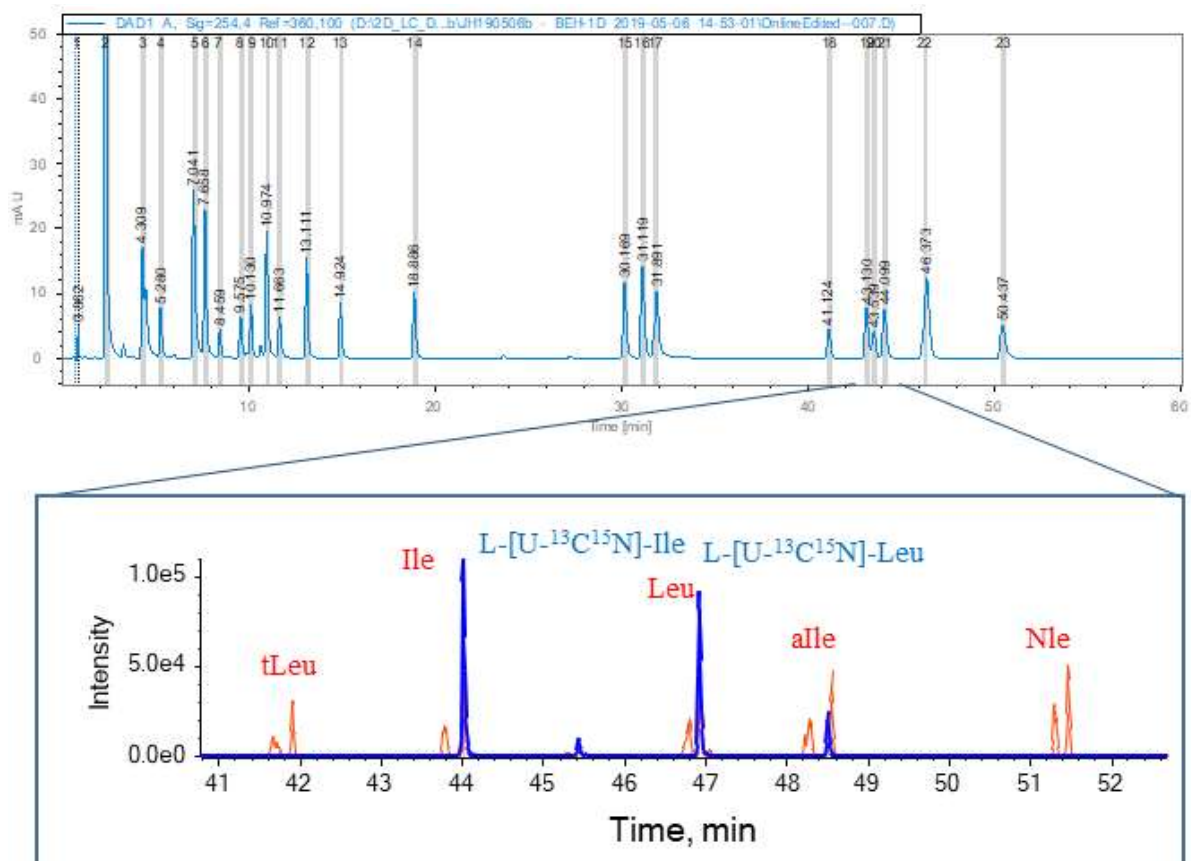
Figure S 10: Best peak based 2D-LC measurement of AQC-derivatized amino acids. Sample: 0.25 mM AA mix (25-DL-AA, 17 L-[u-^{13}C^{15}N]-AA and Cys-IAA-AQC). ^{1}D-column: BEH-C18 (1 x 150 mm, 1.7 μm); mobile phase A: 0.05% FA + 1% MeOH in water; mobile phase B: 0.05% FA in ACN; linear gradient (15% B in 60 min); 0.15 mL min^{-1}; 50 °C, injection volume: 0.5 μL. 2D-column: QNAX core shell (3 x 50 mm, 2.7 μm); mobile phase: 50 mM NH$_4$FA + 50 mM FA + 0.5% H$_2$O in MeOH; 1 mL min^{-1}; 30 °C; no ASM valve, smart peak parking.
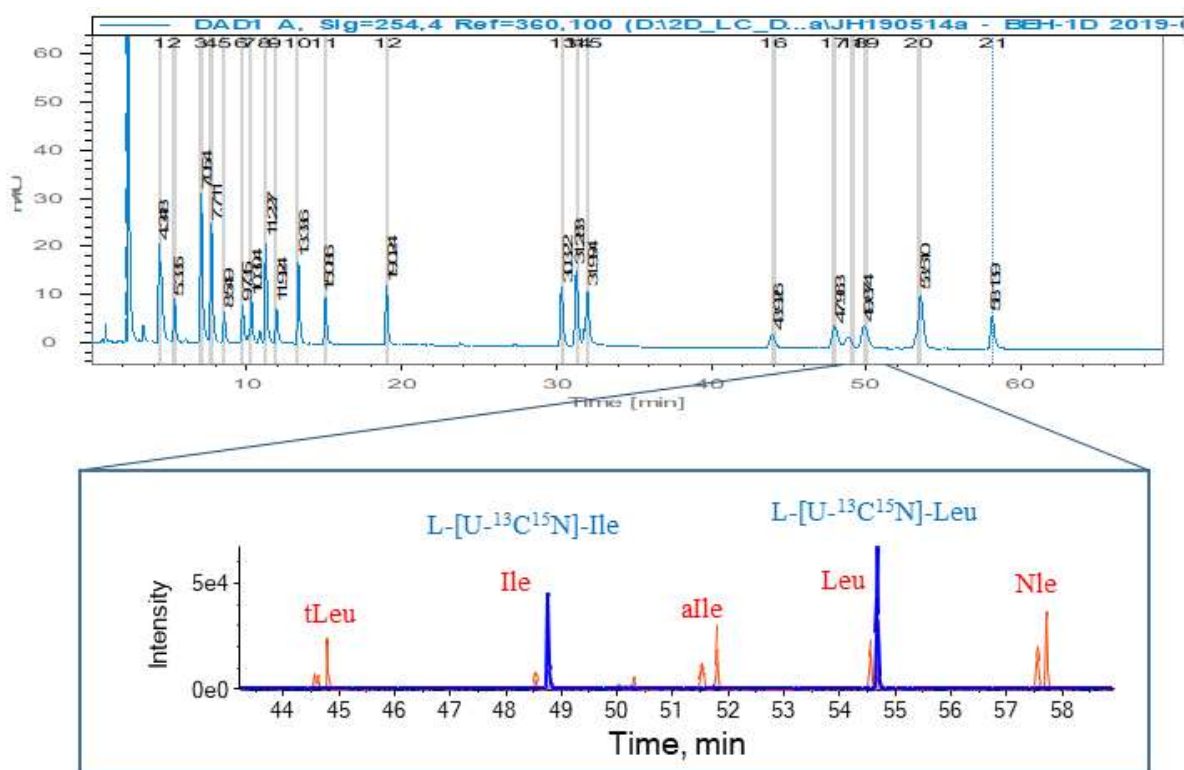
Figure S 11: Best time based 2D-LC measurement of AQC-derivatized amino acids. Sample: 0.25 mM AA mix (25 DL AA, 17 L-[u-^{13}C^{15}N]-AA and Cys-IAA-AQC). ^{1}D-column: BEH-C18 (1 x 150 mm, 1.7 µm); mobile phase: A: 0.05% FA + 1% MeOH in water; mobile phase B: 0.05% FA in ACN; step gradient (0-30 min 0-7.5% B, 30-45 min 7.5-7.5% B, 45-60 min 7.5-15% B); 0.15 mL min^{-1}; 50 ℃, injection volume: 0.5 µL. 2D-column: QNAX core shell (3 x 50 mm, 2.7 µm); mobile phase: 50 mM NH$_4$FA + 50 mM FA + 0.5% H$_2$O in MeOH; 1 mL min^{-1}; 30 °C. no ASM valve, smart peak parking.

Table S 6: Chromatographic parameters obtained from MHC 2D-LC (achiral-chiral) of AQC-derivatized amino acids.

| Amino Acid	Cut #	1D Cut start [min]	Sampling time [min]	Mode	2D Run start [min]	Deck	Loop	1D Ret. time [min]	2D Q-TOF RT [min] D-AAs	2D Q-TOF RT [min] L-AAs	2D RT [min] D-AAs	2D RT [min] L-AAs	k1	k2	w1 (50%) [min]	w2 (50%) [min]	N1	N2	α (Enantio-selectivity)	Elution Order	Resolution
His	1	2.80	0.20	Time	7.66	A	1	2.85	7.975	8.199	0.31	0.54	0.53	1.63	0.06	0.08	176.89	248.68	3.05	D<L	1.95
Asn	2	3.54	0.20	Time	6.53	A	2	3.63	6.904	7.150	0.37	0.62	0.82	2.03	0.03	0.04	823.59	1140.42	2.46	D<L	3.94
Arg	3	5.19	0.20	Time	5.40	A	3	5.26	5.703	6.911	0.30	1.51	0.48	6.40	0.07	0.09	115.39	1668.66	13.40	D<L	9.31
Ser	3	5.19	0.20	Time	5.40	A	3	5.26	5.755	5.891	0.35	0.49	0.73	1.40	0.03	0.03	828.23	1118.85	1.91	D<L	2.53
Gln	4	5.80	0.20	Time	14.81	B	1	5.90	15.387	15.596	0.57	0.78	1.82	2.84	0.04	0.04	960.61	1749.93	1.56	D<L	2.81
Gly	4	5.80	0.20	Time	14.81	B	1	5.90	15.493	-	0.68	-	2.34	-	0.05	-	1126.37	-	-	-	-
Hse	5	6.69	0.20	Time	13.68	B	2	6.76	14.004	14.083	0.32	0.40	0.58	0.96	0.03	0.03	629.21	958.99	1.67	D<L	1.54
Dummy	6	7.17	0.20	Time	12.55	B	3														
Asp	7	7.30	0.20	Time	11.02	B	4	7.36	11.687	11.828	0.67	0.81	2.26	2.95	0.05	0.07	820.16	850.59	1.31	D<L	1.39
aThr	8	8.23	0.20	Time	10.29	B	5	8.35	10.627	10.749	0.34	0.46	0.64	1.24	0.03	0.03	800.02	1161.58	1.93	D<L	2.42
Cys-IAA	9	8.95	0.20	Time	9.16	B	6	9.06	9.562	9.694	0.40	0.53	0.96	1.61	0.03	0.03	1097.43	1348.16	1.67	D<L	2.49
Glu	10	9.46	0.20	Time	19.54	A	1	9.57	20.029	20.096	0.49	0.55	1.38	1.71	0.03	0.04	1074.86	1231.00	1.24	D<L	1.10
Thr	11	10.75	0.20	Time	18.41	A	2	10.86	18.892	19.383	0.48	0.97	1.35	3.75	0.04	0.06	758.97	1676.15	2.79	D<L	6.00
Ala	12	12.10	0.20	Time	17.28	A	3	12.21	17.764	17.911	0.48	0.63	1.36	2.08	0.04	0.04	838.05	1462.36	1.53	D<L	2.23
Pro	13	14.97	0.20	Time	16.15	A	4	15.10	16.697	16.834	0.54	0.68	1.67	2.34	0.04	0.04	896.39	1376.77	1.40	L<D	1.88
Dummy	14	22.50	0.20	Time	22.71	B	1														
Met	15	23.16	0.20	Time	25.00	A	1	23.32	25.345	25.431	0.34	0.43	0.67	1.09	0.03	0.03	811.75	1109.16	1.63	D<L	1.74
Tyr	16	23.63	0.20	Time	23.87	A	2	23.79	24.23	24.351	0.36	0.48	0.74	1.34	0.03	0.03	851.30	1409.88	1.80	D<L	2.44
_ys 2x AQ(	17	24.19	0.20	Time	27.47	B	1	24.28	27.863	27.963	0.39	0.49	0.90	1.39	0.03	0.04	1123.91	786.31	1.54	D<L	1.73
Val	18	24.58	0.20	Time	26.34	B	2	24.71	26.625	26.714	0.28	0.37	0.37	0.81	0.03	0.03	588.91	980.74	2.17	D<L	1.91
Dummy	19	31.63	0.20	Time	31.84	A	1														
tLeu	20	32.10	0.20	Time	34.31	B	1		34.58	34.651	0.27	0.34	0.31	0.66	0.03	0.03	519.51	797.23	2.11	D<L	1.50
	21	32.30	0.20	Time	33.18	B	2	32.36	33.444	33.514	0.26	0.33	0.28	0.63	0.03	0.03	460.69	798.81	2.21	D<L	1.47
Ile	22	34.32	0.20	Time	38.89	A	1		39.175	39.261	0.28	0.37	0.39	0.81	0.02	0.02	882.03	1232.83	2.09	D<L	2.15
	23	34.52	0.20	Time	37.76	A	2	34.69	38.044	38.127	0.28	0.37	0.38	0.79	0.03	0.03	649.94	1026.57	2.06	D<L	1.85
alle	24	35.09	0.20	Time	36.63	A	3	35.26	36.918	37.013	0.29	0.38	0.40	0.87	0.03	0.03	579.42	909.43	2.15	D<L	1.94
	25	35.29	0.20	Time	35.50	A	4		35.793	35.89	0.29	0.39	0.43	0.90	0.03	0.03	678.33	898.32	2.11	D<L	2.01
Leu	26	35.88	0.20	Time	42.49	B	1	36.06	42.782	42.836	0.29	0.34	0.42	0.68	0.03	0.03	645.98	820.15	1.64	D<L	1.16
Phe	27	38.61	0.20	Time	41.36	B	2		41.701	41.801	0.34	0.44	0.66	1.15	0.02	0.03	1094.74	1262.07	1.75	D<L	2.22
Phe	28	38.81	0.20	Time	40.23	B	3	38.92	40.565	40.662	0.33	0.43	0.63	1.10	0.03	0.03	709.87	1228.97	1.76	D<L	1.97
Nle	27	38.61	0.20	Time	41.36	B	2		41.658	41.716	0.30	0.35	0.45	0.73	0.03	0.03	660.77	802.85	1.64	D<L	1.21
Nle	28	38.81	0.20	Time	40.23	B	3	38.92	40.52	40.579	0.29	0.35	0.41	0.70	0.03	0.03	612.23	985.68	1.71	D<L	1.31
Trp	29	43.04	0.20	Time	44.96	A	1	43.04	45.346	45.557	0.38	0.59	0.87	1.91	0.03	0.05	1155.88	873.81	2.18	D<L	3.38
	30	43.24	0.20	Time	43.83	A	2	43.27	44.21	44.419	0.38	0.59	0.85	1.87	0.03	0.04	752.40	1154.55	2.21	D<L	3.39

t_0 = 0.204 min
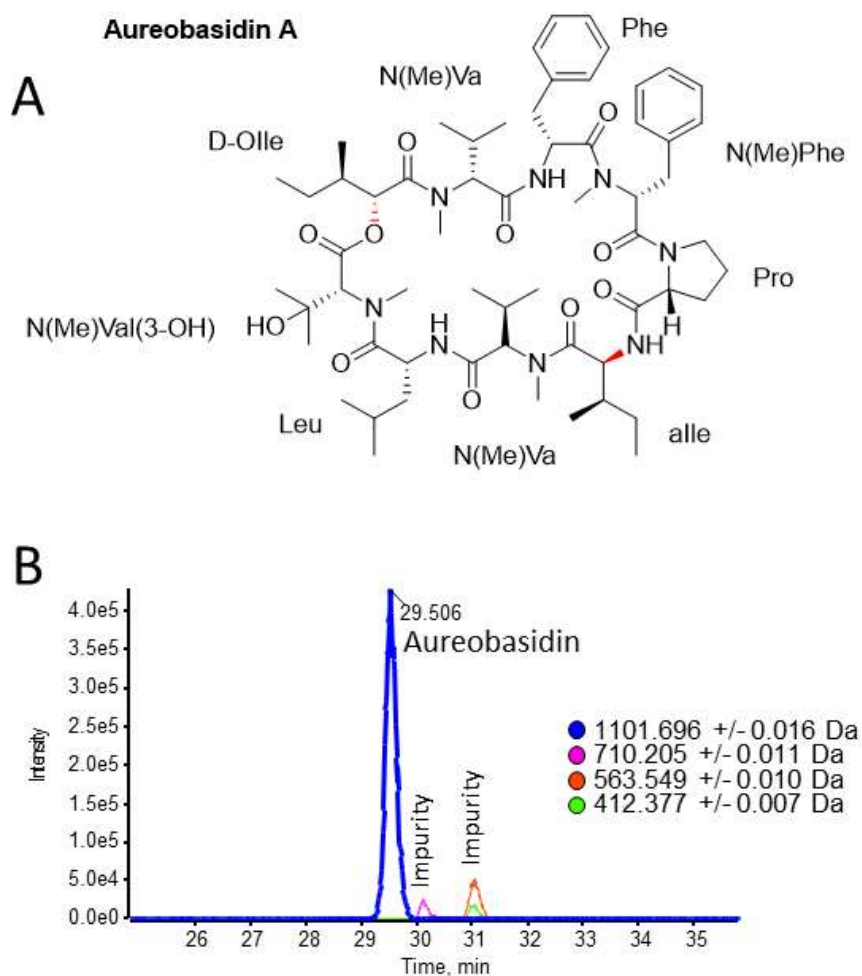
Figure S 12: Chemical Structure of **A)** Aureobasidin A (PubChem CID: 11105152) with the following condensed IUPAC name: cyclo[Leu-N(Me)Val(3-OH)-D-OIle-N(Me)Val-Phe-N(Me)Phe-Pro-aIle-N(Me)Val]. **B)** A RP-LC-ESI-QTOF (IDA pos) of Aureobasidin sample. ^{1}D-column: Zorbax SBRP (2.1 x 100 mm, 1.8 μm); mobile phase: A: 0.1 % FA water; mobile phase B: 0.1 % FA in ACN; gradient (0-1 min 10 %B, 1-30 min 10-100 %B, 30-35 min 100 %B, 35-35.1 min 10 %B, 35.1 – 55 min 10 %B); 0.2 mL min^{-1}; 30 ℃, injection volume: 1 μL.

4.4 Publication IV

Rapid enantioselective amino acid analysis by ultra-high performance liquid chromatography-mass spectrometry combining 6-aminoquinolyl-N-hydroxysuccinimidyl carbamate derivatization with core-shell quinine carbamate anion exchanger separation

Ryan Karongo[a], Min Ge[a], Jeannie Horak[b], Harald Gross[c], Michal Kohout[d], Wolfgang Lindner[e], Michael Lämmerhofer[a]

[a]Institute of Pharmaceutical Sciences, Pharmaceutical (Bio-)Analysis, University of Tübingen, Auf der Morgenstelle 8, Tübingen 72076, Germany

[b]Division of Metabolic and Nutritional Medicine, Dr. von Hauner Children's Hospital University of Munich Medical Center, Ludwig-Maximilians-University Munich, Lindwurmstraße 4, Munich 80337, Germany

[c]Institute of Pharmaceutical Sciences, Pharmaceutical Biology, University of Tübingen, Auf der Morgenstelle 8, Tübingen 72076, Germany

[d]Department of Organic Chemistry, University of Chemistry and Technology, Prague, Czech Republic

[e]Institute of Analytical Chemistry, University of Vienna, Waehringer Strasse 38, Vienna 1090, Austria

Graphical Abstract

Rapid enantioselective amino acid analysis by ultra-high performance liquid chromatography-mass spectrometry combining 6-aminoquinolyl-*N*-hydroxysuccinimidyl carbamate derivatization with core-shell quinine carbamate anion exchanger separation

Ryan Karongo [a], Min Ge [a], Jeannie Horak [a,b,**], Harald Gross [c], Michal Kohout [d], Wolfgang Lindner [e], Michael Lämmerhofer [a,*]

[a] *Institute of Pharmaceutical Sciences, Pharmaceutical (Bio-)Analysis, University of Tübingen, Auf der Morgenstelle 8, Tübingen 72076, Germany*
[b] *Division of Metabolic and Nutritional Medicine, Dr. von Hauner Children's Hospital University of Munich Medical Center, Ludwig-Maximilians-University Munich, Lindwurmstraße 4, Munich 80337, Germany*
[c] *Institute of Pharmaceutical Sciences, Pharmaceutical Biology, University of Tübingen, Auf der Morgenstelle 8, Tübingen 72076, Germany*
[d] *Department of Organic Chemistry, University of Chemistry and Technology, Prague, Czech Republic*
[e] *Institute of Analytical Chemistry, University of Vienna, Waehringer Strasse 38, Vienna 1090, Austria*

ARTICLE INFO

ABSTRACT

Amino acid analysis (AAA) is of central importance for the characterization of the amino acid composition of proteins, peptides, pharmaceutical formulations, dietary supplements, in bioanalysis and metabolomics. Common methodologies are based on achiral assays and hence do not consider distinction of *D* and L-amino acid enantiomers. This may be misleading in many instances, because therapeutic peptides and natural peptides synthesized by non-ribosomal peptide synthetases (NRPSs) frequently contain D-amino acids to achieve proteolytic stability. Furthermore, stereochemical integrity control of peptides made from L-amino acids also need stereoselective assays, and racemization in natural products (proteins, peptides, amino acids) have shown to be useful biomarkers of disease and require assays, which can provide information about the individual stereoisomers. Hence, rapid enantioselective amino acid analysis (ReAAA) is of utmost importance. However, currently employed enantioselective assays are often only focusing on a limited number of amino acids or require long analysis times making them incompatible for high-throughput sample analysis. Here, we present an ReAAA assay, which is based on a fast UHPLC enantiomer separation using a short QN-AX core-shell particle column (2.7 μm) coupled to electrospray ionization quadrupole time of flight mass spectrometric (ESI-QTOF-MS) detection. Amino acid samples are mixed with a [u-^{13}C^{15}N]-labelled L- or DL-amino acid standard mixture, precolumn derivatized with 6-aminoquinolyl-*N*-hydroxysuccinimidyl carbamate (AQC) reagent and subjected to UHPLC-ESI-MS analysis. A number of chromatographic variables have been optimized (buffer additives and concentration, water content, flow rate and temperature) to achieve the goal of simultaneous amino acid enantiomer separation of all proteinogenic amino acids within the shortest possible analysis time. A mobile phase consisting of 50 mM NH$_4$FA, 50 mM FA and 0.5% H$_2$O in MeOH combined with a flow rate of 1 mL/min and a column temperature of 30 °C has been identified as optimal. With these conditions, all of the proteinogenic DL-enantiomers (except for Arg) can be separated in less than 2.5 min. If D-Arg and distinction between D-Leu/D-Ile is of concern, a second-tier method can accomplish this goal. The method can be very useful for ReAAA when high sample throughput is a major demand. Its utility was demonstrated by ReAAA of a lipopeptide hydrolysate which contained several D-amino acids and of an amino acid supplement in which minor D-amino acid impurities could be detected.

Introduction

Amino acid analysis (AAA) is a fundamental technique to determine the amino acid composition of proteins, peptides, amino acid-containing pharmaceutical products and food supplements [1,2]. It is commonly performed by achiral analytical technologies such as reversed-phase HPLC using pre- or post-column derivatization technologies [3]. Pharmacopeias suggest a number of preferred approaches including pre-column (phenylisothiocyanate, 6-aminoquinolyl-*N*-hydroxysuccinimidyl carbamate AQC, 9-fluorenylmethyl-chloroformate FMOC-Cl, 4-fluoro-7-nitro-2,1,3-benzoxadiazole NBD-F) or post-column (ninhydrin, ortho-phthaldialdehyde OPA) derivatization. Unfortunately, in many applications such achiral methods may be greatly misleading as they cannot distinguish between the D- and L-amino acid enantiomers and indeed D-amino acids are often contained in natural products such as synthetic therapeutic peptides, peptides synthesized by non-ribosomal peptide synthetases, or are formed by racemization during aging or as a consequence of disease [4,5]. Meanwhile, D-amino acids are considered as useful biomarkers for disease, which emphasizes the need of analytical assays that can distinguish between the enantiomers [6]. The methodologies that can be used for direct amino acid enantiomer separation have been reviewed by Ilisz et al [7]. It is evident that the comprehensive analysis of all proteinogenic amino acids along with their enantiomers adds an extra level of challenge to the rapid enantioselective amino acid analysis (ReAAA). Approaches that have been described usually focus on a limited number of simultaneously analyzed amino acid enantiomers. Those approaches which attempted to cover the entire profile of proteinogenic amino acid enantiomers typically had long run times (*e.g.* AQC-amino acids on Chiralpak ZWIX [8,9] and tandem column approach [10]), require strongly acidic conditions [11,12], different mobile phases [13] or multiple columns [10,12].

Recently, the sub-2 μm core-shell (superficially porous particle, SPP) particle technology found its way into the field of chiral separation, now enabling fast UHPLC enantiomer separations [14–22]. Sub-minute separations have been shown for enantiomer separations [14,23–29]. The shortest chromatographic run times so far even report sub-second separations for *e.g.* (+/-)-*trans*-stilben oxide [30], DNPyr-DL-leucine [31], *N*-(3,5-dinitrobenzoyl)-DL-leucine [31] and FMOC-DL-Val [32]. However, not for complex, entire proteinogenic amino acid mixtures. In few examples, an extended set of amino acids were resolved into enantiomers on sub 2 μm or core-shell columns [16,24]. Typical run times, however, were in the > 10 min time scale. Reischl et al. accomplished the separation in 11–15 min [16], Mazzoccanti et al. in 20–25 min [24] and Du et al. in 12–16 min [33]. In consideration of the utmost importance of its application, the goal herein was to develop a ReAAA assay, which can accomplish the separation in the 1,2 min time scale utilizing mass spectrometry as a detector. In this study, a wide pore core-shell quinine carbamate anion-exchanger (QN-AX) column from a recent study [20] and AQC pre-column derivatization [34] was employed. The goal of this work was the optimization of the separation conditions to challenge the speed of the comprehensive ReAAA of proteinogenic amino acids and their isobaric variants by UHPLC-MS to make it high throughput compatible.

Material and methods

Materials

Formic acid was from Carl Roth (Karlsruhe, Germany). Ammonium formate, HPLC grade MeOH, DL-norleucine (Nle) and DL-*tert*-leucine (Tle), dithiothreitol (DTT), iodoacetamide (IAA), deuterium oxide (D$_2$O) and deuterium chloride (DCl) were supplied by Sigma-Aldrich (Schnelldorf, Germany). DL-Glutamine and DL-asparagine monohydrate were from Tokyo Chemical Industry (Tokyo, Japan). ACN was from Fisher Chemical (UK). Ultra LC-MS grade ACN and ultra LC-MS grade

MeOH were from Carl Roth (Karlsruhe, Germany). Highly purified water for chromatography was obtained by an Elga Pure Lab Ultra purification system (Celle, Germany). A uniformly labelled L-AA [u-^{13}C^{15}N] internal standard (AA-IS) mix (2.5 mM in 0.1 M HCl) containing all proteinogenic AAs (except Asn, Gln and Trp) was obtained from Euroisotop GmbH (Saarbrücken, Germany). 6-Aminoquinolyl-N-hydroxysuccinimidyl carbamate (AQC, AccQ) was purchased from Synchem (Felsberg/Altenburg, Germany). Essential amino acid supplement complex (Pure Encapsulation) was purchased from a local pharmacy (Tübingen, Germany) containing L-His (150 mg), L-Ile (237 mg), L-Leu (414 mg), L-Lys (330 mg), L-Met (210 mg), L-Phe (345 mg), L-Thr (204 mg), L-Trp (60 mg) and L-Val (225 mg) per 3 capsules. A core-shell QN-AX column (3 × 50 mm, 2.7 μm, 160 Å) from a previous study [20] was employed for chiral UHPLC enantiomer separations.

Sample preparation

AA standard mixture solution ([u-^{12}C^{14}N] L- and DL-amino acids) was prepared at a concentration of 2.5 mM in 0.1 M HCl containing all proteinogenic amino acids plus Hse (homoserine), aThr (*allo*-threonine), aIle (*allo*-isoleucine), Tle (*tert*-leucine) and nLeu (norleucine) as isobaric analogs. Racemic internal standard (IS) solution (0.025 mM, u-^{13}C^{15}N) of DL-AAs was obtained by racemization according to a reported protocol [9,35]. For lipopeptide ReAAA the sample was dissolved in 1 mL of 6 M DCl in D$_2$O (1 mg mL^{-1}) in a glass vial, sealed under nitrogen and hydrolysed at 110 °C for 16 h. Subsequently, the sample was evaporated to dryness, re-dissolved to the original volume (1 mL) with 0.4 M borate buffer (pH 8.8), vortexed, and centrifuged for 60 s at 13,200 rpm. The amino acid complex supplement was dissolved in 0.1 M HCl at 10 mg/mL vortexed and centrifuged for 60 s at 13200 rpm before using the supernatant for further experiments.

Alkylation

Without prior protection of the thiol side chain of Cys, the separation and analysis of this amino acid was rather problematic [36]. Hence, cysteine was prepared according to the following protocol [8]. First, iodoacetamide (IAA) and dithiothreitol (DTT) were prepared (10 mM in ultra-pure water) shortly before their use and kept on ice. Then, solutions of 10 μL AA mix (2.5 mM), 5 μL DTT and 10 μL AA IS (1.25 mM L-AAs or 0.025 mM DL-AAs) were added to a solution of 40 μL 0.4 M sodium borate buffer (pH 8.8) in a 1.5 mL microcentrifuge tube. The reaction solution was placed on a thermoshaker at 800 rpm and 55 °C for 10 min, followed by centrifugation (13,200 rpm, 4 °C, 1 min). Accordingly, 10 μL IAA and 5 μL DTT were added successively and treated likewise. Lastly, 40 μL of the given solution was adjusted to a volume of 50 μL with ultrapure water (0.25 mM AA mix-IAA). For direct MS measurements, the solution was further diluted 1:10 with 0.2 M sodium borate buffer (pH 8.8) prior to derivatization with AQC reagent.

Derivatization

AQC derivatization, which is widely used as part of pharmacopoeias and therefore attractive, was performed. The reaction is carried out at weakly basic conditions which leads to mono- or bis-AQC-tagged (Lys, Cys) derivatives. The side chains of Arg and His are not tagged under weakly basic buffer conditions and therefore adopt a zwitterionic character. Thus, a solution of 3 mg/mL AQC (10.5 mM in dry acetonitrile) was prepared, stored at −20 °C and briefly ultrasonicated before use. If not otherwise stated 10 μL of AA (0.25 mM AA mix) and 10 μL AQC reagent solutions were added to 80 μL of 0.2 M sodium borate buffer (pH 8.8), respectively. The solution was immediately heated to 55 °C for 10 min at 800 rpm. After centrifugation, the sample was ready to use. During measurements, the samples were constantly cooled (4 °C) in the autosampler and were only utilized for a week, then freshly prepared.

Instrumentation

Chiral separation optimization was performed on an Agilent 1290 Infinity UHPLC system (Waldbronn, Germany) comprising a binary pump (G4220A), a thermostated column compartment (G1316C), an Agilent 1100 binary pump for MS-calibrant delivery and a PAL HTC-XS autosampler (CTC Analytics, Zwingen, Switzerland). MS detection was conducted on a TripleTOF 5600+ instrument from Sciex (Ontario, Canada) with Duospray Ion Source operated in positive electrospray ionization mode, using sodium formate clusters for mass calibration. UHPLC-ESI-QTOF-MS measurements were performed in positive ionization mode with a survey TOF-MS full scan combined with information dependent acquisition (IDA) in high sensitivity mode using an inclusion list, which comprised the m/z ratios of the precursor ions of all single and double AQC-derivatized amino acid compounds. The following instrument settings were used: curtain gas (CUR) 40 psi, ion source gas (nebulizing gas; GS1) 60 psi, heater gas (drying gas; GS2) 60 psi, ion spray voltage floating (ISVF) 5500 V, source temperature (TEM) 400 °C, collision energy (CE) 10 V, declustering potential (DP) 100 V. An MS full scan range of m/z 30–2000 with an accumulation time of 250 ms was used for the QTOF-MS runs.

All measurements were performed using [u-^{13}C^{15}N]-AA IS and 1 mg/mL 1,3,5-tri-tert-butylbenzene as void volume marker. The chiral column, a prototype QN-AX core-shell column (3×50 mm, 2.7 μm, 160 Å) from a previous work [20], was selected for its capability to generate fast enantiomer separations (Fig. 1). The thin (0.5 μm thick) porous shell with 160 Å wide pores around the 1.7 μm diameter non-porous particle core greatly reduces mass transfer limitations and, along with lower A-term due to narrower particle distribution and favorable packing characteristics, provides these particles with efficiencies comparable to a corresponding sub-2 μm particle column. Compared to common fully porous particles (FPP), such as commercially available Chiralpak QN-AX, it has about a factor 4 lower specific surface area at comparable surface coverage and a factor 1.4 lower total porosity due to significantly lower intra-particulate porosity [20]. Both factors greatly favor high speed separations and provide this column type with a favorable speed-performance-back pressure profile. As shown previously, it outperforms a corresponding sub-2 μm FPP column regarding the speed-efficiency relationship [20], making it the perfect choice for the current evaluation. Conditions were tested as specified in the figure captions and tables. The flow rate (1 mL/min), the injection volume (1 μL) and the oven temperature (30 °C) were kept constant for all measurements, except when stated otherwise. A summary of precursor ions used for EIC generation are shown in Table S1.

Results and discussion

Derivatization

Amino acid analysis usually involves derivatization of the amino groups to support both chromatographic retention and separation as well as detection. A widely accepted protocol for this purpose is an AQC derivatization. The majority of amino acids are therefore provided with an acidic character for their favorable retention on the chiral anion-exchanger stationary phase QN-AX [34]. Furthermore, with this AQC tagging strategy, favorable urea and quinoline sites for interaction with the quinine carbamate selector of the QN-AX CSP are introduced. The urea group providing the H-donor/acceptor system allows hydrogen bonding with the selector's carbamate group and promotes enantioselectivity in combination with the AQC-quinoline, which can interact with the aromatic moiety of the selector. The *N'*-hydrogen donor introduced by AQC labelling further assures that such an H-donor system is also available for secondary amino acids. This enables the successful enantiomer separation of Pro and other secondary amino acids, although with reversed enantiomer elution order. Other reagents such as chloroformates (*e.g.* FMOC-Cl), fall short for the enantiomer separation of Pro
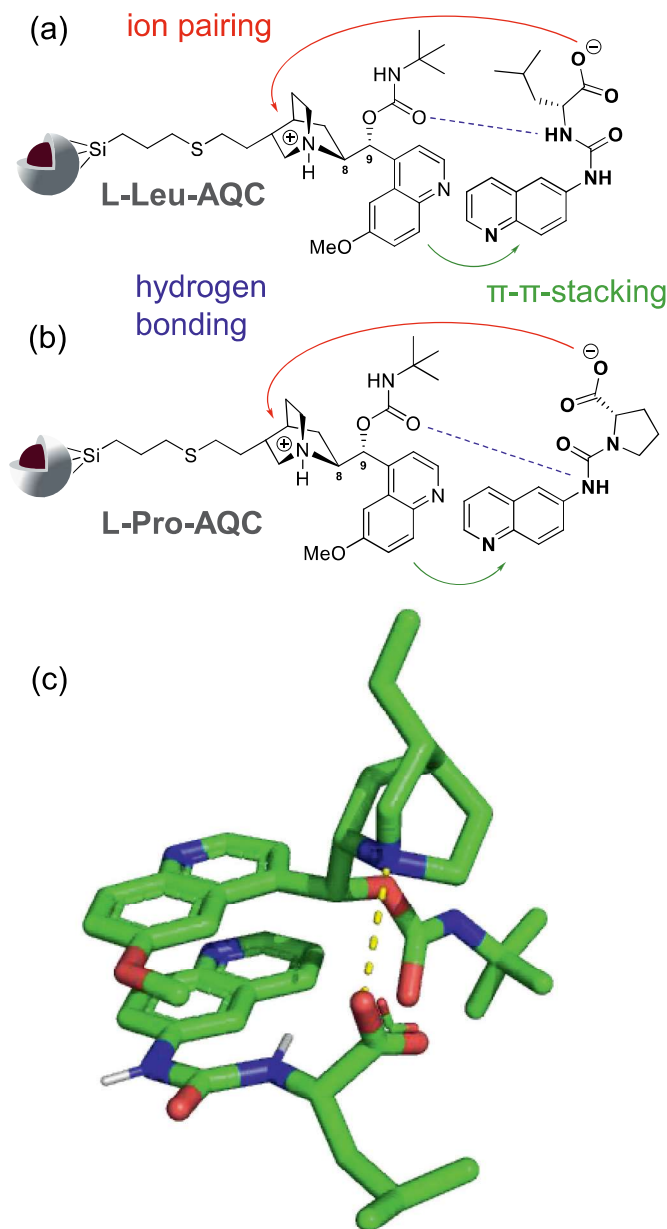

Fig. 1. Selector-selectand interaction between chiral QN-AX and AQC derivatized L-Leu (a) and L-Pro (b) in two- and L-Leu (c) in three-dimensional representation, respectively.

and other secondary amino acids on quinine/quinidine carbamate type CSPs [34].

In addition, the AQC reagent introduces a strong chromophoric and fluorophoric tag, which allows sensitive amino acid analysis *e.g.* by UV as well as fluorescence detection. However, the quinoline label also represents an efficient mass tag with excellent ionization efficiencies in positive ion mode for the AQC-amino acid derivatives. It is therefore highly suitable for sensitive MS detection. To compensate for matrix effects, we utilize a [u-^{13}C^{15}N] labelled amino acid internal standard mixture, which is commercially available in its L-enantiomeric form, but can be readily converted to a D/L-mixture by a simple racemization protocol [9]. The racemized internal standard (DL-[u-^{13}C^{15}N]-AA mix) facilitates identification and enables the correction of (enantioselective) matrix ef-
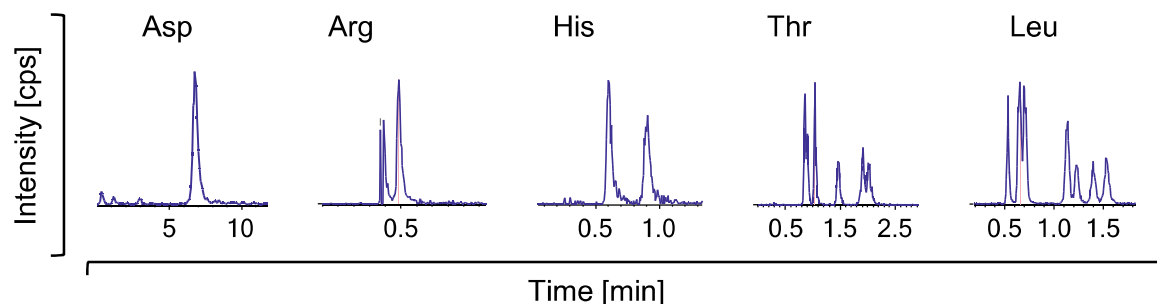
Fig. 2. Influence of different mobile phase compositions on AQC-AA separation. Thr and Leu also contain their isobaric analogues. Mobile Phase: 10 mM NH$_4$FA + 10 mM FA + 0.5% H$_2$O in ACN:MeOH (20:80; v/v), Sample: 0.025 mM AQC-AA mix (25 AAs), isocratic elution.

fects for ESI-MS analysis, which is most pronounced in gradient elution mode [9].

Optimization of separation conditions

Preliminary tests indicated that there are a number of amino acids, which might be considered being the limiting factors for achieving the goal of fast enantiomer separations of the entire set of proteinogenic amino acids. Aspartic acid has an acidic side chain, which competes for ionic interaction at the QN-AX selector that can lead to reduced enantioselectivity, but also increased retention times. Arg and His both have a positively charged side chain under the selected weakly acidic chromatographic elution conditions, which induces repulsive electrostatic interactions that may be detrimental for sufficient retentivity and enantioselectivity, respectively. For Thr, a number of isobaric amino acids exist (Hse and aThr), which cannot be distinguished by MS alone. The same applies for the isobaric variants of Leu and Ile (aIle, Tle and Nle). Although the main goal was the enantiomer separation of the proteinogenic amino acids, these isobaric analogs were included in the optimization as well. The following discussion on the optimization of chromatographic conditions focuses on these challenging amino acids. For the isobaric mixtures we expect 6 peaks for Thr and 10 peaks for Leu analogues, which will not be annotated, while for the other amino acids only two enantiomer peaks are observed in the case of a positive enantiomer separation.

Effect of acid/salt ratio

A polar organic mode eluent type was selected with MeOH as the polar organic solvent basis, partly admixed with ACN. However, it has been found that a small addition of water is favorable for both the solubility of the injected buffer components and electrospray stability. Also buffer additives, which are required in this enantioselective anion-exchange process show better solubility, when a low percentage of water was added.

In a preliminary test series, it was examined whether formic acid, ammonium formate or a mixture of both is favorable for this enantioselective anion-exchange process of AQC-derivatized amino acids. It can be seen in Fig. S1 that the additive type is particularly critical for His and Arg, and that the use of a mixture of both 10 mM NH$_4$FA and 10 mM FA appears to be most advantageous. Further experiments focused on the use of this buffer system as additive to the mobile phase (see Fig. 2).

Buffer concentration

The buffer concentration in the mobile phase was considered being of major importance. It modulates the strength of the ionic interactions of AQC-AA with the QN-AX selector by altered ionic shielding effects around the charged sites and functional groups, respectively, both of the primary anion-exchange interaction, but also the secondary repulsive (Arg, His) and attractive (Asp) side chain interactions. This factor was considered as prime determinant for the overall run time of the separation and enantioselectivity, thus it was evaluated first.

The mobile phase used for these tests was composed of NH$_4$FA at variable molarity and equimolar amounts of FA as well as 0.5% H$_2$O in MeOH. In Fig. S2 the molar concentrations of NH$_4$FA and FA were decreased from 50 mM (Fig. 3) to 1 mM. The enantioseparation improved when the molarity of additives was reduced, but the retention time of acidic amino acids like Asp increased significantly. Arg could not be separated under these conditions, probably due to repulsive interactions between the protonated QN-AX selector and the guanidinium side chain. His on the other hand could be resolved, because its residence time in the column was longer, indicating less repulsive interactions. The greatest benefit, when the buffer concentration was decreased, was observed for the isobaric amino acid mixtures: 6 (out of 6) peaks of Thr, Hse and aThr were all separated and 8 (out of 10) peaks of isobaric Leu, Ile, aIle, Tle and Nle were also resolved at low buffer concentration, yet at the expense of run times. Overall, it becomes evident that outside the buffer range of 10–50 mM the enantiomeric separation takes too long although especially the selectivity for the isobaric leucines was improved.
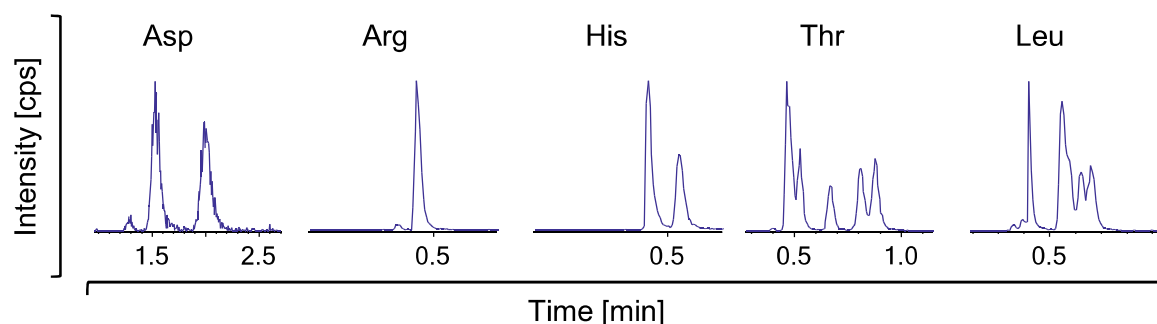

Fig. 3. Influence of the mobile phase additive molarity (50 mM NH$_4$FA + 50 mM FA + 0.5% (v/v) H$_2$O in MeOH) on AQC-AA separation. Sample: 0.025 mM AQC-AA mix (25 AAs), isocratic elution.
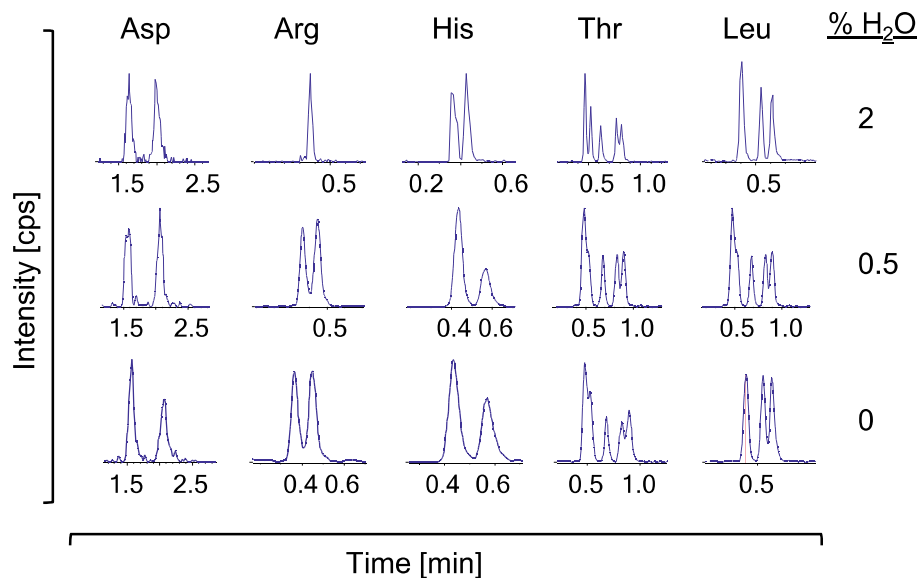
Fig. 4. Influence of the water content in the methanolic mobile phase. 50 mM NH_4FA + 50 mM FA + x% H_2O (v/v) in MeOH (isocratic), Sample: 0.025 mM AQC-AA mix (20 AAs).

Water content in the mobile phase

As shown in Fig. 4, the different water content in the methanolic mobile phase did not have too much of an influence on enantiomeric separation, however, it averts problems with precipitation of the sample or mobile phase buffer in fully nonaqueous mobile phases and associated problems with blockage of the ESI needle. In addition, Arg and His seemed to have a better resolution with low water content. According to various comparisons (Fig. S3), 0.5% water is more suitable for the mobile phase for enantioselective LC-ESI-QTOF-MS analysis of AQC-AAs on the currently investigated QN-AX column.

Effect of flow rate

In order to obtain a full enantioseparation of 25 AAs in the AA mix by a one-dimensional QN-AX system, different flow rates with different mobile phases were tested (Fig. S4). The most important goal was to separate Arg (Fig. 5a) and all the isobaric amino acids (Fig. 5b). However, even at 1 mM buffer concentration, D-Ile and D-aIle, L-Leu and L-Tle could never be separated; D-Thr and D-Hse could not be baseline separated. Since these amino acids (aIle, Tle, Hse) are usually not contained in samples of proteinogenic amino acid mixtures, their coelution is of little practical relevance.

Effect of temperature

Fig.S5 reveals the influence of temperature on peak shape and enantiomer separation. Low column temperature led to a low peak intensity, because of broader peaks, while high temperatures caused a bad peak shape for some of the most critical amino acids in the mixture (Asp, Arg, His). Thus, a column temperature of 30 °C seems to be a good compromise (Fig. 6). His and Asp enantiomers were well resolved in reasonable time (2.5 min for Asp). The enantiomers of AQC-DL-Arg could not be separated under these conditions. However, Arg could be resolved when no water was present in the mobile phase at high ionic strength and low flow rate, which advantageously increased the residence time in the column (Fig. 4). According to these optimization experiments on the QN-AX column, it turns out to be challenging to find a compromise that allows the enantiomer separation of all proteinogenic amino acids using a single mobile phase condition. However, based on these experiments, it can be expected that most of the amino acid enantiomers can be separated using a QN-AX core-shell column with one of two mobile phase conditions (*vide infra*). The remaining critical amino acid pairs are D- and L-Arg, D-Ile and D-aIle, L-Leu and L-Tle. Note that aIle and Tle are usually not present in proteinogenic amino acid samples and hence of less concern.

Optimized UHPLC-ESI-QTOF-MS assay for ReAAA

From the above-described pre-tests, two conditions were finally evaluated for the entire mixture of proteinogenic amino acids and Thr/Leu isobaric analogues. In total 25 amino acids (24 racemates and achiral Gly) and an [u-^{13}C^{15}N]-L-AQC-AA mix (17 labelled AAs), which allows a chiral peak assignment and determination of the enantiomer elution order, were derivatized with the AQC reagent and injected into coreshell QN-AX column using a UHPLC hyphenated to the ESI-QTOF-MS. The first condition tested was 10 mM NH_4FA and 10 mM FA with 0.5% H_2O in MeOH at 1 mL/min, and 30 °C. As shown in Fig. S6. and Table 1 the majority of amino acids are well resolved into their two enantiomers. Problems existed mainly for the two amino acids Arg and Asp. Due to repulsive electrostatic interaction of the side chain, Arg was not sufficiently retained and hence its enantiomers not separated. Asp was strongly retained due to ionic interactions of both α-and β-carboxylate groups with the QN-AX selector, which brings about a disturbance of the preferred molecular recognition mechanism. For this reason, enantioselectivity was lost (only a shoulder is visible on the broad peak which is indicative for a partial separation). The isobaric Thr and Leu analogs on the other hand were quite well resolved (Fig. 7a). In case of isobars of Thr, D-Hse is partially co-eluting with D-Thr, but is usually not present. All other components of this mixture were baseline separated. In case of isobaric amino acids of Leu, 7 out of 10 peaks were resolved. Coelutions concerning Leu isobars were of less importance, since D-Ile/D-Leu and L-Ile/L-Leu were sufficiently separated. Due to the strongly retained AQC-Asp, the analysis time of this method amounted to 10 min. This long run time and the lack of resolution for Arg and Asp limits the practical utility of this method for ReAAA and consequently this method was considered as a second-tier method only if isobaric amino acids D-Ile/D-Leu need to be determined separately (*vide infra*).

As the best conditions for ReAAA, a mobile phase consisting of 50 mM NH_4FA and 50 mM FA with 0.5% H_2O in MeOH at a flow rate of 1 mL/min and a column temperature of 30 °C is suggested (see Fig. 7b and Table 1). Under this condition, all proteinogenic DL-enantiomers except for DL-Arg can be separated in 1.5 min and Asp within 2.5 min (Fig.7b). The isobaric amino acid pair D-Leu/D-Ile coeluted, while the corresponding L-enantiomers were separated. D-Leu/D-Ile can be distinguished employing the second-tier method (Fig. 7a), if this information is required. Similarly, another injection is needed for the enantiomer separation of Arg (fully nonaqueous conditions as shown in Fig. 4 or a method using a commercial Chiralpak ZWIX(+) stationary phase [8]). If D-Arg and the distinction between D-Leu/D-Ile is of no concern,

Table 1

Chiral Separation of 25 AQC derivatized amino acid mixture and 17 AQC-L-[u-13C15N]-AA on a QN-AX core-shell prototype (3 × 50 mm, 2.7 μm) column.

| AQC-AA	50 mM FA + 50 mM NH$_4$FA in MeOH/H$_2$O (99.5: 0.5; v/v) t$_0$= 0.256							10 mM FA + 10 mM NH$_4$FA in MeOH/H$_2$O (99.5: 0.5; v/v) t$_0$= 0.258						
	RT (D)	RT (L)	RT (L-^{13}C^{15}N)	Elution order	k (D)	k (L)	α (L/D)	RT (D)	RT (L)	RT (L-^{13}C^{15}N)	Elution order	k (D)	k (L)	α (L/D)
Gly	–	0.621	0.619	D < L	–	1.426	–	–	1.309	1.304	D < L	–	4.074	–
Ala	0.467	0.577	0.577	D < L	0.824	1.254	1.521	0.871	1.193	1.190	D < L	2.376	3.624	1.525
Ser	0.536	0.829	0.778	D < L	1.094	2.238	2.046	1.082	1.911	1.904	D < L	3.194	6.407	2.006
Thr	0.473	0.878	0.878	D < L	0.848	2.430	2.866	0.884	2.070	2.067	D < L	2.426	7.023	2.895
Cys-IAA	0.681	1.032	1.032	D < L	1.660	3.031	1.826	1.526	2.538	2.534	D < L	4.915	8.837	1.798
Val	0.418	0.647	0.645	D < L	0.633	1.527	2.414	0.669	1.425	1.423	D < L	1.593	4.523	2.839
Leu	0.418	0.550	0.545	D < L	0.633	1.148	1.815	0.712	1.142	1.132	D < L	1.760	3.426	1.947
Ile	0.418	0.622	0.623	D < L	0.633	1.430	2.259	0.693	1.364	1.359	D < L	1.686	4.287	2.543
Met	0.540	0.766	0.766	D < L	1.109	1.992	1.796	1.111	1.797	1.793	D < L	3.306	5.965	1.804
Pro	0.641	0.537	0.536	L < D	1.504	1.098	1.370 [a]	1.402	1.084	1.079	L < D	4.434	3.202	1.385 [a]
Phe	0.536	0.805	0.802	D < L	1.094	2.145	1.961	1.110	1.932	1.924	D < L	3.302	6.488	1.965
Tyr	0.560	0.909	0.906	D < L	1.188	2.551	2.148	1.162	2.333	2.150	D < L	3.504	8.043	2.295
Trp	0.648	1.121	–	D < L	1.531	3.379	2.207	1.364	2.771	–	D < L	4.287	9.740	2.272
Asp	1.531	2.003	1.996	D < L	4.980	6.824	1.370	8.391	–	8.107	D < L	31.523	–	–
Glu	0.933	1.113	1.107	D < L	2.645	3.348	1.266	4.529	5.284	4.754	D < L	16.554	19.481	1.177
Asn	0.627	1.282	–	D < L	1.449	4.008	2.765	1.313	3.190	–	D < L	4.089	11.364	2.779
Gln	0.568	0.720	–	D < L	1.219	1.813	1.487	1.178	1.597	–	D < L	3.566	5.190	1.455
His	0.427	0.544	0.542	D < L	0.668	1.125	1.684	0.540	0.765	0.759	D < L	1.093	1.965	1.798
Lys	0.658	0.923	0.921	D < L	1.570	2.605	1.659	1.354	2.130	2.124	D < L	4.248	7.256	1.708
Arg	0.473	–	0.436	D < L	0.848	–	–	0.443	–	0.443	D < L	0.717	–	–
Hse	0.473	0.669	–	D < L	0.848	1.613	1.903	0.925	1.459	–	D < L	2.585	4.655	1.801
aThr	0.527	0.812	–	D < L	1.059	2.172	2.052	1.068	1.896	–	D < L	3.140	6.349	2.022
aIle	0.418	0.660	–	D < L	0.633	1.578	2.494	0.669	1.485	–	D < L	1.593	4.756	2.985
tLeu	0.418	0.550	–	D < L	0.633	1.148	1.815	0.543	1.142	–	D < L	1.105	3.426	3.102
Nle	0.418	0.550	–	D < L	0.633	1.148	1.815	0.734	1.229	–	D < L	1.845	3.764	2.040

[a] $\alpha = k_D/k_L$
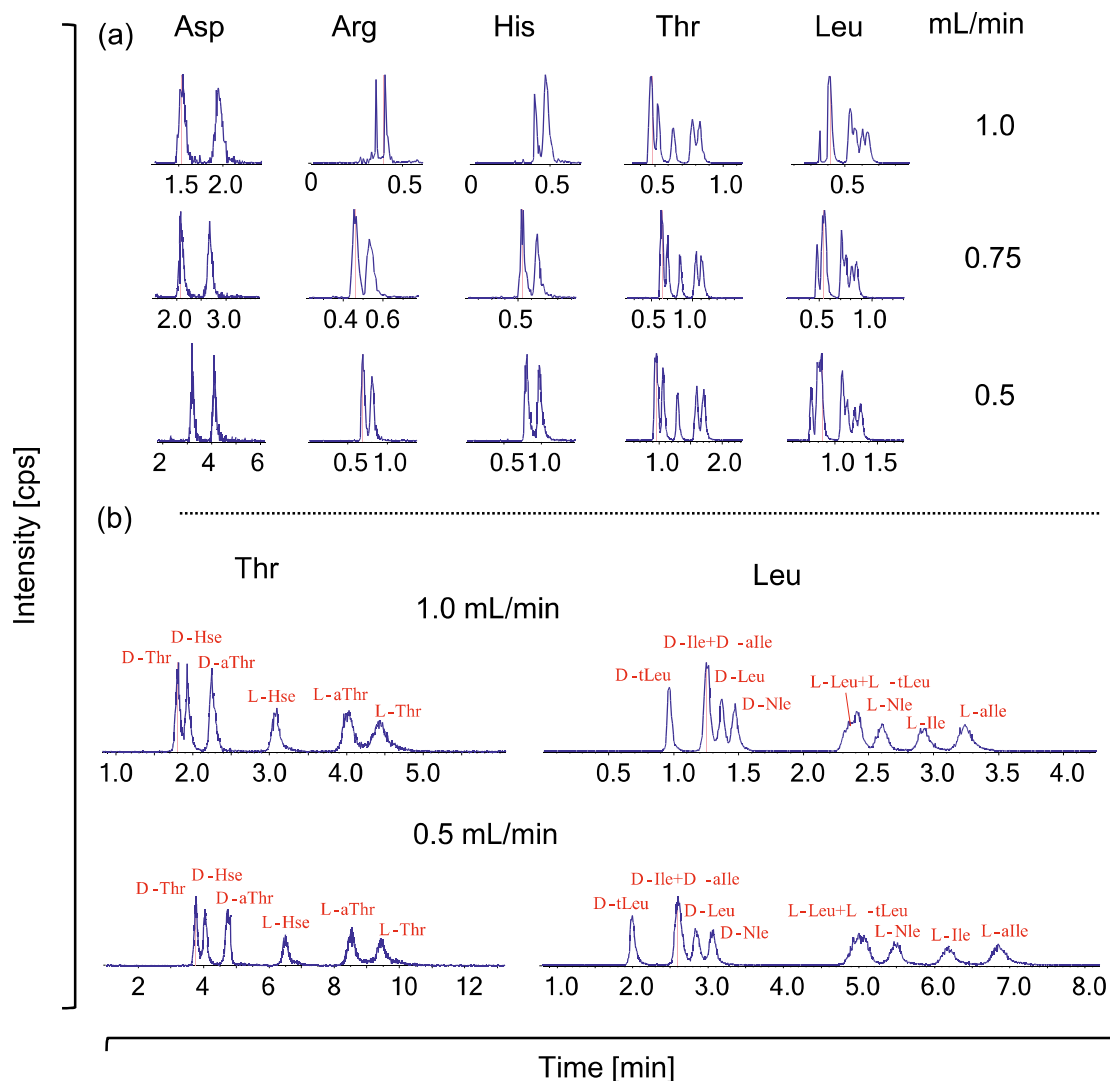
Fig. 5. Influence of the flow rate with varying mobile phase molarity on AQC-AA separation. With x mM NH_4FA + x mM FA + 0.5% (v/v) H_2O in MeOH for (a) x = 50 and (b) x = 1; isocratic elution.
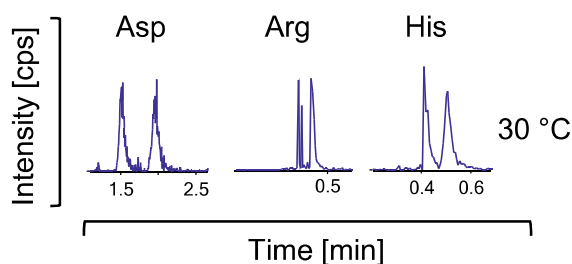

Fig. 6. Influence of the temperature on AQC-AA separation (30 °C, see Fig. S6 for further *T* values). Mobile phase: 50 mM NH_4FA + 50 mM FA + 0.5% (v/v) H_2O in MeOH; Sample: 0.025 mM AQC-AA mix (25 AAs).

the ReAAA can be performed by this enantioselective core-shell QN-AX UHPLC-QTOF-MS method in 2.5 min per sample.

Application

The developed UHPLC-ESI-QTOF-MS assay for fast ReAAA was finally applied for the absolute configuration assignment of the constituent amino acids of a cyclic lipopeptide research sample contain-

ing Glu, Leu, Ser and Val, according to genome sequencing and NMR data [37] (Fig. 8). Their stereoconfiguration was unknown. The prime ReAAA screening method clearly revealed the presence of D-Glu, D-Ser and D- and L-Val (Fig. 8,b,c,d). It further suggested the presence of Leu/Ile (Fig. 8a). For this reason, the sample was also analyzed by the 2nd-tier method (Fig. 7a). It confirmed the presence of D and L-Leu and the absence of L-Ile and also D-Ile which would be observable as a shoulder on the D-Leu peak in the 2nd-tier method. The results finally confirmed the following D/L-AA ratios: Glu (1/0), Leu (2/3), Ser (3/0) and Val (1/2).

Further, an amino acid supplement sample obtained from a local pharmacy which according to specifications contained only L-amino acids was furthermore analyzed (see Fig. 9). The results confirmed the specified amino acid composition. Nonetheless, minor impurities of D-AAs were found for Thr (0.71% area) and Val (1.32% area). Their identity could be verified by the racemized internal standard. The results document that this UHPLC-ESI-QTOF-MS/MS ReAAA method is suitable for fast screening of the amino acid composition and detection of D-amino acids. If other than proteinogenic amino acids are present in a sample, the TOF-MS full scan experiment and stereoselective retention would provide at least some indication that a further validation is necessary for those unexpected constituents.
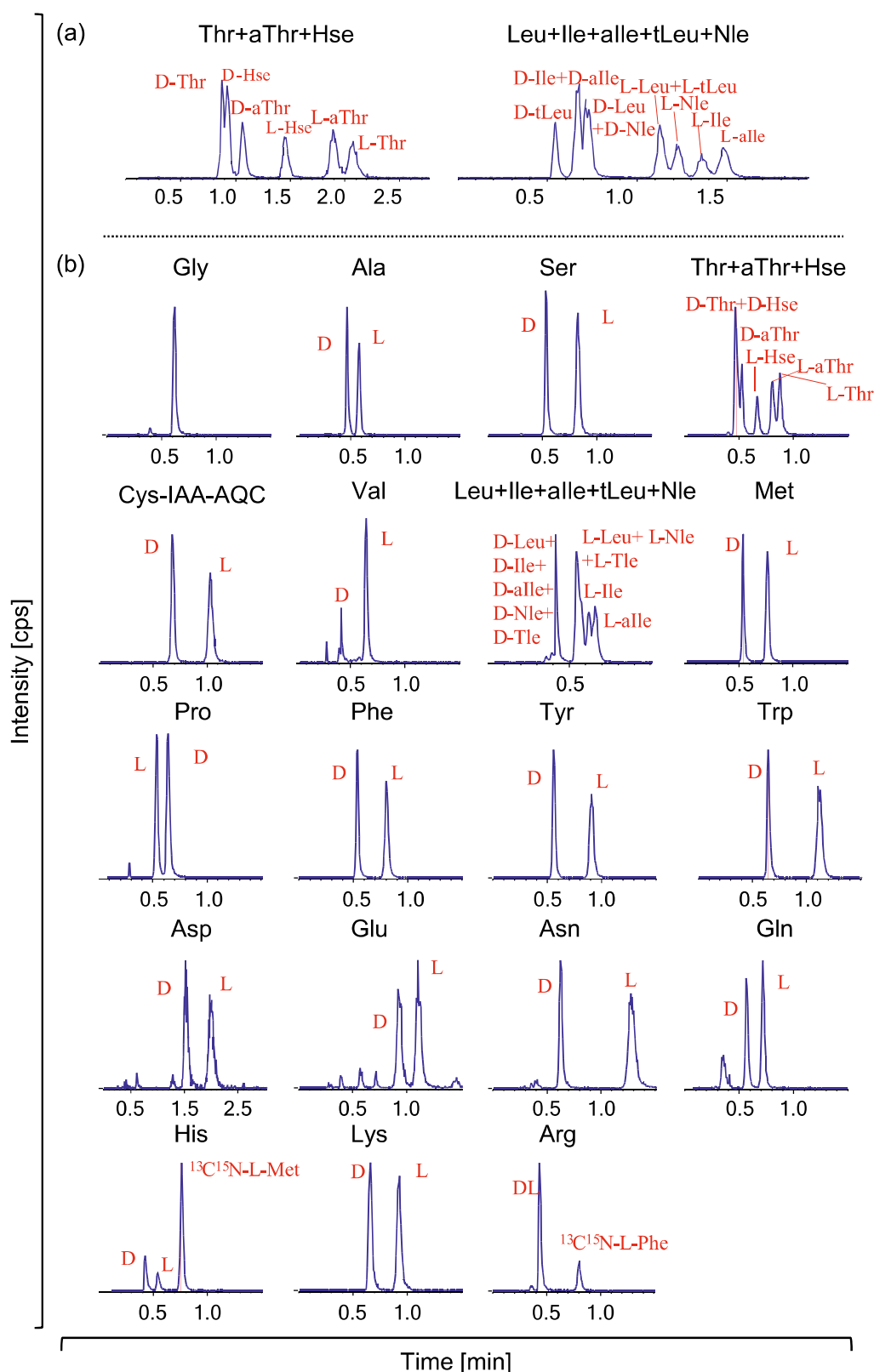
Fig. 7. Final optimized methods: (a) Second tier eAAA method shown for isobars of Thr and Leu with low molarity ($x = 10$) mobile phase. (b) Primary eAAA screening method of AQC-AAs employing the best conditions ($x = 50$). Mobile phase: x mM NH$_4$FA + x mM FA + 0.5% (v/v) H$_2$O in MeOH; Sample: 0.025 mM [u-^{12}C^{14}N]-DL-AQC-AA mix (24 AQC-AA and Cys-IAA-AQC)+ [u-^{13}C^{15}N]-L-AQC-AA mix (17 AQC-AA). Note, isobaric amino acids were also injected as individual standards.
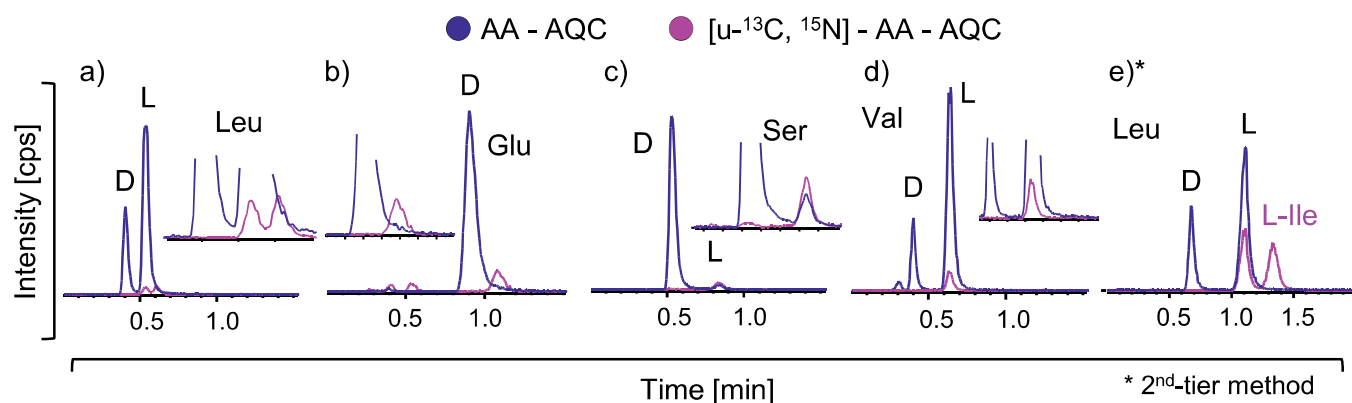
Fig. 8. eAAA of cyclic lipopeptide research sample using optimized conditions, *i.e.* primary (see Fig. 7b caption for conditions) and second-tier method (see Fig. 7a caption for conditions). All proteinogenic AAs (except Trp, Gln and Asn) were included as racemized (15 h) L-[u-^{13}C^{15}N] internal standard for reference.
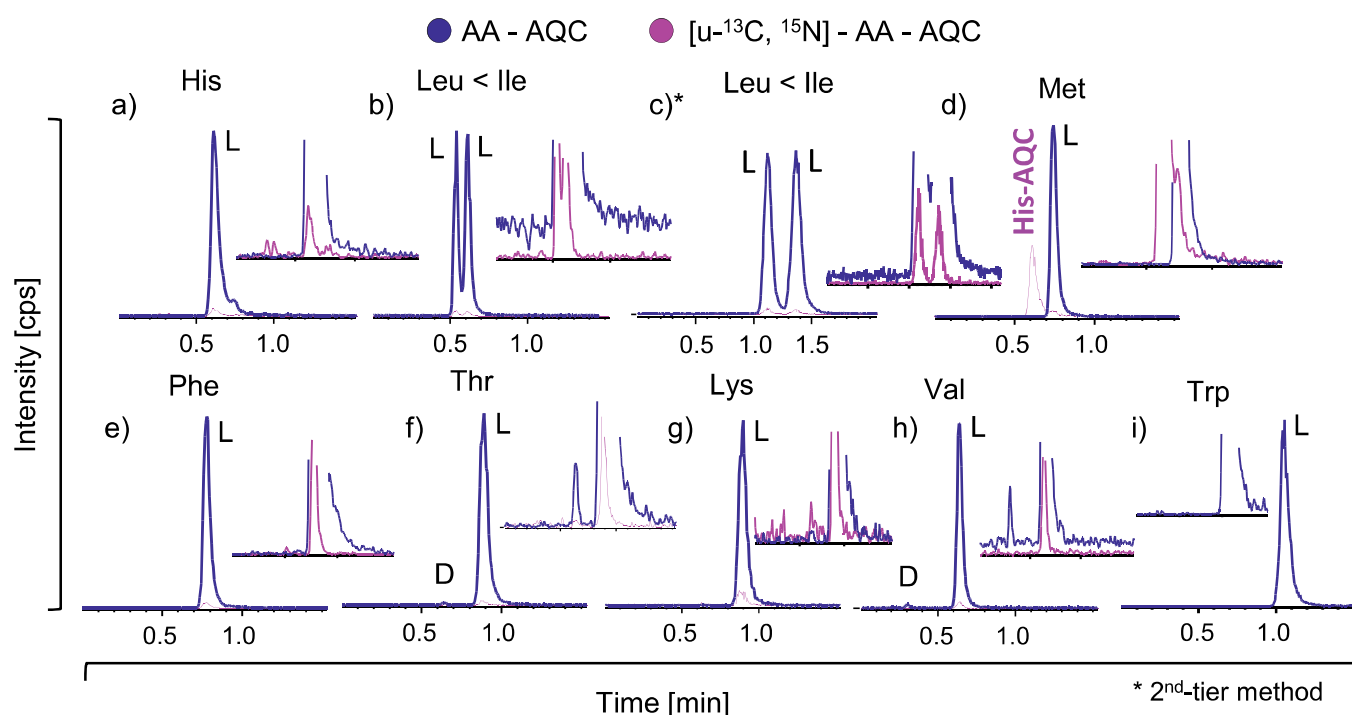

Fig. 9. eAAA of amino acid complex supplement using optimized conditions, *i.e.* primary (see Fig. 7b caption for conditions) and second-tier method (see Fig. 7a caption for conditions). All proteinogenic AAs (except Trp, Gln and Asn) were included as racemized (15 h) L-[u-^{13}C^{15}N] internal standard for reference.

Conclusion

Amino acid analysis is a methodology of broad application in biosciences and well established in many research and routine analytical laboratories. As more and more focus is also directed to D-amino acids as constituents in biomaterials, food supplements and biological samples, efficient methods for the stereoconfiguration control in such samples are becoming of essential importance. There are numerous methods for the enantioselective amino acid analysis, however, they usually require long analysis times. Core-shell chiral columns have been shown to outperform sub-2 μm fully porous particle chiral columns in terms of their speed-performance characteristics and highly qualify as first choice tools for high-throughput eAAA. Here we could achieve this goal in less than 2.5 min for all proteinogenic AAs with a primary method. A 2nd tier method can provide improved resolution for Leu/Ile and their enantiomers and needs 10 min per sample. Higher flow rates, which can further accelerate the separations, are negatively impacting the detection sensitivity in ESI-MS, although in many applications of eAAA there

is no problem with detection limits. Yet, we deemed analysis times of 2.5 min as acceptable for ReAAA screening method. Some further advancements seem necessary to also allow Arg enantiomer separation in a single method with one column and mobile phase [8]. The established ReAAA methodology could be useful for high-throughput quality control of food supplements and (therapeutic) peptide/protein hydrolysates.

Declaration of Competing Interest

The authors declare that they have no known competing financial interests or personal relationships that could have appeared to influence the work reported in this paper.

CRediT authorship contribution statement

Ryan Karongo: Investigation, Methodology, Formal analysis, Data curation, Visualization, Writing – original draft, Writing – review & editing. **Min Ge:** Investigation, Methodology, Formal analysis, Writing –

References

[1] Swietlow A, Rode H, Szajek A, Verlander M, Eggen I, Gregg B. Control strategies for synthetic therapeutic peptide APIs-part I: analytical consideration. Pharm Technol 2014;38.

[2] Wahl O, Holzgrabe U. Amino acid analysis for pharmacopoeial purposes. Talanta 2016;154:150–63. doi:10.1016/j.talanta.2016.03.071.

[3] Ferre S, Gonzalez-Ruiz V, Guillarme D, Rudaz S. Analytical strategies for the determination of amino acids: Past, Present and Future trends. J Chromatogr B Analyt Technol Biomed Life Sci 2019;1132:121819. doi:10.1016/j.jchromb.2019.121819.

[4] Fujii N, Homma H, Usiello A, Sweedler J, Hamase K. The significance of D-amino acids in the homochiral world of life. Biochim Biophys Acta 2021;1869:140565. doi:10.1016/j.bbapap.2020.140565.

[5] Furman C, Howsam M, Lipka E. Recent developments in separation methods for enantiomeric ratio determination of amino acids specifically involved in cataract and Alzheimer's disease. TrAC Trends Anal Chem 2021;141:116287. doi:10.1016/j.trac.2021.116287.

[6] Ishii C, Furusho A, Hsieh CL, Hamase K. Multi-dimensional high-performance liquid chromatographic determination of chiral amino acids and related compounds in real world samples. Chromatography 2020;41:1–17. doi:10.15583/jpchrom.2020.004.

[7] Ilisz I, Péter A, Lindner W. State-of-the-art enantioseparations of natural and unnatural amino acids by high-performance liquid chromatography. TrAC Trends Anal Chem 2016;81:11–22. doi:10.1016/j.trac.2016.01.016.

[8] Horak J, Lammerhofer M. Stereoselective separation of underivatized and 6-aminoquinolyl-N-hydroxysuccinimidyl carbamate derivatized amino acids using zwitterionic quinine and quinidine type stationary phases by liquid chromatography-high resolution mass spectrometry. J Chromatogr A 2019. doi:10.1016/j.chroma.2019.02.060.

[9] Horak J, Lämmerhofer M. Derivatize, racemize, and analyze—an Easy and simple procedure for chiral amino acid standard preparation for enantioselective metabolomics. Anal Chem 2019;91:7679–89. doi:10.1021/acs.analchem.9b00666.

[10] Kimura R, Tsujimura H, Tsuchiya M, Soga S, Ota N, Tanaka A, Kim H. Development of a cognitive function marker based on D-amino acid proportions using new chiral tandem LC-MS/MS systems. Sci Rep 2020;10:804. doi:10.1038/s41598-020-57878-y.

[11] Konya Y, Taniguchi M, Furuno M, Nakano Y, Tanaka N, Fukusaki E. Mechanistic study on the high-selectivity enantioseparation of amino acids using a chiral crown ether-bonded stationary phase and acidic, highly organic mobile phase by liquid chromatography/time-of-flight mass spectrometry. J Chromatogr A 2018;1578:35–44. doi:10.1016/j.chroma.2018.10.004.

[12] Yoshikawa K, Furuno M, Tanaka N, Fukusaki E. Fast enantiomeric separation of amino acids using liquid chromatography/mass spectrometry on a chiral crown ether stationary phase. J Biosci Bioeng 2020;130:437–42. doi:10.1016/j.jbiosc.2020.05.007.

[13] Miller L, Yue L. Chiral separation of underivatized amino acids in supercritical fluid chromatography with chiral crown ether derived column. Chirality 2020;32:981–9. doi:10.1002/chir.23204.

[14] Ciogli A, Ismail OH, Mazzoccanti G, Villani C, Gasparrini F. Enantioselective ultra high performance liquid and supercritical fluid chromatography: the race to the shortest chromatogram. J Sep Sci 2018;41:1307–18. doi:10.1002/jssc.201701406.

[15] Catani M, Felletti S, Ismail OH, Gasparrini F, Pasti L, Marchetti N, De Luca C, Costa V, Cavazzini A. New frontiers and cutting edge applications in ultra high performance liquid chromatography through latest generation superficially porous particles with particular emphasis to the field of chiral separations. Anal Bioanal Chem 2018;410:2457–65. doi:10.1007/s00216-017-0842-4.

[16] Reischl RJ, Hartmanova L, Carrozzo M, Huszar M, Frühauf P, Lindner W. Chemoselective and enantioselective analysis of proteinogenic amino acids utilizing N-derivatization and 1-D enantioselective anion-exchange chromatography in combination with tandem mass spectrometric detection. J Chromatogr A 2011;1218:8379–87. doi:10.1016/j.chroma.2011.09.046.

[17] Lomsadze K, Jibuti G, Farkas T, Chankvetadze B. Comparative high-performance liquid chromatography enantioseparations on polysaccharide based chiral stationary phases prepared by coating totally porous and core–shell silica particles. J Chromatogr A 2012;1234:50–5. doi:10.1016/j.chroma.2012.01.084.

[18] Spudeit DA, Dolzan MD, Breitbach ZS, Barber WE, Micke GA, Armstrong DW. Superficially porous particles vs. fully porous particles for bonded high performance liquid chromatographic chiral stationary phases: isopropyl cyclofructan 6. J Chromatogr A 2014;1363:89–95. doi:10.1016/j.chroma.2014.08.022.

[19] Kotoni D, Ciogli A, Molinaro C, D'Acquarica I, Kocergin J, Szczerba T, Ritchie H, Villani C, Gasparrini F. Introducing enantioselective ultrahigh-pressure liquid chromatography (eUHPLC): theoretical inspections and ultrafast separations on a new Sub-2-μm whelk-O1 stationary phase. Anal Chem 2012;84:6805–13. doi:10.1021/ac301335b.

[20] Schmitt K, Woiwode U, Kohout M, Zhang T, Lindner W, Lämmerhofer M. Comparison of small size fully porous particles and superficially porous particles of chiral anion-exchange type stationary phases in ultra-high performance liquid chromatography: effect of particle and pore size on chromatographic efficiency and kinetic performance. J Chromatogr A 2018. doi:10.1016/j.chroma.2018.07.056.

[21] Geibel C, Dittrich K, Woiwode U, Kohout M, Zhang T, Lindner W, Lammerhofer M. Evaluation of superficially porous particle based zwitterionic chiral ion exchangers against fully porous particle benchmarks for enantioselective ultra-high performance liquid chromatography. J Chromatogr A 2019. doi:10.1016/j.chroma.2019.06.026.

[22] Pantsulaia S, Targamadze K, Khundadze N, Kharaishvili Q, Volonterio A, Chitty M, Farkas T, Chankvetadze B. Potential and current limitations of superficially porous silica as a carrier for polysaccharide-based chiral selectors in separation of enantiomers in high-performance liquid chromatography. J Chromatogr A 2020;1625:461297. doi:10.1016/j.chroma.2020.461297.

[23] Patel DC, Breitbach ZS, Wahab MF, Barhate CL, Armstrong DW. Gone in seconds: praxis, performance, and peculiarities of ultrafast chiral liquid chromatography with superficially porous particles. Anal Chem 2015;87:9137–48. doi:10.1021/acs.analchem.5b00715.

[24] Mazzoccanti G, Manetto S, Ricci A, Cabri W, Orlandin A, Catani M, Felletti S, Cavazzini A, Ye M, Ritchie H, Villani C, Gasparrini F. High-throughput enantioseparation of Nα-fluorenylmethoxycarbonyl proteinogenic amino acids through fast chiral chromatography on zwitterionic-teicoplanin stationary phases. J Chromatogr A 2020;1624:461235. doi:10.1016/j.chroma.2020.461235.

[25] Khundadze N, Pantsulaia S, Fanali C, Farkas T, Chankvetadze B. On our way to sub-second separations of enantiomers in high-performance liquid chromatography. J Chromatogr A 2018;1572:37–43. doi:10.1016/j.chroma.2018.08.027.

[26] Welch CJ. Are we approaching a speed limit for the chromatographic separation of enantiomers? ACS Central Sci 2017;3:823–9. doi:10.1021/acscentsci.7b00250.

[27] Barhate CL, Joyce LA, Makarov AA, Zawatzky K, Bernardoni F, Schafer WA, Armstrong DW, Welch CJ, Regalado EL. Ultrafast chiral separations for high throughput enantiopurity analysis. Chem Commun 2017;53:509–12. doi:10.1039/C6CC08512A.

[28] Patel DC, Breitbach ZS, Yu J, Nguyen KA, Armstrong DW. Quinine bonded to superficially porous particles for high-efficiency and ultrafast liquid and supercritical fluid chromatography. Anal Chim Acta 2017;963:164–74. doi:10.1016/j.aca.2017.02.005.

[29] Wahab MF, Roy D, Armstrong DW. The theory and practice of ultrafast liquid chromatography: a tutorial. Anal Chim Acta 2021;1151:238170. doi:10.1016/j.aca.2020.12.045.

[30] Ismail OH, Pasti L, Ciogli A, Villani C, Kocergin J, Anderson S, Gasparrini F, Cavazzini A, Catani M. Pirkle-type chiral stationary phase on core-shell and fully porous particles: are superficially porous particles always the better choice toward ultrafast high-performance enantioseparations? J Chromatogr A 2016;1466:96–104. doi:10.1016/j.chroma.2016.09.001.

[31] Wahab MF, Wimalasinghe RM, Wang Y, Barhate CL, Patel DC, Armstrong DW. Salient sub-second separations. Anal Chem 2016;88:8821–6. doi:10.1021/acs.analchem.6b02260.

[32] Patel DC, Wahab MF, O'Haver TC, Armstrong DW. Separations at the speed of sensors. Anal Chem 2018;90:3349–56. doi:10.1021/acs.analchem.7b04944.

[33] Du S, Wang Y, Weatherly CA, Holden K, Armstrong DW. Variations of l- and d-amino acid levels in the brain of wild-type and mutant mice lacking d-amino acid oxidase activity. Anal Bioanal Chem 2018;410:2971–9. doi:10.1007/s00216-018-0979-9.

[34] Hellinger R, Horak J, Lindner W. Enantioseparation of 6-aminoquinolyl-N-hydroxysuccinimidyl carbamate tagged amino acids and other zwitterionic compounds on cinchona-based chiral stationary phases. Anal Bioanal Chem 2013;405:8105–20. doi:10.1007/s00216-013-7121-9.

[35] Horak J, Lämmerhofer M. Racemization without deamidation: effect of racemization conditions on 6-aminoquinolyl-N-hydroxysuccinimidyl carbamate tagged amino acids. J Chromatogr A 2019;1604:460492. doi:10.1016/j.chroma.2019.460492.

[36] Pucciarini L, González-Ruiz V, Zangari J, Martinou JC, Natalini B, Sardella R, Rudaz S. Development and validation of a chiral UHPLC-MS method for the analysis of cysteine enantiomers in biological samples. J Pharm Biomed Anal 2020;177:112841. doi:10.1016/j.jpba.2019.112841.

[37] Gross H, Stockwell VO, Henkels MD, Nowak-Thompson B, Loper JE, Gerwick WH. The genomisotopic approach: a systematic method to isolate products of orphan biosynthetic gene clusters. Chem Biol 2007;14:53–63. doi:10.1016/j.chembiol.2006.11.007.

4.5 Publication V – Revised Manuscript

Comprehensive Online Reversed-phase×Chiral Two-dimensional Liquid Chromatography-Mass Spectrometry with Data-independent SWATH-Acquisition for Untargeted Enantioselective Amino Acid Analysis
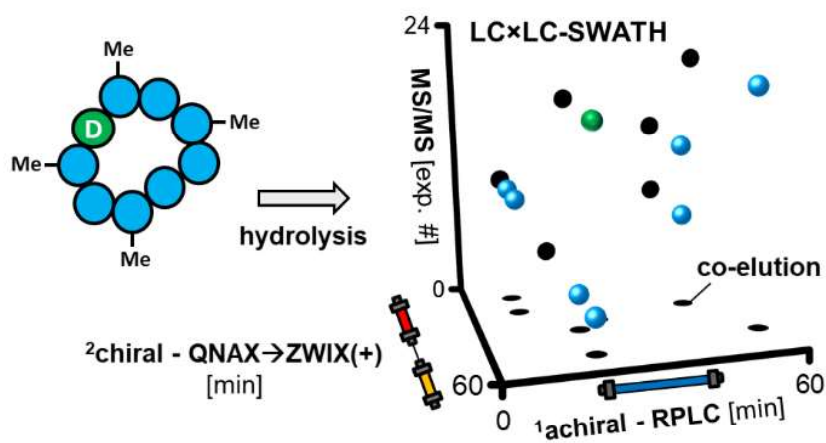
Ryan Karongo[a], Jeannie Horak[b], Michael Lämmerhofer[a]

[a]Institute of Pharmaceutical Sciences, Pharmaceutical (Bio-)Analysis, University of Tübingen, Auf der Morgenstelle 8, Tübingen 72076, Germany

[b]Division of Metabolic and Nutritional Medicine, Dr. von Hauner Children's Hospital University of Munich Medical Center, Ludwig-Maximilians-University Munich, Lindwurmstraße 4, Munich 80337, Germany

Graphical Abstract

Comprehensive Online Reversed-phase×Chiral Two-dimensional Liquid Chromatography-Mass Spectrometry with Data-independent SWATH-Acquisition for Untargeted Enantioselective Amino Acid Analysis

Ryan Karongo[a], Jeannie Horak[b], Michael Lämmerhofer[a]*

[a]Institute of Pharmaceutical Sciences, Pharmaceutical (Bio-)Analysis, University of Tübingen, Auf der Morgenstelle 8, 72076 Tübingen, Germany

[b]Division of Metabolic and Nutritional Medicine, Dr. von Hauner Children's Hospital, Ludwig-Maximilians-University Munich Medical Center, Lindwurmstraße 4, 80337 Munich, Germany

ABSTRACT: This work presents an advanced analytical platform for untargeted enantioselective amino acid analysis (eAAA) by comprehensive achiral × chiral 2D-LC hyphenated to ESI-QTOF-MS/MS utilizing data-independent SWATH (Sequential Window Acquisition of all Theoretical Fragment-Ion Spectra) technology. The methodology involves *N*-terminal pre-column derivatization with 6-aminoquinolyl-*N*-hydroxysuccinimidyl carbamate (AQC; AccQ) as retention, selectivity and MS tag, supporting retention and UV detection in RPLC (^{1}D), chiral recognition and thus enantioselectivity by the core-shell tandem column composed of a quinine carbamate weak anion exchanger (QN-AX) and a zwitterionic chiral ion-exchanger (ZWIX(+)) (^{2}D), as well as the ionization efficiency during positive electrospray ionization due to a high proton affinity of the AQC label. Furthermore, the urea-type MS tag gives rise to the generation of AQC-tag characteristic signature fragments in MS^2. The latter allows the chemoselective mass spectrometric filtering of targeted and untargeted *N*-derivatized amino acids or related labelled species. The chiral core-shell tandem column provides a complete enantioselective amino acid profile of all proteinogenic amino acids within 1 minute, with full baseline separation of all enantiomers, but without resolution of isomeric Ile/*allo*-Ile (aIle)/Leu, which can be resolved by RPLC. The entire LC×LC separation occurs within a total run time of 60 min (^{1}D), with the chiral ^{2}D operated in gradient elution mode and a cycle time of 60 seconds. A strategy to mine the 2D-LC-SWATH data is presented and demonstrated for the qualitative eAAA of two peptide hydrolysate samples of therapeutic peptides containing common and uncommon as well as primary and secondary amino acids. Absolute configuration assignment of amino acids using template matching for all proteinogenic amino acids was made feasible due to method robustness and the inclusion of an isotopically labelled L-[U-^{13}C^{15}N]-AA standard. The quantification performance of this LC×LC-MS/MS assay was also evaluated. Accuracies were acceptable for the majority of AAs enabling AA composition determination in peptide hydrolysates simultaneously with configuration assignment, as exemplified by oxytocin. This methodology represents a step towards truly untargeted enantioselective amino acid analysis and metabolomics, respectively.

INTRODUCTION. There is growing evidence that the presence of D-AAs in various biochemical environments has significant biological implications. D-AAs can be found in tissues and physiological fluids[1] indicating various diseases like cataract,[2] multiple sclerosis[3] and Alzheimer's disease[4] thus having potential as biomarkers. They are also present in (natural, synthetic and therapeutic) peptides requiring their analytical determination as part of structure elucidation and/or quality control.[5] A direct enantioresolution of underivatized and derivatized AAs using chiral stationary phases is nowadays the first choice.[6-14] Common examples for achiral precolumn derivatization supporting chiral separation comprise 6-aminoquinolyl-*N*-hydroxysuccinimidyl carbamate (AQC),[15,16] 1-fluoro-2,4-dinitrobenzene (DNB-F, Sanger's reagent),[17] 4-fluoro-7-nitro-2,1,3-benzoxadiazole (NBD),[18] dansyl chloride (Dns)[19,20] and 9-fluorenylmethyl-chloroformate (Fmoc-Cl).[21-23] These reagents commonly improve the retention and enantioselectivity behavior,[24,25] introduce chromophoric and

fluorophoric detectability,[12] can enhance detection sensitivity of AAs with poor electrospray ionization efficiency and deliver signature ions (in MS/MS detection).[26,27] Chiral stationary phases, the workhorses for direct HPLC enantiomer separation, have often remarkable enantioselectivity, but suffer from limited chemoselectivity and lower efficiencies (compared to highly efficient RP congeners).[28,29] Hence, the combination of the two principles is quite obvious and should lead to an enhanced separation technology platform.

With the rise of commercial two-dimensional (2D) instrumentation, its use has gained popularity, despite the complex and tedious method development.[30-35] 2D-LC with an achiral first dimension (^{1}D) can resolve problems of 1D-LC such as limited (achiral) chemoselectivity in complex samples, interferences and matrix effects, while the second dimension (^{2}D) is enantioselective, or vice versa.[30] Eluent fractions are transferred from the ^{1}D, in a targeted (e.g. by time-based

1

sampling) or untargeted manner (e.g. peak-based sampling or full comprehensive approach), to the ²D, whereby orthogonality between both dimensions is of paramount importance.[36, 37] One distinct mode of operation is multiple heart-cutting (mLC-LC), in which specific peaks of interest are transferred from the ¹D to the ²D (representing typically a targeted approach).[36, 37] Such targeted 2D-LC methods (achiral-chiral) have been applied for AA analysis, but were most frequently limited to a subset of AAs only.[18, 19, 38, 39] The main advantage is the relaxed constraint in terms of speed posed on the second dimension, since storage loops for the isolated fractions can be employed decoupling ¹D sampling from ²D run time.[39] The common consideration is that chiral separations possess slow kinetics, lead to loss of resolution at high flow velocities, and require long re-equilibration times if gradient elution is employed, which disqualifies them for ²D separation. However, very fast chiral separations have been demonstrated employing superficially porous particles and sub 2-µm fully porous particles.[23 40-46 47-49] Their integration in a multiple heart cutting 2D-LC setup finally enabled the targeted enantioselective analysis of all 20 proteinogenic amino acids in a single run within 120 min[39] and 45 min.[38] Such targeted analysis requires prior knowledge of the targets or preliminary information from an independent prior analysis. More appealing appears to be an untargeted assay, which provides comprehensive information from single injection and without prior knowledge or analysis. This can be accomplished by comprehensive 2D-LC (LC×LC), another mode of operation, in which the entire effluent from the ¹D is sampled and transferred to the ²D. In online LC×LC very fast ²D separations are required (typically less than 60 s to avoid excessive undersampling), since the sampling time is directly linked (and is equal) to the ²D cycle time. This major constraint is the reason why only few examples of LC×LC with fast chiral separations in the ²D exist.[22, 43] In one study, chiral×achiral 2D-LC with the chiral separation of *N*-derivatized amino acids in the ¹D and fast achiral separation by RPLC in the ²D was suggested for eAAA in honey samples.[17]

The goal of the present study is to establish the first comprehensive LC×LC method with data-independent SWATH MS/MS detection and demonstrate its applicability for untargeted analysis of peptide-derived AQC derivatized AAs. The idea is to enhance assay specificity on both the chromatographic level, through comprehensive LC×LC, and also on the MS level, through SWATH acquisition. SWATH-MS provides comprehensive MS¹ and MS² data, yielding quantifiable signals not only for precursor ions (like it is common for state-of the-art LC×LC methods published so far that were based on data-dependent acquisition), but also for fragment ions through a series of consecutive MS² spectra recorded via intermediate-sized (herein 20 *m/z* units wide) precursor isolation windows. By this novel LC×LC-SWATH-MS approach a truly comprehensive untargeted analysis becomes feasible for the first time. The achiral RPLC separation in the ¹D of the LC×LC approach allows for pre-separation of amino acids, in particular of interest for isobaric amino acids like Thr/aThr/Hse and Leu/Ile/aIle/Tle/Nle, and also of matrix components such as reagent peaks. It avoids interferences in the ²D in which the chiral column accomplishes their enantiomer separation. The chromatographic challenge that needed to be solved was to achieve sub-minute enantiomer separations in the

²D for both primary and secondary amino acids, which was addressed by a tandem column setup with a core-shell *tert*-butyl quinine carbamate based chiral stationary phase (QN-AX) followed by a core-shell zwitterionic quinine type stationary phase (ZWIX(+)).[14, 47, 48, 50] In fact, this is the first enantioselective LC×LC assay in which sub-1 min ²D enantiomer separations has been accomplished. In general, previous untargeted LC×LC-MS assays were based on data-dependent acquisition which do not allow the generation of MS² chromatograms and their corresponding 2D-contour plots, respectively. The here described novel approach combines LC×LC with DIA by SWATH significantly enhances the flexibility in untargeted analysis of samples by 2D-LC. It should also lead to an advanced power of 2D-LC when applied to other types of samples, e.g. peptides, where substructure filtering is of interest, e.g. of conjugates or a certain structural impurity pattern. The applicability and potential of the developed LC×LC setup with SWATH-MS is demonstrated herein by the amino acid configuration determination of the non-ribosomal therapeutic peptide aureobasidin (**Figure 1A**) and the synthetic therapeutic peptide octreotide (**Figure 1B**) both containing uncommon AAs. The prime focus lies on qualitative analysis for the determination of the amino acid composition of peptides with regard to D- and L-enantiomers. The potential of quantitative analysis using the developed method is evaluated as well, with the goal to elucidate whether accuracy is adequate to derive information on amino acid stoichiometry in a peptide hydrolysate simultaneously with untargeted qualitative profiling. To keep the entire analysis time somehow acceptable, the ¹D run time, which is essentially equal to the total run time, was restricted to 60 min.

EXPERIMENTAL SECTION

Chemicals and Reagents. Aureobasidin (**Figure 1A**) and octreotide (**Figure 1B**) were supplied by AvaChem Scientific (San Antonio, TX, USA) and BOC Sciences (Shirley, NY, USA), respectively. Acetonitrile, methanol and formic acid (FA) purchased from Carl Roth (Karlsruhe, Germany) were of ultra-LC–MS grade quality. All amino acids (AAs) (**Table S1**), ammonium formate (NH₄FA), hydrochloric acid (HCl), dithiothreitol (DTT), deuterium oxide, deuterium chloride, boric acid, sodium hydroxide, iodoacetamide (IAA) were provided by Sigma Aldrich (Schnelldorf, Germany). A solution of uniformly labelled [U-¹³C¹⁵N] L-amino acid metabolomics standard mix (2.5 mM in 0.1 M HCl), which contained 17 (without Gln, Asn and Trp) amino acids as well as an all labelled proteinogenic amino acid mix was acquired from Eurisotop GmbH (Saarbrücken, Germany) and was used as an internal standard. Single L- or DL-amino acid stock solutions (50 mM in 0.1 M HCl) were used to prepare 2.5 mM stock solutions for each amino acid. All amino acid standard solutions were stored at −20 °C prior to use. Water was purified using a Water Purelab Analytics Purification System from ELGA (Celle, Germany). 6-Aminoquinolyl-*N*-hydroxysuccinimidyl carbamate (AQC, AccQ) was purchased from Synchem (Felsberg/Altenburg, Germany). Derivatization reactions were performed in 1.5 mL Crystal Clear microcentrifuge tubes from Starlab (Hamburg, Germany) using a Thermo-Shaker PHMT Grant-bio from Grant Instruments Ltd. (Shepreth, England). The procedures of sample preparation and pre-column

2

derivatization, respectively, are described in detail in the **Supporting Information**.

An ACQUITY BEH C18 (150 x 1.0 mm, 1.7 μm) column from Waters (Eschborn, Germany) was used for the ^{1}D achiral chromatographic separation and a chiral QNAX-ZWIX(+) tandem column setup consisting of an experimental prototype of a superficially porous particle (SPP) QN-AX (50 x 3.0 mm, 2.7 μm, 160 Å) column[47] coupled to an experimental prototype SPP ZWIX(+) (50 x 3.0 mm, 2.7 μm, 160 Å) column[48] using a short stainless-steel capillary (0.12 mm ID, 75 mm) for the ^{2}D.

Instrumentation. An Agilent 1290 Infinity II 2D-LC Solution from Agilent Technologies (Waldbronn, Germany) was used for full comprehensive 2D-LC. The ^{1}D LC consisted of a quaternary low pressure gradient UHPLC pump (flexible pump, G7104A), a multisampler (G7167B), a multicolumn thermostat (G7116B), a diode array detector (DAD, G7117B) with 1 μL flow cell (#G4212-60008) and a pressure release kit (G4236-60010) between UV-detector and 2D-interface. The ^{2}D comprised a binary high-pressure gradient UHPLC pump (High Speed Pump, G7120A), a valve drive (G1170A) with a 2-pos/4-port duo valve (5067-4244) equipped with two 60 μL loops (operated in countercurrent fill/analyze mode) and a multicolumn thermostat (G7116B). The ^{2}F was directed through a DuoSpray™ Ion Source to a TripleTOF 5600+ QTOF mass spectrometer from Sciex (Concord, Ontario, Canada) using a contact closure connection for peripheral devices. The data acquisition rate was set to 10 Hz in the ^{1}D for the ^{1}DAD. These instrumental components were assembled into an LC×LC instrumental setup without flow splitting as depicted in **Figure S1**. Dwell volumes were determined using a zero dead volume union connector in place of the column. The measured dwell volumes were 550 μL in the ^{1}D and 120 μL in the ^{2}D at a flow rate of 0.20 mL/min. The 2D-chromatographic data were processed with OpenLab Data Analysis (Build 2.204.0.661) from Agilent Technologies (Waldbronn, Germany) and LC Image™ Version 2.9r3 LC×LC-HRMS (GC Image, LLC, Nebraska).

QTOF-MS measurements were performed using a Duospray ion source operated in positive electrospray ionization mode. The following MS instrument parameters were used: curtain gas (CUR) 40 psi, ion source gas (nebulizing gas; GS1) 60 psi, heater gas (drying gas; GS2) 60 psi, ion spray voltage floating (ISVF) 5500 V, source temperature (TEM) 550 °C and declustering potential (DP) 100 V. Data acquisition was performed in data independent acquisition (DIA) with SWATH (Sequential Window Acquisition of all Theoretical fragment-ion spectra) in high sensitivity mode, covering the precursor ions of all single and double derivatized amino acid compounds (**Table S1**). The SWATH design is shown in **Table S5**. The mass range of the TOF-MS full scan comprised m/z 100-2000 with an accumulation time of 50 ms and a collision energy (CE) of 10 V. MS/MS in SWATH was performed with 40 V CE, 15 V CE spread (CES) and an accumulation time of 12.5 ms. Mass calibration was conducted with a calibrant delivery system (Sciex, Darmstadt, Germany) through the APCI inlet using the positive calibration solution for the SCIEX X500 System. Data acquisition was performed with Analyst TF 1.7 (Sciex) and analysis with PeakView (Sciex), Skyline (Version 21.1.0.278)

and LC Image. Chromatographic conditions are specified in the respective figure captions.

Data Analysis with LC-Image. For data analysis with LC Image, the raw .wiff files were imported and a selected ion chromatogram (SIC) view of all targets was saved as a .cgf file for all runs. Then an exemplary run was used to create a configuration file (.cfg) with the following settings CLIC (computer language to identify chemicals) filter settings: (Area $\geq$ 15.0) & (Volume $\geq$ 0) & ((Peak_II $\geq$ 15.0) & (Peak_II $\leq$ 51.25)) & (SNR $\geq$ 8.02)) for blob detection. Then, a template file (.bt) was further created for the proteinogenic AQC derivatized AAs containing their m/z as quantifier ions. The LC-Image project software was used to batch process all SIC images (.cgf) by automatically applying the .cfg and .bt for matching the detected blobs against the template and saving the results as .gci files ready for reviewing and editing (**Table S6**).

RESULTS AND DISCUSSION

Preoptimization of ^{1}D and ^{2}D. The development of ^{1}D and ^{2}D separations started on the basis of a previously published multiple heart cutting 2D-LC enantiomer separation method.[38] The first RP separation dimension was optimized regarding repeatability and selectivity to achieve a precision with RSD of <0.5 % for the analysis of 25 AAs and the separation of critical peak pairs of the isomers Leu, Ile, aIle, Tle, Nle, and Thr, aThr, Hse, respectively. ^{1}D Column selection turned out to be critical as not every RP stationary phase showed sufficient selectivity between AQC-labelled Ile and aIle. An Acquity BEH C18 (150 x 1 mm, 1.7 μm) was finally selected (**Figure 2A**). As can be seen, the most critical peak pair Ile/aIle is close to baseline separation. The other isobaric leucines, Tle, Leu, and Nle, were fully baseline resolved from the Ile/aIle peaks and each other. The ^{1}D RP separation in **Figure 2A** further documents a good run-to-run repeatability (mean RSDs < 0.21%; n=8) and with this a robust separation, which is of particular importance if a full enantioselective amino acid analysis with calibrants, quality controls, and study samples must be performed in an extended analytical batch.

According to the concept of Giddings on sample dimensionality, the entirety of the AQC-labelled amino acids clearly differ in two properties, their lipophilicity and stereochemistry. The first one was addressed herein in the ^{1}D RP separation as discussed above, and the second one in a ^{2}D enantiomer separation. It could be clearly demonstrated in our recent work that a wide-pore 160 Å core-shell particle CSP was favourable for fast separations compared to both corresponding narrow pore (90 Å) core-shell CSP and wide- and narrow-pore sub-2 μm FPP CSPs, because it could achieve the enantiomer separations with equal efficiency at higher speed.[47, 48] The mass-transfer resistance term (C-term) was lower on wide-pore SPP CSPs and comparable to sub-2μm FPP CSPs. Resultant flat H/u curves were advantageous for fast sub-minute enantiomer separations. AQC-tagged amino acids with mostly net acidic character were resolved on a core-shell QN-AX anion-exchanger CSP[16] under isocratic conditions (**Figure S2**). Two major problems were observed: i) The amino acids with basic side chain, Arg and His (note, Lys was doubly labelled and hence lost its basic side chain character), were not resolved into enantiomers due to repulsive electrostatic interactions of the

3

cationic side chains with the cationic anion-exchanger site leading to insufficient retention and enantioselectivity. ii) The acidic amino acid Asp carries two carboxylate groups and is strongly retained.
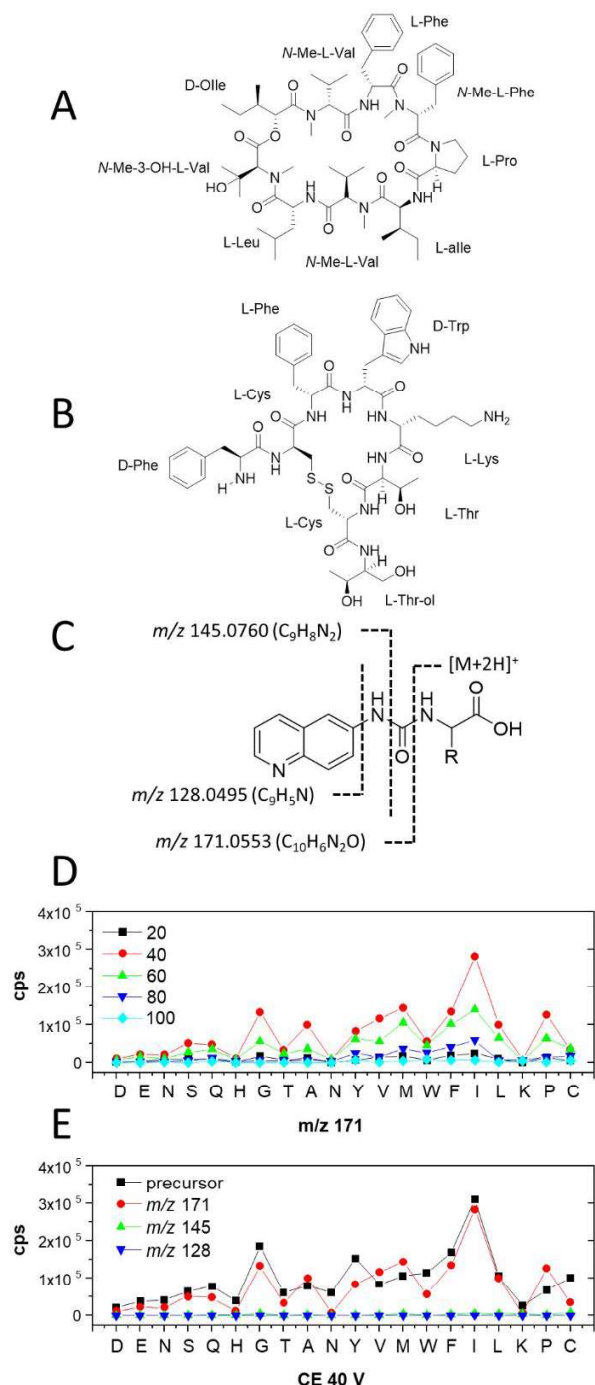

Figure 1. Chemical structure of **A**: Aureobasidin A and **B**: Octreotide. **C**: AQC derivatized AA fragmentation pattern producing signature ions in positive mode. **D:** Intensity of signature ion $C_{10}H_6N_2O$ (*m/z* 171.055) at different CE settings for all proteinogenic AAs. **E:** Comparison of signature ion intensities in MS^2 at CE: 40 V.

For this reason, it could not be eluted within 1 min, but took 3 min. This would lead to a wrap around (which however would not be extremely problematic). Nevertheless, in the final untargeted RP×chiral 2D-LC method, a gradient elution enantiomer separation method with a unified gradient throughout the ^{2}D separations of the 2D-LC run was developed utilizing a DoE approach as described in detail in the Supporting Information (chapter 5.1). This method, which was based on a tandem column of core-shell QNAX-ZWIX(+) (both 5 cm long with 3 mm ID, 2.7 μm, 160 Å), enabled the acquisition of a full enantioselective amino acid profile within 1 min by a one-dimensional UHPLC method, if there was no need to distinguish between isobaric Leu/Ile/aIle and Thr/aThr (**Figure 2B**). For these isobaric amino acids, the opposite (D and L) enantiomers were fully baseline separated, yet the constitutional isomers with the same configuration at the α-amino group coeluted in a pack. Their complete resolution was accomplished by the 2D-LC setup through combination of the orthogonal selectivity of the two dimensions. As an elegant solution a buffer (salt) gradient for the ^{2}D including full re-equilibration was employed. This optimized ^{2}D method was found to be superior, due to the ion exchange properties of the CSPs. Hereby, formate acts as the counter ion on the quinuclidinium WAX site of the CSPs whereas ammonium as the counter ion on the SCX site of ZWIX(+).

From a fundamental viewpoint, there were some discrepancies regarding ion concentrations in the two distinct ion exchange columns in this complex ion exchange gradient mode, e.g. the initial buffer concentrations that arrived at the second column once analytes had entered ought not to be the same as the initial concentration of buffer in the first column (when the 2D run began). However, the optimization was based on a phenomenological approach using a DoE (as reported in suppl. Table S2) and was mainly focused on getting the enantiomer separations of all AAs done within 1 min with baseline resolution. In this tandem column, the QNAX column could separate all AQC amino acid enantiomers except for Arg and His. Arg and His were the two amino acids, which were due to the additional SCX interaction strongest retained on the ZWIX(+) column and their enantiomers were also well resolved. Owing to the SCX moiety and its intramolecular counterion effect, all other AQC amino acids eluted with t_0 on the ZWIX(+) column. Thus their enantiomer separation achieved on QNAX was not at all negatively affected by the ZWIX(+) column. This way all amino acids could be resolved by the tandem column approach.

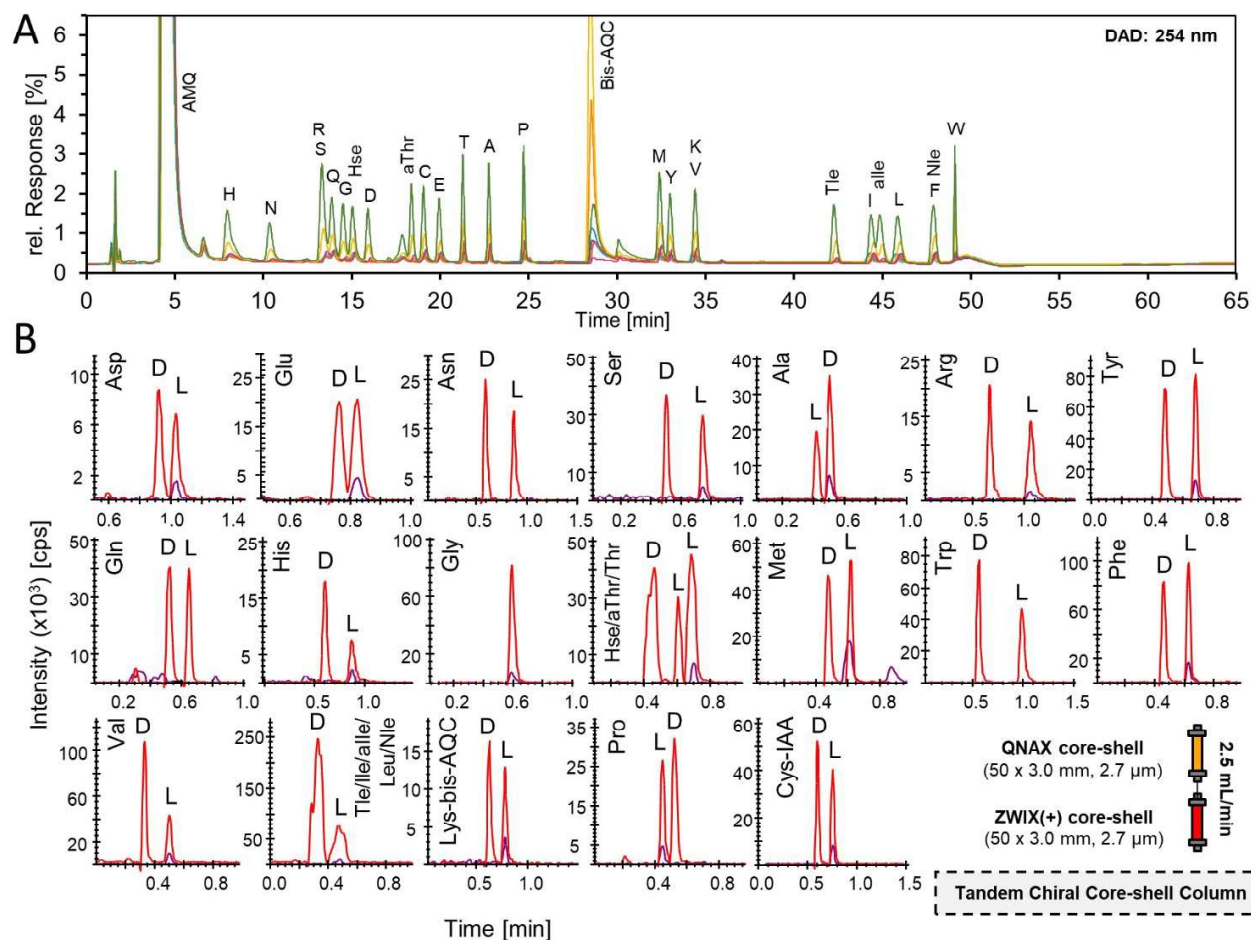The implementation of ^{1}D RPLC and ^{2}D chiral LC in an LC×LC approach is described in the following section.

4

Figure 2. Optimized [1]D (**A**) and [2]D (**B**) LC separations of AQC-derivatized amino acids. **A:** [1]D DAD chromatogram of 7 consecutive runs of 25 DL-AAs (proteinogenic plus aThr, Hse, Tle, Nle and aIle) with varying sample concentration (0.01, 0.05, 0.1, 0.5, 1, 5 and 10 pmol on column injection). Column: BEH-C18 (1 x 150 mm, 1.7 μm); MP-A: 0.05% FA + 1% MeOH in water; MP-B: 0.05% FA in ACN; Gradient: 0 min (0% B) – 9.33 min (2.5% B) – 17.5 min (9% B) – 23.33 min (9% B) –29.17 min (13% B) –40.83 min (13 %B) – 44.33 min (25% B) – 45.50 min (50% B) – 46.67 min (50% B) – 47.83 min (0% B, 150 μL/min) – 58.33 min (0% B, 150 μL/min) – 59.50 min (13% B) – 60 min (13% B). F: 0.06 mL/min; T: 50 °C, Inj. vol.: 1 μL. **B:** Extracted ion chromatograms (EICs) from the 1D-LC separation of 25 DL-AAs (red trace) and 17 L-[U-[13]C[15]N]-AA (purple trace) under optimized conditions. Column (tandem): QNAX core-shell (3.0 x 50 mm, 2.7 μm, 160 Å)- ZWIX(+) core-shell (3.0 x 50 mm, 2.7 μm, 160 Å); MP-A1: 10 mM NH4FA + 10 mM FA + 0.5% H2O in MeOH; MP-B1: 50 mM NH4FA + 50 mM FA + 0.5% H2O in MeOH, Gradient (DoE Exp. N9, Table S3): 0 min (0% B) – 0.2 min (0% B) – 0.5 min (100% B) – 1.5 min (100% B) – 1.6 min (0% B) – 5 min (0% B), F: 2.5 mL/min; T: 50 °C. The final LC×LC 2D Gradient without initial hold was: 0 min (0% B) – 0.35 min (100% B) – 0.83 min (100% B) – 0.85 min (0% B) – 1 min (0% B), F: 2.5 mL/min; T: 50 °C (note, the U-^{13}C,[15]N-IS mix (from Eurisotop) used for method development (Fig. 2B) contained only 17 AAs: The labile AAs Trp, Asn, Gln were missing; [2]D chromatogram of Hse/aThr/Thr in Fig. 2B, peak 1 contains all coeluted D-forms, and peak 2 (Hse) and 3 (Thr and aThr) all L-forms).

Establishing the final LC×LC method. For the final setup (**Figure S1**), a sub2 micron [1]D column (ACQUITY BEH C18, 150 x 1.0 mm, 1.7 μm) was used to reduce the [1]F (60 μL/min) and achieve selectivity and resolution between Ile and aIle. This was accomplished with low organic (1% MeOH) in channel A of the mobile phase and a shallow acetonitrile gradient (in B). Both contained 0.05% (v/v) formic acid, which corresponds to a molar concentration of around 13 mM. Considering that

formic acid represents a counterion at the anion-exchange site of the QNAX and ZWIX(+) columns, it is important to note that this ionic strength in the [1]D eluent roughly corresponds to the weak starting conditions of the [2]D gradient. In other words, the [1]D eluent was well compatible with the [2]D mobile phase and no breakthrough was observed in spite of a large transfer volume ([2]V$_{inj}$ = 60 μL). It corresponds to a transfer volume of around 30% and 15% of the [2]D total pore volume related to the first

5

core-shell column only ($\varepsilon_T = 0.559$ in both) and total tandem column, respectively. Due to the gradient elution ion-exchange process (from low to high counterion concentration), efficient refocusing could be accomplished. [1]D chromatograms remained reproducible under these conditions (**Figure 2A**). A sampling loop volume of 60 µL for both loops was selected to match the [1]F and [2]cycle time (60 s). While this 100% loop fill is suboptimal, it was an acceptable compromise as it was not possible to get faster [2]D separations without significant loss in resolution. The [2]F was already increased to 2.5 mL/min according to DoE results and directed entirely to the MS. A buffer gradient from 10 mM to 50 mM ammonium formate (with formate representing the counterion at the quinine anion-exchange site of QN-AX and ZWIX and the ammonium ion being the counterion at the SCX site of the ZWIX phase) was selected for elution in the [2]D. This ensured sufficient retention of early eluted AQC-amino acids (in spite of a large transfer volume) and fast elution of the strongly retained AQC-amino acids. The final optimized conditions for the separation of all AAs in the [2]D were thus: t_G: 20 s (without initial hold), followed by a 35 s hold time, F: 2.5 mL/min, T: 50 °C, re-equilibration: 5 s, cycle time: 60 s (**Figure 2B**). In spite of an unusually high flow rate (2.5 mL/min), the ESI process was robust due to the efficient Turbo-Ion-Spray source and the high volatility of the [2]D mobile phase (composed of MeOH with 1% water and 10 – 50 mM NH_4FA buffer).

Establishing the MS/MS method. For fast 2D-LC it was necessary to establish an MS/MS method, in which the data acquisition rate matched the speed of the [2]D (peak widths ~ 4s). Thus, in order to accommodate 10 data points per peak, the maximum MS cycle time was set to 400 ms. For truly untargeted analysis, SWATH-MS was preferred as a data independent acquisition method, which availed chromatogram extraction at both MS[1] and MS[2] level. The accumulation time was set to 50 ms for the MS[1] scan and 12.5 ms for each consecutive MS[2] experiment (24 in total per MS cycle).

Since all amino acids were derivatized with AQC, reagent specific signature fragments (**Figure 1C**) were extracted on MS[2] level to indicate the presence of unknown AQC derivatized amino acids.[51] Thus, the collision energy was optimized for the dominant qualifier AQC fragment $C_{10}H_6N_2O$ (*m/z* 171.055), with the aim to maximize its intensity. As shown in **Figure 1D**, the maximum was achieved at 40 V CE, while the intensities of other AQC specific fragments remained less abundant at various CE settings regarding their intensity (**Figure 1E and S11**). No dominating fragments were observed in negative mode (CE: -40 V). As shown in **Figure 1E**, at CE of 40 V also the precursor ion was reasonably well detected in the corresponding SWATH windows which facilitated the establishment of the precursor-fragment link which was lost in DIA.

Elucidation of AA Stereoconfiguration in Peptides. The elucidation of the absolute configurations of amino acid building blocks was performed on peptide hydrolysates of Aureobasidin A and Octreotide (**Figure 1A and 1B**) utilizing the developed enantioselective LC×LC method.

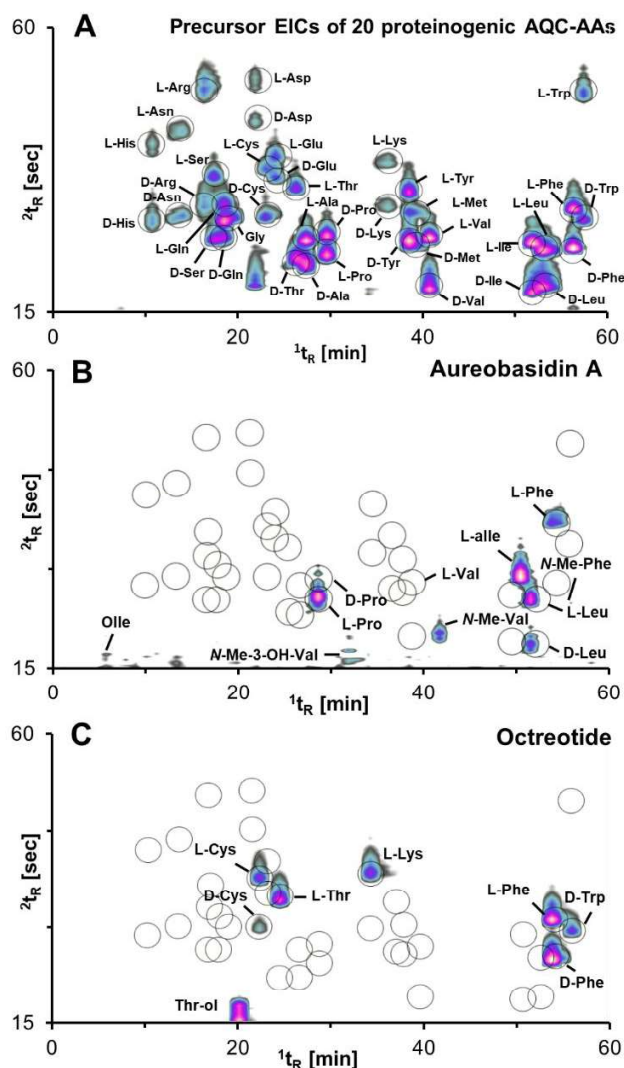**Figure 3**. Overlay of MS[1] EICs of an LC×LC analysis of **A)** all proteinogenic AAs (standard mix), **B)** aureobasidin A and **C)** octreotide peptide hydrolysate on a tandem column by 2D-LC-SWATH-MS, separated according to the conditions stated in Figure 2A (ACQUITY BEH C18, 150 x 1.0 mm, 1.7 µm) and Figure 2B (core-shell tandem column of QN-AX and ZWIX(+), 50 x 3 mm, 2.7 µm, 160 Å), for the [1]D and [2]D, respectively. Note, except for isomeric amino acids all amino acids were also separated in z-dimension, i.e. by their distinct m/z in MS[1]. Note, circles indicate spots of elution of targets (i.e. proteinogenic amino acids) present in the data processing template.

The general strategy to analyze the LC×LC-SWATH-MS data to identify AQC-derivatized amino acids is simple and straightforward (**Figure S12**). First, all expected amino acids are extracted from MS[1] in conjunction with a template matching using a 2D library (*m/z*, [1]RT and [2]RT) for known targets (**Figure S12A-B**), e.g. the 20 proteinogenic amino acids (**Figure 3A**). In order to detect unknown AQC-derivatized species, the AQC signature fragment *m/z* = 171.055 is extracted on MS[2] level in all SWATH windows (**Figure S12C**). When a new peak is found, the MS[1] spectra of the respective SWATH window at the

6

specific x,y-coordinate is inspected for the particular precursor ion by extracting the corresponding 2D chromatogram (**Figure S12D**). The overlap of spots from the signature fragment (MS^2) and precursors (MS^1) confirm the correct assignment of precursor to fragments. Lastly, the ion is once again matched to the library to rule out e.g. IS (U-^{13}C^{15}N-labelled) ions that may be found in the same or a different SWATH window; then it is identified and added to the library (**Figure S12E**). The strategy was applied to the peptide hydrolysate of Aureobasidin A and depicted for the exemplary AAs Phe, Pro and Leu/Ile (see 2D-MS^1-EICs and 2D-MS^2-EICs in **Figure 4**).

Aureobasidin A is a natural cyclic depsipeptide with antifungal activity, that contains a number of proteinogenic amino acids (L-Leu, L-Pro, and L-Phe) as well as special amino and hydroxy acids (*allo*-Isoleucine, *N*-methyl-L-valine, *N*-methyl-L-phenylalanine, 2-(*R*)-hydroxy-3-(*R*)-methylpentanoic acid (D-OIle) and β-hydroxy-*N*-methyl-L-valine).[52, 53] The results indeed revealed the presence of L-aIle, L-Leu, L-Pro, and L-Phe which could be matched with the 20-AA 2D template (**Figure 3B**). Although slight undersampling occurs, the resolution of Leu and aIle in the ^{1}D guaranties their identification (**Figure S13**). D-Leu, L-Val and D-Pro were found as peptide impurities by the template. By virtue of full comprehensive 2D-LC the uncommon amino acids *N*-Me-Phe, *N*-Me-3-OH-Val, *N*-Me-Val could be analyzed enantioselectively without prior run or prior information in the template through their detection in the ^{1}D and confirmation by

their 2D EICs (on MS^1 and MS^2 level) as well as the co-eluting signature fragment from the respective SWATH window (**Figure S14-15**). The stereoconfiguration of *N*-Me-Phe and *N*-Me-Val can be derived according to the elution times of DL-Phe/Val applying analogy considerations. The *N*-methyl substituent adds a slight retention increment in ^{1}D RPLC and as secondary amino acids, their enantiomer elution order is reversed (like for Pro) in the ^{2}D. Such tentative assignments must, however, be verified by independent experiments. Standards would be required for confirmation, especially for uncommon AAs with significant retention time shifts (e.g. *N*-Me-3-OH-Val or Thr-ol in **Figure 3C**) from their proteinogenic counterpart. One possibility to generate both enantiomers from an uncommon amino acid of natural origin of which no standards are available, is to take an aliquot of the sample, derivatize it with AQC and racemize it, as described by Horak et al..[15, 54] This gives at least rise to the retention times of the two corresponding enantiomers with tentative enantiomer elution orders (D<L for primary amino acids and L<D for secondary amino acids in the ^{2}D chiral QNAX-ZWIX(+) tandem column). Moreover, it was striking that the secondary amino acids (*N*-Me-Phe and *N*-Me-Val) showed significantly lower signals (Fig. 3B), which could be due to a slower derivatization kinetics or lower ionization efficiency (reduced fragmentation efficiency in MS^2).
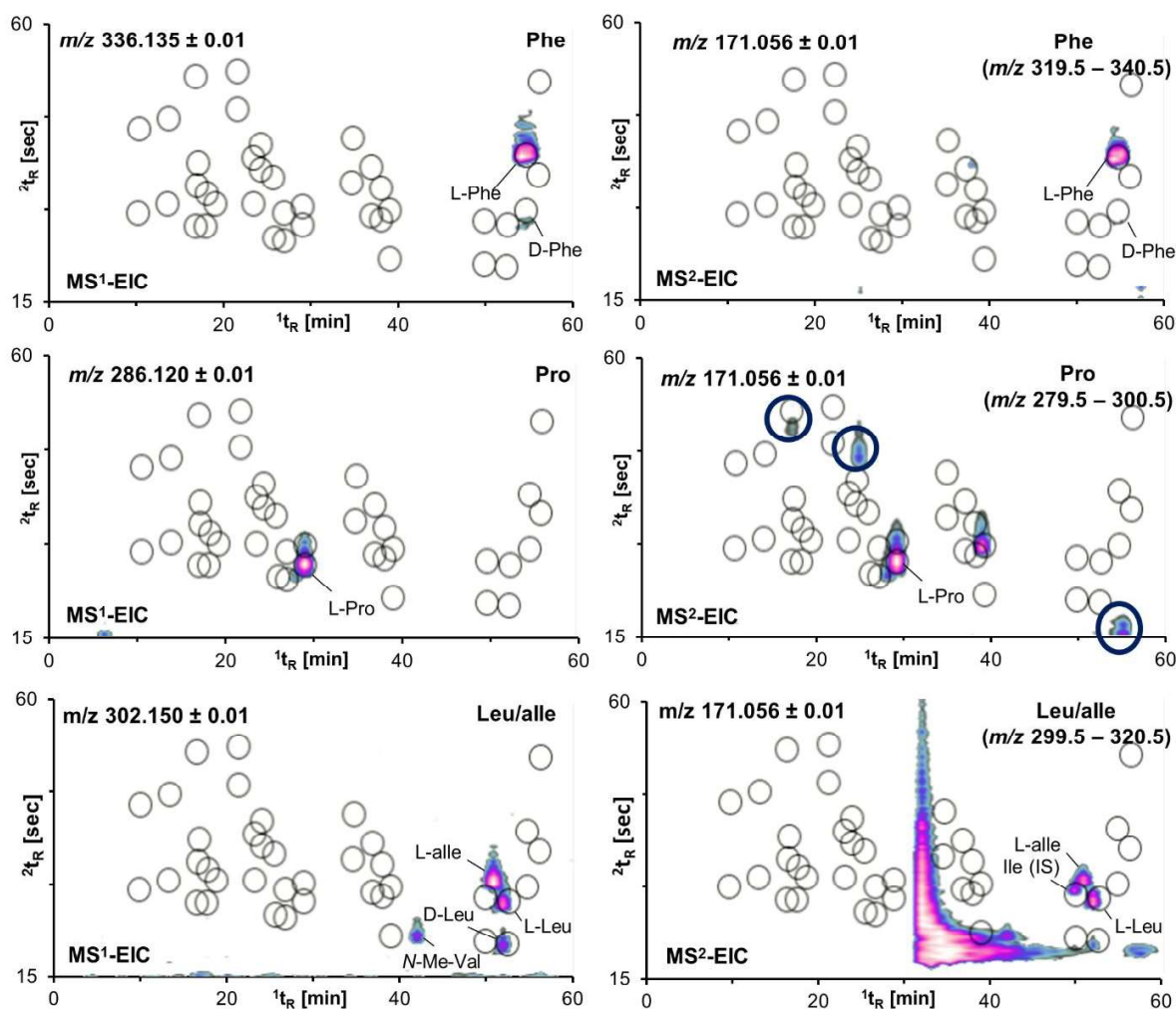
7

Figure 4. Exemplary 2D-chromatograms extracted from MS[1] (left panel) and MS[2] data (right panel) illustrating comprehensiveness on the LC and MS dimensions. EIC contour plots of the respective AQC-AA (MS[1]) expected in Aureobasidin A and the signature fragment m/z 171 from the respective AQC-AA SWATH window (MS[2]) are shown. Unknown peaks found by the peak finding strategy are circled in bold blue. Black circles indicate targeted AAs from the template. MS[2] SWATH (i.e. precursor isolation) window information is given in the 2D contour plots in the top right corner. The strongly tailing peak in the SWATH window of m/z 299.5 – 320.5 corresponds to the AQC reagent peak (N,N'-bis-quinolyl-urea; ideally the reagent excess is quenched by another compound that elutes with t_0 or after all the relevant AAs to avoid interferences).

The elution order of the N-methylated AAs was L < D, as expected for secondary amino acids, and was observed for N-Me-Phe which was slightly stronger retained than D-Phe in the [1]D but eluted slightly earlier in the [2]D (**Figure 3B** and **Figure S14**) as well as for N-Me-L-Val which closely eluted to D-Val (**Figure 3B** and **Figure S15**). As D-OIle did not contain an N-terminus it did not feature the signature fragment for AQC-derivatization and was therefore not detected in the MS[2] contour plot for the fragment ion with m/z 171.055 (however, there was a small spot in the MS[1] contour plot corresponding to free OIle although this hydroxy carboxylic acid was more sensitively detected in negative mode; its stereoisomer separation required different conditions as shown recently[55]). Unknown or non-targeted AQC derivatized species and AA

impurities found by the signature fragment were discovered using the above-mentioned strategy (**Figure 4** and **Figure S16-17**). All identified AAs are summarized as overlay of their MS[1] EICs in the 2D contour plot shown in **Figure 3B**.

Likewise, an octreotide (**Figure 1B**) hydrolysate containing only proteinogenic AAs, except for Thr-ol (Threoninol) was analyzed. All expected amino acids were detected successfully on MS[1] and MS[2] level (**Figure S18-19**) and unknown impurities could be revealed by the signature fragment (**Figure S20**). For this example, the signature ion was extracted in all SWATH windows (**Figure S21-23**). The first two windows largely reveal low molecular AQC reagent derivatives eluting at around [2]t_0 (0.15 min), but also covered low molecular in-source fragments, e.g. from Lys-bis-AQC matching the

8

template coordinates. Ions covered by the edges of two SWATH windows (e.g. L-Ser (IS), m/z 280.1) were detected by virtue of the overlapping window design in both (**Figure S21**). Other impurities such as *m/z* 317.2, *m/z* 379.1, *m/z* 391.1 and *m/z* 407.1 should be elucidated further, either by the 2D retention time deconvoluted MS[2] spectra (**Figure S24**) or a targeted MS/MS method, which was however out of the scope of this work. All identified AAs are summarized by an overlay of MS[1] EICs in form of a 2D contour plot in **Figure 3C**.

Quantification. The primary application focus of the established method was qualitative analysis for the determination of the configurations of amino acids in hydrolysates of natural and synthetic peptides (*vide supra*). In an attempt to combine untargeted qualitative AA profiling simultaneously with quantification for the determination of the stoichiometry of amino acids in peptides, we herein elucidated the quantification performance of the present LC×LC-MS/MS assay. In order to evaluate the quantitation ability of the established LC×LC method using blob (peak volume) detection (see suppl. Fig S25 and Table S6), a dilution series (0.01 – 10 pmol on column) of a 20 proteinogenic AA mix was measured for calibration. Three features (^1t_R, ^2t_R and *m/z* in MS[1]) were used to create a template of the AA mix to match against all consecutive runs by automated batch processing, which included baseline correction and blob detection. In most cases the blobs were distinguished properly. Detection errors (e.g. one blob quantifying two ions) resulting from unresolved peaks or co-elutions were corrected by peak deconvolution/unmixing (e.g. D-Glu and L-Thr) based on *m/z* (multi-channel data) or split/merge for D-Leu and D-Ile based on their partial separation. The latter could result in a slight bias, since it relied on a manual split/merge editing due to the absence of distinct mass spectra. The resulting blob table containing the quantifier (precursor) ion peak volume (PV) and peak height (PH), respectively, and the signal-to-noise ratio (SNR of local maximum peak to calculate the noise), was used as the raw input file for further analysis.

As mentioned above, SWATH-MS offers the possibility of using MS[2]-signals for quantification. However, assay specificity needs to be carefully assessed due to the intermediate-wide precursor isolation windows with co-fragmentation of precursors with similar *m/z* if there is coelution. Since herein a non-specific fragment (*m/z* 171.055 or 145.076) would be selected as MS[2] quantifier, assay specificity problems may arise in some instances, e.g. due to ^{13}C-labelled ISs. Some of the ^{13}C-labelled ISs are co-fragmented in the same SWATH window as their ^{12}C-analogues. Since both afford the same fragments, this strategy cannot be used herein for quantification. Therefore, quantification was performed on the MS[1] level in this study. In some instances, the ^{13}C-labelled IS was fragmented in a different SWATH window so that no assay specificity problems would arise.

Quantification (including calibration and validation) was performed for all proteinogenic AAs. In a single analytical batch, calibrants (7 levels), quality controls and samples (peptide hydrolysates) were injected and analyzed by the developed LC×LC-SWATH-MS method. The entire sequence ran unattended continuously over 3 days without interruption in spite of the high ^{2}D flow rate of 2.5 mL/min, which appears stressful for the ESI source. The calibration functions (based on MS[1]-EICs) and the validation data are summarized in **Table S7**. The calibration curves (without IS) generally showed mostly

satisfactory values for linear response function evaluation (R^2 >0.91) and LOQs in the range between 0.02 and 0.33 pmol (S/N = 10) (for the PV method) (**Figure 5A**). The intra-batch accuracies (as % recovery) and precisions (as % RSD) are depicted for the PV method in Figure 5B and 5C, respectively. A comparison of these figures of merit between PV and PH is shown in suppl. Figure S27. It can be seen that PV is the preferred method. The majority of values were within the acceptable range < 15% RSD and 85-115%, however, several AAs were outside, especially instable AAs such as Met, Trp, Cys. In some instances, peak height provided better results (Arg with tailing, D-Ile/Leu due to incomplete resolution).

To evaluate the applicability of AA quantification by this LC×LC-MS/MS assay, the amino acid composition of oxytocin was determined using external calibration (without ISs). The results are summarized in suppl. Table S8. All AAs of oxytocin could be detected (Asn as Asp and Gln as Glu due to acidic hydrolysis of the peptide; low quantities of D-Cys were found owing to racemization). The sum of the pmol of AAs determined was divided by the number of (expected) amino acids in the peptide and afforded the pmol amount per AA. After dividing all determined AA quantities by this number and after converting to integer numbers, the correct AA composition was obtained. For the majority of the AAs the recovery was within acceptable range. However, 3 amino acids were slightly outside (Gly, Leu, Asp), yet still acceptable as a first estimate of the AA stoichiometry in a peptide and providing the correct integer i.e. AA stoichiometry. In general, this 2DLC method can provide a first assessment of concentration levels and AA stoichiometries in peptide hydrolysates, but further advancement of the method for improvement of accuracy and precision is recommended. This should be possible with the inclusion of ^{13}C-labeled IS (not included in this quantitative analysis). To avoid extensive calibration runs, future focus will be to incorporate internal calibration with ^{13}C-ISs for accurate quantification as suggested recently.[56] For accurate trace level enantiomeric impurity determination, the current method is not suitable yet.

However, the current work can be regarded as an intermediate step to a quantitative untargeted LC×LC-MS/MS platform method for the analysis of AQC-derivatized amino acids.
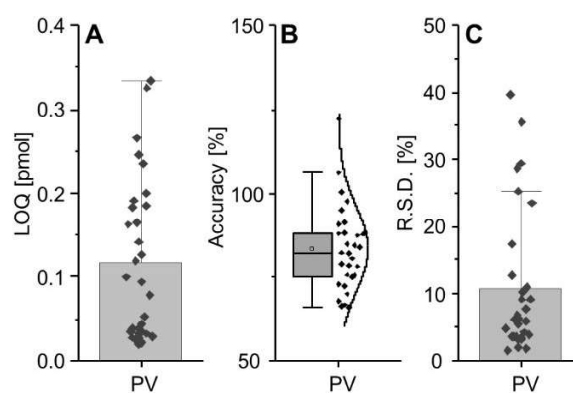

Figure 5. Summary of calibration and validation data (Table S7) for A) LOQ (S/N=10), B) accuracy (as % recovery) and C) precision (as % RSD) for all AAs (except instable ones) using peak volume (PV) as dependent variable and QC (5 pmol or 10 pmol depending on range).

CONCLUSIONS

An untargeted enantioselective LC×LC-ESI-QTOF-MS/MS amino acid analysis method with SWATH acquisition was established for the simultaneous enantioseparation of all proteinogenic amino acids, including the side chain isomeric analogues of Leu (aIle, Nle, Tle), and Thr (aThr, Hse) (in total 25 components), within a total runtime of 60 min (including re-equilibration).

The chemoselective [1]RPLC separation resolved the majority of amino acids from each other and from their isomeric analogs, while the [2]D achieved the enantioselective resolution of all species under gradient elution within a minute using core-shell technology for the short tandem column (both 50 x 3.0 mm) of QN-AX and ZWIX(+) chiral selectors. The [2]D elution order was determined by the use of an L-[U-[13]C[15]N]-AA internal standard mixture for all proteinogenic AAs. The pre-column derivatization with AQC, did not only introduce a chromophore and a fluorophore, but also an easily ionizable mass tag, which was sensitive and chemoselective, as it allowed the extraction of AQC-specific signature fragments in MS[2]. A peak finding strategy utilizing the most intense product ion (m/z 171.055) was used to identify AQC-derivatized amino acids in a two-dimensional space, along with a template to match a 2D library (m/z, [1]RT and [2]RT) containing known AQC-AA entries, was presented. This strategy was used to control the stereochemical integrity of therapeutic peptide hydrolysates of Octreotide and Aureobasidin A, resulting in 2D fingerprinting plots. The produced untargeted data was not only qualitative, but also quantitative on MS[1] and MS[2] level and ultimately open for retrospective targeted analysis. The capability for quantification was exemplified by an extended calibration and validation exercise, and application to AA composition determination of oxytocin.[57] In conclusion, the presented method combines comprehensive separation with comprehensive MS/MS detection and represents a new platform for untargeted profiling with new feasibilities including quantification. It should be further noted, that the [2]D separation could be used as a 1D-LC high throughput method for (1 min) enantioselective amino acid analysis, just losing the information for Leu/Ile/aIle which are analysed as their sum for both D and L-forms. This comprehensive analytical approach could serve as a model for other applications in the pharmaceutical analysis of new complex therapeutic modalities.

ASSOCIATED CONTENT

Supporting Information

The Supporting Information is available free of charge on the ACS Publications website.

Additional information on instrumental setups, detailed design of experiment and re-equilibration optimization for enantiomer separations, optimization of MS parameters and SWATH design, additional targeted and untargeted 2D-LC-MS/MS contour plots of Octreotide and Aureobasidin A as well as detailed results of validation (docx).

AUTHOR INFORMATION

Corresponding Author

* E-mail: michael.laemmerhofer@uni-tuebingen.de. Tel.: +49 7071 29 78793. Fax: +49 7071 29 4565.

Author Contributions

R.K., J.H. and M.L. conceptualized the method. R.K. performed all experiments and analyzed the data. The manuscript was written through contributions of all authors. / All authors have given approval to the final version of the manuscript.
Notes
The authors declare no competing financial interest.

REFERENCES

(1) Miyoshi, Y.; Hamase, K.; Tojo, Y.; Mita, M.; Konno, R.; Zaitsu, K. *J. Chromatogr. B* **2009**, *877* (24), 2506-2512.

(2) Masters, P. M.; Bada, J. L.; Samuel Zigler, J. *Nature* **1977**, *268* (5615), 71-73.

(3) Friedrich, M. G.; Hancock, S. E.; Raftery, M. J.; Truscott, R. J. W. *Acta Neuropathologica Communications* **2016**, *4* (1), 83.

(4) Lambeth, T. R.; Riggs, D. L.; Talbert, L. E.; Tang, J.; Coburn, E.; Kang, A. S.; Noll, J.; Augello, C.; Ford, B. D.; Julian, R. R. *ACS Central Science* **2019**, *5* (8), 1387-1395.

(5) D'Hondt, M.; Bracke, N.; Taevernier, L.; Gevaert, B.; Verbeke, F.; Wynendaele, E.; De Spiegeleer, B. *J. Pharm. Biomed. Anal.* **2014**, *101*, 2-30.

(6) Horak, J.; Lammerhofer, M. *J. Chromatogr. A* **2019**, *1596*, 69-78.

(7) Du, S.; Wang, Y.; Weatherly, C. A.; Holden, K.; Armstrong, D. W. *Anal. Bioanal. Chem.* **2018**, *410* (12), 2971-2979.

(8) Yoshikawa, K.; Furuno, M.; Tanaka, N.; Fukusaki, E. *J. Biosci. Bioeng.* **2020**, *130* (4), 437-442.

(9) Mast, D. H.; Liao, H.-W.; Romanova, E. V.; Sweedler, J. V. *Anal. Chem.* **2021**, *93* (15), 6205-6213.

(10) Mast, D. H.; Checco, J. W.; Sweedler, J. V. *BBA - Proteins and Proteomics* **2021**, *1869* (1), 140553.

(11) Calderón, C.; Lämmerhofer, M. *J. Pharm. Biomed. Anal.* **2022**, *207*, 114430.

(12) Ilisz, I.; Péter, A.; Lindner, W. *TrAC, Trends Anal. Chem.* **2016**, *81*, 11-22.

(13) Ianni, F.; Pucciarini, L.; Carotti, A.; Natalini, S.; Raskildina, G. Z.; Sardella, R.; Natalini, B. *J. Sep. Sci.* **2019**, *42* (1), 21-37.

(14) Kimura, R.; Tsujimura, H.; Tsuchiya, M.; Soga, S.; Ota, N.; Tanaka, A.; Kim, H. *Scientific Reports* **2020**, *10* (1), 804.

(15) Horak, J.; Lämmerhofer, M. *Anal. Chem.* **2019**, *91* (12), 7679-7689.

(16) Hellinger, R.; Horak, J.; Lindner, W. *Anal. Bioanal. Chem.* **2013**, *405* (25), 8105-8120.

(17) Acquaviva, A.; Siano, G.; Quintas, P.; Filgueira, M. R.; Castells, C. B. *J. Chromatogr. A* **2020**, *1614*, 460729.

(18) Ishii, C.; Akita, T.; Mita, M.; Ide, T.; Hamase, K. *J. Chromatogr. A* **2018**, *1570*, 91-98.

(19) Ianni, F.; Sardella, R.; Lisanti, A.; Gioiello, A.; Cenci Goga, B. T.; Lindner, W.; Natalini, B. *J. Pharm. Biomed. Anal.* **2015**, *116*, 40-46.

(20) Yao, X.; Tan, T. T. Y.; Wang, Y. *J. Chromatogr. A* **2014**, *1326*, 80-88.

(21) Molnár-Perl, I. *J. Chromatogr. B* **2011**, *879* (17), 1241-1269.

(22) Woiwode, U.; Reischl, R. J.; Buckenmaier, S.; Lindner, W.; Lämmerhofer, M. *Anal. Chem.* **2018**.

(23) Mazzoccanti, G.; Manetto, S.; Ricci, A.; Cabri, W.; Orlandin, A.; Catani, M.; Felletti, S.; Cavazzini, A.; Ye, M.; Ritchie, H.; et al. *J. Chromatogr. A* **2020**, *1624*, 461235.

(24) Ferre, S.; Gonzalez-Ruiz, V.; Guillarme, D.; Rudaz, S. *J Chromatogr B Analyt Technol Biomed Life Sci* **2019**, *1132*, 121819.

(25) Karongo, R.; Ge, M.; Horak, J.; Gross, H.; Kohout, M.; Lindner, W.; Lämmerhofer, M. *Journal of Chromatography Open* **2021**, *1*, 100004.

(26) Karakawa, S.; Shimbo, K.; Yamada, N.; Mizukoshi, T.; Miyano, H.; Mita, M.; Lindner, W.; Hamase, K. *J. Pharm. Biomed. Anal.* **2015**, *115*, 123-129.

(27) Santa, T. *Biomed. Chromatogr.* **2011**, *25* (1-2), 1-10.

(28) Sardella, R.; Lämmerhofer, M.; Natalini, B.; Lindner, W. *J. Sep. Sci.* **2008**, *31* (10), 1702-1711.

(29) Welsch, T.; Schmidtkunz, C.; Müller, B.; Meier, F.; Chlup, M.; Köhne, A.; Lämmerhofer, M.; Lindner, W. *Anal. Bioanal. Chem.* **2007**, *388* (8), 1717-1724.

(30) Ishii, C.; Furusho, A.; Hsieh, C.-L.; Hamase, K. *Chromatography* **2020**, *41* (1), 1-17.

(31) Stoll, D. R.; Carr, P. W. *Anal. Chem.* **2017**, *89* (1), 519-531.

(32) Dugo, P.; Cacciola, F.; Kumm, T.; Dugo, G.; Mondello, L. *J. Chromatogr. A* **2008**, *1184* (1), 353-368.

(33) Gargano, A. F. G.; Duffin, M.; Navarro, P.; Schoenmakers, P. J. *Anal. Chem.* **2016**, *88* (3), 1785-1793.

(34) Pirok, B. W. J.; Stoll, D. R.; Schoenmakers, P. J. *Anal. Chem.* **2019**, *91* (1), 240-263.

(35) Wang, H.; Lhotka, H. R.; Bennett, R.; Potapenko, M.; Pickens, C. J.; Mann, B. F.; Ahmad, I. A. H.; Regalado, E. L. *J. Chromatogr. A* **2020**, 460895.

(36) Pursch, M.; Buckenmaier, S. *Anal. Chem.* **2015**, *87* (10), 5310-5317.

(37) Pursch, M.; Lewer, P.; Buckenmaier, S. *Chromatographia* **2017**, *80* (1), 31-38, journal article.

(38) Karongo, R.; Ge, M.; Geibel, C.; Horak, J.; Lämmerhofer, M. *Anal. Chim. Acta* **2021**, *1180*.

(39) Woiwode, U.; Neubauer, S.; Lindner, W.; Buckenmaier, S.; Lämmerhofer, M. *J. Chromatogr. A* **2018**, *1562*, 69-77.

(40) Ciogli, A.; Ismail, O. H.; Mazzoccanti, G.; Villani, C.; Gasparrini, F. *J. Sep. Sci.* **2018**, *41* (6), 1307-1318.

(41) Khundadze, N.; Pantsulaia, S.; Fanali, C.; Farkas, T.; Chankvetadze, B. *J. Chromatogr. A* **2018**, *1572*, 37-43.

(42) Welch, C. J. *ACS Central Science* **2017**, *3* (8), 823-829.

(43) Barhate, C. L.; Regalado, E. L.; Contrella, N. D.; Lee, J.; Jo, J.; Makarov, A. A.; Armstrong, D. W.; Welch, C. J. *Anal. Chem.* **2017**, *89* (6), 3545-3553.

(44) Patel, D. C.; Breitbach, Z. S.; Yu, J.; Nguyen, K. A.; Armstrong, D. W. *Anal. Chim. Acta* **2017**, *963*, 164-174.

(45) Pantsulaia, S.; Targamadze, K.; Khundadze, N.; Kharaishvili, Q.; Volonterio, A.; Chitty, M.; Farkas, T.; Chankvetadze, B. *J. Chromatogr. A* **2020**, *1625*, 461297.

(46) Patel, D. C.; Breitbach, Z. S.; Wahab, M. F.; Barhate, C. L.; Armstrong, D. W. *Anal. Chem.* **2015**, *87* (18), 9137-9148.

(47) Schmitt, K.; Woiwode, U.; Kohout, M.; Zhang, T.; Lindner, W.; Lämmerhofer, M. *J. Chromatogr. A* **2018**.

(48) Geibel, C.; Dittrich, K.; Woiwode, U.; Kohout, M.; Zhang, T.; Lindner, W.; Lammerhofer, M. *J. Chromatogr. A* **2019**.

(49) Ismail, O. H.; Ciogli, A.; Villani, C.; De Martino, M.; Pierini, M.; Cavazzini, A.; Bell, D. S.; Gasparrini, F. *J. Chromatogr. A* **2016**, *1427*, 55-68.

(50) Grecsó, N.; Kohout, M.; Carotti, A.; Sardella, R.; Natalini, B.; Fülöp, F.; Lindner, W.; Péter, A.; Ilisz, I. *J. Pharm. Biomed. Anal.* **2016**, *124*, 164-173.

(51) Siegel, D.; Meinema, A. C.; Permentier, H.; Hopfgartner, G.; Bischoff, R. *Anal. Chem.* **2014**, *86* (10), 5089-5100.

(52) Katsushige IkaiI, K. T., Kazuro Shiomi, Makoto Moriguchi, Yoshihisa Umeda, Junko Yamamoto, Ikunoshin Kato, Hiroshi Naganawa. *The Journal of Antibiotics* **1991**, *44* (9), 925-933.

(53) In, Y.; Ishida, T.; Takesako, K. *J. Peptide Res.* **1999**, *53* (5), 492-500.
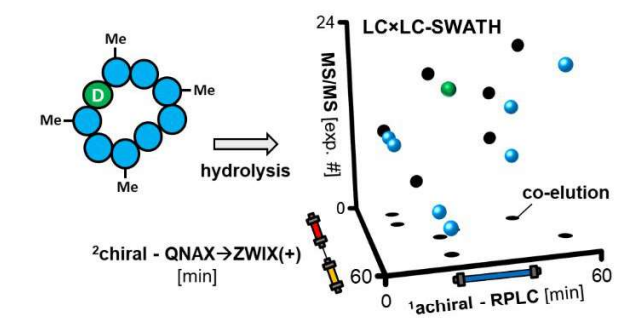
(54) Horak, J.; Lämmerhofer, M. *J. Chromatogr. A* **2019**, *1604*, 460492.

(55) Calderón, C.; Santi, C.; Lämmerhofer, M. *J. Sep. Sci.* **2018**, *41* (6), 1224-1231.

(56) Visconti, G.; Olesti, E.; González-Ruiz, V.; Glauser, G.; Tonoli, D.; Lescuyer, P.; Vuilleumier, N.; Rudaz, S. *Talanta* **2022**, *240*, 123149.

(57) Li, P.; Lämmerhofer, M. *Anal. Chem.* **2021**, *93* (27), 9583-9592.

For Table of Contents Only

4.5.1 Supporting Information

4.5.1.1 Targeted analytes and their 3-letter (and one-letter if available) amino acid code used herein

Table S1. Labels of 20 proteinogenic amino acids (1-20), the 5 isobaric (21-25) amino acids and the uncommon amino acids, amino alcohols and hydroxy acids (26-30).

1. Glycine (Gly, G)	11. Phenylalanine (Phe, F)	21. Homoserine (Hse)
2. Alanine (Ala, A)	12. Tyrosine (Tyr, Y)	22. *allo*-Threonine (aThr)
3. Serine (Ser, S)	13. Tryptophan (Trp, W)	23. *allo*-Isoleucine (aIle)
4. Threonine (Thr, T)	14. Aspartic Acid (Asp, D)	24. tert-Leucine (Tle)
5. Cysteine (Cys, C)	15. Glutamic Acid (Glu, E)	25. Norleucine (Nle)
6. Valine (Val, V)	16. Asparagine (Asn, N)	26. *N*-Methylvaline (*N*-Me-Val)
7. Leucine (Leu, L)	17. Glutamine (Gln, Q)	27. *N*-Methylphenylalanine (*N*-Me-Phe)
8. Isoleucine (Ile, I)	18. Histidine (His, H)	28. 3-Hydroxy-*N*-methylvaline (*N*-Me-3-OH-Val)
9. Methionine (Met, M)	19. Lysine (Lys, K)	29. 2-Desamino-2-hydroxy-isoleucine (OIle)
10. Proline (Pro, P)	20. Arginine (Arg, R)	30. Threoninol (Thr-ol)

4.5.1.2 Sample Preparation

For peptide hydrolysis the sample was dissolved in 1 mL of 6 M DCl in D_2O (1 mg/mL). The glass vial was sealed under nitrogen and heat-treated at 110 °C for 16 h. Subsequently, the sample was evaporated to dryness, the residue was re-dissolved to the original volume (1 mL) with 0.4 M borate buffer (pH 8.8), vortexed, and centrifuged for 60 s at 13,200 rpm. The supernatant was used for AQC derivatization of the liberated amino acids. Non-isotopically labelled AA stock solutions (L-[U-^{12}C^{14}N]-amino acids) as standard mixtures were prepared at a concentration of 2.5 mM in 0.1 M HCl containing all proteinogenic amino acids and additionally Hse, aThr, alle, Tle and Nle as isobaric analogs.

4.5.1.2.1 Alkylation

Cysteine-containing mixtures were prepared according to the following protocol.[1, 2] Iodoacetamide (IAA) and dithiothreitol (DTT) were freshly prepared at a concentration of 10 mM in ultra-pure water shortly before use and kept on ice. Solutions of 10 µL AA mix (2.5 mM), 5 µL DTT and 10 µL L-[U-^{13}C^{15}N]-AA IS (0.25 mM) were added to a solution of 40 µL 0.4 M sodium borate buffer (pH 8.8) in a 1.5 mL microcentrifuge tube. The reaction solution was placed on a thermoshaker (Grand Instruments) and allowed to react at 800 rpm and 55 °C for 10 min. After short centrifugation (13200 rpm, 4 °C, 1 min), 10 µL IAA was added followed by heating (55 °C) and shaking (800 rpm) for 10 min. After centrifugation, 5 µL DTT were added followed by yet another step of heating and shaking. Subsequently, 40 µL of this solution was filled up to 50 µL with ultrapure water (0.25 mM AA mix-IAA). For direct MS measurements, the solution was further diluted 1:10 with 0.4 M sodium borate buffer (pH 8.8) prior to derivatization with AQC reagent.

4.5.1.2.2 Derivatization.

The derivatization reagent AQC was prepared at a concentration of 3 mg/mL in dry acetonitrile (AQC: 10.5 mM), stored at −20 °C and shortly ultrasonicated before use. If not otherwise stated 10 µL sample solution (0.25 mM AA mix or hydrolyzed sample) was added to 80 µL 0.4 M sodium borate buffer (pH 8.8), followed by the addition of 10 µL AQC reagent solution. This reaction solution was immediately heated to 55 °C for 10 min at 800 rpm. After centrifugation, the sample was ready for analysis. According to the European Pharmacopoeia 10.0 peak areas for AQC-amino acids remain unchanged for at least a week at room temperature. Nevertheless, the samples were constantly cooled in the autosampler at 4 °C and were only utilized for a week, then freshly prepared.

4.5.1.3 Instrumental setup

The components of the 2D-LC system are described in the main document. They have been assembled in the following instrumental setup.
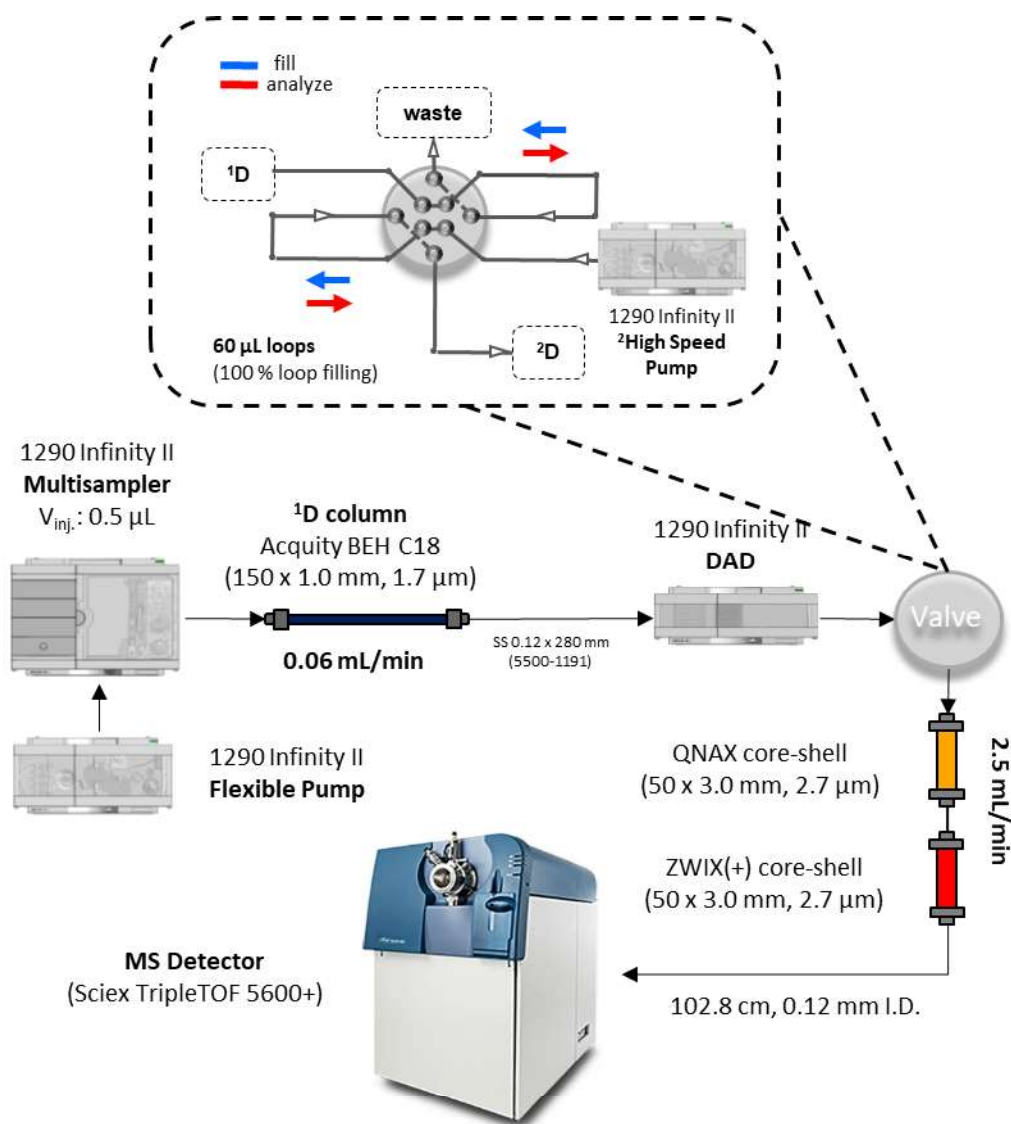

Figure S1. Final LC×LC setup without flow splitting utilizing 60 µL storage loops for full transfer of ^{1}D effluent.
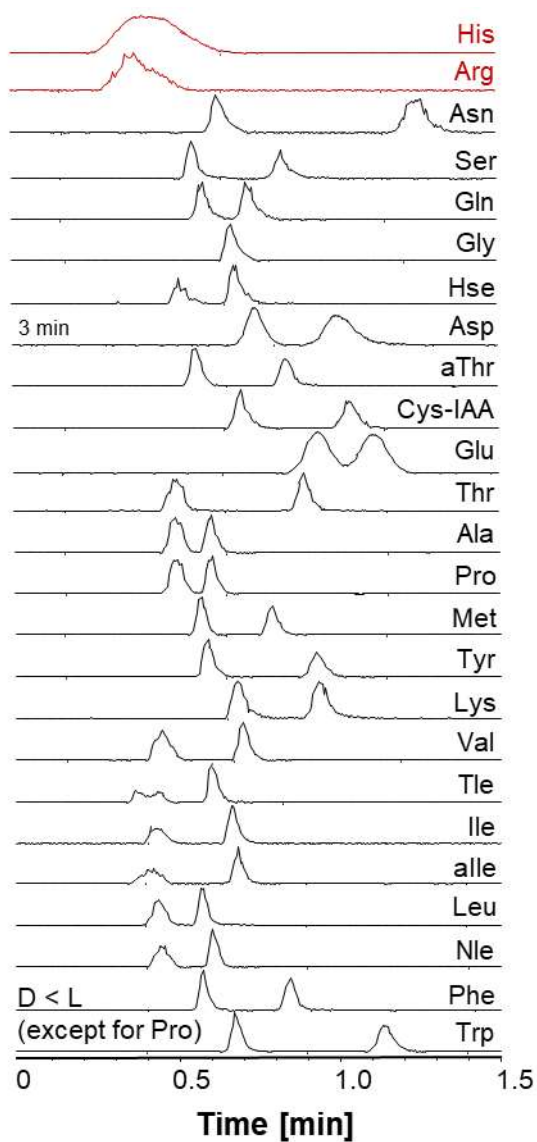
4.5.1.4 Optimization of ²D separation

Figure S2. Enantiomer separations of 20 proteinogenic amino acids and some isobaric analogs on core-shell QN-AX column (50 x 3 mm; 2.7 µm, 160 Å).

4.5.1.5 Comprehensive RP×chiral 2DLC-ESI-QTOF-MS without flow splitting

4.5.1.5.1 Optimization of sub-minute gradient elution AA enantiomer separation
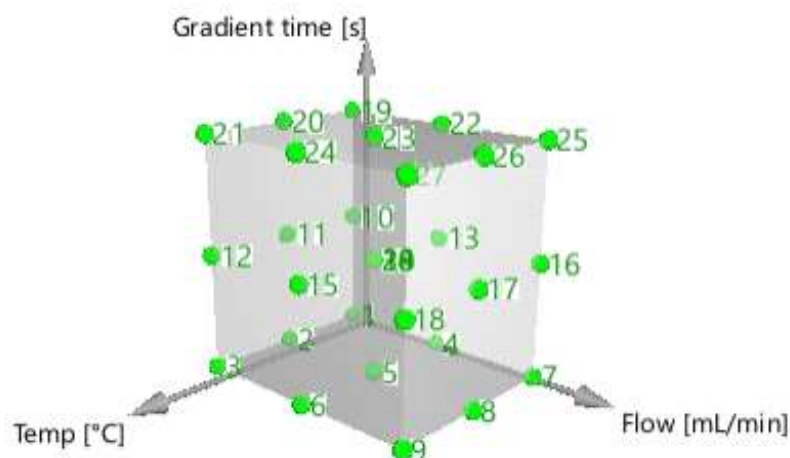
Figure S3. Full factorial design (3 levels) for the [2]D optimization.

Under isocratic elution condition, certain AAs require low (10 mM) and others high (50 mM) buffer concentrations in order to achieve reasonable retention times on the column for sufficient enantioselectivity and resolution ($R_S \approx 1.5$).[3] For mLC-LC different isocratic conditions can be chosen for each cut, but for LC×LC, gradient elution is the favored solution to assure elution of all amino acids, while keeping the method generic. The main expectation for gradient elution was the ability to separate all amino acids within reasonable timescales suitable for a LC×LC setup. The maximum [2]cycle time is imposed by the [1]flow rate and modulation loop volume; it was tolerated at maximum 60 s including the re-equilibration time. Next, a full factorial design (FFD) response surface modelling approach was used to optimize the most important quantitative factors flow rate ([2]F), linear gradient (10 – 50 mM) time ([2]t_G) and temperature ([2]T) for the problematic amino acids Asp, Arg and His (note, this i.e. a FFD was readily possible due to the short run times).[4, 5] L-Asp as the last eluting AA determines the gradient time, while His and Arg as basic amino acids needed special attention for their resolution.[6] To this end, the response factors for the DoE were $RT_{L\text{-}Asp}$, $R_{s\text{-}(Arg)}$ and $R_{s\text{-}(His)}$ (**Table S3**). The high-level factors were restricted by the column's maximum backpressure (800 bar) and temperature (60 °C).[7] Experiments (N = 30) were run in a randomized order and a quadratic model including interaction terms was fitted to encode between three levels of each factor (**Figure S8**). Insignificant model terms were removed after evaluating the regression coefficients.

The response surface plots (**Figure S9**) for each response reveal a minimized $RT_{L\text{-}Asp}$ at maximum [2]F and [2]T, and minimum [2]t_G. The resolution for His and Arg is sufficient at all

conditions (**Figure S10-S11**), which can be attributed to the high enantioselectivity of the ZWIX column towards basic amino acids. Thus, the separation for all AAs was achieved under optimized conditions (**Figure S13**): t_G: 20 s, F: 2.5 mL/min, T: 50 °C.

Table S2. DoE experimental design for the optimization of Temperature, Flow and Gradient Time. Main response is the retention time of the last eluting peak (L-Asp) and the resolution of the basic amino acids His and Arg (critical amino acids).

Exp No	Exp Name	Run Order	Incl/Excl	Temp	Flow	Gradient time	Response $R_{s\text{-(His)}}$	Response $R_{s\text{-(Arg)}}$	Response $RT_{L\text{-Asp}}$ [min]
1	N1	2	Incl	30	1.5	20	6.29	5.06	2.01
2	N2	27	Incl	40	1.5	20	4.83	5.31	1.92
3	N3	20	Incl	50	1.5	20	4.40	6.76	1.64
4	N4	11	Incl	30	2	20	3.62	4.41	1.51
5	N5	12	Incl	40	2	20	4.18	4.35	1.53
6	N6	15	Incl	50	2	20	5.11	5.02	1.34
7	N7	5	Incl	30	2.5	20	4.21	4.61	1.10
8	N8	8	Incl	40	2.5	20	3.69	5.90	1.01
9	N9	7	Incl	50	2.5	20	2.95	4.59	1.07
10	N10	22	Incl	30	1.5	40	3.47	5.61	1.98
11	N11	26	Incl	40	1.5	40	7.38	5.53	1.90
12	N12	4	Incl	50	1.5	40	5.04	6.69	1.76
13	N13	13	Incl	30	2	40	4.60	4.56	1.53
14	N14	6	Incl	40	2	40	3.30	5.48	1.59
15	N15	21	Incl	50	2	40	4.60	5.04	1.35
16	N16	10	Incl	30	2.5	40	3.30	4.13	1.22
17	N17	14	Incl	40	2.5	40	4.33	3.99	1.26
18	N18	19	Incl	50	2.5	40	3.33	5.43	1.14
19	N19	28	Incl	30	1.5	60	3.89	5.61	2.16
20	N20	1	Incl	40	1.5	60	4.47	6.12	2.07
21	N21	17	Incl	50	1.5	60	6.11	6.61	2.00
22	N22	29	Incl	30	2	60	4.18	5.21	1.73
23	N23	23	Incl	40	2	60	3.33	5.73	1.69
24	N24	24	Incl	50	2	60	6.03	5.72	1.53
25	N25	30	Incl	30	2.5	60	4.13	5.06	1.39
26	N26	25	Incl	40	2.5	60	5.90	6.93	1.18
27	N27	3	Incl	50	2.5	60	3.86	4.92	1.26
28	N28	18	Incl	40	2	40	4.46	4.93	1.39
29	N29	9	Incl	40	2	40	3.25	5.21	1.44
30	N30	16	Incl	40	2	40	4.72	5.47	1.38
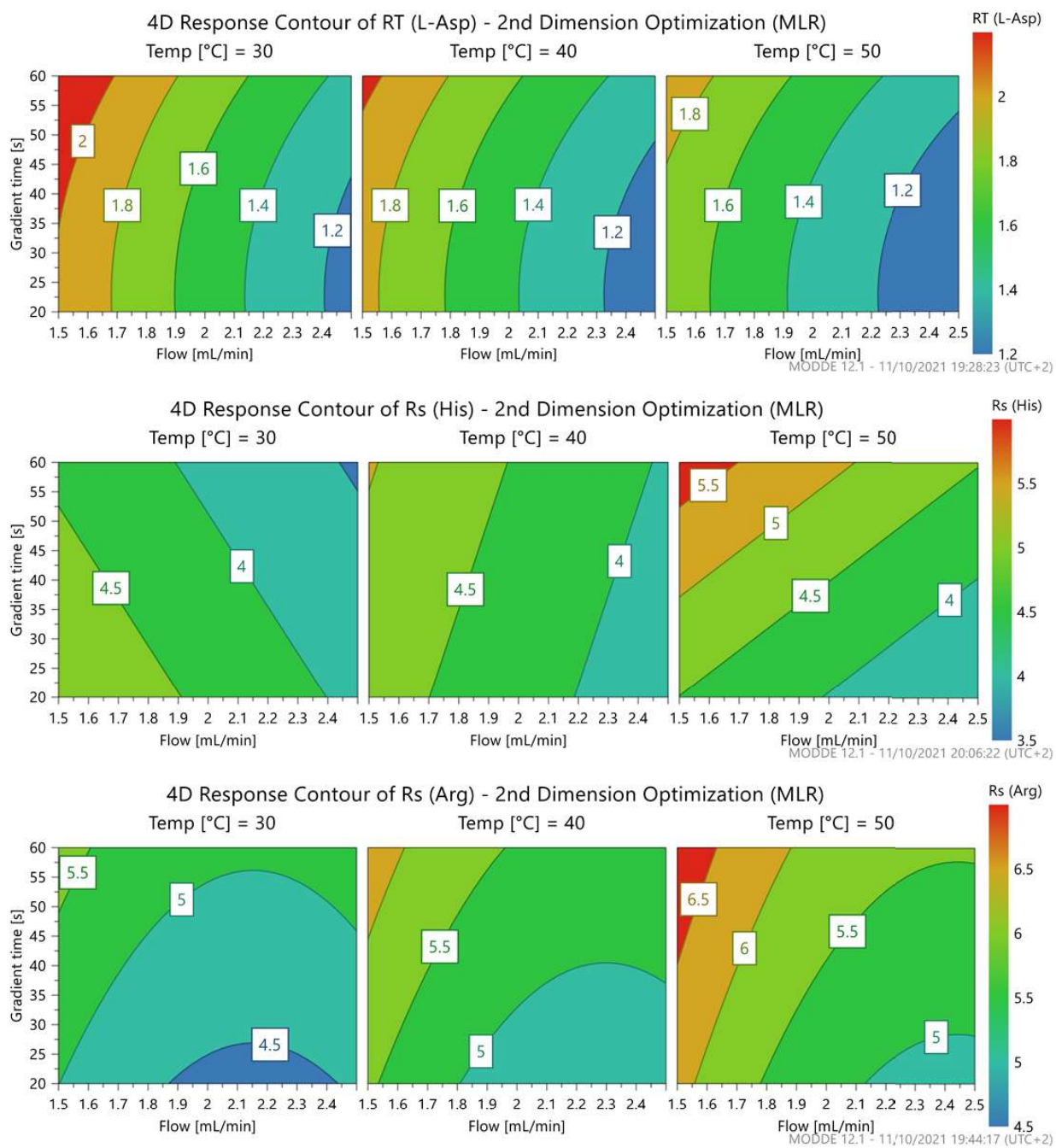
Figure S4. Response surface plots for the optimization of ^{2}Flow, ^{2}Temp. and ^{2}t$_G$, and the response factors RT$_{L-Asp}$, R$_{s-(Arg)}$ and R$_{s-(His)}$.
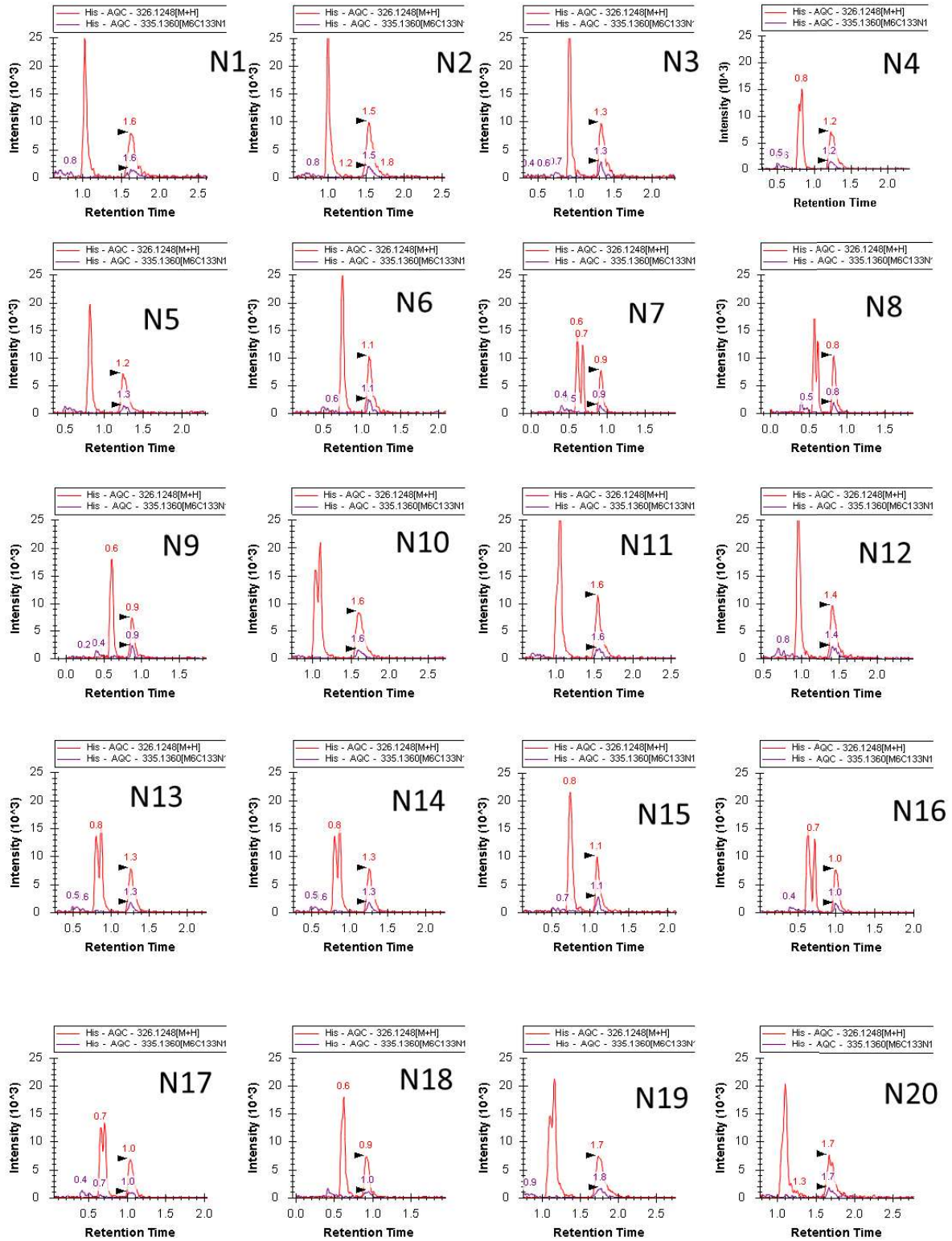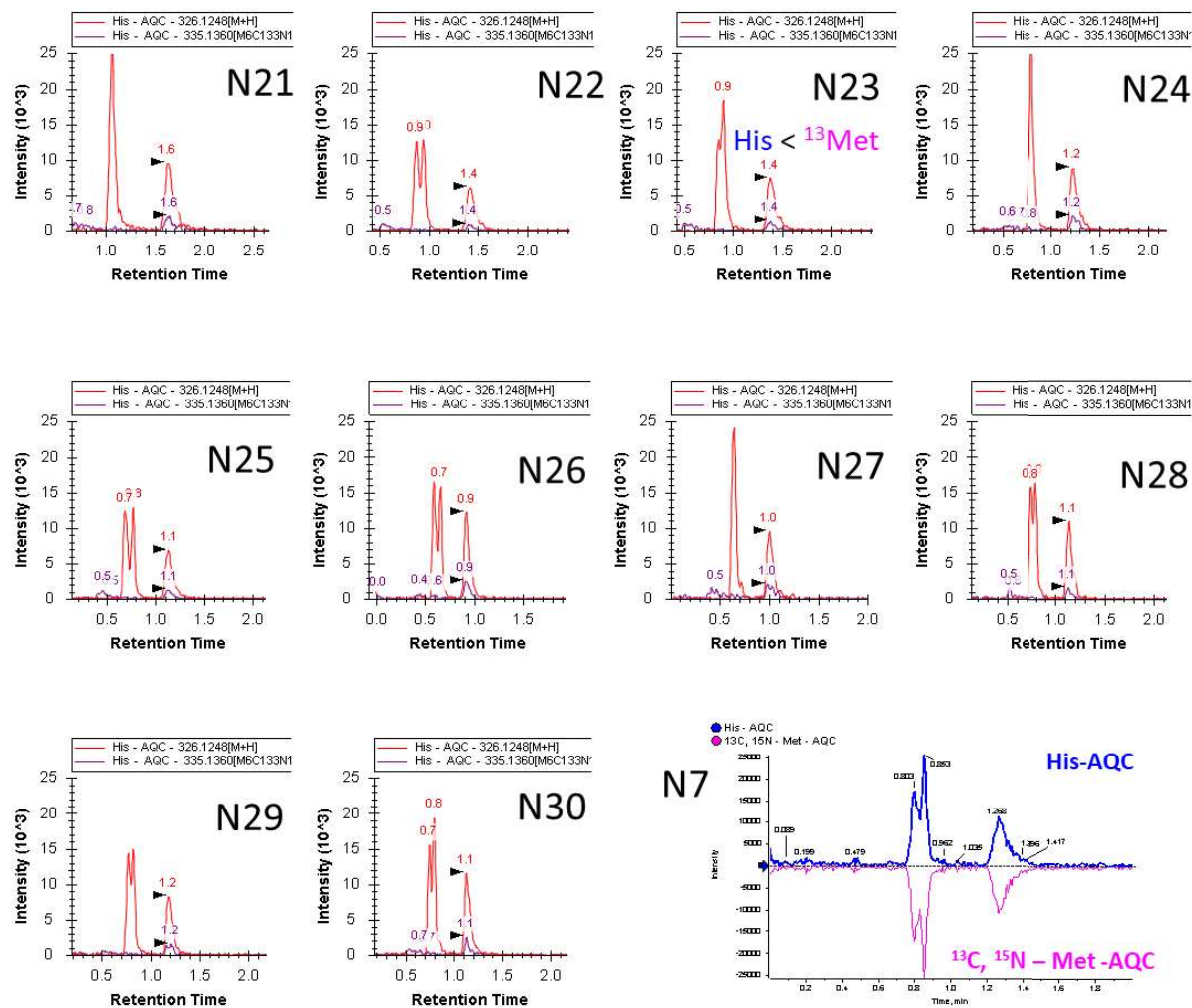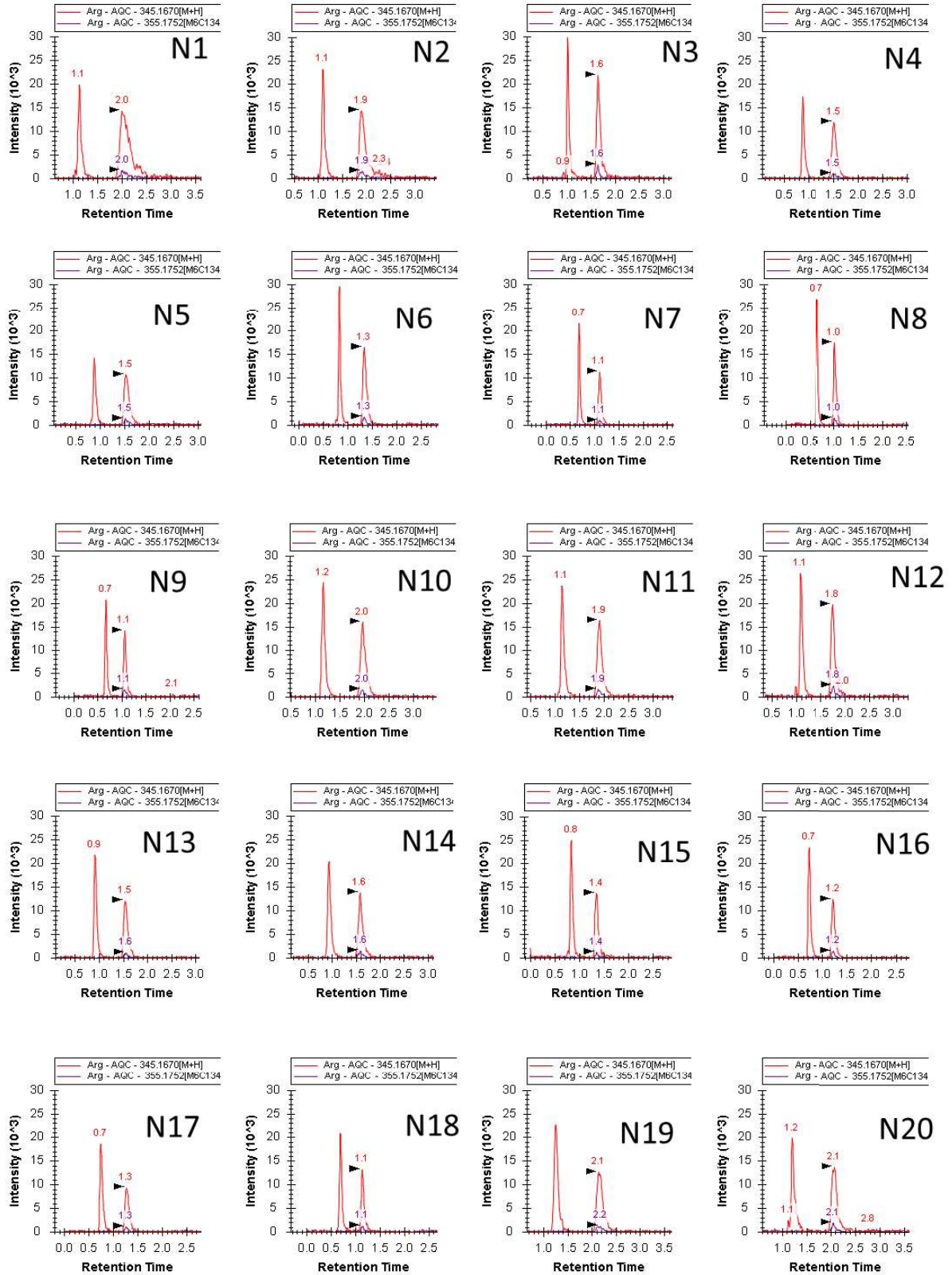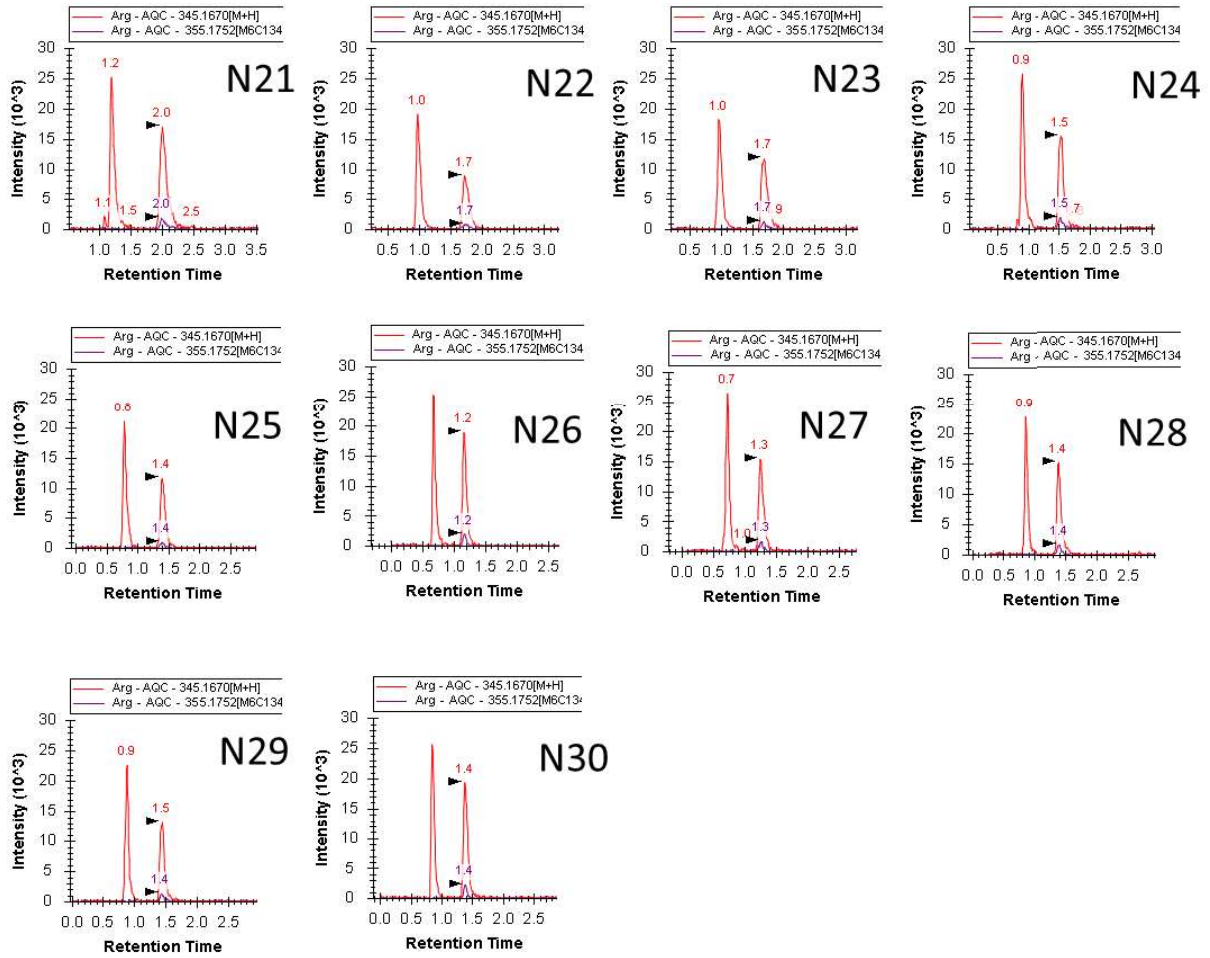
Figure S5. Extracted ion chromatograms for the separation of DL-Histidine (red trace) and [U-^{13}C^{15}N]-L-His (purple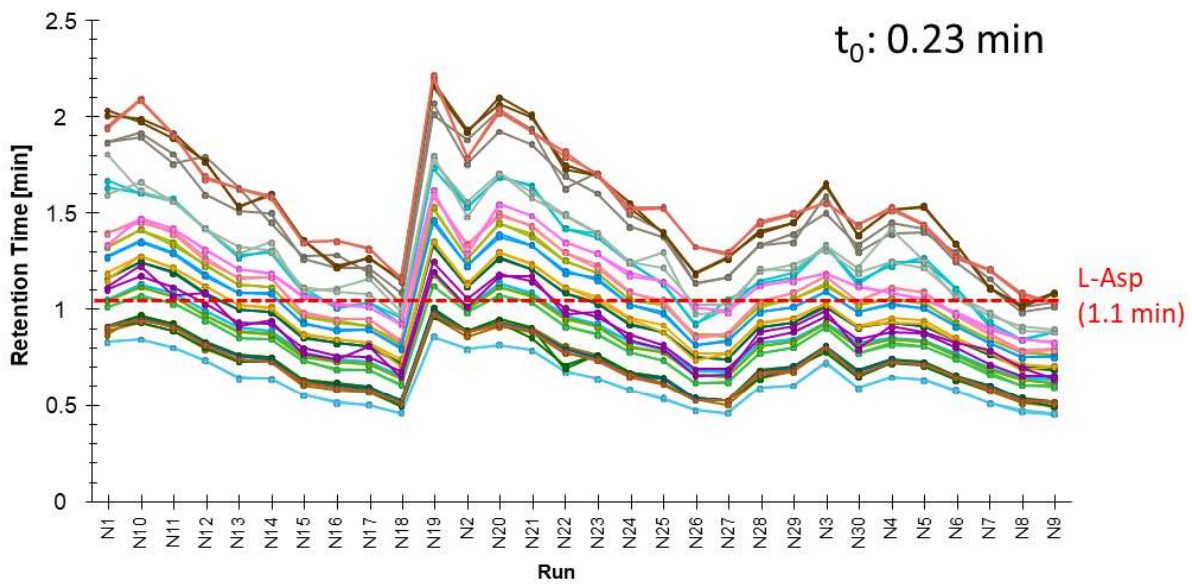 trace) under all DOE conditions (N1-N30). His-AQC and ^{13}C,^{15}N – Met-AQC co-eluted and were not resolved by MS (see panel on the bottom right) resulting in double peaks where partial separation occurs.

Figure S6. Extracted ion chromatograms for the separation of DL-Arginine (red trace) and [U-^{13}C^{15}N]-L-Arg (purple trace) under all DOE conditions (N1-N30).

Figure S7. Run to run comparison of retention times for 25 amino acids under conditions N1 to N30 as listed in **Table S2**.

146

4.5.1.5.2 Optimization of column re-equilibration of ^{2}D gradient elution AA enantiomer separation

In order to minimize the re-equilibration time, a study design for overlapping injections to compensate for autosampler movements was carried out (**Figure S14**), considering equilibration times of 5 s, 10 s, 15 s, 20 s and 30 s (**Table S4**). The measurements were run in triplicates, revealing sufficient retention time precision (average RSD = 1.43) for all D- and L-AAs with the shortest re-equilibration time of 5 s (Table S5, Figure 15-16).
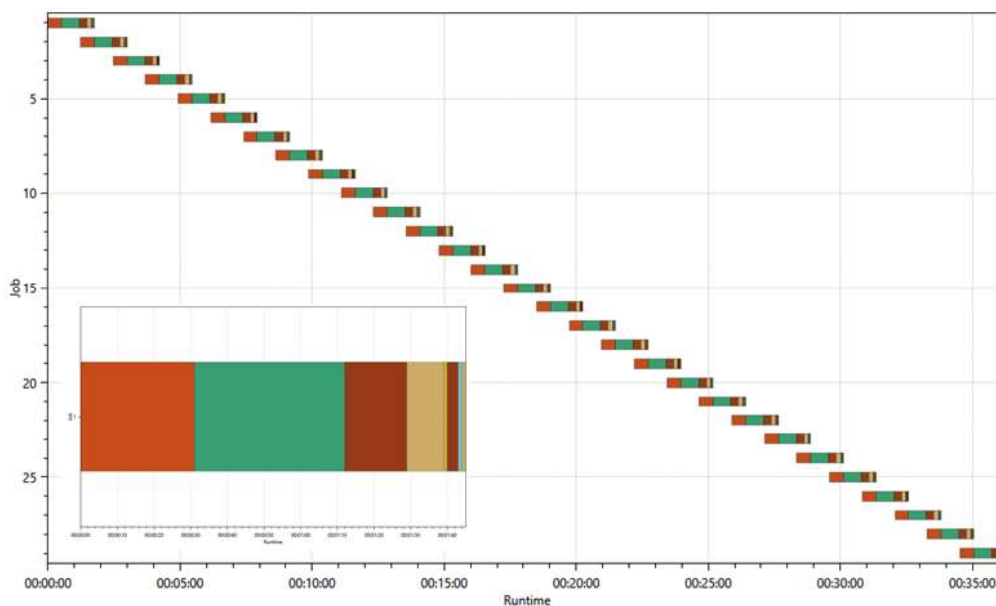
Figure S8. Chronos study design for overlapped injections (compensate autosampler movements) to optimize re-equilibration time. One period contains 10 tasks: 1: wait, 2: clean syringe for second injection, 3: get sample from vial, 4: park in the needle seat, 5: send acquisition data to Analyst (blocks and waits for previous run equilibration to finish), 6: switch valve to bypass for loop fill, 7: dispense syringe to loop, 8: switch valve to main pass for injection, 9: send start signal to MS and LC, 10: move arm to home position.

Table S3. Experimental replicates to optimize re-equilibration time, initial hold and gradient.

Experiments	Runs	Experiment	Comment
	3	30 sec	
	3	20 sec	
	3	15 sec	re-equilibration time
	3	10 sec	
1D-LC	3	5 sec	
	3	no hold	initial hold
	3	30-50B	gradient
	3	30-50B no hold	initial hold

Table S4. Retention time precision (RSD, n=3) for overlapped injections to optimize re-equilibration time, initial hold and gradient.

| Amino Acid	Enantiomer	RT 30-50B	RSD 30-50B	RT no hold 30-50B	RSD no hold 30-50B	RT no hold	RSD no hold	RT re-eq 10s	RSD re-eq 10s	RT re-eq 15s	RSD re-eq 15s	RT re-eq 20s	RSD re-eq 20s	RT re-eq 30s	RSD re-eq 30s	RT re-eq 30s	RSD re-eq 30s	RT re-eq 5s	RSD re-eq 5s
Asp - AQC	D	0.73	1.57	0.72	2.11	0.90	2.94	0.89	0.65	0.89	0.65	0.89	1.29	0.89	1.29	0.90	0.64	0.90	0.64
Glu - AQC	D	0.53	1.08	0.52	2.21	0.73	0.00	0.74	0.00	0.74	0.78	0.74	0.78	0.75	0.77	0.75	0.00	0.74	0.78
Asn - AQC	D	0.44	3.45	0.45	1.27	0.58	2.62	0.58	1.00	0.58	0.99	0.58	1.00	0.58	0.99	0.58	1.72	0.57	2.01
Ser - AQC	D	0.37	1.55	0.40	0.00	0.50	3.46	0.51	1.14	0.51	2.98	0.50	3.03	0.50	1.16	0.50	1.16	0.50	2.00
Gln - AQC	D	0.31	1.88	0.30	1.90	0.30	1.90	0.31	3.23	0.31	1.84	0.32	1.82	0.31	1.88	0.32	4.82	0.31	1.84
His - AQC	D	0.48	2.08	0.46	2.17	0.58	2.62	0.59	1.97	0.58	2.62	0.60	0.00	0.59	0.98	0.59	3.51	0.57	2.70
Gly - AQC	D	0.43	1.33	0.44	1.32	0.58	1.72	0.58	1.00	0.58	0.00	0.58	1.00	0.58	0.00	0.58	0.00	0.58	0.00
Thr - AQC	D	0.34	1.68	0.35	0.00	0.44	3.45	0.44	0.00	0.43	2.33	0.44	0.00	0.43	4.03	0.43	3.53	0.43	1.35
Ala - AQC	D	0.34	2.94	0.33	0.00	0.42	0.00	0.42	1.39	0.43	1.35	0.42	1.36	0.42	1.39	0.42	1.36	0.42	1.36
Arg - AQC	D	0.54	1.06	0.54	1.06	0.64	2.40	0.65	1.79	0.65	0.89	0.64	0.90	0.65	1.54	0.65	0.89	0.64	0.90
Tyr - AQC	D	0.38	2.63	0.37	0.00	0.47	1.22	0.48	1.19	0.47	0.00	0.48	0.00	0.48	2.42	0.48	1.21	0.48	1.21
Val - AQC	D	0.27	-	0.29	0.00	0.34	2.94	0.34	1.68	0.34	0.00	0.34	3.36	0.33	3.46	0.34	0.00	0.34	2.94
Met - AQC	D	0.36	0.00	0.37	1.57	0.47	1.24	0.47	1.22	0.47	0.00	0.47	1.24	0.47	2.47	0.47	1.22	0.48	1.21
Trp - AQC	D	0.43	1.35	0.43	0.00	0.55	2.11	0.56	1.79	0.55	0.00	0.56	2.07	0.55	0.00	0.55	1.06	0.55	1.04
Phe - AQC	D	0.36	2.78	0.36	1.62	0.46	1.25	0.46	0.00	0.47	0.00	0.46	1.26	0.45	1.27	0.45	1.27	0.46	2.17
Ile - AQC	D	0.29	3.45	0.28	4.17	0.34	3.36	0.34	1.71	0.34	0.00	0.34	1.68	0.34	3.43	0.33	1.73	0.35	4.41
Leu - AQC	D	0.29	3.45	0.29	2.01	0.34	3.43	0.34	1.71	0.34	1.68	0.34	1.71	0.35	4.41	0.34	2.94	0.35	4.41
Lys - 2x AQC	D	0.49	2.37	0.47	0.00	0.60	0.97	0.60	0.97	0.60	0.96	0.60	0.96	0.59	1.69	0.60	0.97	0.60	0.00
Pro - AQC	D	0.35	1.67	0.35	1.67	0.45	0.00	0.44	0.00	0.45	3.42	0.44	1.30	0.44	1.30	0.45	0.00	0.44	1.30
Cys - IAA-AQC	D	0.45	3.37	0.45	2.22	0.58	2.00	0.58	0.00	0.59	0.98	0.59	0.98	0.58	0.99	0.57	1.01	0.59	0.98
Asp - AQC	L	0.82	0.70	0.82	0.70	0.97	0.59	0.98	1.02	0.99	1.17	0.98	0.59	0.99	0.59	0.99	0.59	0.98	0.00
Glu - AQC	L	0.62	0.94	0.60	0.96	0.79	0.00	0.80	0.00	0.80	0.72	0.80	0.00	0.79	0.73	0.80	0.00	0.79	0.73
Asn - AQC	L	0.68	0.84	0.68	1.47	0.83	0.70	0.84	0.69	0.84	0.69	0.84	0.69	0.85	1.18	0.85	1.36	0.83	1.83
Ser - AQC	L	0.55	0.00	0.56	2.07	0.71	0.82	0.71	2.14	0.71	1.41	0.72	0.81	0.72	0.81	0.72	0.00	0.71	0.00
Gln - AQC	L	0.48	1.21	0.48	2.08	0.62	1.61	0.63	0.92	0.62	0.93	0.63	0.00	0.63	3.29	0.64	1.56	0.62	0.93
His - AQC	L	0.71	0.82	0.70	2.17	0.73	16.67	0.80	0.72	0.80	1.25	0.79	1.27	0.81	0.00	0.80	0.72	0.79	0.73
Gly - AQC	L	0.43	1.33	0.44	1.32	0.58	1.72	0.58	1.00	0.58	0.00	0.58	1.00	0.58	0.00	0.58	0.00	0.58	0.00
Thr - AQC	L	0.52	2.23	0.51	1.12	0.66	1.74	0.68	0.85	0.67	0.86	0.67	0.87	0.69	5.23	0.68	0.00	0.67	1.49
Ala - AQC	L	0.38	1.53	0.38	0.00	0.51	1.14	0.51	1.14	0.50	0.00	0.50	2.29	0.50	0.00	0.50	1.15	0.50	0.00
Arg - AQC	L	0.85	2.04	0.85	2.35	0.97	2.15	0.96	0.60	0.95	0.00	0.97	1.03	0.97	1.19	0.97	1.19	0.96	1.59
Tyr - AQC	L	0.51	0.00	0.50	1.15	0.66	0.00	0.66	0.87	0.66	0.87	0.66	0.00	0.66	0.87	0.66	0.87	0.66	0.00
Val - AQC	L	0.35	14.23	0.36	1.59	0.51	1.14	0.50	0.00	0.50	1.15	0.51	3.40	0.51	1.14	0.50	1.15	0.50	0.00
Met - AQC	L	0.45	2.22	0.46	1.26	0.60	0.97	0.59	1.95	0.60	0.96	0.60	0.00	0.59	0.97	0.59	2.57	0.59	0.98
Trp - AQC	L	0.78	1.97	0.76	2.00	0.93	1.65	0.93	0.62	0.92	0.63	0.92	1.09	0.93	1.86	0.93	1.08	0.93	0.62
Phe - AQC	L	0.46	0.00	0.45	1.27	0.61	0.00	0.61	0.94	0.62	0.94	0.62	0.94	0.61	0.00	0.62	0.94	0.61	0.00
Ile - AQC	L	0.36	2.78	0.36	0.00	0.48	2.42	0.45	8.91	0.45	3.85	0.44	2.60	0.45	3.37	0.45	1.29	0.45	5.88
Leu - AQC	L	0.36	2.78	0.36	0.00	0.45	6.37	0.43	0.00	0.44	0.00	0.44	2.60	0.44	2.27	0.45	1.29	0.45	2.59
Lys - 2x AQC	L	1.32	-	1.19	-	1.16	-	0.99	-	0.74	0.78	0.74	0.78	1.13	-	0.74	1.35	0.74	1.57
Pro - AQC	L	0.23	2.47	0.23	2.55	0.23	4.35	0.23	4.35	0.23	0.00	0.24	2.44	0.23	4.95	0.23	2.47	0.23	4.35
Cys - IAA-AQC	L	0.59	0.97	0.58	0.99	0.72	0.00	0.72	0.80	0.72	0.80	0.73	0.79	0.73	1.37	0.73	0.00	0.73	0.79
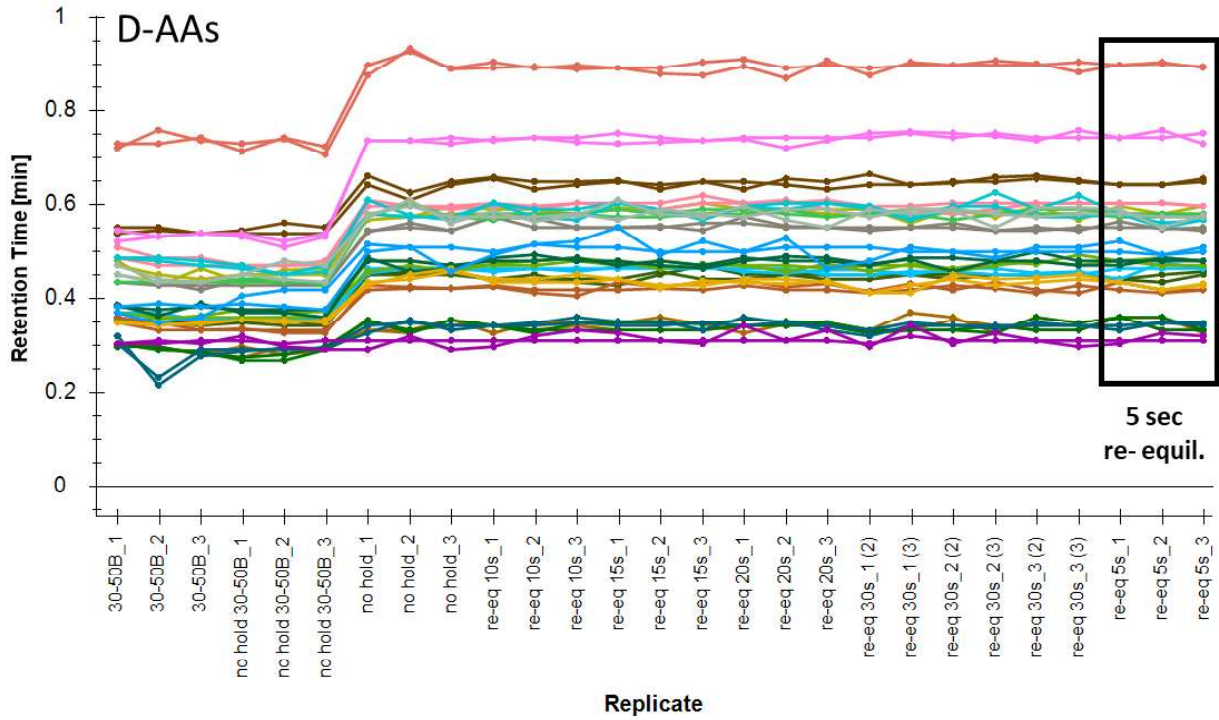
Figure S9. Retention time analysis of D-AAs replicates (n=3) performed under various conditions as stated in **Table S5**.
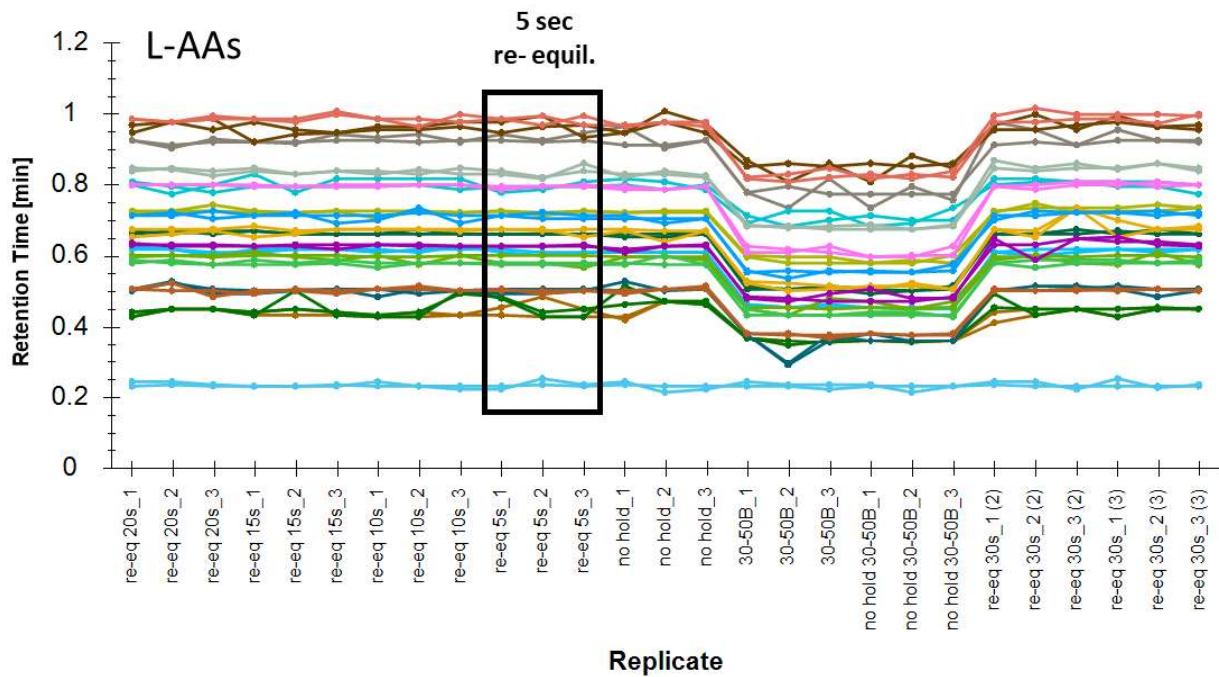

Figure S10. Retention time analysis of L-AAs replicates (n=3) performed under various conditions as stated in **Table S6**.

4.5.1.5.3 Optimization of MS parameters and SWATH windows

Table S7. Final design of the SWATH experiment for ESI+.

Experiment	MS Type	SWATH label	Start (m/z)	End (m/z)	Accumulation time [ms]
1	SCAN	N/A	100	2000	50
2	SWATH	125	50	200	12.5
3	SWATH	210	199.5	220.5	12.5
4	SWATH	230	219.5	240.5	12.5
5	SWATH	250	239.5	260.5	12.5
6	SWATH	270	259.5	280.5	12.5
7	SWATH	290	279.5	300.5	12.5
8	SWATH	310	299.5	320.5	12.5
9	SWATH	330	319.5	340.5	12.5
10	SWATH	350	339.5	360.5	12.5
11	SWATH	370	359.5	380.5	12.5
12	SWATH	390	379.5	400.5	12.5
13	SWATH	410	399.5	420.5	12.5
14	SWATH	430	419.5	440.5	12.5
15	SWATH	450	439.5	460.5	12.5
16	SWATH	470	459.5	480.5	12.5
17	SWATH	490	479.5	500.5	12.5
18	SWATH	510	499.5	520.5	12.5
19	SWATH	530	519.5	540.5	12.5
20	SWATH	550	539.5	560.5	12.5
21	SWATH	570	559.5	580.5	12.5
22	SWATH	590	579.5	600.5	12.5
23	SWATH	700.25	600	800.5	12.5
24	SWATH	700.25	800	1000.5	12.5
25	SWATH	1125	1000	1250	12.5
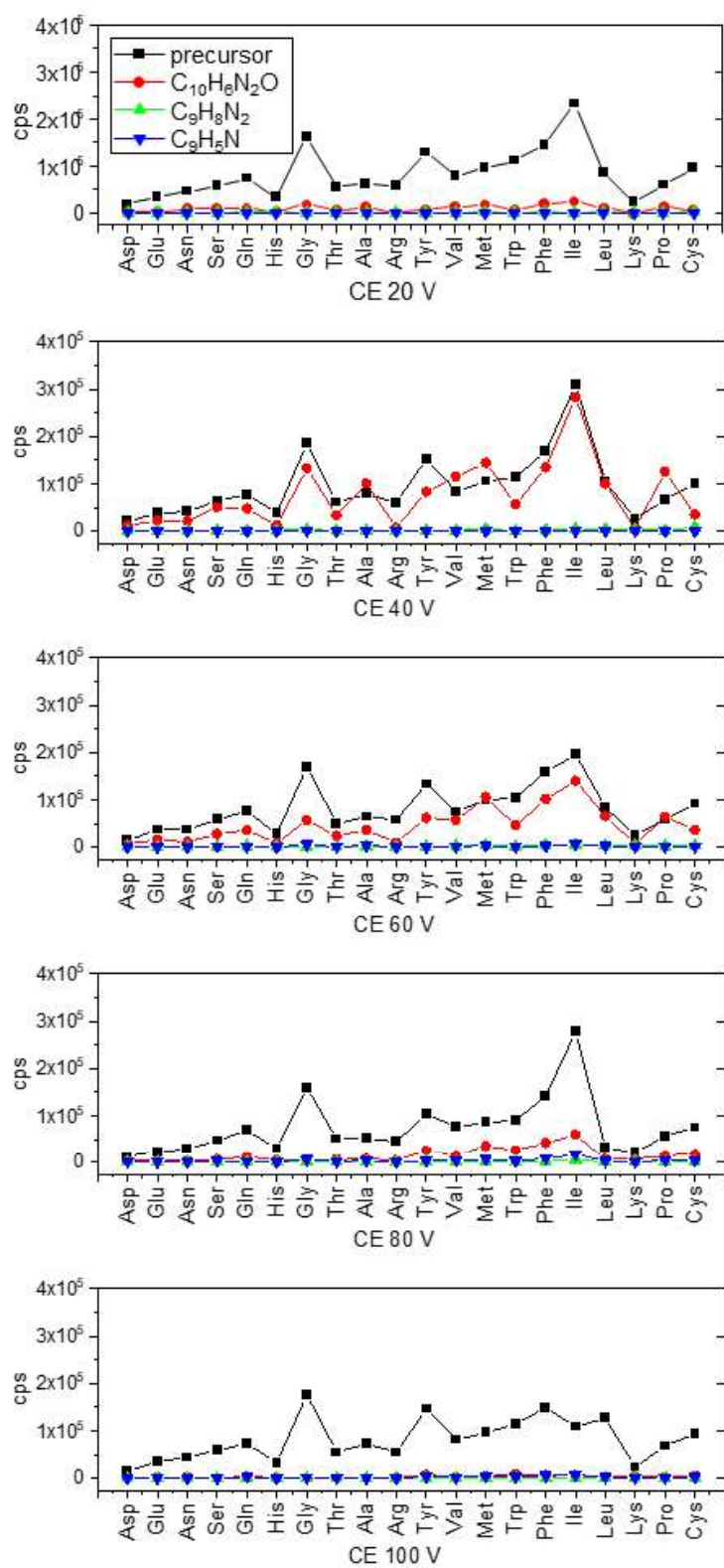
Figure S11. Collision energy optimization to obtain AQC signature fragments for all proteinogenic AAs. Cys and Lys are alkylated (IAA) and double derivatized (2x AQC), respectively.

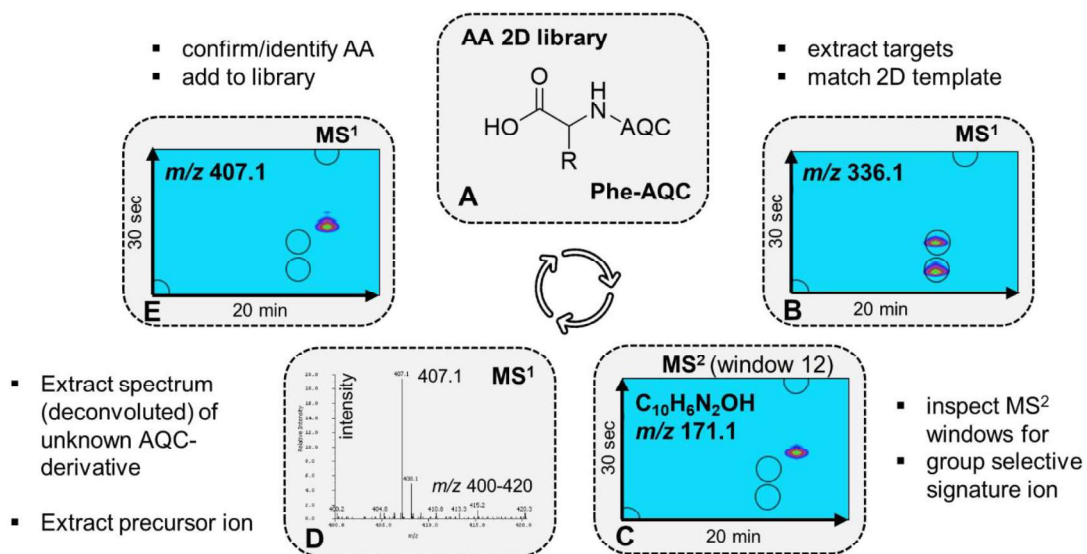### 4.5.1.5.4 A general strategy to analyze 2D-LC-SWATH data

Figure S12. A general strategy to analyze 2D-LC-SWATH data by exploiting the signature ion introduced by AQC derivatization (see main text for explanation).

4.5.1.5.5 RP×chiral 2DLC-ESI-QTOF-MS/MS analysis of aureobasidin

4.5.1.5.5.1 [1]RP chromatogram
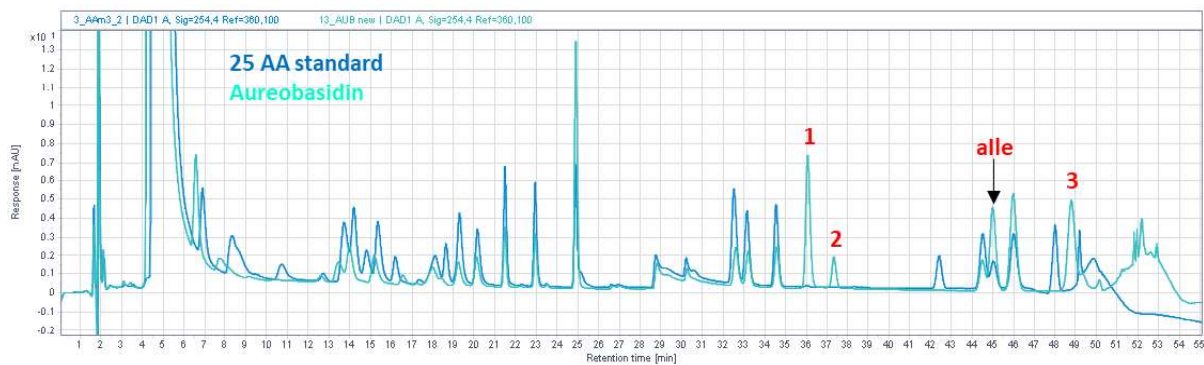
Figure S13. [1]D RPLC-DAD chromatogram of a 25 AQC-AAs standard mix and an aureobasidin hydrolysate AQC-AAs mix. The [1]D chromatography provides the information on three unidentified peaks. These were later identified by MS detection as (1) m/z 256.11, (2) N-Me-Val and (3) N-Me-Phe. Unknown (1) was also revealed on a 2D-LC level by the peak finding strategy described in **Figure S12**.

4.5.1.5.5.2 MS1 and MS2 2D-Extracted Ion Chromatograms (2D-contour plots) of targeted amino acids
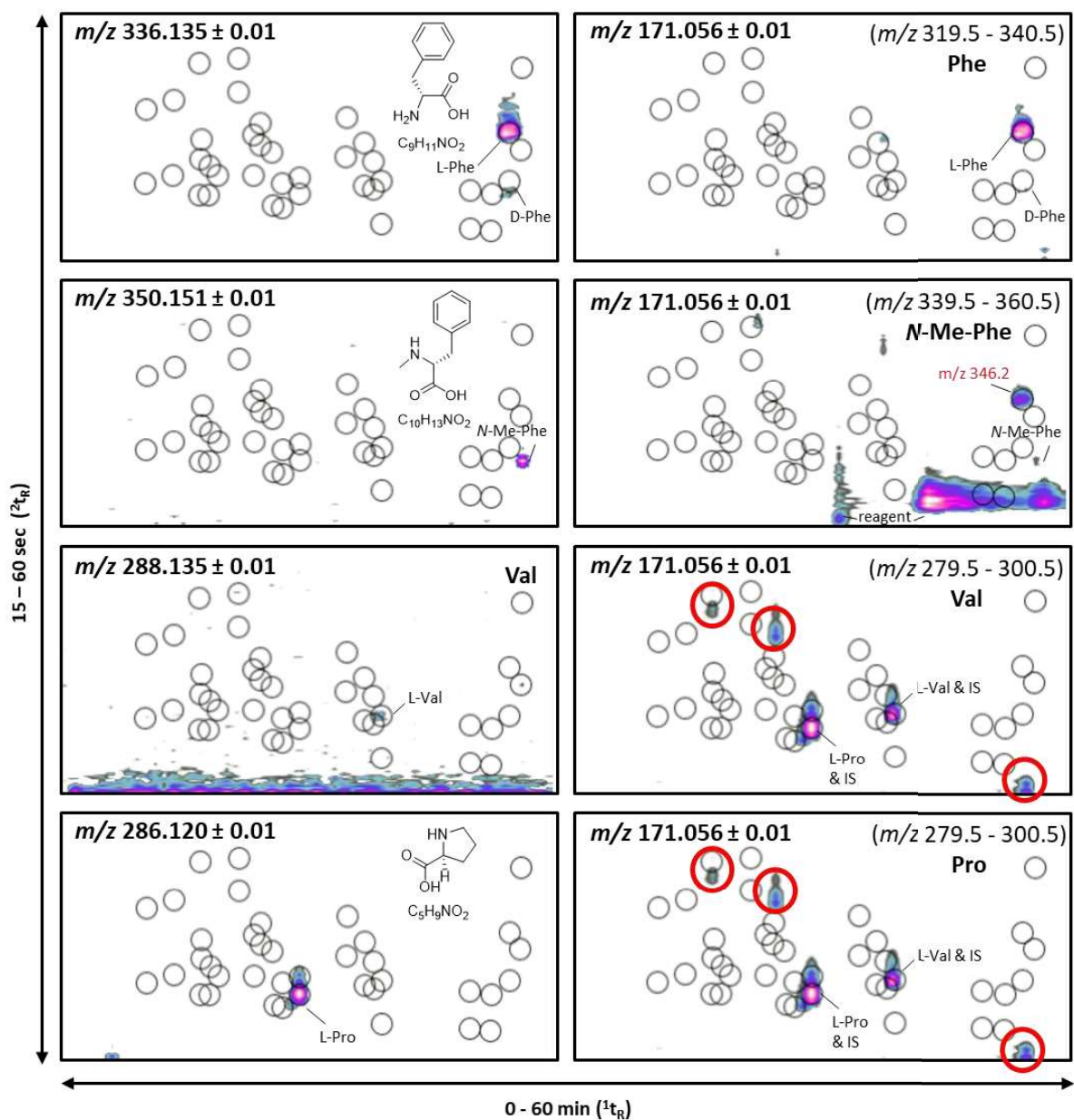
Figure S14. Extracted ion chromatograms (EIC) from MS[1] (left panel) of the respective AQC-AA expected in Aureobasidin A and MS[2] EIC of the signature fragment m/z 171 from the respective AQC-AA SWATH window (right panel). The red circles correspond to unknown compounds and red labels to the precursor ions of unknowns).
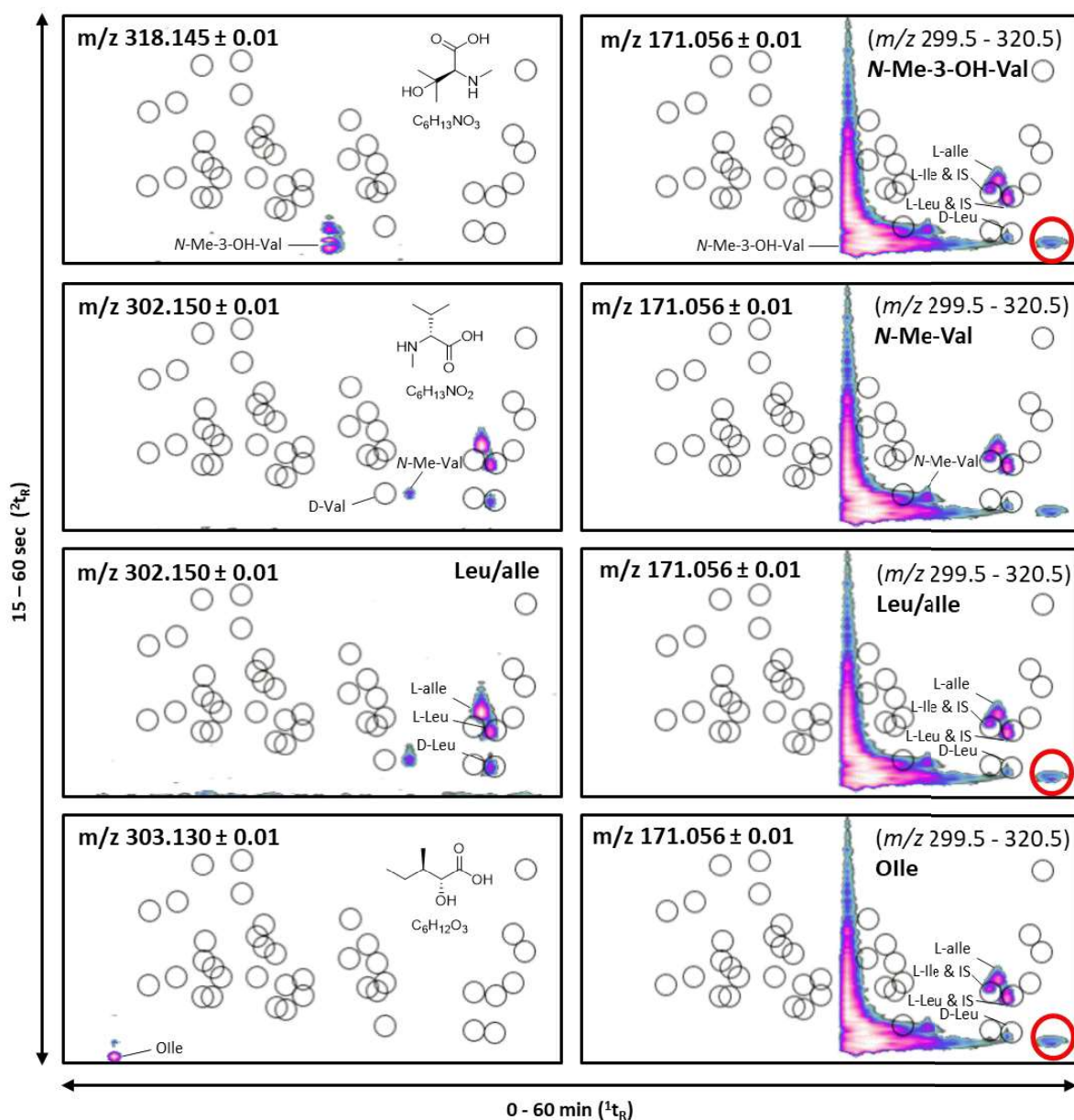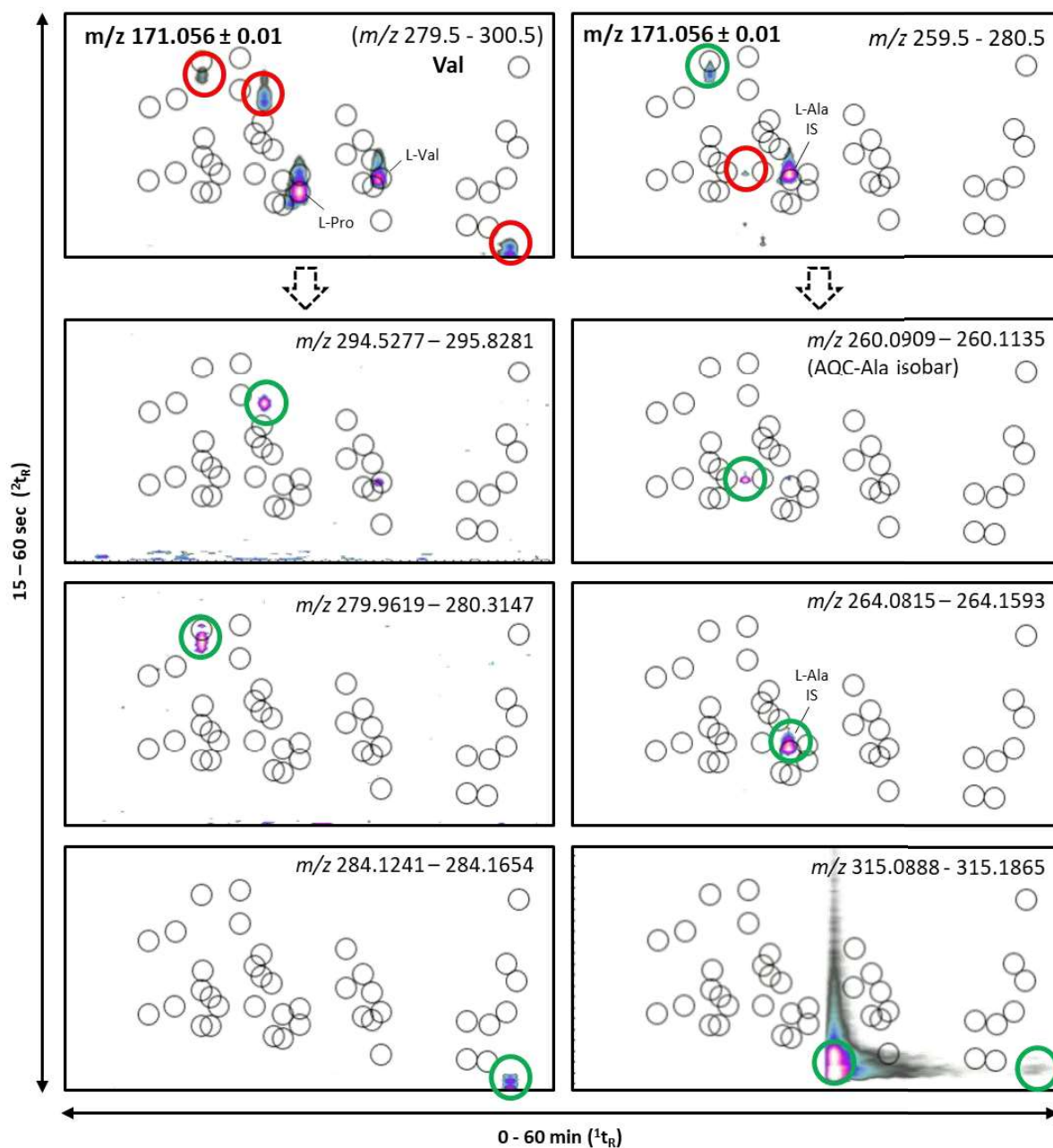
Figure S15. (Continued) Extracted ion chromatograms from MS[1] (left) of the respective AQC-AA expected in Aureobasidin A and MS[2] EIC of the signature fragment m/z 171 from the respective AQC-AA SWATH window (right). The red circles correspond to unknown compounds.
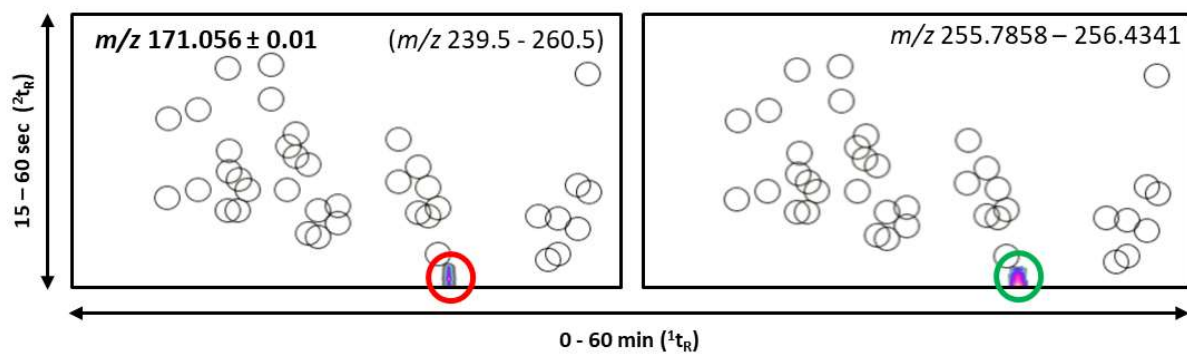
4.5.1.5.5.3 Untargeted analysis

Figure S16. Unknown impurities from Aureobasidin A revealed through the AQC signature fragment m/z 171 on MS[2] level (red circled) and the corresponding retrospectively extracted precursor ions (at FWHM) from MS[1] (green circles).

Figure S17. (continued). Unknown impurities from Aureobasidin A revealed through the AQC signature fragment m/z 171 on MS^2 level (red circled) and the corresponding retrospectively extracted precursor ions (at FWHM) from MS1 (green circles).

4.5.1.5.6 RP×chiral 2DLC-ESI-QTOF-MS/MS analysis of octreotide

4.5.1.5.6.1 MS[1] and MS[2] 2D-Extracted Ion Chromatograms (2D-contour plots) of targeted amino acids
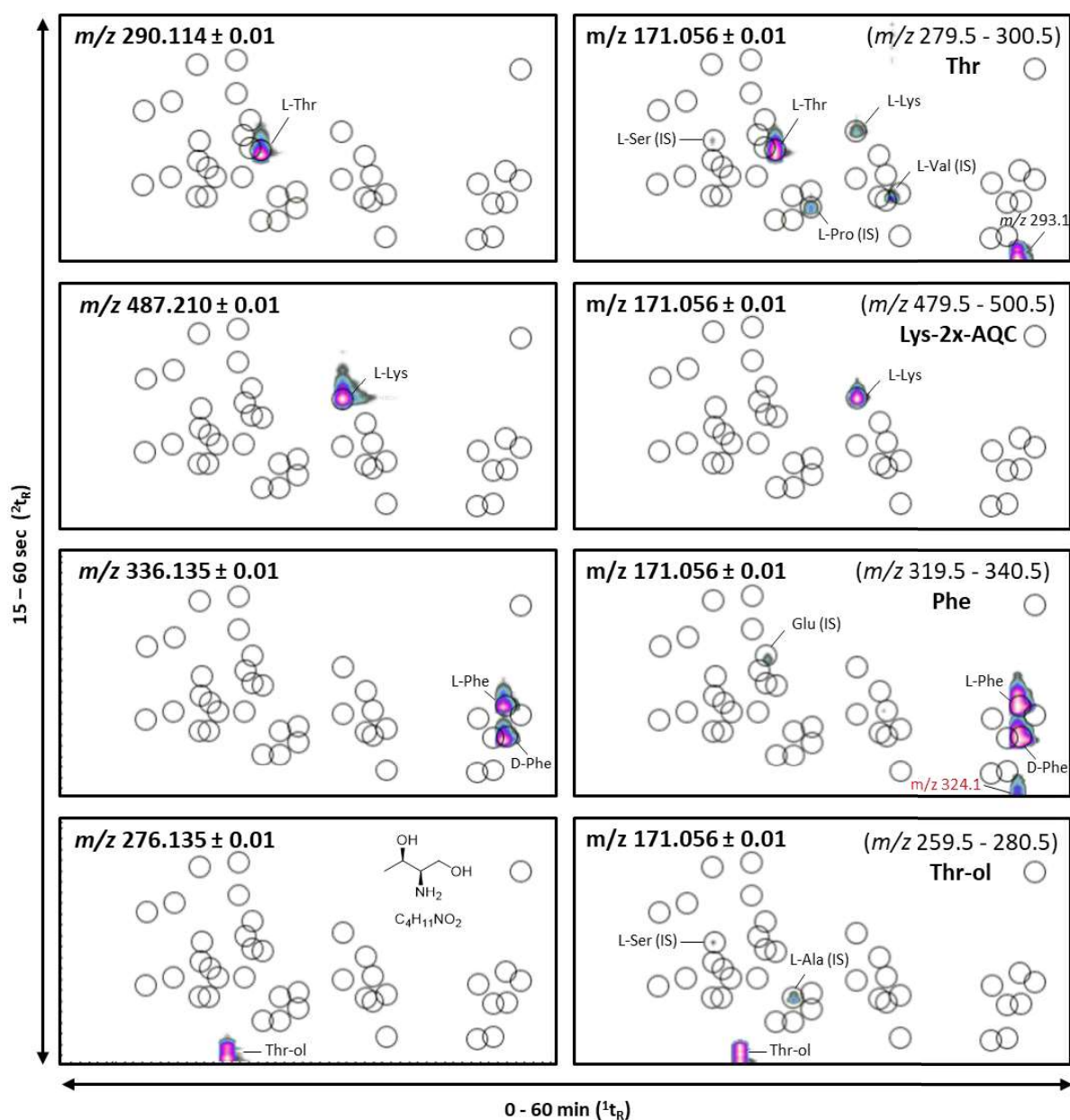

Figure S18. Extracted ion chromatograms from MS[1] (left) of the respective AQC-AA expected in Octreotide and MS[2] EIC of the signature fragment m/z 171 from the respective AQC-AA SWATH window (right). Red labels indicate the precursor ions of unknowns.
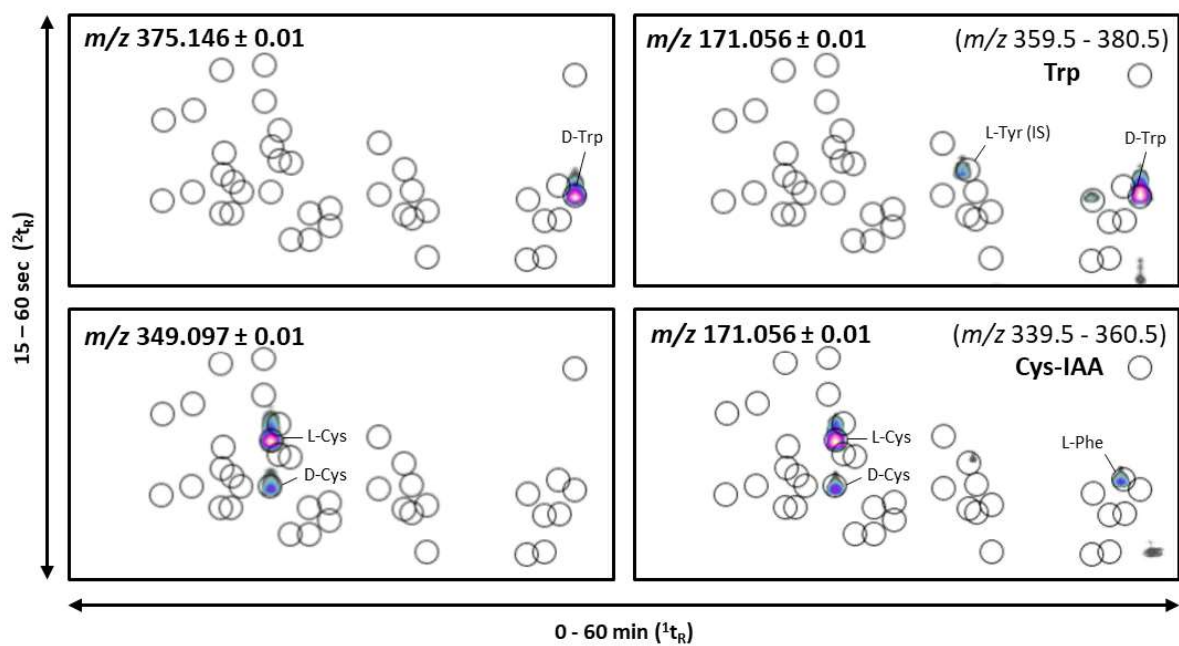
Figure S19. (Continued) Extracted ion chromatograms from MS[1] (left) of the respective AQC-AA expected in Octreotide and MS[2] EIC of the signature fragment m/z 171 from the respective AQC-AA SWATH window (right).

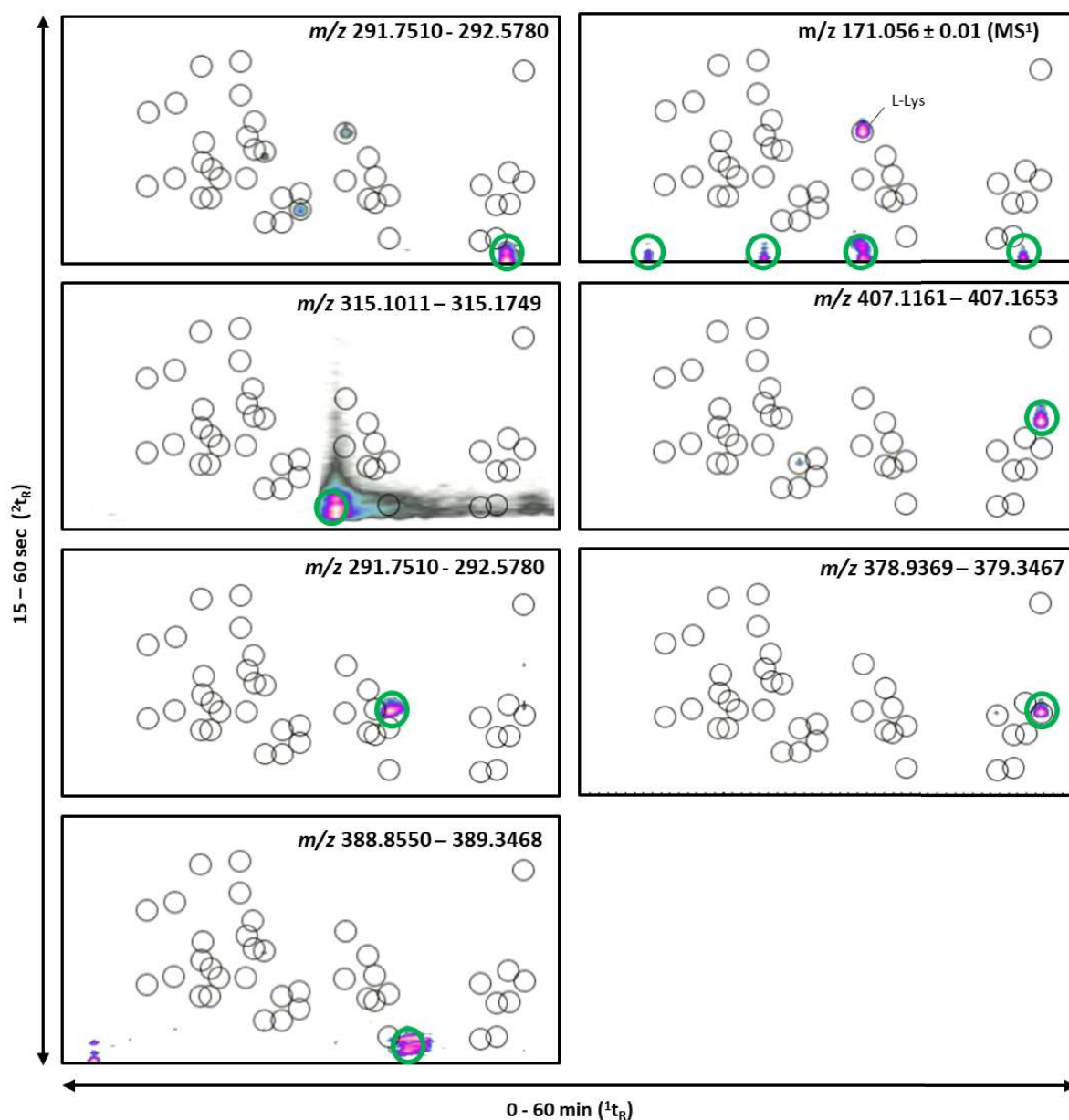### 4.5.1.5.6.2 Untargeted analysis

Figure S20. Unknown impurities from Octreotide revealed through the AQC signature fragment m/z 171 on MS[2] level and the corresponding retrospectively extracted precursor ions (at FWHM) from MS[1] (green circles). Ions corresponding to m/z 171.056 on MS1 level and unretained by the [2]D, can be attributed to insource fragments of AQC reagent peaks.

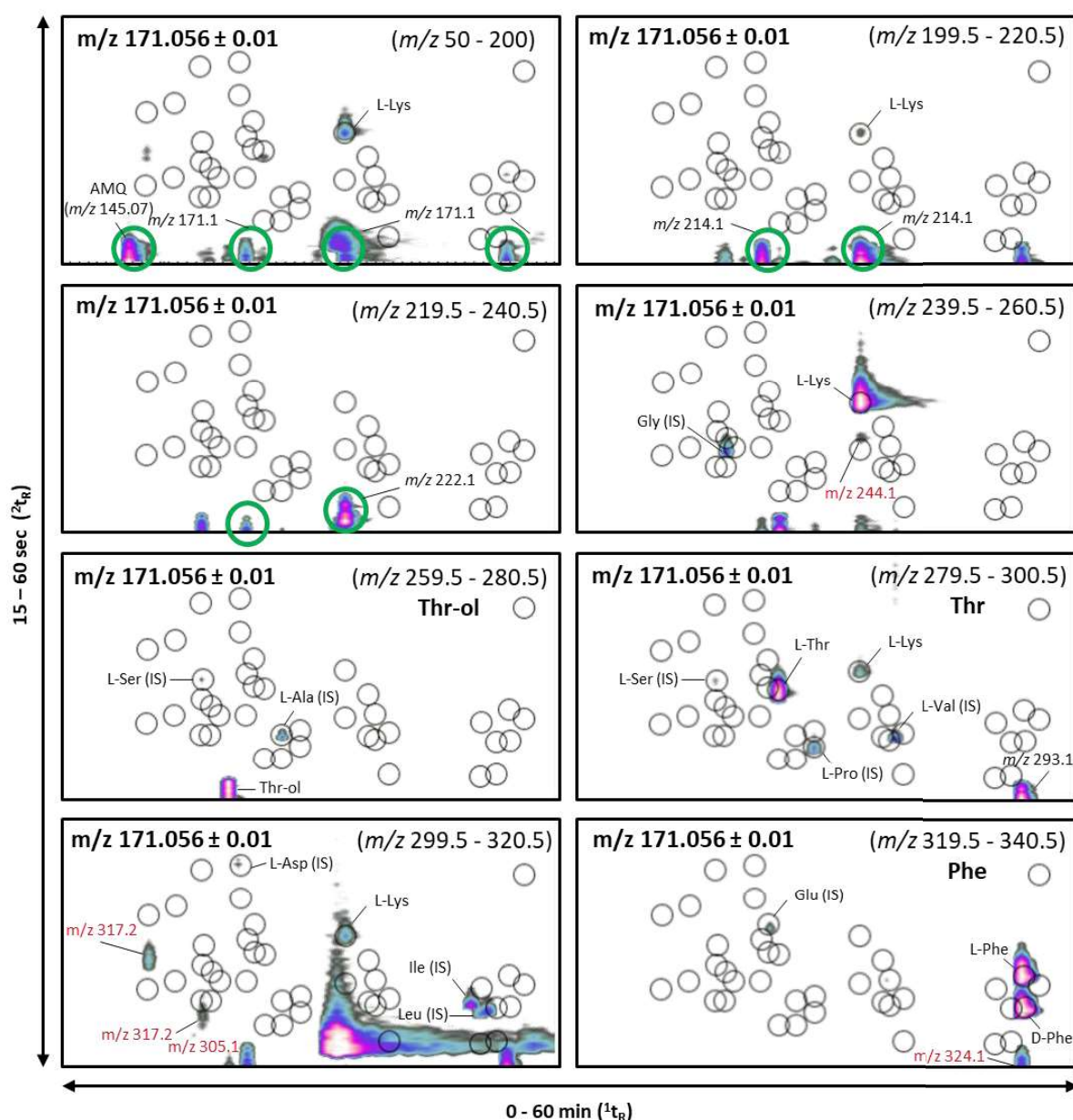### 4.5.1.5.6.3 Untargeted analysis: All consecutive SWATH windows

Figure S21. Octreotide MS[2] chromatograms of signature fragment m/z 171 extracted from SWATH windows 1-8 (red labels indicate the precursor ions of unknowns). Ions corresponding to m/z 171.056 in MS[2] (m/z 50 - 200) level and unretained by the [2]D, can be attributed to insource fragments of AQC reagent peaks. The dominant L-shaped peak (bottom left) corresponds to bis-AMQ urea (m/z 315.1240). L-Lys-bis-AQC is represented in multiple SWATH windows with ions (e.g. L-Lys-AQC and L-Lys) produced by insource fragmentation or adducts analogues.
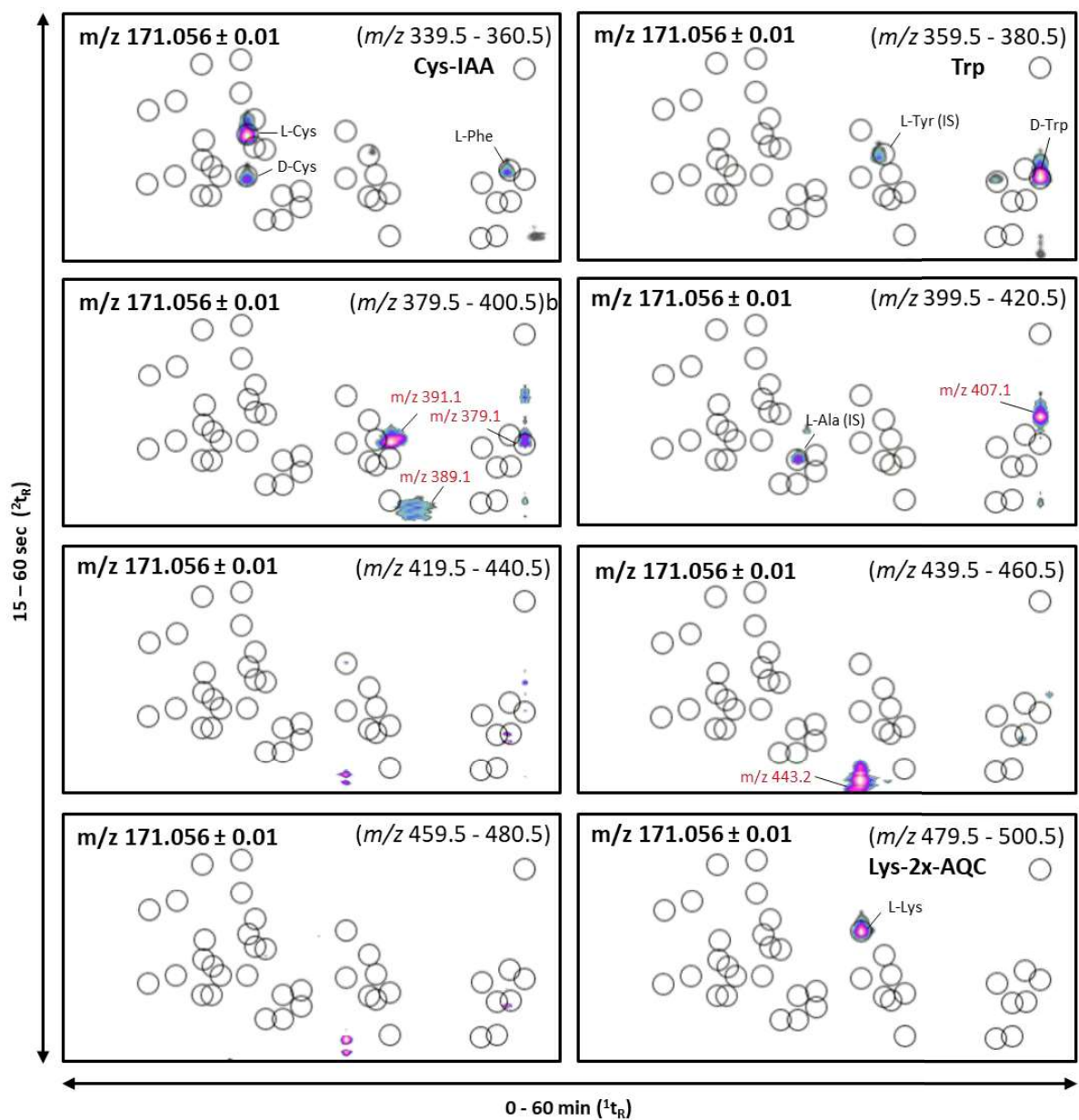
Figure S22. Octreotide MS[2] chromatograms of signature fragment m/z 171 extracted from SWATH windows 9-16 (red labels indicate the precursor ions of unknowns).
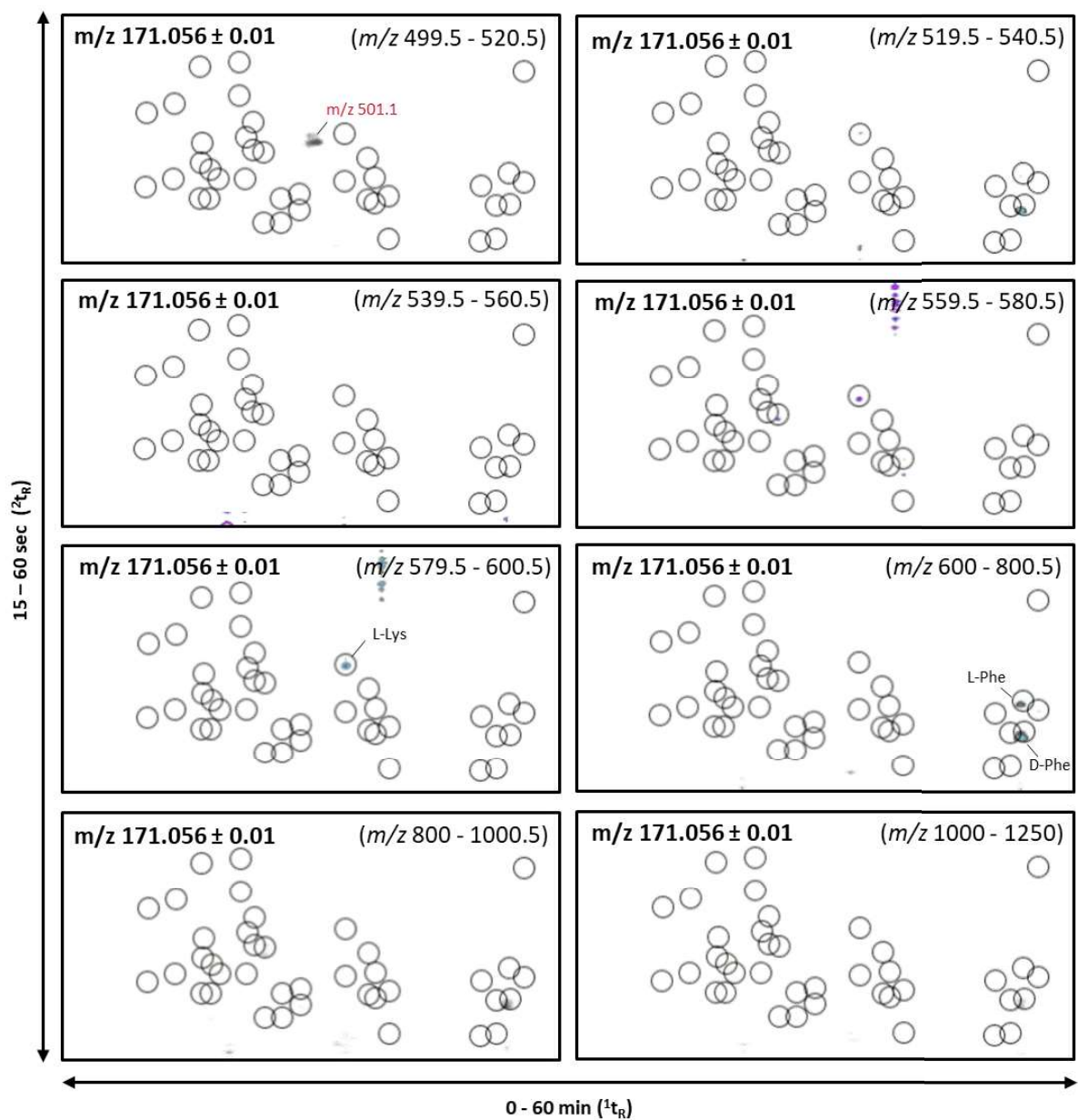
Figure S23. Octreotide MS[2] chromatograms of signature fragment m/z 171 extracted from SWATH windows 17-24 (red labels indicate the precursor ions of unknowns). Ions co-eluting with Lys and Phe correspond to the formation of adducts and dimers, respectively.
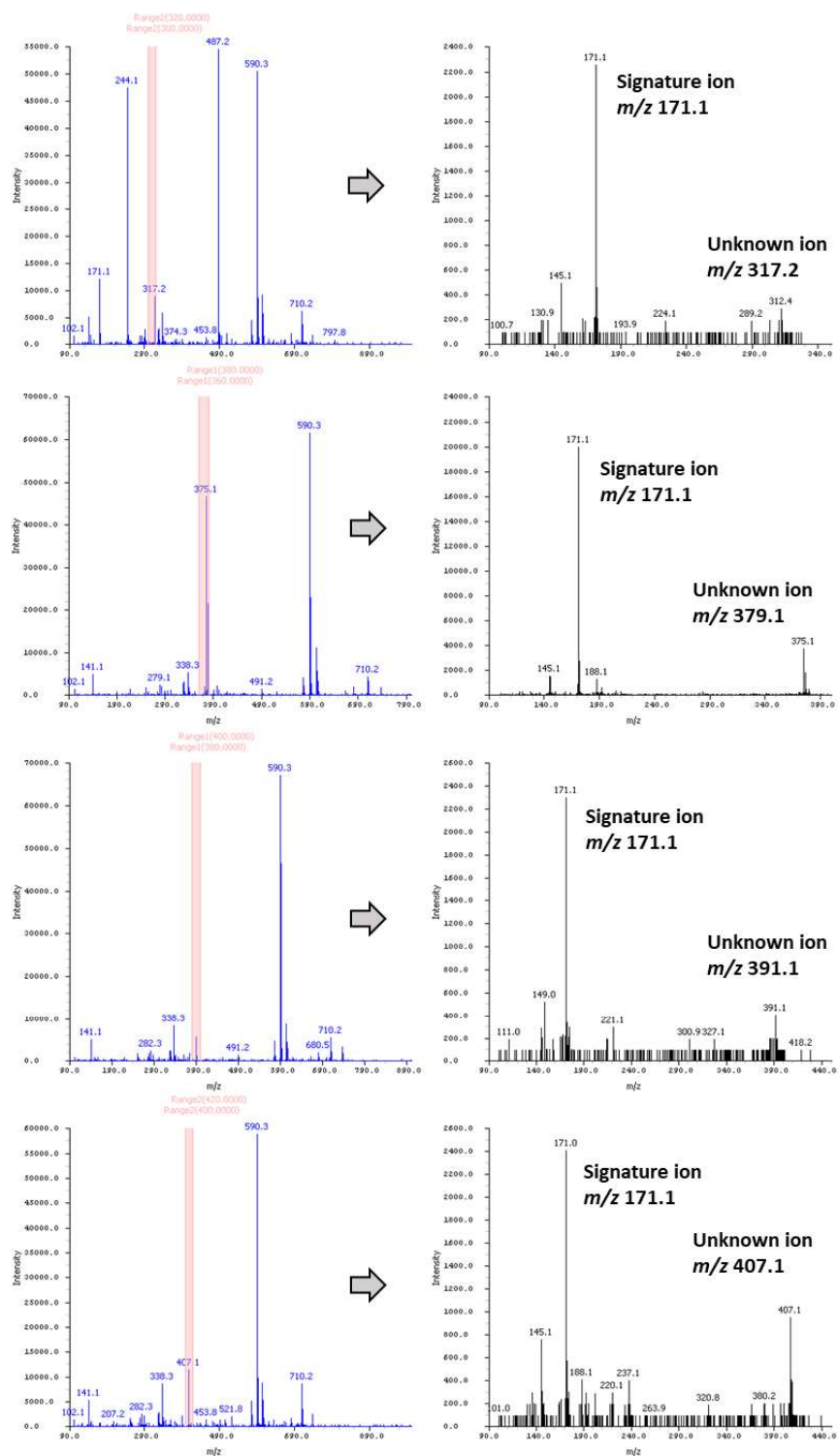
Figure S24. MS[1] (left) and the corresponding MS[2] (right) spectra for m/z 317.2 (t_R(^{1}D): 9.00 min, t_R(^{2}D): 33.72 s), m/z 379.1 (t_R(^{1}D): 51.00 min, t_R(^{2}D): 29.78 s), m/z 391.1 (t_R(^{1}D): 36.00 min, t_R(^{2}D): 29.78 s) and m/z 407.1 (t_R(^{1}D): 51.00 min, t_R(^{2}D): 34.60 s) as unknowns found in octreotide.

4.5.1.6 Calibration functions for all proteinogenic AAs comparing peak volume and peak height as response
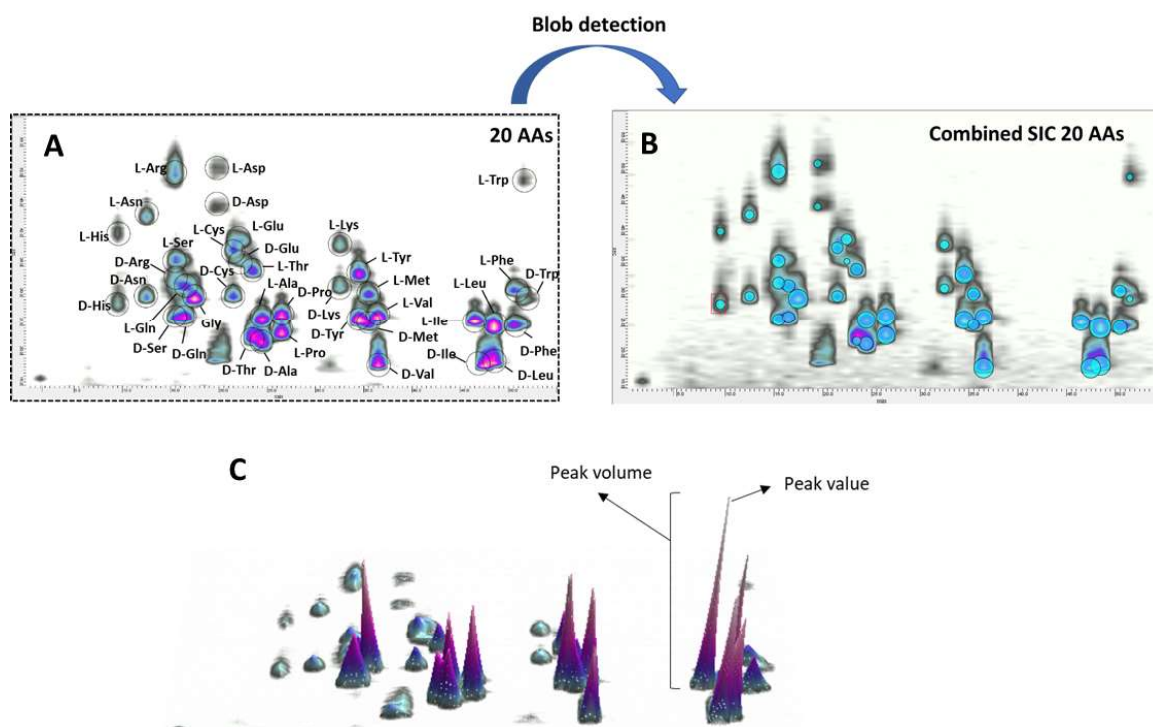
Figure S25. Exemplary blob detection workflow using LC-Image. **A**) First the raw MS data files (.wiff) are loaded to LC Image and the corresponding targets (e.g. AA mix) extracted. **B**) The combined SIC (selected ion chromatogram) is saved as ".gci", on which blob detection is performed using **C**) peak volume (PV) and peak value (i.e. peak height, PH) as responses. Detailed commentary on LC-Image parameters is given in **Table S8**.

Table S8. Comments to LC-Image workflow and parameters.

Untargeted analysis	1. Load data via direct import.
	2. View any spectrum after the direct import. The MS Viewer will show MS^1 and all MS^2 spectra.
	3. Make a preferred MS^2 spectrum (SWATH window) active > Open EIC (signature ion or specific ion).
Targeted analysis (i.e. using a template)	1. Import the raw data > View > EIC View with the formula list of AQC-AAs
	2. With the EIC view in focus, File > Save Image as ".gci".
	3. Open the saved EIC image (.gci), then process.

Background subtraction → Configuration settings → **B**lob detection/editing → **T**emplate matching → **E**xport blob table

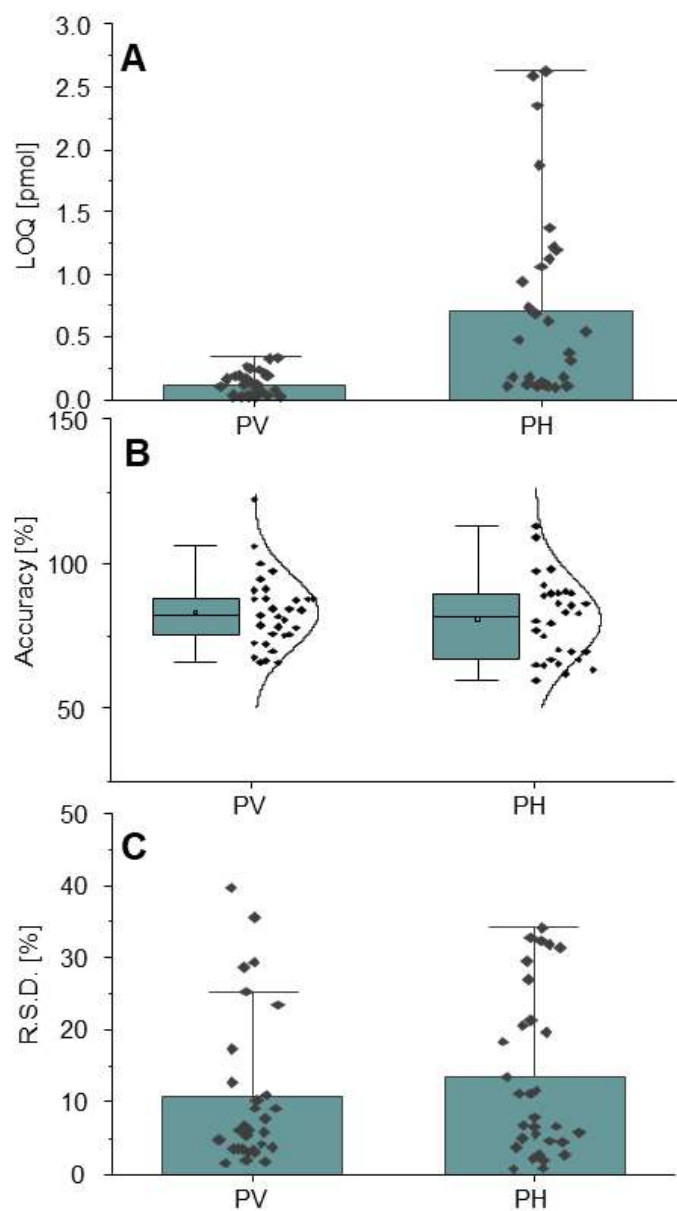|		
Processing	Background subtraction	Removal of the baseline (or background) level introduced by the system (important for precise quantification).
	Configuration settings	Settings for processing and analyzing images (e.g. color map, blob display, blob detection settings, baseline correction settings, template settings and blob table configuration) are exported in a configuration file (.cfg).
	Blob detection	Peaks (or blobs) are identified by the pixels that make up each peak. The sum of the pixel values in each blob is related to the quantity of the chemical that produced it, so the sum of pixel values of a blob is useful in quantifying each chemical in a sample.
	Blob editing	Automated blob detection sometimes fails to detect blobs correctly (e.g. split what should be a single blob and merge what should be two separate blobs). Therefore, deconvolve/unmix blobs: Separate co-eluting peaks by their spectral signature (i.e. the extracted precursor ions of D-Glu & L-Thr), merge: Merge selected blobs (e.g. of same spectral signature after deconvolution), split: Split the currently selected blob along a horizontal or vertical line (e.g. for co-eluting isobaric AAs, i.e. Leu/Ile).
	Template matching	Area objects (i.e. black circles) containing quantifier ions are added to a template of all targeted peaks (exported as .bt). The CLIC (Computer Language to Identify Chemicals) tool further supports blob selection using customizable constraints (i.e. quantifier ion), i.e. a CLIC column is added to the Blob/Area Table to check area objects against detected blobs.
	Export blob table	Blob table is exported. Array (Compound Name, Group Name Inclusion, Retention I (min), Retention II (sec), Peak Value, Volume, Quantifier Peak Value(1), Quantifier Volume(1), Quantifier(1), SNR).
Batch processing		Performed in LC Project. Images (.gci of EICs) are processed automatically using the defined processing parameters (.cfg, .bt,), resulting in blob tables for each sample. Perform blob editing (convenient in LC Project).

Figure S26. Summary of calibration and validation data (**Table S9**) for **A**) LOQ (S/N=10), **B**) accuracy (as % recovery) and **C**) precision (as % RSD) for all AAs (except instable ones) using peak volume (PV) and peak height (PH) as dependent variable and QC (5 pmol or 10 pmol depending on range).

Table S9. Calibration/validation/quantification results for all AAs using EICs of precursor ions from MS[1].

AA	Response	Range [pmol]	Regression equationa	R2	LOD [pmol]	LOQ [pmol]	Intra batch/day (n = 3), QC 10 pmola		
							calc. conc. [pmol]	Acurracy [%]	Precision R.S.D [%]
D-Ala	PV	0.1 – 5	y = 126568x 19015	0.999	0.01	0.04	9.08	90.80	17.42
	PH	0.1 – 5	y = 33313x 2379	0.999	0.04	0.14	8.03	80.26	5.57
D-Arg	PV	1 – 10	y = 41029x -9297	0.997	0.05	0.17	8.79	87.87	28.64
	PH	1 – 10	y = 5691x -748	0.997	0.36	1.19	13.54	135.39	4.67
D-Asn	PV	0.1 – 10	y = 35816x 6978	0.987	0.06	0.19	7.29	72.87	3.54
	PH	0.1 – 10	y = 7270x 3008	0.987	0.28	0.94	8.93	89.26	3.82
D-Asp	PV	0.5 – 10	y = 17166x 5575	0.995	0.10	0.33	7.89	78.88	9.22
	PH	0.5 – 10	y = 2444x 1945	0.995	0.70	2.35	7.73	77.27	11.25
D-Cys-IAA	PV	0.05 – 5	y = 45907x 214	0.977	0.03	0.11	4.21	84.27	17.52
	PH	0.05 – 5	y = 7810x 2410	0.977	0.20	0.67	5.77	115.36	18.00
D-Gln	PV	1 – 10	y = 40015x 36271	0.926	0.05	0.16	10.63	106.26	1.54
	PH	1 – 10	y = 13641x 10870	0.926	0.14	0.48	8.96	89.62	0.77
D-Glu	PV	0.5 – 10	y = 22533x 2983	0.992	0.07	0.24	8.23	82.25	10.30
	PH	0.5 – 10	y = 7155x 1355	0.992	0.22	0.74	9.76	97.60	20.67
D-His	PV	0.5 – 10	y = 24698x -5463	0.999	0.07	0.25	8.80	88.00	6.13
	PH	0.5 – 10	y = 3239x 378	0.999	0.56	1.87	9.27	92.67	2.31
D-Ilec	PV	0.5 – 10	y = 132165x 18637	0.997	0.01	0.03	12.23	122.26	39.73
	PH	0.5 – 10	y = 37606x 5408	0.997	0.04	0.12	10.95	109.46	11.23
D-Leuc	PV	0.05 – 5	y = 211013x 35591	0.997	0.01	0.02	3.39	67.75	29.47
	PH	0.05 – 5	y = 35584x 3983	0.997	0.04	0.13	3.26	65.30	7.89
D-Lys-bis-AQC	PV	1 – 5	y = 23780x -7404	0.996	0.06	0.19	6.64	66.35	7.79
	PH	1 – 5	y = 3909x -861	0.996	0.34	1.13	7.51	75.07	0.96
D-Metb	PV	1 – 5	y = 27680x -4777	>0.999	0.05	0.17	13.05	130.53	22.43
	PH	1 – 5	y = 9591x -2180	>0.999	0.15	0.50	16.43	164.30	20.33
D-Phe	PV	0.1 – 10	y = 89450x 54184	0.905	0.02	0.05	4.49	44.89	26.28
	PH	0.1 – 10	y = 21315x 18910	0.905	0.06	0.21	4.55	45.50	10.89
D-Pro	PV	0.5 – 5	y = 147737x -4702	>0.999	0.01	0.03	3.33	66.66	12.75
	PH	0.5 – 5	y = 36407x 1874	>0.999	0.03	0.11	3.25	64.93	21.38
D-Ser	PV	0.5 – 5	y = 64647x 2881	>0.999	0.03	0.10	4.24	84.70	4.79
	PH	0.5 – 5	y = 17544x 3531	>0.999	0.11	0.37	4.32	86.47	4.52
D-Thr	PV	0.01 – 5	y = 90287x 18363	0.999	0.02	0.05	5.02	100.39	4.19
	PH	0.01 – 5	y = 27623x 1853	0.999	0.05	0.17	3.36	67.14	6.67
D-Trpb	PV	0.5 – 10	y = 20580x -2791	0.982	0.06	0.20	4.41	44.09	29.91
	PH	0.5 – 10	y = 7572x -436	0.982	0.16	0.55	2.81	28.06	32.54
D-Tyr	PV	0.05 – 10	y = 146479x -6639	0.974	0.01	0.03	9.50	94.98	1.76
	PH	0.05 – 10	y = 40054x 2229	0.974	0.04	0.12	8.34	83.38	11.76
D-Val	PV	0.5 – 5	y = 198032x 14049	0.998	0.01	0.03	8.20	82.02	6.08
	PH	0.5 – 5	y = 49497x -11519	0.998	0.03	0.10	6.55	65.53	32.34
Gly	PV	0.1 – 10	y = 144571x 34034	0.998	0.01	0.04	8.05	80.54	3.50
	PH	0.1 – 10	y = 35796x 7074	0.998	0.05	0.18	11.33	113.27	6.80
L-Ala	PV	0.5 – 10	y = 131385x 20222	0.975	0.01	0.03	8.44	84.41	9.22
	PH	0.5 – 10	y = 34528x 8498	0.975	0.04	0.13	6.20	62.03	5.00
L-Arg	PV	0.5 – 10	y = 71303x 6251	0.997	0.03	0.09	6.99	69.90	35.57
	PH	0.5 – 10	y = 6325x 414	0.997	0.32	1.06	9.84	98.37	6.60

168

L-Asn	PV	0.5 – 10	y = 31509x 1497	0.992	0.06	0.20	7.25	72.48	5.96
	PH	0.5 – 10	y = 4591x 955	0.992	0.41	1.37	9.01	90.05	2.01
L-Asp	PV	0.05 – 10	y = 22065x 2709	0.990	0.08	0.27	9.14	91.35	6.91
	PH	0.05 – 10	y = 2261x 959	0.990	0.78	2.59	8.57	85.70	29.65
L-Cys-IAA	PV	0.1 – 5	y = 23980x -285	0.988	0.07	0.24	20.32	203.22	8.54
	PH	0.1 – 5	y = 5626x 1733	0.988	0.30	1.00	21.63	216.29	14.73
L-Gln	PV	0.01 – 10	y = 42777x 6901	0.954	0.04	0.14	8.74	87.44	5.51
	PH	0.01 – 10	y = 11169x 2211	0.954	0.16	0.54	9.06	90.55	5.81
L-Glu	PV	0.01 – 10	y = 41585x 2270	0.997	0.04	0.13	7.58	75.78	3.12
	PH	0.01 – 10	y = 7665x 1096	0.997	0.21	0.68	9.00	90.05	27.01
L-His	PV	0.5 – 10	y = 18774x -1826	0.995	0.10	0.33	8.40	83.96	10.97
	PH	0.5 – 10	y = 2322x 393	0.995	0.79	2.63	7.96	79.63	2.63
L-Ile	PV	0.05 – 10	y = 162714x -12620	0.995	0.01	0.03	9.76	97.57	23.53
	PH	0.05 – 10	y = 43119x -5	0.995	0.03	0.11	6.98	69.82	31.42
L-Leu	PV	0.01 – 5	y = 224808x 20773	0.997	0.01	0.02	4.39	87.77	6.34
	PH	0.01 – 5	y = 42209x 3433	0.997	0.03	0.11	3.52	70.41	18.41
L-Lys-bis-AQC	PV	0.01 – 10	y = 22979x -2087	0.998	0.05	0.18	7.84	78.42	3.66
	PH	0.01 – 10	y = 3446x -56	0.998	0.37	1.22	8.32	83.16	19.66
L-Met[b]	PV	0.5 – 5	y = 28058x -10070	>0.999	0.05	0.17	3.35	66.97	4.29
	PH	0.5 – 5	y = 6633x -1211	>0.999	0.22	0.73	3.86	77.27	5.80
L-Phe	PV	0.01 – 10	y = 71940x 10434	0.988	0.02	0.06	4.98	49.82	17.80
	PH	0.01 – 10	y = 19662x 3373	0.988	0.07	0.22	4.13	41.34	13.29
L-Pro	PV	0.01 – 5	y = 153701x 713	0.999	0.01	0.03	7.52	75.19	25.30
	PH	0.01 – 5	y = 40530x -95	0.999	0.03	0.10	6.71	67.10	32.79
L-Ser	PV	0.01 – 10	y = 52233x 2967	0.993	0.04	0.12	7.56	75.56	3.56
	PH	0.01 – 10	y = 9898x 2396	0.993	0.19	0.63	5.98	59.82	34.11
L-Thr	PV	0.01 – 10	y = 64044x 5062	0.987	0.02	0.08	6.60	65.96	3.87
	PH	0.01 – 10	y = 16257x 1817	0.987	0.09	0.31	6.97	69.72	2.69
L-Trp[b]	PV	0.5 – 10	y = 26100x -5884	0.995	0.05	0.16	3.48	34.79	39.23
	PH	0.5 – 10	y = 3535x -29	0.995	0.35	1.17	2.98	29.80	21.29
L-Tyr	PV	0.01 – 10	y = 114097x -6498	0.991	0.01	0.04	8.81	88.11	2.04
	PH	0.01 – 10	y = 24326x 243	0.991	0.05	0.18	8.62	86.17	13.43
L-Val	PV	0.01 – 5	y = 148756x 3854	0.998	0.01	0.03	7.81	78.06	3.05
	PH	0.01 – 5	y = 49116x -5818	0.998	0.03	0.10	6.32	63.23	31.95

[a] Analytical batch was running over three days, i.e. intra-batch validation is equivalent to inter-day precision accuracy; QC level: 5 or 10 pmol (depending on range)
[b]unstable amino acids
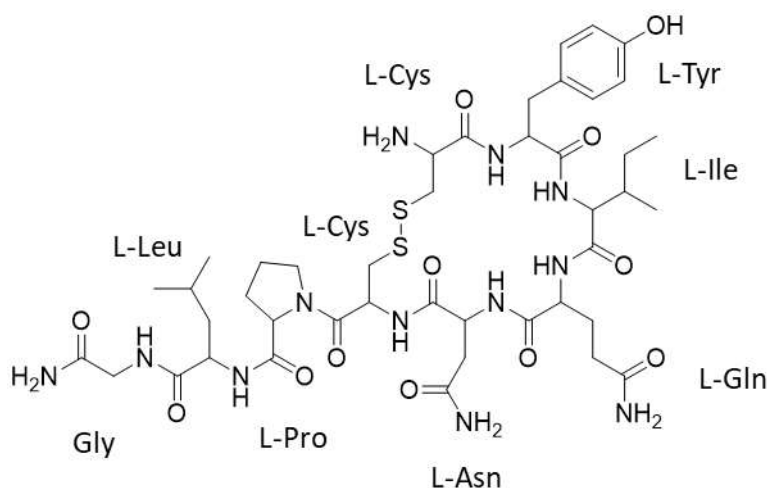[c]partial co-elution brings about problems with blob editing (splitting)

Figure S27: Structure of Oxytocin

Table S10. The calculation of the amino acid composition of oxytocin using PV integration. The molar concentration of each amino acid is calculated and divided by the average (number of AAs is known or estimated) molar concentration to determine the observed AA composition.

AA	c [pmol on column]	pmol AA/pmol peptide[a]	Observed composition[b]
D-Cys-IAA	0.83	0.33	0
Gly	1.60	0.63	1
L-Asp (Asn)	3.13	1.24	1
L-Cys-IAA	4.65	1.85	2[c]
L-Glu (Gln)	2.82	1.12	1
L-Ile	2.63	1.04	1
L-Leu	1.89	0.75	1
L-Pro	2.91	1.15	1
L-Tyr	2.21	0.88	1
Sum pmol AAs/9 AAs	2.52		

[a] calculated as pmol on column divided by mol equivalent of single amino acid (obtained from sum pmol AAs/n AAs in peptide

[b] Obtained from integer of pmol AA per pmol peptide

[c] sum of D and L (minor D-Cys quantities observed due to racemization during hydrolysis; can be ruled out by performing the hydrolysis in DCl/D$_2$O)

Literature

(1) Horak, J.; Lammerhofer, M. *J. Chromatogr. A* **2019**, *1596*, 69-78.

(2) Horak, J.; Lämmerhofer, M. *Anal. Chem.* **2019**, *91* (12), 7679-7689.

(3) Karongo, R.; Ge, M.; Geibel, C.; Horak, J.; Lämmerhofer, M. *Anal. Chim. Acta* **2021**, *1180*.

(4) Hanafi, R. S.; Lämmerhofer, M. *J. Chromatogr. A* **2018**, *1534*, 55-63.

(5) Araujo, P. W.; Brereton, R. G. *TrAC, Trends Anal. Chem.* **1996**, *15* (2), 63-70.

(6) Karongo, R.; Ge, M.; Horak, J.; Gross, H.; Kohout, M.; Lindner, W.; Lämmerhofer, M. *Journal of Chromatography Open* **2021**, *1*, 100004.

(7) Geibel, C.; Dittrich, K.; Woiwode, U.; Kohout, M.; Zhang, T.; Lindner, W.; Lammerhofer, M. *J. Chromatogr. A* **2019**.

5. Acknowledgements

I would like to acknowledge and thank everyone who contributed to the making of this thesis.

Special thanks,

And finally, to my mother, who has constantly sacrificed her present for my future. You brought me to Germany and made everything possible. Without you, I could never be where I am. To you I dedicate this thesis.

"Science investigates; religion interprets. Science gives man knowledge, which is power; religion gives man wisdom, which is control. Science deals mainly with facts; religion deals mainly with values. The two are not rivals. They are complementary."

Martin Luther King, Jr